THÈSE POUR OBTENIR LE GRADE DE DOCTEUR DE L'UNIVERSITÉ DE MONTPELLIER

En Génie des Procédés

École doctorale GAIA-APAB- Agroressources, Procédés, Aliments, Bioproduits

Unité de recherche BioWooEB – Biomasse, Bois, Énergie, Bioproduits (CIRAD – UR114)

Conversion thermochimique des coques de noix de cajou : comportement des extractibles

Présentée par Kelly Wen Yee CHUNG
Le 6 Novembre 2024

Sous la direction de Laurent VAN DE STEENE

Devant le jury composé de

Sylvain CAILLOL, Directeur de recherche, CNRS, Institut Charles Gerhardt de Montpellier	Président du jury
Anthony DUFOUR, Directeur de recherche, CNRS, LRGP Nancy	Rapporteur
Jean-Henry FERRASSE, Professeur des Universités, Aix Marseille Université, Laboratoire M2P2	Rapporteur
Capucine DUPONT, Maître de conférences HDR, IHE Delft Institute for Water Education	Membre du jury
Dorothee LAURENTI, Directeur de recherche, CNRS, laboratoire IRCELYON	Membre du jury
Laurent VAN DE STEENE, Chargé de recherche HDR, CIRAD BioWooEB	Directeur de thèse
Joël BLIN, Chargé de recherche, CIRAD BioWooEB	Encadrant de thèse

UNIVERSITÉ DE MONTPELLIER

Acknowledgements

I was not able to fully express my extensive gratitude during my defense, so I am happy to do so here.

First and foremost, I would like to express my gratitude to **AgroGazelec** and **Biostar**, as well as the **regional funding** authorities, for providing the financial support for my thesis.

But most importantly, I would like to express my heartfelt gratitude to my two primary supervisors, **Laurent and Joël**, who have guided me throughout my thesis. Your patience and trust in my work, along with your availability for numerous discussions, have been invaluable. Thank you for teaching me what research truly entails, helping me understand my shortcomings in this field, and showing me what I was, am, and will be capable of achieving in the realm of research.

Laurent, thank you for teaching me everything about pyrolysis kinetics and thermochemical processes-related knowledge. From someone who did not know what tar was, I became someone who knows how they are formed, how they can be analyzed, how they could be manipulated according to operating conditions. And it was not only that, I have learnt a lot more, and most I did not know before my thesis. During my university years, I studied thermochemical processes but had never applied them experimentally. You have given me the opportunity to do so. From you, the most important thing I have learned was the rigor of research. You also offered me a different perspective about research by emphasizing the importance of applied research.

Joël, thank you for guiding me and making my thesis both interesting and fulfilling. Your ability to interpret scientific results is something I deeply admire and aspire to master in the future. I still remember when you shared your perspective on passion in research; it inspired me to seek a domain where I could feel the same enthusiasm and dedication as you.

Thank you, Laurent and Joël, for your unwavering support throughout these three years, especially in the lead-up to my defense. Because of you both, I was able to deliver a presentation I was proud of, despite not being someone who is usually confident or proud of her achievements. From you both, I have learned that becoming a good researcher involves overcoming many intellectually challenging moments. Research is not just about obtaining results; it requires persistence, critical thinking, and the willingness to tackle complex problems, often requiring deep focus and creative problem-solving. These "brain-breaking" moments are

where the most significant growth happens, pushing one to question assumptions, explore new approaches, and ultimately contribute meaningful insights to the field.

My sincere gratitude goes to the two examiners of my thesis, **Anthony Dufour** and **Jean-Henry Ferrasse**, as well as the jury president, **Sylvain Caillol**, and the other jury members, **Capucine Dupont** and **Dorothée Laurenti**. Thank you for accepting to be a part of the jury and your presence during my defense. Your advice and the discussions we had opened up numerous opportunities for improvement and new ideas in the domain of my thesis research.

Next, I would also like to extend my thanks to **Jean-Michel**, the unit director of BioWooEB, for letting me integrate into BioWooEB.

Thank you, **Diakaridia**, for the insightful discussions and the knowledge you shared with me, particularly in the area of kinetic modeling. Your encouragement throughout my thesis journey has been greatly appreciated. I am glad to have worked with you.

I am deeply thankful to **Diakaridia**, **François**, and **Jean-Michel** for their assistances in helping me prepare for my defense.

I would like to highlight my gratitude to **Jérémy**, a truly skilled technician at BioWooEB. Thank you for your availability, patience, and for teaching me so many valuable technical skills. You have always been present when I encountered technical difficulties and I am really grateful to you.

Thank you, **Charline**, expert in analytical methods as well, for developing the HPLC method, which allowed us to make significant progress in the characterization of CNSL. Thank you for your kindness and assistances throughout these 3 years.

Thank you, **Eric**, for setting up the laboratory reactor, especially during the early stages of my thesis, and for always being available to address my technical needs. Thank you for your good humor as well.

I would also like to express my gratitude to the other members of BioWooEB and my B16 colleagues: Florent, Coline, Laurent, Priscilla, Frank, Annabelle, Agnès, Alfredo, Philippe and others whom I have not named here. Thank you for your friendliness and your kindness.

I am particularly thankful to four essential PhD students—**Johnrell**, **Imen**, **Askar**, and **Chaisiri** and **Sam**—for their support and advice during my presentations.

I am also grateful to the other PhD students and interns I encountered along the way: Lisa, Sabba, Fabrice, Landry, Wadii, Men, Edwige, Nawel, Charlotte, Nafiu, Souha, Lucie, Solène, Mourad, Estelle, Charnelle, Meriam, Tessembou and others whom I might have missed out in the list. Thank you for the wonderful moments we have shared together.

A special thank you to two very important friends, **Dino** and **Chian Huey**, who were unconditionally present for me, offering their virtual support and care, especially during my final year of the thesis. Thank you for bringing me light during my last year of thesis.

I would also like to express my deepest gratitude to my partner, **Louis**, for his understanding and unwavering support throughout my thesis. Thank you for making the difficult moments easier to overcome.

Finally, thank you to my family : my dear parents, my brother Eric, Matherin, and my aunt Professor Chua, for your support and love despite being 7k miles away.

Your presence has been essential to me during this 3-year journey, and I am sincerely touched and profoundly grateful.

Résumé

Résidu agricole abondant dans les pays du Sud, les coques de noix de cajou (CNC) sont peu ou pas valorisées sur le plan énergétique, notamment en raison de la présence de composés extractibles. Ces derniers, connus sous le nom de CNSL (Cashew Nut Shell Liquid), contiennent trois constituants principaux : les acides anacardiques, les cardanols et les cardols (ACC).

Cette thèse a pour objectif de comprendre les réactions impliquées lors de la conversion thermochimique de ces coques de noix de cajou, avec un focus particulier sur le comportement des composés extractibles. L'amélioration des connaissances de la composition de ce résidu et des produits issus de sa transformation a nécessité, en amont, la mise au point de méthodes spécifiques d'extraction et d'analyse. Par ailleurs, l'analyse thermogravimétrique a été utilisée pour étudier les cinétiques de pyrolyse, tandis qu'un réacteur à lit fixe a permis de quantifier les produits obtenus après pyrolyse et craquage thermique. Une attention particulière a été portée aux mécanismes de dégradation des composés extractibles ACC et à l'influence des conditions opératoires sur la production de charbon, de condensats, et de gaz, ainsi que sur leur composition.

L'analyse détaillée des coques de noix de cajou a permis d'identifier 91% de leur composition. La teneur totale en composés extractibles est de 58%, dont 40% pour les ACC et 18% pour les tanins. Les cinétiques de pyrolyse des coques, des coques « hors ACC », et des ACC ont été étudiées, et les interactions entre la matrice solide et les composés extractibles pendant la pyrolyse ont été mises en évidence. Les ACC sont les principaux contributeurs à la formation de condensats et de CO_2 lors de la pyrolyse des coques à 400 °C. Une réduction significative de leur quantité a été observée durant la pyrolyse, les cardanols étant les seuls ACC résiduels dans les condensats. Les ACC se dégradent selon les réactions suivantes : (1) décarboxylation des acides anacardiques, (2) polymérisation des cardanols et des cardols, (3) dévolatilisation des cardanols des cardols, et (4) dégradation thermique des polymères à base de cardanols et de cardols, ainsi que l'évaporationdes cardanols. Des expériences de craquage thermique des gaz de pyrolyse ont permis de mesurer des conversions de 25 %, 48%, et 77 % respectivement à 600, 800, et 900 °C.

Mots clés: pyrolyse, extractibles, composition, cinétique

Abstract

Cashew nut shells (CNS), an abundant agricultural residue in South countries, are little or not valorized into energy due to the presence of extractives, known as Cashew Nut Shell Liquid (CNSL), which contains 3 main constituents: anacardic acids, cardanols and cardols (ACC).

The aim of this thesis is to understand the reactions involved in the thermochemical conversion of these cashew nut shells, with a particular focus on the behavior of extractives. The composition and pyrolysis of CNS and CNSL were investigated through the development of characterization methods and experiments. Thermogravimetry analysis was used to study pyrolysis kinetics, while a laboratory scale reactor allowed quantification of products after pyrolysis and thermal cracking. Particular attention was paid to the ACC thermal degradation mechanisms and the influence of operating conditions on the production of char, condensates and gas, and their composition.

The comprehensive analysis of cashew nut shells (CNS) identified 91% of the composition. ACC accounted for 40% of the CNS, while additional findings suggested the presence of tannins, which contributed a further 18%, bringing the total identified extractives to 58%. The pyrolysis kinetics of CNS, ACC-free CNS and ACC were determined and interactions between the solid matrix and the extractives during pyrolysis were demonstrated. Results also showed that ACC were the major contributors to condensates and CO_2 formation during CNS pyrolysis at 400°C, with significant reductions in ACC content observed in the pyrolysis products: Cardanols were the only ACC constituents in the condensates. ACC degraded by several reactions: decarboxylation of anacardic acids, polymerization of cardanols and cardols, devolatilization of cardanols and cardols, as well as thermal degradation of cardanol and cardol based polymers and evaporation of cardanols. Thermal cracking experiments on the CNS pyrolysis gas showed that temperature increases the rate of conversion of organic condensates: 25% at 600°C, 48% at 800°C and 77% 900°C.

Key words: pyrolysis, extractives, composition, kinetic

Thermochemical conversion of cashew nut shells: behavior of extractives

Table of contents

Acknowledgements 3

Résumé long en français 17

General introduction 29

1. General context: Biomass to energy 35

1.1 Issue of biomass energy 35

1.2 Bioenergy conversion 36

1.2.1 Biochemical conversion 37

1.2.2 Physicochemical conversion 37

1.2.3 Thermochemical conversion 38

1.3 Thermochemical conversion processes 39

1.3.1 Pyrolysis 39

1.3.2 Gasification 39

1.3.3 Combustion 41

1.4 Biomass 41

1.4.1 Lignocellulosic biomass 42

1.4.2 Cashew nut shells (CNS) 48

1.5 Issues and challenges related to CNS 51

2. State of art and literature review 57

2.1 Biomass thermochemical reactions 57

2.1.1 Pyrolysis 58

2.1.2 Conversion of pyrolysis gas 60

2.2 Cashew nut shells (CNS) characterization and composition 62

2.2.1 Characterization methods of cashew nut shells 63

2.2.2 Composition of cashew nut shells 68

2.3 Pyrolysis of cashew nut shells 75

2.3.1 Thermal degradation of cashew nut shells 75

2.3.2 Kinetic studies of cashew nut shells pyrolysis 76
2.3.3 Pyrolysis products 80
2.4 Thermal degradation of ACC constituents 85
2.4.1 Thermal degradation of anacardic acids 85
2.4.2 Thermal degradation of cardanols and cardols 86
2.5 Scientific positioning and objectives 92
2.5.1 Positioning 92
2.5.2 Objectives 93
3. Material and methods 97
3.1 Preparation of cashew nut shells 97
3.2 Characterization techniques of cashew nut shells (CNS) 99
3.2.1 Ultimate and proximate analysis 99
3.2.2 Extractives content 100
3.2.3 Determination of macromolecular composition 102
3.3 Thermochemical studies of biomass 103
3.3.1 Description and experimental procedure of thermogravimetric analyzer 104
3.3.2 Description and experimental procedure of tar conversion reactor 105
3.4 Analysis of pyrolysis/cracking products 111
3.4.1 Permanent gas 111
3.4.2 Condensates 112
3.5 Definitions and calculations 113
4. Cashew nut shells composition: Development of analytical methods and study of CNS composition 117
4.1 CNS proximate and ultimate analysis 117
4.2 Molecular composition of CNS 119
4.2.1 Lignocellulosic content 119
4.2.2 Protein and starch content 119

4.2.3 Extractives content 120
4.2.4 Tannin content in water extractives 131
4.3 Summary: Composition of cashew nut shells 133
5. Pyrolysis of cashew nut shells 137
5.1 Pyrolysis kinetics 137
5.1.1 Pyrolysis of CNS, ACC-free CNS and ACC 137
5.1.2 Limitation of CNS kinetic studies 140
5.2 ACC thermal degradation mechanisms 142
5.2.1 Selection of temperatures for analysis of ACC conversion products 142
5.2.2 Analysis of ACC conversion residues at various temperatures 144
5.2.3 Evolution of each ACC isomers at different temperatures 156
5.3 Products from CNS pyrolysis 158
5.3.1 Pyrolysis products yield 159
5.3.2 Permanent gas composition 162
5.3.3 Condensates composition 163
5.3.4 Influence of temperature on pyrolysis products 169
5.4 Summary 172
6. Cracking of CNS pyrolysis gas 177
6.1 Definition and calculations 178
6.1.1 Conversion rate of organic condensates 178
6.1.2 Temperature profile in the cracking zone 178
6.1.3 Residence time of thermal cracking experiments 179
6.1.4 Variation of constituent mass during thermal cracking 180
6.2 Thermal cracking of CNS pyrolysis gas 180
6.2.1 Conversion and product distribution 181
6.2.2 Permanent gas composition 183
6.2.3 Condensates composition 184

6.3 Influence of temperature on thermal cracking of CNS pyrolysis gas 186
6.3.1 Conversion and product distribution 186
6.3.2 Permanent gas composition 189
6.3.3 Condensates composition 190
6.4 Catalytic cracking of CNS pyrolysis gas 191
6.5 Conclusion 194
Conclusions and perspectives 197
References 203
Appendices 233
List of figures 243
List of tables 248

Résumé long en français

Contexte

Les coques de noix de cajou (CNC) représentent un déchet abondant des unités agroalimentaires, dont la valorisation constitue un enjeu majeur, économique, environnemental, et sociétal, notamment en Afrique de l'Ouest.

Malgré le fait que l'Afrique soit l'un des plus grands producteurs de noix de cajou, la transformation ne représente que 10% de sa production [1]. Les unités de transformation ont connu pendant de nombreuses années des difficultés d'approvisionnement en noix brutes en raison de la forte concurrence des acheteurs asiatiques (indisponibilité et augmentation des prix), ce qui a contribué à freiner le développement des procédés de transformation. Aujourd'hui, la grande majorité de la production est exportée, principalement vers le Vietnam et l'Inde, pour être transformée et commercialisée. Par ailleurs, l'accès limité à l'électricité, le manque de technologies appropriées et de compétences freinent la transformation des noix de cajou en Afrique [2].

Les coques produites en grande quantité (2 à 3 tonnes par tonne d'amande), posent de nombreux problèmes lorsqu'elles sont mal ou pas valorisées. Sur le plan environnemental, la présence d'extractibles appelés CNSL (Cashew Nut Shell Liquid) dans les coques, entraînent des risques de pollution des sols par lixiviation lors du stockage, ainsi que des émissions polluantes dans l'air lors de leur combustion. Le CNSL, de nature acide, peut modifier le pH du sol, affectant ainsi la croissance des plantes et perturbant les microbiomes du sol [3]. Par ailleurs, pour les petites et moyennes entreprises (PME), la gestion de ces résidus entraine des surcouts de production difficilement supportables économiquement.

Il existe cependant de nombreuses voies potentielles de valorisation du CNSL, notamment pour la production de résines, de peintures, de vernis, ou encore de produits pharmaceutiques. Plusieurs solutions techniques permettent de récupérer ces extractibles et sont principalement mise en œuvre par de grandes unités industrielles dans des pays comme l'Inde et le Brésil. Malheureusement, les petites unités artisanales en Afrique manquent actuellement de solutions pratiques pour valoriser ce CNSL [2].

Positionnement de thèse

Cette thèse s'inscrit dans le cadre des projets AgroGazelec et Biostar, dont l'objectif final est la valorisation propre et efficace des Coques de Noix de Cajou (CNC) pour satisfaire les besoins énergétiques de PME agroalimentaires en Afrique de l'Ouest. Ces deux projets visent en particulier le développement et/ou l'optimisation de procédés de combustion et de gazéification de cette biomasse problématique. Dans ce contexte, les recherches menées se focalisent sur l'étude de la pyrolyse des coques et de la conversion des gaz de pyrolyse, les deux premières étapes essentielles des procédés thermochimiques. Et naturellement, une attention particulière a été portée au comportement des extractibles CNSL.

La recherche bibliographique a montré que les études antérieures sur la caractérisation des coques se sont principalement concentrées sur la composition lignocellulosique, notamment les hémicelluloses, cellulose et lignines. Il n'existe aucune méthode normalisée pour extraire le CNSL, ce qui constitue une limite pour accéder à la connaissance précise de la composition de ces coques. L'identification et la quantification des acides anacardiques, des cardanols et des cardols (ACC), principales molécules présentent dans le CNSL, nécessitent le développement d'une méthode analytique adaptée, prenant notamment en compte tous les 12 isomères des ACC contenus dans ces extractibles.

En ce qui concerne la pyrolyse des CNC, divers auteurs ont mené des études avec des réacteurs d'analyse thermogravimétrique, mettant principalement l'accent sur les températures de dégradation des macromolécules (hémicelluloses, celluloses et lignines) [4–10]. Seules quelques études ont prêté attention à la dégradation du CNSL [6,7,10–12].

D'autres études ont été réalisées sur des réacteurs à l'échelle laboratoire (400-600°C) [2,4,6,13–16] afin d'étudier le rendement et la composition des produits de pyrolyse des CNC. Cependant, les données sur la composition de ces condensats est mal connue en raison des limitations dans l'analyse de ces extractibles. Plus généralement, nous avons fait le constat que peu d'études ont été publiées sur la pyrolyse de biomasses riches en extractibles.

Naturellement le même constat a été fait sur la conversion du gaz issu de la pyrolyse des CNC. A noter toutefois que l'effet de la température sur le craquage des gaz de pyrolyse a été étudié par Das et al., à 600 °C, et Moreira et al. à 700 °C [4,17].

En résumé, l'état actuel de la recherche révèle un manque de connaissance du rôle des extractibles ACC sur le comportement thermochimique des CNC et des mécanismes de

dégradation thermique des ACC. De même les cinétiques de conversion des CNC et de ses composants (extractibles) n'ont été que peu étudiées jusqu'à présent.

Objectifs de thèse

Dans ce contexte scientifique, les objectifs de la thèse étaient :

1. Déterminer la composition chimique détaillée des CNC et de leurs extractibles CNSL par le développement de méthodes analytiques.
2. Étudier la pyrolyse des CNC, en se concentrant sur la cinétique et la quantification des produits formés.
3. Mieux appréhender les mécanismes de dégradation thermique des ACC.
4. Étudier le craquage thermique et catalytique des gaz de pyrolyse du CNC.

Matériel et méthodes

Deux réacteurs ont été utilisés pour étudier le comportement thermochimique des CNC :

- un analyseur thermogravimétrique (ATG), pour les études cinétiques de dégradation thermique des coques et des ACC ;
- un réacteur de pyrolyse et de conversion des goudrons (PyTar) (Figure 1), afin de collecter pour analyse les produits issus de la pyrolyse et du craquage des gaz de pyrolyse.

(1) Réacteur à pyrolyse
(2) Tube de quartz à pyrolyse
(3) Disque filtrant
(4) Résistance électrique
(5) Thermocouple
(6) Thermocouple
(7) Débitmètre
(8) Joint d'arbre
(9) Verrouillage de la pince
(10) Réacteur de craquage
(11) Tube en acier inoxydable
(12) Tube en quartz
(13) Résistances électriques
(14) Bride en acier inoxydable
(15) Joint d'arbre
(16) Résistance électrique
(17) Bloc noir contenant un isolant et une résistance électrique
(18) Débitmètre
(19) Condenseur serpentin
(20) Condenseur avec isopropanol
(21) Condenseur avec gel de silice et coton
(22) Micro GC

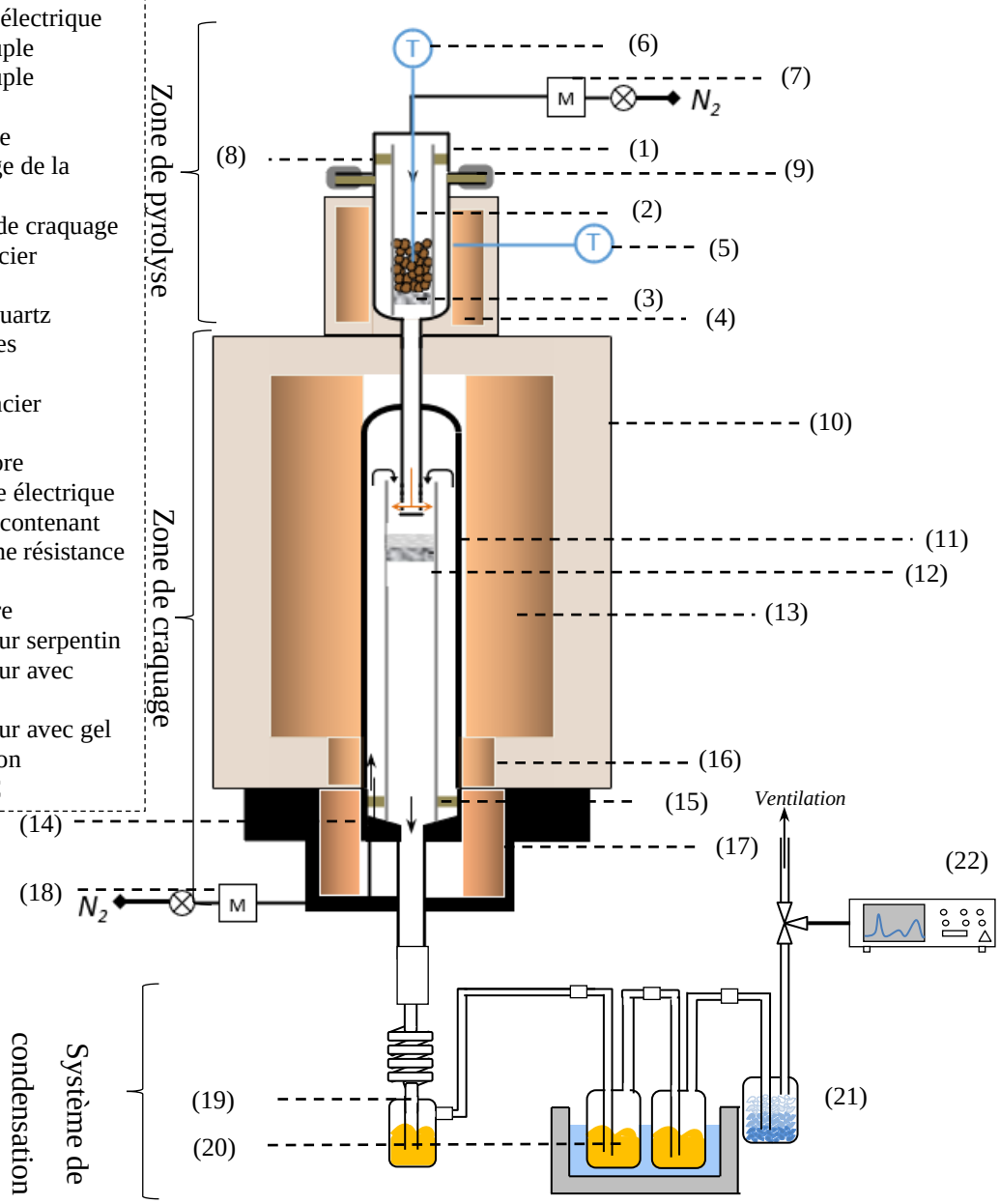

Figure 1: Réacteur de pyrolyse et de conversion des goudrons

Principaux résultats

1. Caractérisation des coques de noix de cajou

Une caractérisation approfondie des CNC a été réalisée (Figure 2), elle comprenait entre autres la quantification des extractibles, protéines et amidon.

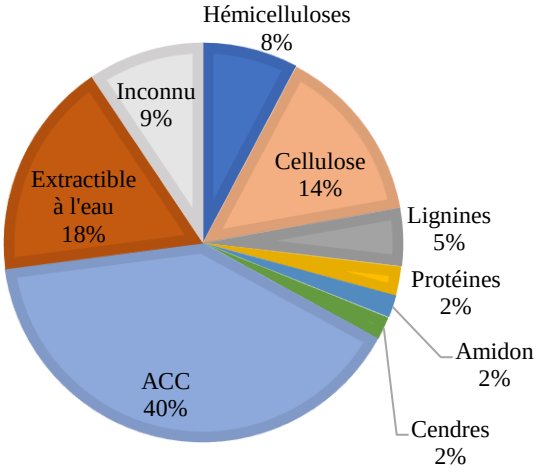

Figure 2 : Composition de coques de noix de cajou

Avec l'optimisation de la méthode d'extraction et le développement de la méthode HPLC, l'acétone a été choisie pour extraire les constituants ACC. Une extraction successive par triple solvant a été réalisée afin de récupérer tous les extractibles des CNC. L'acétone a été utilisée pour extraire la majorité des ACC (99%), l'hexane pour éliminer les matières grasses restantes et l'eau pour les autres extractibles potentiels.

Les constituants ACC dans les extractibles ont été identifiés, en prenant en compte les 12 isomères. La majorité des ACC a été retrouvée dans les extractibles à l'acétone, représentant jusqu'à 40% de la masse des CNC. Cette caractérisation a également mis en évidence la présence potentielle de tannins, représentant 18% massique des CNC.

À notre connaissance, il s'agit de la première caractérisation des CNC incluant la teneur en protéines et en amidon, ainsi que l'extraction exhaustive et l'identification des ACC. Cependant, 9% des substances présentes dans les coques de noix de cajou n'ont pas encore pu être identifiées.

L'identification possible des ACC a ouvert la voie à une étude détaillée de leur dégradation thermique.

2. Pyrolyse de coques de noix de cajou

Les différents pics de dégradation des CNC et de leurs composants ont été identifiés et commentés à l'aide d'un réacteur ATG. L'étude cinétique de la pyrolyse des CNC a mis en évidence une limitation due à l'impossibilité d'atteindre un régime chimique, en raison de la présence des ACC, même avec une masse très faible et une vitesse de chauffe minimale.

La distribution des produits de pyrolyse du CNC, du CNC sans ACC et des ACC a été étudiée en utilisant le réacteur PyTar. Une méthode analytique détaillée a été mise en œuvre pour mieux identifier les constituants des ACC et les goudrons dans les condensats.

L'étude a également révélé des interactions intermoléculaires entre la matrice solide et les extractibles des CNC au cours de la pyrolyse à 400 °C. En effet, la matrice solide influence la conversion des ACC, réduisant le taux de conversion de 61 % à 52 % lors de la pyrolyse en présence de la matrice solide (CNC) par rapport à celle des ACC seuls.

Les expériences de pyrolyse ont révélé que les ACC contribuent principalement à la formation de condensats et de CO_2 lors de la pyrolyse à 400°C. À 400°C, seuls les cardanols ont été détectés dans les condensats. La répartition des produits de la pyrolyse des CNC à 400°C est présentée sur la Figure 3.

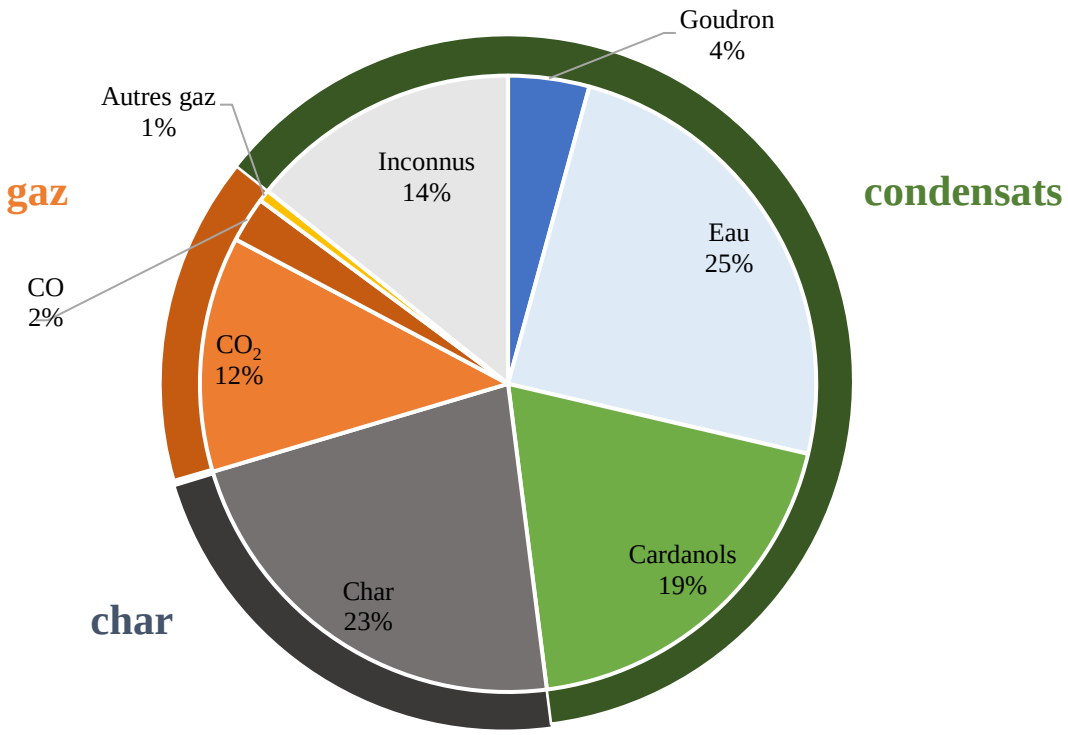

Figure 3 : Répartition des produits de la pyrolyse du CNC à 400 °C (hors cendres et base sèche)

À l'aide du réacteur ATG et de la méthode HPLC développée, ainsi qu'en nous appuyant sur la littérature scientifique, nous avons pu examiner les mécanismes de dégradation des ACC lors de la pyrolyse des CNC.

Initialement, les acides anacardiques subissent une décarboxylation (autour de 125-190°C), produisant des cardanols et du CO_2.

Ensuite, la polymérisation des cardanols a lieu (autour de 190-250°C).

Par la suite, dans une plage de température de 250 à 385°C, plusieurs réactions concurrentes ont lieu : polymérisation des cardanols et des cardols pour former des polymères à base de cardanol et de cardol, dévolatilisation des cardanols et des cardols, ainsi qu'évaporation des cardanols. La dégradation des polymères formés a lieu également. Il est à noter qu'une quantité élevée d'ACC favorise les réactions de polymérisation en raison d'interactions intermoléculaires accrues.

Enfin (T° > 385°C), les polymères formés au cours de ces processus subissent une dégradation thermique supplémentaire, qui entraîne la production secondaire de gaz. Ces polymères peuvent subir une dépolymérisation, comme l'indique la présence de cardanols avec des chaînes aliphatiques en C17 et C13 dans les condensats de pyrolyse de l'ACC. La dégradation des polymères contribue à la formation de charbon en fin de réaction.

Les mécanismes et les produits de dégradation des ACC au cours de la pyrolyse des CNC sont détaillés sur la figure 4.

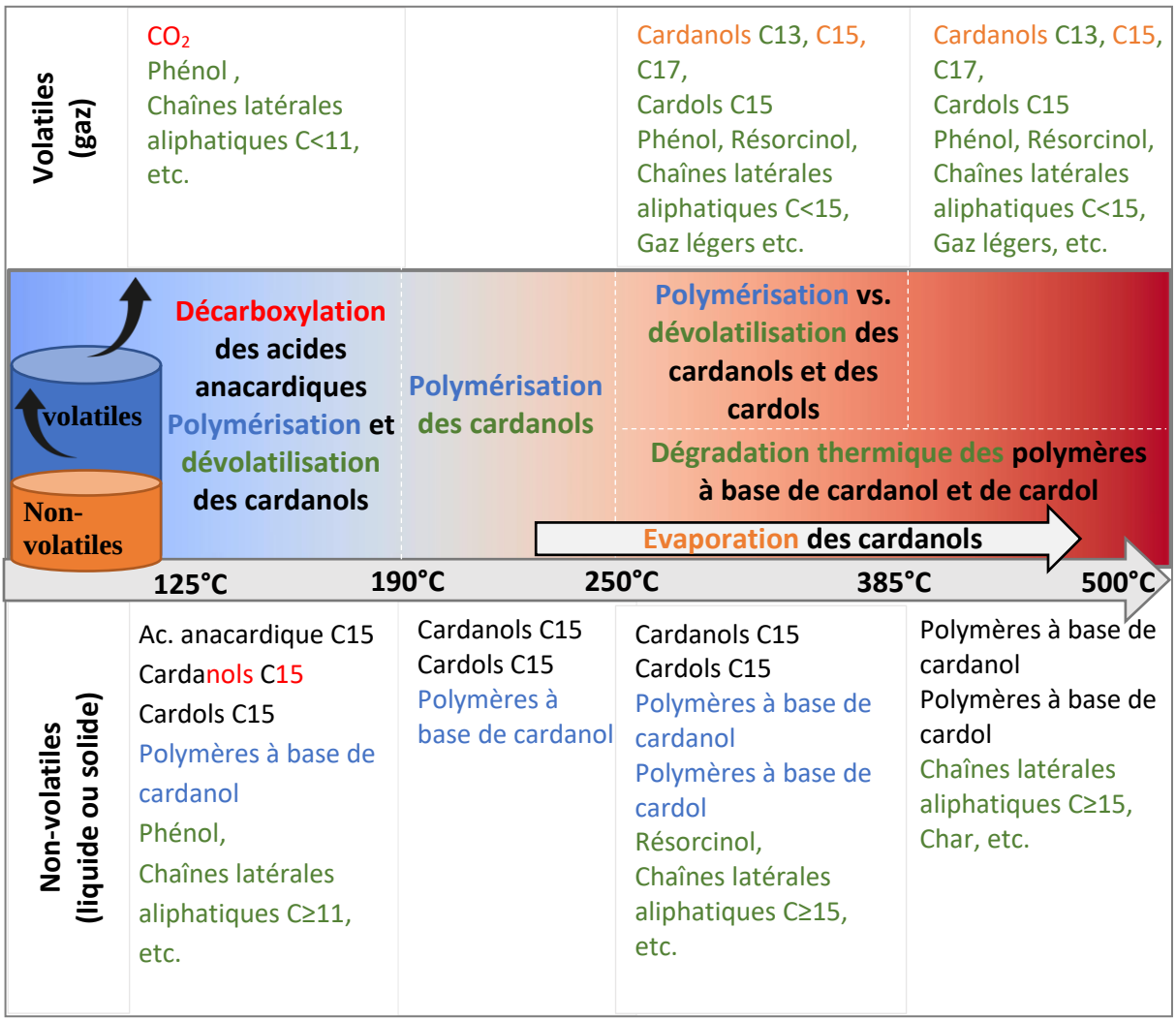

Figure 4 : Mécanismes et produits de dégradation des ACC lors de la pyrolyse des CNC, produits initiaux (noir), produits de décarboxylation (rouge), produits de polymérisation (bleu), produits de dégradation thermique et de dévolatilisation (vert), produits d'évaporation(orange)

3. Etude de la conversion du gaz de pyrolyse des coques de noix de cajou

3.1 Craquage thermique du gaz de pyrolyse des CNC

Les expériences de craquage thermique ont été réalisées sur les gaz de pyrolyse des CNC, des CNC sans ACC, des ACC et des plaquettes forestières (PF) à 800°C.

Pour tous ces échantillons, le craquage thermique a réduit la proportion de condensats à moins de 27%, tout en augmentant proportionnellement la part de gaz permanent dans le gaz de pyrolyse (jusqu'à un maximum de 55%).

Les expériences avec des échantillons contenant des ACC (CNC et ACC) présentent des taux de conversion des condensats plus faibles par rapport aux échantillons sans ACC (CNC sans ACC et PF). Les extractibles ACC forment donc des gaz condensables plus stables et plus résistants à la dégradation thermique que les ceux dérivés de la partie lignocellulosique.

Par cette étude, il est observé que les ACC contribuent indirectement, c'est-à-dire, par l'intermédiaire des gaz de pyrolyse, à la production de CO lors du craquage thermique des gaz. Ils contribuent également à la formation des goudrons tertiaires dans le gaz de craquage des CNC.

3.2 Influence de la température sur le craquage thermique du gaz de pyrolyse des CNC

Le taux de conversion des condensats augmente de 25%, 48% et à 77% lorsque la température de craquage augmente de 600, 800 et à 900°C. Une augmentation de la production de CO_2 a été constatée quand la température de craquage augmente. Ceci est due à l'intensification des réactions de craquage, accentuées par la réaction du gaz à l'eau.

La dominance des goudrons tertiaires est significative au-delà de 800°C, représentant plus de 95 % des goudrons quantifiés. Cela signifie qu'au-delà de 800°C, la plupart des goudrons lourds sont déjà convertis en molécules légères.

3.3 Craquage catalytique du gaz de pyrolyse des CNC

L'étude de craquage catalytique (600°C) sur un lit de charbon a été menée, néanmoins aucun effet a été constaté sur le taux de conversion des condensats organiques.

Conclusion

Le développement de nouvelles méthodes analytiques a permis de réaliser des progrès significatifs dans la caractérisation des CNC. Ce fut une étape nécessaire pour l'étude de la dégradation thermique des ACC, et la quantification des produits de transformation lors de la pyrolyse des CNC.

L'étude détaillée de la dégradation thermique des ACC a révélé des interactions complexes des réactions thermochimiques impliquant ses principaux constituants. Néanmoins, les mécanismes de dégradation des ACC ont pu être expliqués au cours de cette étude, améliorant la compréhension du comportement thermochimique des ACC et des CNC lors de la pyrolyse et du craquage thermique.

Ainsi, il a été établi que la dégradation des ACC lors de la pyrolyse des CNS se déroule à travers une série de réactions successives :

- Tout d'abord, les acides anacardiques subissent une décarboxylation (environ 125-190°C), produisant des cardanols et du CO_2.
- Ensuite, la polymérisation des cardanols a lieu (environ 190-250°C).
- Cette réaction est suivie par plusieurs réactions concurrentes : la polymérisation des cardanols et des cardols pour former des polymères à base de cardanols et de cardols, la dévolatilisation des cardanols et des cardols, ainsi que l'évaporation des cardanols (environ 250-385°C).
- Les polymères à base de cardanols et de cardols formés au cours de ces processus subissent ensuite une dégradation thermique supplémentaire.

En perspectives, Il serait pertinent d’approfondir l’étude des tannins ainsi que des 9 % de composants non identifiés présents dans les CNS, afin de compléter la caractérisation chimique de ce matériau. Par ailleurs, une analyse détaillée des polymères formés lors de la pyrolyse des ACC permettrait de mieux comprendre les mécanismes de polymérisation.

L’optimisation des paramètres favorisant les réactions de craquage tout en limitant la polymérisation serait également intéressante à réaliser essentielle pour réduire la formation de goudrons indésirables.

Cette thèse a ainsi permis des avancées significatives dans la compréhension des mécanismes de pyrolyse des CNS, et plus généralement des biomasses riches en extractibles.

General Introduction

General introduction

The utilization of fossil fuels has been identified as detrimental to the environment due to its primary role in CO_2 emissions and its significant contribution to climate change. This situation has expedited the transition towards renewable energy sources such as wind, geothermal, solar, hydro, and biomass.

The global demand for bioenergy has been steadily increasing, driven by its potential to produce heat, electricity, fuels, and other valuable products. Notably, Africa has emerged as a major consumer of traditional biomass energy, primarily derived from firewood, charcoal, and agricultural residues, making it the world's largest user of these resources.

Bioenergy encompasses thermochemical, biochemical and physicochemical conversion processes. Biochemical conversions are most suitable for biomass rich in sugar or starch. In contrast, physicochemical conversions are primarily applied to oleaginous biomass, which contains oils such as triglycerides, including sources such as colza, palm, jatropha and shea nut. **Thermochemical conversions,** i.e., pyrolysis, gasification and combustion, are particularly adapted to lignocellulosic biomass.

Lignocellulosic biomass consists of cellulose, hemicelluloses and lignins, though it may contain other components, such as extractives and minerals. Extractives, as non-structural components, include wax, fats, resins, gums, phenolic acids etc. While the thermochemical conversion of lignocellulosic biomass, particularly woody biomass, has been extensively studied and optimized, there is a lack of research on **extractive-containing biomass**. The presence of extractives impacts the mechanisms involved in the thermochemical conversion of biomass, necessitating adjustments to the processes to ensure satisfactory performance.

Cashew nut shells are lignocellulosic biomass, with a particularity due to the presence of extractives. Cashew nuts are one of the most exported agricultural products in Africa. Ivory Coast is currently the first exporter of cashew nuts, and accounts for around 1 million metric tons of raw cashew [18] whereas global raw cashew nut production in 2022/2023 accounts for approximately 4.41 million metric tons [18]. Yet, shortage of electricity, lack of technology and skills hinder the processing of cashew nuts in Africa [1]. Despite the fact that some African countries are among the largest cashew nut producers, they still process less than 10% of their cashew nuts [1]. The cashew nuts are mostly exported to Vietnam and India for further processing. This is undeniably a huge loss for the economic growth in Africa.

The cashew nut shells (CNS), account for around 70% of the weight of a raw cashew nut [19]. They are by-products issued from cashew nut shelling units. CNS are sometimes burnt to generate steam for heat or electricity purposes, but majority of the shells are discarded (75-95%) [19]. Although cashew nut shells possess high energy content (20.42 MJ/kg) [5], they are difficult to convert into energy in conventional open fireplaces due to the presence of extractives known as **Cashew Nut Shell Liquid (CNSL)**.

CNSL is an oil found between the inner and the outer shell of the cashew nut. CNSL is a viscous brown liquid which contains phenolic compounds with long-chain substitution [20]. Once extracted, it is interesting for various applications or utilization due to its biological properties but also its phenolic constituents. Indeed, CNSL has found broad applications in industries such as brake linings, cements, varnishes, paints and coatings. It also has been reported to be a promising and accessible source for the development of pharmaceutical drugs [21]. According to Caillol, CNSL can potentially replace phenol in many applications and it could provide equivalent and even better results than ordinary phenols [22].

Concerning the use of CNS as a fuel, incineration and direct combustion in boilers emit black smoke that is both irritating and carcinogenic due to CNSL [23]. In Côte d'Ivoire, only 15% of the CNS are used as fuels for boilers in processing units [24], the rest are mainly disposed in the bushes. Improper stockage or disposal of CNS on the ground leads to soil degradation due to the lixiviation of the CNSL. CNSL which is acidic, can alter the pH of the soil, thus affect plant growth and soil microbiomes [3]. The soil degradation later leads to water pollution by contaminating water with the acidic and toxic substances in the CNSL. This poses risks to human health and the ecosystems.

The current state of research on cashew nut shells highlights significant gaps in the understanding of their composition, particularly regarding the extractives content. There is no standardized method for extraction and analysis to accurately identify the primary constituents of CNSL: **anacardic acids, cardanols and cardols (ACC)**. Moreover, very few studies focused on the degradation kinetics of CNSL, with even less attention given to the behavior of ACC during CNS pyrolysis. Furthermore, the literature lacks comprehensive investigations into the conversion of pyrolysis gas derived from CNS. Addressing these gaps is crucial for advancing knowledge in this field of research.

This thesis is in conjunction with the two ongoing projects: Agrogazelec and Biostar which focus on energy recovery from agri-food residues like cashew nut shells through

thermochemical conversion processes such as combustion and gasification. Therefore, this work aims to study the **thermochemical behavior of cashew nut shells**, focusing on their pyrolysis and gas conversion, which are crucial steps in thermochemical conversion processes.

Therefore, the scientific objectives of this thesis are as follows:

1. To determine the detailed chemical composition of cashew nut shells (CNS) and of cashew nut shell liquid (CNSL), which involves the development of analytical methods.
2. To study the pyrolysis of CNS by focusing on both the kinetics and the quantification of resulting products.
3. To investigate the thermal degradation mechanisms of ACC.
4. To study the conversion of CNS pyrolysis gas through thermal cracking and catalytic cracking processes.

Based on experimental results, this research aims to provide insights into the utilization and improved valorization of cashew nut shells (CNS) as a sustainable alternative to fossil fuels for energy production, particularly for semi-industrial units in Africa. By promoting the use of CNS as an energy source, this approach can contribute to reducing air and ground pollution, as well as decreasing dependency on unreliable energy supply systems that are common in many parts of Africa.

Chapter 1 presents the general context and the main issues addressed in this study, concluding with an introduction to the biomass of interest: cashew nuts shells.

Chapter 2 consists of a bibliographical review of pyrolysis and conversion of pyrolysis gas. It includes literature review on the characterization methods and the composition of cashew nut shells and their extractives Cashew Nut Shell Liquid (CNSL). This chapter regroups the literature review on the thermochemical reaction studies carried out by other authors, including thermal degradation, kinetic studies as well as the pyrolysis products of CNS.

Chapter 3 details the methodology used to achieve these objectives. The experimental equipment such as Soxhlet extractor, micro thermogravimetric analyzer (micro-TG), and pyrolysis and tar conversion reactor (PyTar) and the experimental procedures were described in detail in this chapter. The methods used to analyze and characterize the transformation products (permanent gas, condensates and char) are also detailed.

Chapter 4 presents the study of the composition of cashew nut shells. It includes the development of analytical methods and the study of CNS composition. Focus was put on the

method development to analyze the extractives content, starting from the optimization of extraction method for ACC recovery and then the development of multiple solvent extraction method for determination of extractives content in CNS. With the development of analytical methods as well as those already set up before this thesis, the physicochemical properties of CNSL and the extractives content in CNS were determined and presented.

Chapter 5 deals with the pyrolysis of cashew nut shells and their components. It starts with a pyrolysis kinetics study on CNS and their components (ACC-free CNS and ACC). This chapter includes an in-depth study of the **thermal degradation mechanisms of ACC**. It also presents the results on the distribution of the pyrolysis products, as well as the influence of temperature on the pyrolysis products (condensates, permanent gas and char) of CNS and ACC.

Chapter 6 consists of the study of the conversion of pyrolysis gas from CNS, in which two main reactions were studied: thermal cracking and catalytic cracking. The thermal cracking studies are divided into two main parts: thermal cracking of CNS pyrolysis gas; and the influence of temperature on the thermal cracking products. This chapter ends with the study of catalytic cracking of CNS pyrolysis gas, in which we used CNS char as catalyst.

CHAPTER 1

General context: Biomass to Energy

1. General context: Biomass to energy

As the world grapples with the pressing challenges of climate change and the finite nature of fossil fuel resources, the need for renewable energies has never been more urgent. Among these renewable options, biomass energy holds a significant promise, particularly in regions like Africa where traditional biomass resources such as firewood, charcoal, and agricultural residues are widely used. Africa's reliance on biomass is substantial, with the continent consuming millions of tons of biomass energy annually. This is particularly true in Sub-Saharan Africa, where the use of biomass energy is deeply embedded in daily life and essential for cooking, heating, and even small-scale industrial activities.

However, the heavy reliance on biomass in Africa presents both opportunities and challenges. While biomass is a renewable resource, its traditional forms are often inefficient and environmentally taxing. Moreover, the rural areas of West Africa face significant energy challenges, with limited access to reliable electricity. This lags down the economic development of West Africa, particularly for small and medium-sized enterprises (SMEs) in the food processing sector, leading to post-harvest losses and unoptimized energy usage. Therefore, it is crucial to explore and implement more efficient and sustainable biomass energy solutions.

This chapter outlines the general context and primary themes of this study, emphasizing the issue of biomass energy in West Africa. It details the various biomass valorization pathways, including physicochemical, biochemical, and thermochemical methods. The chapter then provides a bibliographical review of biomass types: lignocellulosic biomass and its composition, followed by the specific biomass under study, **cashew nut shells**. It concludes by addressing the issues and challenges associated with cashew nut shells.

1.1 Issue of biomass energy

Fossil fuels such as coal, oil and natural gas will eventually deplete and dwindle one day, unlike renewable resources. Therefore, it is essential to replace the non-renewable energies with renewable ones, which could be solar energy, hydraulic energy, wind energy, geothermal energy and biomass energy. The demand of bio-energy has been increasing in the world. In Africa, traditional biomass energy sources such as firewood, charcoal, and agricultural residues are extensively utilized, making the continent the largest consumer of such resources worldwide.

According to data from the AFREC Energy Statistics Database, Africa consumed a total of 269 million tons of oil equivalent (Mtoe) of biomass and 295 Mtoe of conventional energy in 2019 [25].

In the rural areas of West Africa, energy supply is derived from autonomous internal combustion engine-based systems, photovoltaic systems, and occasionally from the national electric power grid [26]. Autonomous systems using fossil fuels face challenges such as inconsistent fuel supply and high energy costs due to transportation difficulties [26,27] and import shortages [26]. Photovoltaic systems are insufficient for non-industrial or industrial activities due to their limited and intermittent power output [26]. National power grids are unreliable in the rural parts as the distribution of electricity is privileged in the capitals and main cities. The World Bank's 2022 estimates indicate that the average electrification rate in West Africa is 42%, with rural areas having a significantly lower rate of just 8% [28]. The rural areas are also subject to recurrent power outages.

These situations limit the development of food processing small and medium-sized enterprises (SMEs) in rural areas. This is because the food processing SMEs cannot function properly and have to export local products to other countries for transformation. These situations cause huge loss in terms of post-harvest revenues due to high transportation costs. On top of that, many agri-food residues, which are also biomass are produced by these food processing units, and yet not properly managed, cause problem to public health and environmental pollution.

Therefore, it is essential to properly manage the post-treatment of agricultural residues in Africa. The development of bioenergy conversion processes emerges as a pertinent solution to address these issues effectively.

1.2 Bioenergy conversion

Biomass is a combustible that contain around 50% of carbon. Therefore, it produces energy during oxidation. However, the bulky and inconvenient heterogeneous form of biomass is a major barrier to the shift from fossil fuels to biomass fuels. In this section, the 3 main biomass conversion pathways will be briefly described: biochemical, physicochemical and thermochemical conversion.

1.2.1 Biochemical conversion

The biochemical pathway consists of transforming biomass through the reaction of microorganisms including fermentation and anaerobic digestion (methanization) for the production of bio-ethanol and biogas respectively. They rely on the usage of microorganisms to convert a biomass. Biochemical conversion methods are currently the most widely used methods for producing biofuels from biomass, accounting for approximately 80% of all biofuels produced worldwide [29].

Methanization or anaerobic digestion represents a natural biological process that stabilizes organic wastes in the absence of oxygen, converting them into bio-fertilizer and biogas. The predominant gas produced in this process are methane (approximately 60%) and carbon dioxide (around 40%). Anaerobic digestion stands out as a reliable technology specifically designed for the treatment of wet organic waste.

Alcoholic fermentation, on the other hand, involves the conversion of biomass containing sugar or starch to yield bioethanol (or butanol), aided by enzymatic treatment. The process typically involves pretreatment of the biomass, followed by enzymatic hydrolysis to generate simple sugars. These sugars are then subjected to fermentation to produce biofuels, such as ethanol.

1.2.2 Physicochemical conversion

Physicochemical conversions include extraction and transesterification for the extraction of oils in biomass to produce biodiesel. Most of the physicochemical conversions involve oleaginous biomass such as rapeseed, sunflower, and palm oil.

Extraction is based on the separation of useful chemical compounds with physicochemical methods: pressing, supercritical fluid extraction, microwave and ultrasound. In the recent years, there has been a growing utilization of cavitation-assisted techniques, including ultrasound-assisted extraction processes, across various stages of biomass processing. These applications include biomass pretreatment, delignification, hydrolysis, oil extraction, fermentation, and the synthesis of bio-alcohol [30].

The transesterification of plant is a well-established process wherein triglycerides undergo a reaction with alcohol, facilitated by a catalyst. Extracted vegetable oils or animal fats, characterized by esters of both saturated and unsaturated monocarboxylic acids with the trihydric alcohol glyceride (triglycerides), are subjected to transesterification when exposed to

alcohol and a catalyst. This process leads to the formation of fatty acid alkyl esters and glycerol as main products [30].

1.2.3 Thermochemical conversion

Thermochemical conversion accounts for around 20% of the production of biofuels in the world. Through thermochemical conversion, bio-oil and syngas could be produced from sources like wood chips, agricultural waste, and municipal solid waste [29].

The three major technologies for the thermochemical conversion of biomass are pyrolysis, gasification and combustion. These three processes can be distinguished by the quantity of oxidizing agent and the process temperature [31]. These technologies can transform biomass into heat, electricity and liquid or gaseous intermediates for the production of biofuels or chemicals [32].

The different biomass valorization pathways are summarized in the figure below (Figure 1.1).

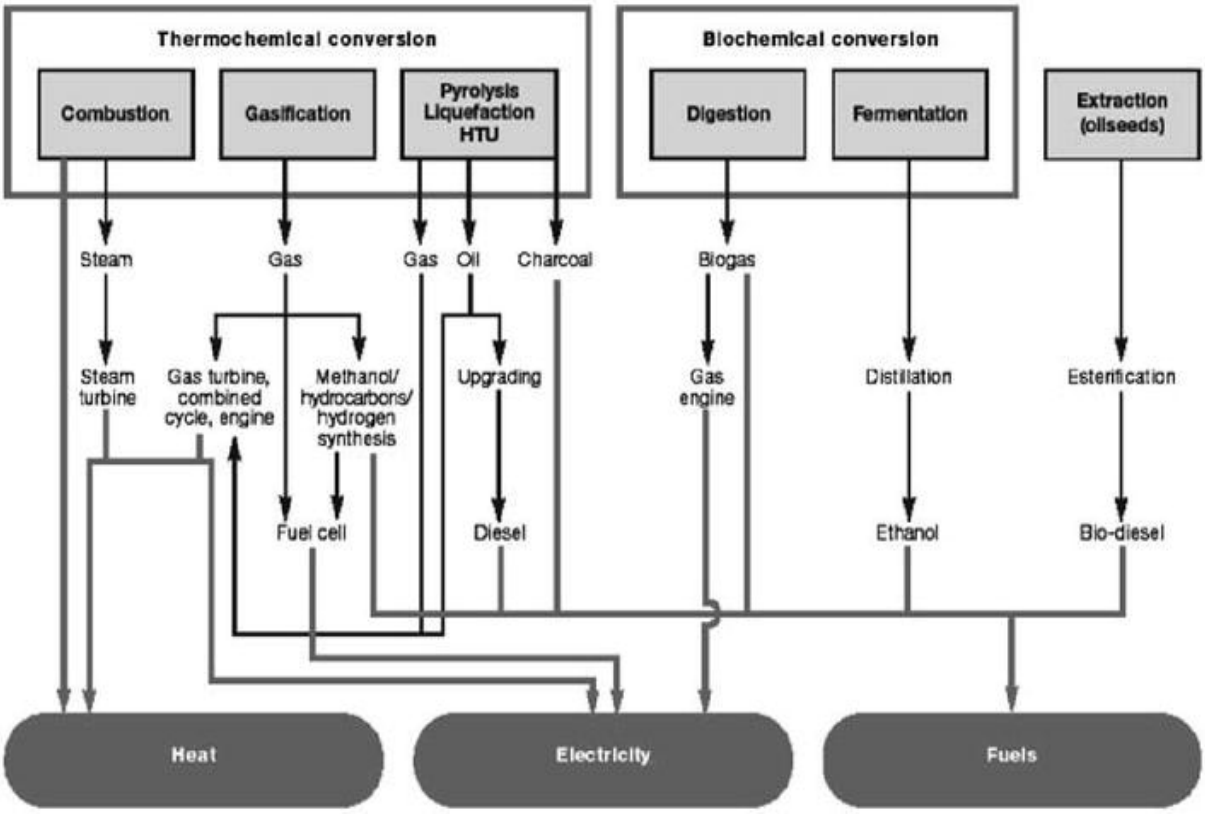

Figure 1.1: Biomass valorization pathways [33]

1.3 Thermochemical conversion processes

1.3.1 Pyrolysis

Pyrolysis is a thermochemical process that involves the breakdown of biomass molecules at moderate temperatures (typically between 250-700°C) in the absence of, or with limited, oxidizing agents. This procedure leads to the decomposition of large and complex hydrocarbon molecules found in biomass, resulting in the formation of smaller and simpler molecules in gaseous, liquid, and solid forms. The outcomes of the pyrolysis process can be harnessed as bio-char through carbonization, or as bio-oil through fast pyrolysis. Alternatively, these products react in subsequent stages of gasification or combustion processes.

Slow pyrolysis, characterized by a prolonged heating period at lower temperatures, yields biochar primarily, while fast pyrolysis, occurring at higher temperatures with a faster heating rate, produces bio-oil suitable potentially for various applications. The process also generates a combustible gas which can be used for heat and power generation. Overall, pyrolysis stands as a versatile and environmentally sustainable technology, facilitating the conversion of biomass into valuable products with diverse applications.

1.3.2 Gasification

Gasification is a thermochemical conversion method that allows the transformation of carbonaceous solids into synthesis gas, a gaseous product composed mainly of H_2 and CO and to a lesser extent of light hydrocarbons (CH_4, C_2H_2, C_2H_4, C_2H_6) [34]. It requires an oxidizing agent such as water, air and carbon dioxide. In the case of air gasification, non-combustible gases such as CO_2, H_2O and N_2 could also be produced. This process is usually operated at temperature above 800°C.

Gasification involves different stages: drying, pyrolysis, combustion (oxidation) and reduction. The overall diagram of thermochemical reactions involved in a gasification process is shown in Figure 1.2.

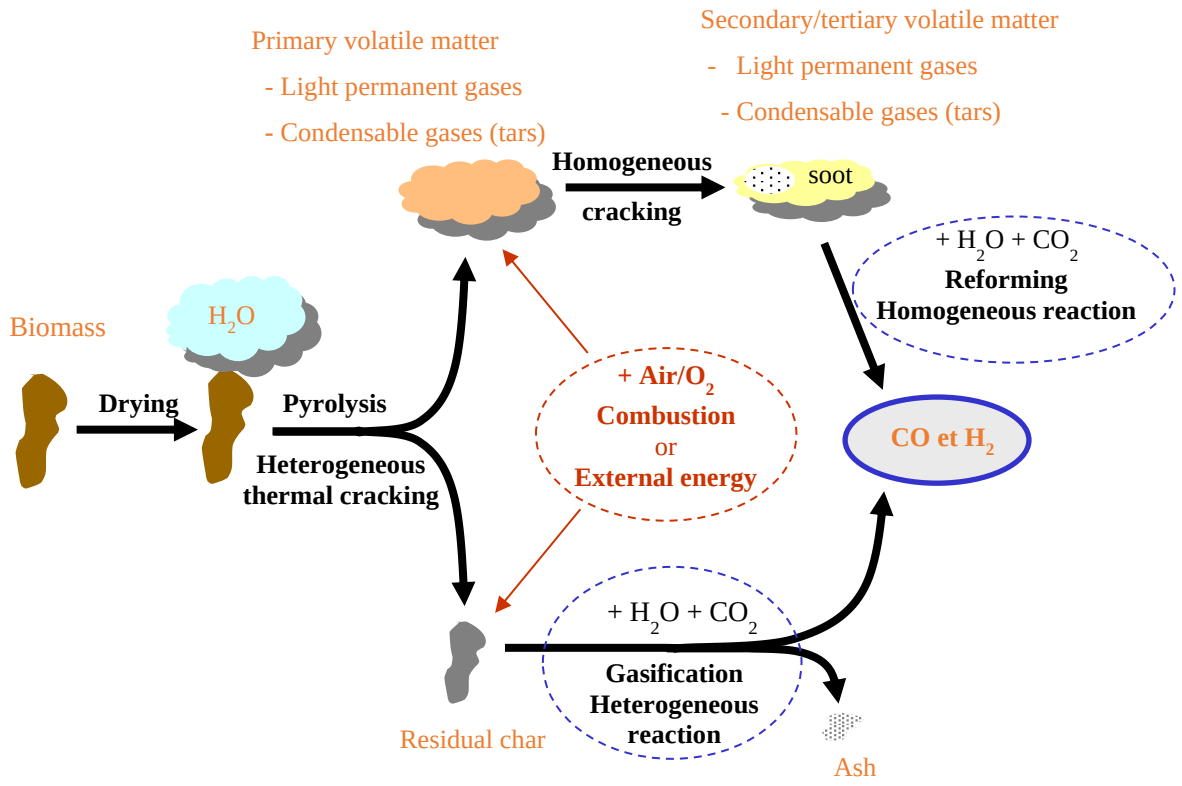

Figure 1.2: Simplified overall diagram of reactions involved in a gasification process (adapted from S. Salvador)

The main problematic regarding a gasification process is that while it produces useful syngas for the electricity and heat production, it also releases undesirable by-products such as tars [18].

The Gasification Task from the IEA Bioenergy Agreement, US Department of Energy (DOE) and the DGXVII from the European Commission agreed to define tar as hydrocarbons with molecular weight higher than benzene [35]. Tar is a complex mixture with more than 1000 compounds and it condenses at a temperature <400°C which easily blocks and corrodes the downstream pipes and installation equipment, poisons catalysts, releases irritating gas, and produces secondary pollutants, such as phenolic-water [36].

Thus, it is essential to understand the mechanisms of tar cracking in order to tackle the constraints related to tars in a gasification process. There are various methods to tar removal: physical methods and chemical methods.

Physical methods include water washing, filtration, cyclone separation, electric trapping and absorption. Chemical conversion methods include thermal cracking, catalytic cracking, plasma method and partial oxidation.

1.3.3 Combustion

Combustion involves the thorough oxidation of intricate hydrocarbon molecules found in biomass but also primary compounds (CxHyOz), char, CO, H_2, etc., resulting in the formation of carbon dioxide and steam. This exothermic process generates heat, with combustion temperatures reaching between 800 and 1200°C. This heat release makes combustion a readily applicable method for various purposes, including heating, drying, cooking, lighting, and electricity generation. Direct combustion is better suited for biomass feedstock with low moisture content [29].

Combustion represents a relatively straightforward and well-established technology, boasting numerous existing installations that can be readily adapted to utilize biomass in lieu of fossil fuels. Furthermore, it demonstrates versatility by accommodating a diverse array of feedstocks, including wood, agricultural residues, and municipal solid waste.

However, direct combustion faces certain challenges. Emissions such as particulate matter (coke) and nitrogen oxides can be generated during the process, contributing to air pollution and adverse health effects. The efficiency of the system is also subject to variations based on factors like the quality of the biomass feedstock and the design of the combustion system [37].

1.4 Biomass

According to Legifrance (Article L 211-2 of the Energy Code which has entered into force since 12 March 2023), biomass is the biodegradable fraction of products, waste, and residues of biological origin from agriculture, including plant and animal substances, forestry and related industries, including fishing and aquaculture, as well as the biodegradable fraction of waste, including industrial waste as well as household and similar waste of biological origin [38].

This section will explain lignocellulosic biomass and its components, ending with a detailed discussion on the specific biomass investigated in this work: cashew nut shells.

1.4.1 Lignocellulosic biomass

Lignocellulosic biomass is defined as all non-edible parts of field crops and products from the forest-wood sector. Lignocellulosic biomass is composed mainly of cellulose and hemicelluloses which are the parietal polysaccharides, and lignins which are polymers consisting of units derived from phenylpropane [30] (Figure 1.3). The quality and proportion of these 3 macromolecules vary according to the nature of the biomass. Biomass also contains extractives such as lipids, essential oils, resins, proteins, starches, water, simple sugars and ash [39].

In general, lignocellulosic biomass is composed 20-60 % of cellulose, 15-40 % of hemicellulose, 10-40 % of lignin, 0-15 % of extractives and 0-20 % inorganic matters [40].

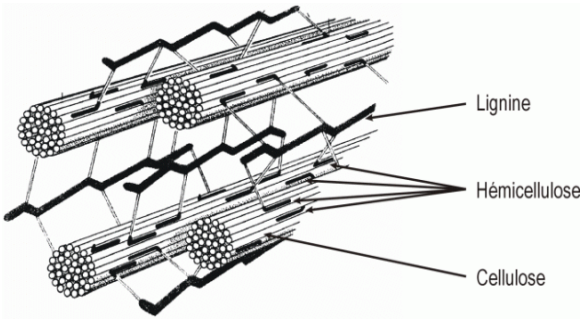

Figure 1.3: Structure of a lignocellulosic biomass [41]

Hemicelluloses and lignins form an envelope where cellulose is enclosed. Cellulose gives the rigidity of the plant cell wall. Hemicelluloses are located between microfibers and macrofibers which act as a binding between fibers and lignins. Lignins permeate the polysaccharide complex and ensure the reinforcement of mechanical properties and resistance to the environment and aggressors.

1.4.1.1 Components of lignocellulosic biomass

Hemicelluloses, cellulose and lignins are organic components of lignocellulosic biomass, whereas ash is the inorganic residue that remains after the combustion of a biomass. Some biomass can contain extractives, which are a group of non-structural organic compounds that can be separated from the lignocellulosic fraction of biomass.

Hemicelluloses

Hemicelluloses include hydrocarbon polymers consisting of monosaccharides associated with each other by different glycosidic bonds [42]. The monosaccharides (Figure 1.4) are: pentoses

(xylose, rhamnose and arabinose), C6 hexoses (glucose mannose and galactose) and uronic acids (e.g. D-glucuronic acid) [43].

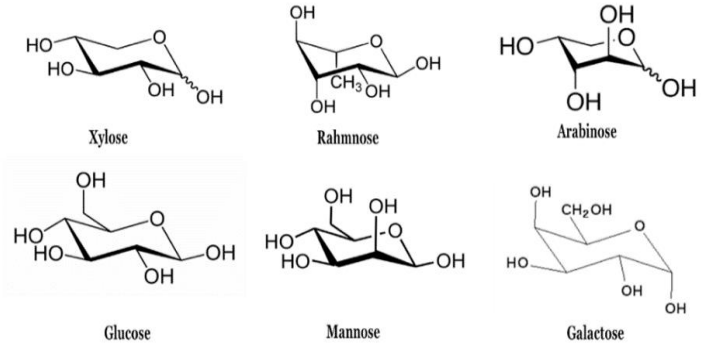

Figure 1.4: Hemicelluloses monosaccharides [44]

Cellulose

Cellulose is the main structural component of plant cell walls and accounts for about 20-30% of the primary cell wall and 40-90% of the secondary cell wall [45]. Cellulose (Figure 1.5) with the chemical formula $(C_6H_{10}O_5)_n$ is a unit polymer of β-D-glucopyranose (one of the isoforms of glucose) [46].

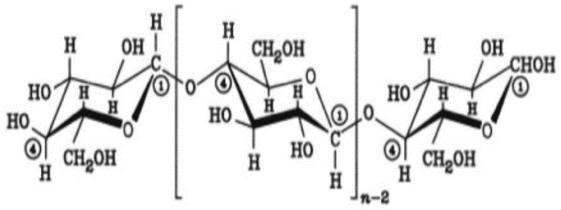

Figure 1.5: Structure of the glucose polymer that forms cellulose [47]

Lignins

Lignins (Figure 1.6) are one of the major constituents of lignocellulosic biomass. They are the third most abundant polymers constituent on Earth [46]. They give cell walls their impermeability, rigidity and extensibility. Lignins are three-dimensional structures that are insoluble in water and are highly resistant to chemical and enzymatic attacks [48]. Lignins are polymers consisting of 3 alcohols: p-coumaryl alcohol, coniferyl alcohol and synapyl alcohol [48] (Figure 1.7).

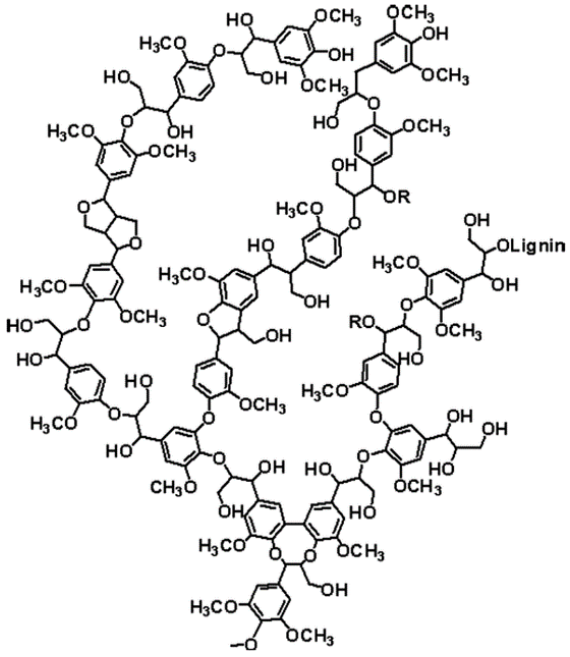

Figure 1.6: Lignins structure [49]

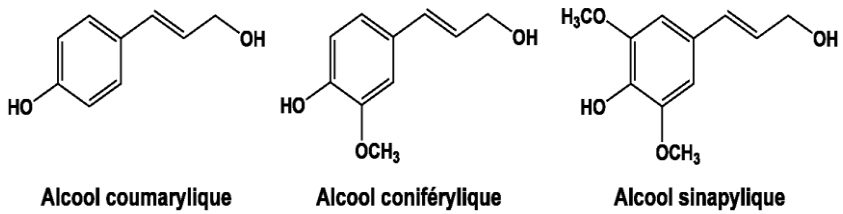

Figure 1.7: Structure of p-coumaryl alcohol, coniferyl alcohol and synapyl alcohol main structural monomers of lignins [50]

Ash

Biomass ash constitutes 2–20% of the biomass [51]. Ash content varies according to the type of biomass. Biomass ash contains macronutrients essential for plant growth, and is rich in calcium, potassium, magnesium [52]. Straw and herbaceous fuels like grass have a higher ash content than wood.

Ash can be problematic due to several reasons. Firstly, ash content in biomass negatively affects the calorific value of biomass. Moreover, ash can be highly abrasive [53], especially if it contains hard minerals like silica and alumina. This abrasion can cause significant wear on the internal surfaces of gasification equipment, including feeders, reactors, and cyclones. Over time, this wear can lead to increased maintenance costs and downtime. Ash can also cause

slagging in equipment [30]. Slagging refers to the formation of molten or partially molten deposits [54] which can occur on the walls of the reactor and other surfaces within the equipment.

Extractives

A lignocellulosic biomass such as wood can contain up to 10% of extractives [55]. Some tropical species of wood can even go up to 15% [56].

Extractives are substances within plant tissues that can be extracted using solvents; they often have economic or functional value. They could be fats, waxes, lipids, gums, resins, terpenes, phenolics etc. [57]. These extractives play different roles in the physiology of the plants. For instance, fats provide energy storage in the biomass and are stored inside parenchyma cells [55]. Lipids and waxes help reduce water loss from the plant surface and protect the plants against pathogens. Resins and gums are produced when plants encounter physical damage. Sticky resins trap and fester herbivores. Terpenes act as a defense against herbivores and pathogens. The phenolics components protect the lignocellulose of the biomass from fungal and microbial attack [55].

Extractives in biomass can be classified into: hydrophilic extractives, which are soluble molecules in high polarity solvents; and hydrophobic extractives which are soluble only in low polarity solvents [58].

Extractives content influence the high-heating value (HHV) of lignocellulosic materials. Since there are many different extractives, the HHV of each biomass can vary significantly. The HHV of resin, for instance, is 34.9-37.2 MJ/kg, which is relatively high due to the low oxygen content in extractives [59].

The table 1.1 shows the composition of several biomasses in the literature. The biomasses are categorized into softwood biomass, hardwood biomass and herbaceous and agricultural biomass.

Table 1.1: Major components of biomass adapted from Pham (wt% on dry basis) [30]

Biomass	Hemicellulose	Cellulose	Lignin	Ash	Extractives	Ref.
Softwood biomass						
Pine	20.3	46.9	27.3	0.3	5.1	[60]
Spruce	29.4	43.0	27.6	0.6	1.7	[61]
Fir	22.0	45.0	30	0.5	2.6	[62]
Japanese cedar	23.1	38.6	33.8	0.3	4.0	[63]
Hardwood biomass						
Aspen	21.7	52.7	19.5	0.3	5.7	[60]
Willow	16.7	41.7	29.3	2.5	9.7	[60]
Poplar	24.0	49.0	20.0	1.0	5.9	[62]
Breech	33.0	45.0	21.8	0.5	2.6	[62]
Herbaceous and agricultural biomass						
Hazelnut shells	25.2	28.2	42.1	1.4	3.1	[61]
Rice straw	16.5	37.0	13.6	19.8	13.1	[64]
Rice husk	23.4	37.0	24.77	17.23	3.19	[62]
Corn straw	23.2	42.7	17.5	6.8	9.8	[62]

In general, softwood and hardwood biomass have higher cellulose content than herbaceous and agricultural biomass. The extractives content in the biomass shown in these examples varies from 2 to 13%.

1.4.1.2 Proximate and ultimate analysis of lignocellulosic biomass

Proximate and ultimate analyses (Figure 1.8) are main standard laboratory test methods for solid biofuels used for assessing the quality of fuels and, besides determination of calorific value, as a basis for fuel trade [65].

The main components analyzed include moisture, volatile matter, fixed carbon and ash on a mass percent basis. Moisture is the amount of water present in the biomass. It affects the energy content and the combustion efficiency. Volatile matter consists of the fraction of biomass that volatilizes in the absence of oxygen. Ash, as mentioned previously is the inorganic residue left after biomass combustion. Fixed carbon is the material remaining after the determination of volatile matter, moisture and ash – that is a measure of the solid combustible material in the fuel after expulsion of volatile matter [65].

The 3 major elemental composition of a biomass are carbon (C), hydrogen (H) and oxygen (O). Ultimate analysis is employed to determine the proportions of key elements in fuels: carbon (C), hydrogen (H), nitrogen (N), oxygen (O), and sulfur (S). Carbon is the most critical element in fuels, contributing the most to the fuel's heating value. Hydrogen is also a major component in a biomass, which is why organic compounds are typically referred to as hydrocarbons. Oxygen is essential for the combustion process and reduces the amount of air required for combustion. Nitrogen does not contribute to the heating value [66] but serves as plant nutrient. Sulfur, found in organic compounds such as amino acids, proteins, and enzymes, is present in small quantities and, along with nitrogen, which also serves as a plant nutrient [66].

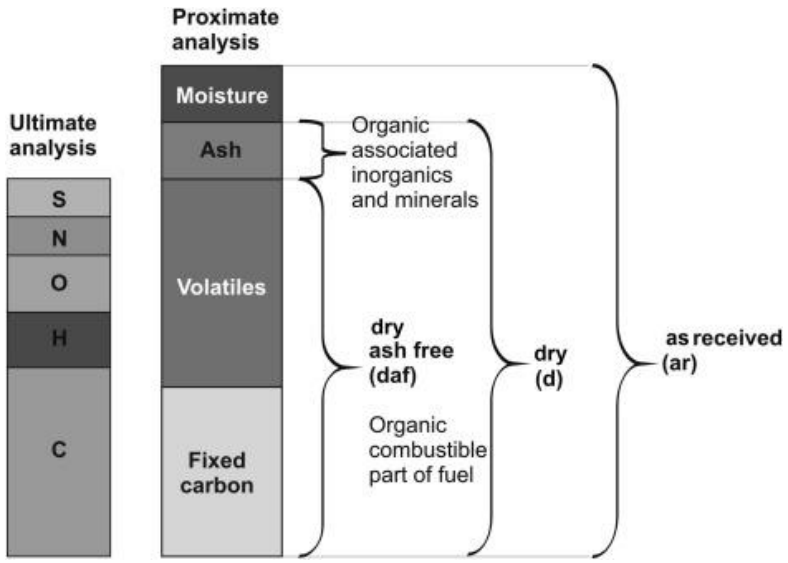

Figure 1.8: Proximate and ultimate analysis and different analysis basis [65]

Table 1.2 shows some examples of proximate and ultimate analysis of biomass.

Table 1.2: Proximate and ultimate analysis of biomass. Volatile Matter, Ash, Fixed Carbon, C, H, O, N, S in wt%, High Heating Value in MJ/kg.

Biomass	Proximate analysis				Ultimate analysis					Ref.
	VM	FC	Ash	HHV	C	H	O	N	S	
Softwood biomass										
Pine	85.80	14.10	0.20	20.10	48.40	6.00	45.30	0.10	0.00	[67]
Spruce	70.20	29.30	1.50	-	51.90	6.10	40.90	-	-	[68]
Fir	87.30	12.60	0.10	-	50.60	6.18	43.00	-	-	[69]
Japanese cedar	78.80	20.80	0.40	-	50.00	6.10	43.90	-	-	[70]
Hardwood biomass										
Aspen	87.10	12.4	0.50	18.80	47.8	6.00	45.40	0.20	0.03	[67]
Willow	80.80	16.80	2.40	18.20	47.20	5.60	44.40	0.40	0.00	[67]
Poplar	82.32	16.35	1.33	-	48.45	5.85	43.69	-	-	[71]
Beech	85.70	13.90	0.50	19.10	46.7	5.90	46.80	0.20	0.02	[67]
Herbaceous and agricultural biomass										
Hazelnut shells	68.90	30.00	1.10	19.90	50.90	5.90	42.80	0.40	-	[72]
Rice straw	65.47	15.86	18.67	15.09	38.24	5.20	36.26	0.87	0.18	[51]
Rice husk	61.20	16.30	22.50	16.47	38.20	5.60	33.70	-	-	[73]
Corn straw	73.15	19.19	7.65	17.68	44.73	5.87	40.11	0.60	0.07	[74]

The proximate analysis reveals that softwoods like pine, spruce, fir, and Japanese cedar have high volatile matter (VM) content, low ash content, and varying fixed carbon (FC) levels. Hardwoods, such as aspen and beech, exhibit similar high VM and low ash content. Herbaceous and agricultural biomass, such as rice husk and rice straw, tend to have higher ash content and varying HHV. Softwoods generally having higher carbon content, while agricultural biomass displays more variability in composition.

1.4.2 Cashew nut shells (CNS)

The origin of the cashew tree, also known as *Anacardium Occidentale*, comes from northeastern Brazil. European explorers introduced the tree to other parts of the world such as Asia and Africa during the sixteenth century [75]. Cashew nuts (Figure 1.9) belong to the *Anacardiaceae* family, which includes mango and pistachio [76].

In 2019, Vietnam accounted for the highest raw cashew nut production in the world, with 2,598,220 metric tons of production, followed by India with 786,326 metric tons, Côte d'Ivoire with 731,917 metric tons, the Philippines with 236,925 tons, and Benin with 206,004 metric tons [77].

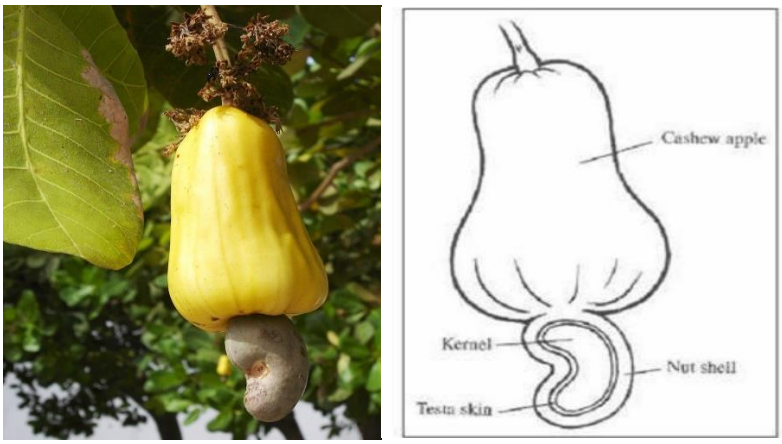

Figure 1.9: Photo and pictogram of cashew fruit with apple and nut [78,79]

In 2023, raw cashew nut production in West Africa was estimated to increase by 400,000 tons, which accounted probably more than 3 million barrels of crude oil. 51% of the production was exported to Vietnam and 33% to India. 13% was transformed locally each year [80].

The cashew tree can grow up to 12 m [81]. The bark and the leaves of the cashew tree could be used to treat sickness such as malaria and toothaches [82].

The cashew apple (Figure 1.9) is edible and can be consumed as juice and other food products such as jelly, jam and syrup [83]. It is rich in reducing sugars such as fructose and glucose, vitamins C, minerals and amino acids [84]. The vitamin C content is 5 times higher than an orange [85]. Cashew apple juice possesses antitumor and antimicrobial properties [86].

The cashew nut (Figure 1.9) is attached beneath the cashew apple, and it represents about 90% in terms of the weight of the whole fruit [87]. It is kidney shaped and its size varies from 2.5 to 4 cm [81]. Inside the shell contains a cashew kernel.

Cashew kernels are nutritious and are covered by a thin skin of brown color, known as testa. Testa makes up 1-3% of the total weight of cashew nuts and this part is rich in hydrolysable tannins with proanthocyanins as major polyphenols [88]. The phenolic acids present in cashew skin are syringic acids, gallic acids and p-coumaric acids [89].

The cashew kernel is enclosed in a shell, called **cashew nut shell (CNS)**,which protects them from aggressors such as pests. This rigid brown shell, is particular, because it contains a honeycomb structure (3.tial zone), which contains an oily phenolic liquid, commonly named as **Cashew Nut Shell Liquid (CNSL)** [14]. This interstitial zone refers to the zone situated between the hard outer shell and the soft kernel of the cashew nut.

The world production of CNSL reaches a value of 450,000 tons per year [90]. CNSL accounts for 18-27% of the total weight of the raw nuts [81] and contributes approximately 40 % to the total weight of the cashew nut shell.

CNSL has found broad applications in industries such as brake linings, cements, varnishes, paints and coatings. CNSL is also studied to produce intermediates such as 3-pentadecylcyclohexanone which has many potentially application in polymer chemistry [91]. According to Caillol, CNSL can potentially replace phenol in many applications and it could provide equivalent and even better results than ordinary phenols [22].

CNSL has been reported to be a promising and accessible source for the development of new sustainable pharmaceutical drugs [21]. It was studied as a drug to treat metabolic diseases [92], Alzheimer's Disease [93], oral diseases (dental caries and chronic apical periodontitis) [94], etc.

In agricultural industry, CNSL can be applied as pesticides, larvicides, and termiticide.

CNSL can also serve as a potential alternative fuel that can be used in diesel engines with modifications [95] or as a CNSL-diesel blend [12,96–98] and CNSL-based antioxidants in biofuel [99]. Eke et al. did a study on the application of modified CNSL to improve the flow of paraffinic crude oils [100].

CNSL polymers are also being studied for their application in rubber plasticizers and antioxidants in polyurethanes synthesis, epoxy resin curing and phenol formaldehyde resin [101]. Nambela et al. proved that anacardic acid in the CNSL can be a cheaper and green raw material for the synthesis of anthraquinone dyes [102].

Depending on the extraction method, CNSL can be classified into two types: natural CNSL and technical CNSL (t-CNSL). The first type of CNSL is obtained using extraction techniques such as Soxhlet extraction and supercritical fluid extraction (such as supercritical carbon dioxide). It is defined as "natural" because the extraction methods mentioned above do not result in chemical changes in biomass. This form of CNSL is known for its diverse properties including

antimicrobial, antioxidant, fungicidal, insecticidal, termiticidal and enzymatic inhibition properties. T-CNSL is obtained by heating natural CNSL at temperatures above 180-200°C [103]. This form of CNSL is more likely to be used as a raw material in the manufacture of friction linings, paints, varnishes, laminating and epoxy resins.

Figure 1.10 shows the different valorization pathways of CNSL [104]. Other applications of CNSL include the manufacture of azo dyes, superplasticizers, rubber modification, rubber inhibitor and UV absorbers.

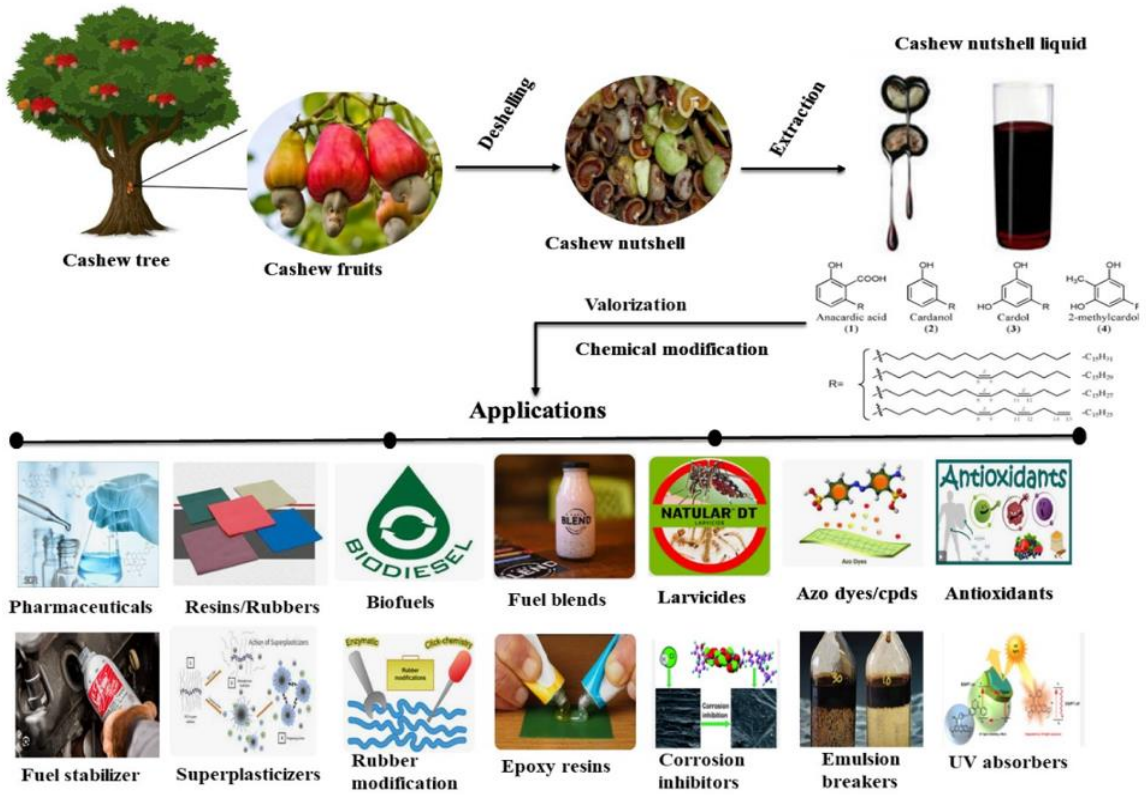

Figure 1.10: Potential applications of CNSL in different fields [76]

1.5 Issues and challenges related to CNS

Cashew nut shells (CNS) are by-products generated during the processing of cashew nuts, and their valorization (utilization or conversion into added-value products) addresses several environmental, economic, and social challenges in West Africa.

Despite the fact that Africa is one of the largest cashew nut producers, it still processes less than 10% of its cashew nuts [1]. For several consecutive years, cashew processing units in West Africa have had difficulty sourcing raw nuts due to strong competition from Asian buyers

(unavailability and price increases), and are not functioning at full capacity. Today, the vast majority of this production is exported, mainly to Vietnam and India, to be processed and made suitable for consumption. Shortage of electricity, lack of technology and skills hinder the processing of cashew nuts in Africa [1].

Most shelling units in West Africa rely on wood and natural gas for energy in the deshelling process, contributing to environmental issues such as deforestation and global warming. Additionally, managing CNS waste presents significant challenges for small and medium enterprises (SMEs) due to the large quantities produced—generating 2.3 to 3 tons of shells per ton of almonds, which adds to the waste management costs.

CNS possess high heating value, yet their energetic valorization presents difficulties due to the presence of extractives CNSL. Consequently, there is an abundance of CNS which most of them are not properly handled in West Africa. Improper stockage of CNS on the grounds lead to water and soil pollution through lixiviation, because the CNSL could be very acidic (pH 3) and toxic. This is mainly due to the presence of anacardic acids. Although CNSL is known for its antimicrobial property, excessive lixiviation can negatively impact and harm beneficial microbes (such as nitrogen fixing bacteria) in the soil [3]. CNSL lixiviation could cause plant toxicity and affect plant growth [3]. The availability of plant nutrients such as phosphorus and molydenum is decreased by soil acidity [105].

Furthermore, the open incineration of CNS without optimized criteria degrades air quality by producing toxic fumes.

A way of valorizing CNS is through CNSL as it possesses interests in many industrial applications (resins, paints, varnishes, pharmaceutical products, etc.). Technical solutions for extracting these extractives are available, but they are primarily utilized by large industrial units in countries like India and Brazil. Unfortunately, small artisanal units in Africa currently lack practical solutions tailored to their specific context [2] .

CNS produced from cashew shelling units could be used as a combustible to produce energy and heat. If CNS were strategically leveraged for energy in suitable conditions, they could potentially fulfill the energy requirements of these smaller-scale processing units. Consequently, the problem of waste production by cashew nut shells could be reduced.

In conclusion, CNS hold significant potential for energy production, industrial applications, and contributing to carbon neutrality. However, they remain undervalued in West Africa. Improved

valorization is essential to reduce the environmental problems associated with CNS and enhance the economic situation in West Africa by reducing dependence on foreign processing of cashew nuts.

The challenge of adding value to CNS requires a deeper knowledge of its composition and, in the context of bioenergy, a better understanding of their behavior during thermochemical conversion. Therefore, a comprehensive review of the current state of scientific knowledge is presented in the next chapter.

CHAPTER 2

State of art and literature review

2. State of art and literature review

This chapter aims to provide a scientific overview of the composition of cashew nut shells (CNS) and their thermochemical behavior. By examining current scientific advancements and highlighting existing gaps, this chapter intends to lay a solid foundation for guiding this thesis but also future research and innovations in the bio-energy field.

This chapter is divided into five comprehensive sections.

The first section provides description of the different biomass thermochemical reactions, with a specific focus on biomass pyrolysis.

The second section offers a summary of the characterization methods used for analyzing cashew nut shells, with an in-depth review on the techniques employed to extract and analyze the extractives CNSL in the CNS.

The third section presents a literature review on the thermochemical behavior of cashew nut shells, highlighting pyrolysis kinetics and products.

The fourth section describes the state of art regarding the thermal degradation ACC (anacardic acids, cardanols and cardols) constituents.

Finally, the chapter concludes with the positioning and objectives of this thesis.

2.1 Biomass thermochemical reactions

In a thermochemical conversion process, such as pyrolysis, gasification and combustion, different thermochemical reactions take place. For instance, gasification process starts with pyrolysis, and then homogeneous (thermal cracking, oxidation and reforming) and heterogeneous reactions (catalytic cracking, oxidation) occur simultaneously.

In this work, we focus on biomass pyrolysis and the conversion of pyrolysis gas as shown in Figure 2.1. Both steps are present and play a major role in all thermochemical conversion processes.

The two main types of reactions that could take place during the conversion of pyrolysis gas are heterogeneous (gas-solid) and homogeneous reactions (gas-gas) [106] Heterogeneous reactions involve the usage of char as catalyst to break down the pyrolysis gas into lighter gases.

Homogeneous reactions of pyrolysis gas include **thermal cracking** which consists of breaking down the molecules by heat. They also include **reforming and oxidation**, which requires an oxidizing agent (CO_2, H_2O and O_2). Depending on the pyrolysis gas produced, **water gas-shift reaction** could also take place.

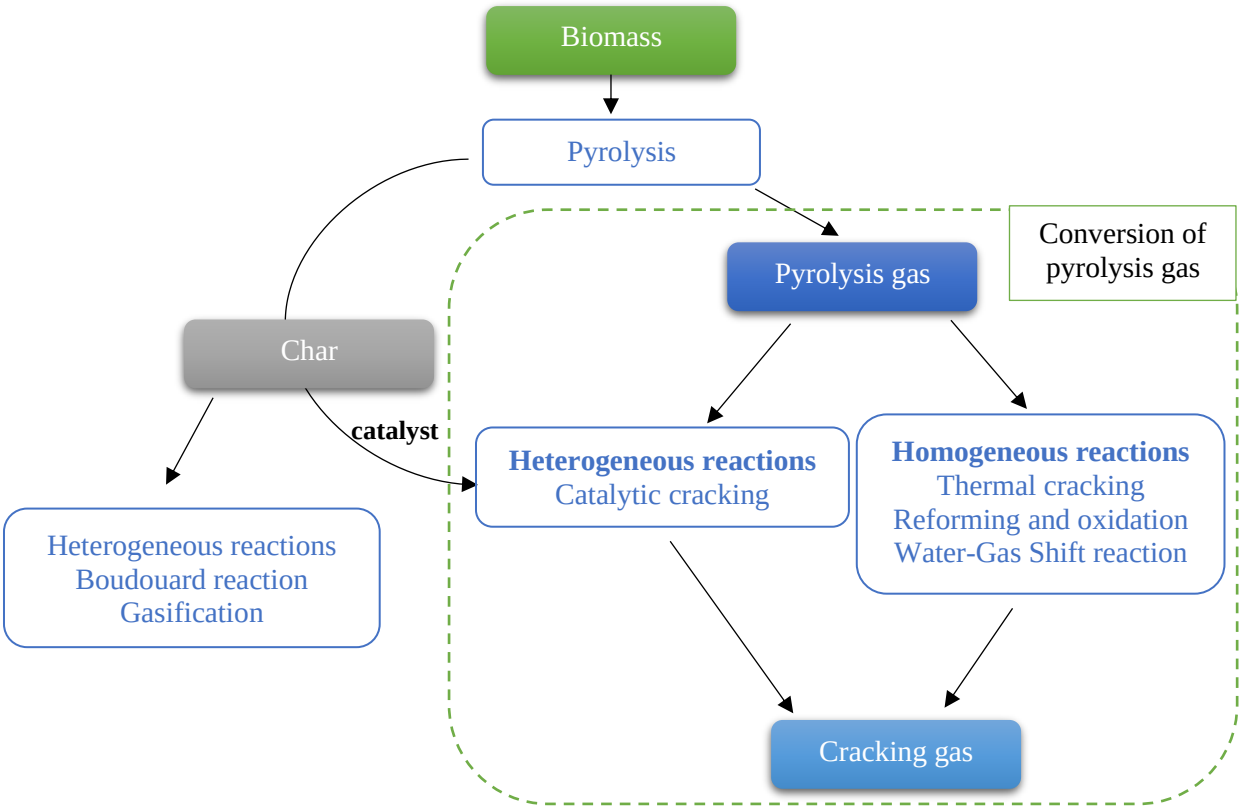

Figure 2.1: Pyrolysis and the conversion of pyrolysis gas

In this section, the biomass pyrolysis reactions will be first presented, followed by the different conversion reactions of pyrolysis gas: thermal cracking, reforming and oxidation, Water-Gas Shift reaction and lastly, catalytic cracking.

2.1.1 Pyrolysis

Pyrolysis consists of converting a biomass into char, permanent gas and condensates (oxygenated organic compounds) through the action of heat in an inert atmosphere [107,108].

Organic compounds are produced via the depolymerization or rupture of C-C or C-O bonds, and permanent gas from dehydration, decarboxylation or decarbonylation [106] and debranching [109]. The solid residue (char) formed is therefore rich in carbon.

2.1.1.1 Pyrolysis mechanisms

The mechanisms of pyrolysis could be divided into two types: primary and secondary mechanisms [110].

Primary mechanisms can be described into 3 pathways: char formation, depolymerization and fragmentation.

a) Char formation

During pyrolysis, the ordered organic macrostructure in raw biomass first decomposes and converts into a network-like structure, described as a 3D network of benzene rings. This transformation occurs during the initial decomposition stage (<450°C).

During the second stage (450-550°C), the 3D network of benzene rings transitions to a 2D structure of fused rings through the cleavage of functional groups containing methyl, methylene, and oxygen.

Finally, during the third stage (>550°C), the enlargement of fused rings, along with dehydrogenation and cleavage of ether bonds, may lead the 2D structure of fused rings to transition into a graphite microcrystalline structure [109].

b) Depolymerization

Depolymerization involves breaking the bonds between the monomer units of polymers. Each rupture is followed by stabilization reactions at the newly formed chain ends [110]. This process reduces the degree of polymerization of the chains until the resulting molecules become volatile. These volatile molecules, which condense at ambient temperature, are typically found in the condensates as derived monomers, dimers, or trimers [111,112].

c) Fragmentation

Fragmentation consists in the linkage of many covalent bonds of the polymer, even within the monomer units [113], and results in the formation of permanent gas and of a diversity of small chain organic compounds which are condensable at ambient temperature [113–115].

When released, volatiles gases are not stable, they can undergo **secondary reactions** such as cracking [113,116] and recombination [116,117].

a) Cracking

Cracking reactions consist in the breaking of chemical bonds within the volatile compounds, which result in the formation of lower molecular weight molecules [118,119].

b) Recombination

Recombination reactions lead to the formation of a secondary char [117,119] Reactive intermediates such as free radicals, ions, or small molecules can interact and recombine. This can occur through various mechanisms including radical-radical reactions, ion-molecule reactions, and condensation reactions.

2.1.1.2 Pyrolysis of cellulose, hemicelluloses and lignins

This section aims to describe the mechanism of the pyrolysis of each of these lignocellulosic components. The pyrolysis behaviors of these components are usually studied using thermogravimetric analysis (TGA).

Thermogravimetric analysis measures the change in weight when the sample is heated. In general, carrier gases such as N_2, H_2O, CO_2, He, Ar are used to analyze the thermal decomposition of a sample for different temperature profiles (isotherm or temperature ramp). The analyzer allows accurate weight measurement, up to 0.001 mg. The differential mass loss is also applied for the kinetic study through the Differential Thermogravimetric Analysis (DTG).

a) Cellulose

The pyrolytic breakdown of cellulose occurs within a specific temperature range. It results in a large amount of volatile matter due to its linear chains [120]. When a heating rate of 5°C/min is applied in TGA, cellulose decomposition becomes noticeable at approximately 225°C. The temperature at which the peak mass loss occurs is around 350°C, and the pyrolysis process is completed at about 400°C [121].

The cellulose pyrolysis initiates with an intra-molecular dehydration, leading to the formation of water and the production of anhydrocelluloses [155].

Tar steam reforming reaction:

$$C_nH_m + nH_2O \rightarrow nCO + (\frac{m}{2})H_2 \qquad \textit{Equation 2.5}$$

$$C_nH_m + 2nH_2O \rightarrow nCO_2 + \left(2n + \frac{m}{2}\right)H_2 \qquad \textit{Equation 2.6}$$

Dry reforming

Dry reforming is the reforming using CO_2 as gasification agent [156]. The outcome of the process is a gas mixture containing CO and H_2.

An example of dry reforming of methane is shown below (Equation 2.7).

$$CH_4 + CO_2 \rightarrow 2CO + 2H_2 \quad \Delta H = 247 \frac{kJ}{mol} \qquad \textit{Equation 2.7}$$

Dry reforming of tar typically requires catalysts [157], if not the reaction rates are too slow and high temperature will be required. The tar dry reforming reaction is shown in Equation 2.8.

Tar dry reforming reaction:

$$C_nH_m + nCO_2 \rightarrow 2nCO + \left(\frac{m}{2}\right) H_2 \qquad \textit{Equation 2.8}$$

a) Oxidation

During the oxidation phase in a gasifier, the gas produced from the pyrolysis step meets the gasifying agent (oxidizing agent). The reactions are exothermic and therefore are a heat source for endothermic reactions.

Oxidation (using methane as example) can be presented in 3 reactions (Equations 2.9-2.11).

$$CH_4 + 2O_2 \rightarrow CO_2 + 2H_2O \quad \Delta H = -803 \frac{kJ}{mol} \qquad \textit{Equation 2.9}$$

$$CH_4 + O_2 \rightarrow CO_2 + 2H_2 \quad \Delta H = -319 \frac{kJ}{mol} \qquad \textit{Equation 2.10}$$

$$CH_4 + \frac{1}{2}O_2 \rightarrow CO + 2H_2 \quad \Delta H = -36 \frac{kJ}{mol} \qquad \textit{Equation 2.11}$$

Tar can also undergo partial oxidation to form CO and H_2 (Equation 2.12).

Tar partial oxidation:

$$C_nH_m + \left(\frac{n}{2}\right) O_2 \rightarrow nCO + \left(\frac{m}{2}\right) H_2 \qquad \textit{Equation 2.12}$$

2.1.2.3 Water-Gas Shift reaction (WGS)

Water-Gas Shift Reaction (WGS) (Equation 2.13) is the reaction of carbon monoxide and water vapor to form carbon dioxide and hydrogen. It is an exothermic reaction, thus lower temperature favorizes the reactions to produce hydrogen [154].

$$CO + H_2O_{(g)} \leftrightarrow CO_2 + H_2 \quad \Delta H = -41 \frac{kJ}{mol} \qquad \textit{Equation 2.13}$$

2.1.2.4 Catalytic cracking

Catalytic cracking is a heterogeneous reaction, which primarily involves the cracking of volatiles on char, with potential catalytic effects from ash (mineral oxides) or catalysts that have been introduced into the biomass bed.

The transformation of tars into lighter gases at temperatures lower than those conventionally employed can be achieved through thermal cracking, facilitated by catalysts [31] (Equation 2.14). The presence of catalysts lowers the activation energy of cracking reactions. Numerous catalysts have been investigated for their efficiency in catalyzing the cracking of tars, encompassing both mineral-derived ones such as calcined rocks, clay minerals, or iron-based minerals, and synthetic counterparts like zeolites and catalysts based on transition metals, activated alumina, or alkali/alkaline earth metals [158,159].

Tar cracking on char:

Tar (heavy hydrocarbons)+ C (catalyst) → Gases (lighter hydrocarbons, etc.) + Char (partially regenerated) *Equation 2.14*

Catalytic conversion on char could also be enhanced by the dry reforming and steam reforming reactions. The presence of char makes these heavier tars (macromolecules) react more with oxidizing agents (H_2O, CO_2) and inhibits their polycondensation [152].

Several studies investigated the catalytic cracking of gas by char and compared to the conversion of gas during thermal cracking [36,152]. At temperatures exceeding 600 °C, the introduction of char exhibited a superior secondary conversion rate compared to thermal cracking, showing an increase of approximately 14% [36,152]. This observation underscores the catalytic efficiency of char in facilitating the transformation of heavy tar fractions, particularly at the specified reaction temperature threshold above 600 °C. The importance of temperature on the tar catalytic conversion was studied, showing that the efficiency of tar conversion improved from 61% to 94% from 850 to 950°C [160].

2.2 Cashew nut shells (CNS) characterization and composition

Given the large quantities of CNS available in countries that process cashew nuts and the difficulty in valorizing this by-product, numerous research studies have been conducted to explore the composition of this resource.

2.2.1 Characterization methods of cashew nut shells

In order to understand the thermochemical behavior of the cashew nut shells, it is essential to be able to characterize the biomass comprehensively. In this section, a particular attention was put on the characterization methods of CNSL, including extraction methods as well as quantification and qualification of CNSL.

CNSL contains long-chain saturated and unsaturated phenolics. CNSL is a viscous, dark brown liquid. Unlike other nut oils, it is not a triglyceride. It contains mainly 4 major constituents in which all of them are phenolic acids and their derivatives: 60-65% anacardic acid (3-n-pentadecylsalicylic acid), 15-20% cardanol (3-n-pentadecylphenol), 10% cardol (5-n-pentadecylresorcinol) and traces of 2-methylcardol (2-methyl-5-n-pentadecylresorcinol).

These constituents are present in different side chain unsaturations [161] : saturated (5-8%), monoene (48-49%), diene (16-17%) and triene (29-30%) [162] (Figure 2.10). As the CNSL contains readily extractable phenol compounds, it presents innumerable interests technologically.

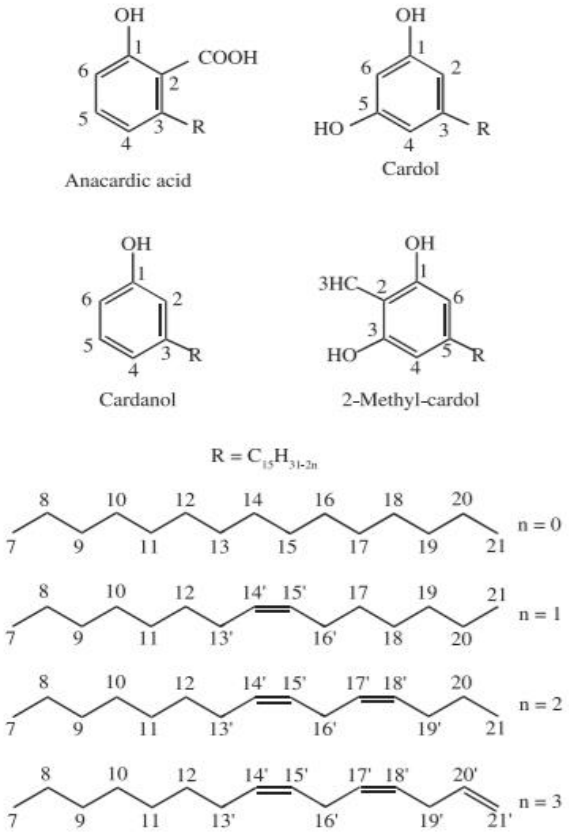

Figure 2.10: Structure of main constituents of CNSL

The characterization of extractives in a biomass is divided into two main steps. The first step includes the optimal extraction of the compounds of interest from the biomass. Second, the most suitable analytical method is chosen to identify and quantify the chemical compounds in the extractives.

2.2.1.1 Extraction methods of CNSL

The extractives content depends on the extraction method. Until now, there is no standardized method to extract CNSL from CNS. Moreover, the methods for characterizing hemicelluloses, cellulose, and lignins require a prior extraction of "extractives". The discrepancies in the yields and composition of extractives observed in the literature suggest that there may be issues with the extraction methods of CNSL. A rigorous and comprehensive study on this subject is therefore required.

There are several methods to extract CNSL from cashew nut shells: hot oil process, roasting, solvent extraction, mechanical extraction, vacuum distillation, and supercritical fluid extraction [163]. In general, only solvent extraction (Soxhlet extraction and Accelerated Solvent Extraction) and supercritical fluid extraction are used for the analysis of CNSL. Soxhlet extraction is the most common method for the extraction of CNSL.

a) Supercritical fluid extraction

The Supercritical Fluid Extraction Unit (SCFE) consists of an extraction vessel, pump and preheater to compress and heat carbon dioxide to its supercritical temperature. A gas flow meter allows precise flow of carbon dioxide into the extraction vessel. The recovery of extractives occurs when the charged solvent flow expands at ambient pressure [164]. The CNSL obtained by SCFE using carbon dioxide contains mainly cardanol (70–90%). It hardly contains anacardic acid, while traces of cardol is found only at high pressures [164]. Other supercritical extraction of CNSL includes using a mixture of CO_2 and isopropyl alcohol [165]. The extraction of CNSL using supercritical carbon dioxide (SC-CO2) has also been reported by Shobha and Ravindranath (1991) [166] and Smith et al. (2003) [167].

b) Soxhlet extraction

Soxhlet extraction is a liquid-solid extraction that is carried out using a Soxhlet that consists of a bulb condenser, a thimble, a distillation path and a round bottomed flask to collect the extractives (Figure 2.11). The solvents used can be polar or non-polar depending on the target of the extracted compounds. The solvents commonly used for the extraction of CNSL

are hexane, ethanol, acetone, petroleum ether and dichloromethane. Although water can also be used to extract CNSL, this method is less applied because the recovery of products is more difficult via rotavapor. On top of that, it is more difficult to remove water from the compounds of interest.

During extraction, the solvent vaporizes and flows along the distillation path. The steam reaches the condenser and the vapor turns into a liquid form. The solvent fills the chamber and, once it reaches the top, the siphon empties the contents of the chamber into the round-bottomed flask. During the recirculation of the solvent in the Soxhlet system, the solvent dissolves a desired compound, and this process is repeated to extract the maximum possible from the desired compound.

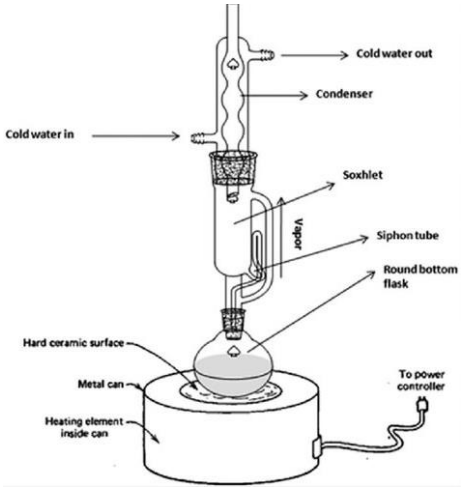

Figure 2.11: Soxhlet extraction

c) Accelerated solvent extraction (ASE)

An Accelerated Solvent Extractor (ASE) is a device used to extract chemical compounds from solid and semi-solid samples more efficiently than traditional extraction methods. The ASE operates usually by using high pressure and elevated temperatures to accelerate the extraction process. Accelerated solvent extraction of CNSL has been reported by Ahmadou et al. in which water-methanol mixture was utilized under pressure at 100 bars [166] .

Other extraction methods for CNSL include the hot oil process, roasting, mechanical extraction, and vacuum distillation. These techniques are generally employed on an industrial scale due to their efficiency in processing large quantities of material. Hot oil process involves involves heating the cashew nut shell using CNSL. In this process, about 50% of extractives is extracted from the CNS [168]. Roasting method involves a sudden change in the temperature of the CNS,

resulting in an explosive pressure change in the nut shell that causes the cell structure to break and the CNSL to seep through the shells [168]. Mechanical extraction includes the cold extrusion method. Cold extrusion method consists of applying high pressure on the sample without heat to extract the desired compounds (oil, juices, extractives etc.). CNSL extracted by this method contains about 70% anacardic acid, 18% cardol and 5% cardanol. The remaining consists of substituted phenols and less polar substances [164]. Vacuum distillation is a type of distillation carried out under reduced pressure. It facilitates the distillation of compounds that have high boiling points or have more difficulty evaporating at normal ambient pressure. The extraction of products depends mainly on the boiling temperature of the desired compound. Cardanol was obtained from a vacuum distillation process at 4-8 mmHg, and the optimum temperature was achieved at 280°C with 74.22% yield [169].

2.2.1.2 Quantification and qualification of CNSL

The three main methods of quantification and qualification of CNSL are high-performance liquid chromatography (HPLC), thin layer chromatography (TLC) and gas chromatography coupled with mass spectroscopy (GC-MS).

Thin layer chromatography makes it possible to give a qualitative measurement of CNSL but not quantitative. This means that the concentration of constituents cannot be determined by this method. GC-MS is not suitable for determining the composition of CNSL because the CNSL constituents are heat-sensitive, and injection system operates at 250°C. Increasing temperature of the CNSL will cause the transformation of anacardic acid into cardanol by decarboxylation. On top of that, the chromatogram peaks of anacardic acids, cardanols and cardols tend to superpose each other, hence forming a big and wide peak in the chromatogram. Therefore, it is impossible to identify the components clearly.

Table 2.1 shows different operating conditions of HPLC used to analyze the components in the CNSL. It is shown that the volumetric ratio of the mobile phase is identical (80:20:1 with acetonitrile: water: acetic acid) whatever the author, and the elution rate is in between 1.5-1.8 ml/min.

Table 2.1: Operating conditions of HPLC of CNSL by different studies

Year	2011	2012	2013	2017	2017	2020
Authors (s)	Feitosa et al. [170]	Patel et al. [171]	Gandhi et al. [172]	Oiram Filho et al. [173]	Morais et al. [174]	Chen et al. [175]
Mobile phase	acetonitrile: water: acetic acid					
Proportion of mobile phase	60:20:1	80 :20 :1	80 :20 :1	80:20:1	80:20:1	80:20:1
Stationary phase	Reverse phase	supelcosil LC-18	supelcosil LC-18	Inverse phase C18	Phase inverse - Hypersil GOLD 25 cm	Polysil-UC18 Columns
Column size	4.6 mm ; Granulation 15 cm et 5µm	4.6 mm ; Granulation 15 cm et 5µm	4.6 mm ; Granulation 15 cm et 5um	4.6 mm ; Granulation 15 cm et 5um	Not specified	4.6 mm ; Granulation 25 cm et 5um
Elution rate	1,8 ml/min	1,8 ml/min	1,8 ml/min	1,5 ml/min	1,75 ml/min	1,5 ml/min
Sample preparation	25 mg/5 ml acetonitrile	25 mg/5 ml acetonitrile	25 mg/5 ml acetonitrile	1 mg/ml	Not specified	1g/L
Sample volume injected	20 µL	20 µL.	20 µL.	20 µL.	Not specified	Not specified

While the quantification and qualification of CNSL presents a great interest, none of the articles stated above did a complete calibration of the standards present in the CNSL. A complete calibration should include all the ACC isomers: Anacardic acid 15:0, 15:1, 15:2, 15:3 , Cardanol 15:0, 15:1, 15:2, 15:3 and Cardol 15:0, 15:1, 15:2, 15:3 and eventually 2-methylcardol 15:0, 15:1, 15:2, 15:3.

2.2.1.3 Lignocellulosic, protein and starch analysis of CNS

The lignocellulosic composition (hemicelluloses, cellulose and lignins) of biomass is usually measured by Van Soest method, if not Klason Lignin method. Before the study of Melzer et al. 2013 [6,10] , the lignocellulosic composition of CNS has not been reported yet.

There are various protocols of protein and starch analysis that exist in the literature, which could cause discrepancy in the results of protein and starch content in CNS. Yuliana et al. has published works on the extraction and quantification of protein and starch in the cashew nut shells [176,177] .

2.2.2 Composition of cashew nut shells

The composition of cashew nut shells is first detailed, comprising their CNSL content, lignocellulosic content, proximate and ultimate analysis, followed by their vitamin, proteins and starch content.

2.2.2.1 Composition of cashew nut shells

a) CNSL content

As mentioned in the previous chapter, cashew nut shells contain a significant proportion of CNSL (>40%). However, the percentage of extractives in the CNS varies significantly in the literature.

Soxhlet extraction is the main method used in many studies [6,10,15,82,103,178] to extract CNSL from cashew nut shells. Soxhlet extraction can be carried out using one or several solvents. The extractives yields of soxhlet extraction from different works and using different solvents are figured in Table 2.2.

Table 2.2: Soxhlet extraction yield of CNSL in the CNS (wt%)

Melzer et al. [6,10]	**Yuliana et al.** [82]	**Yuliana et al.** [82]	**Nyirenda et al.** [103]	**Nyirenda et al.** [103]	**Nyirenda et al.** [103]	**Kaur et al.** [15]
26.5 (water) 38.3 (petroleum)	32.0 (hexane)	38.4 (methanol)	24.6 (petroleum ether)	38.2 (hexane)	40.1 (ethanol)	37.2 (hexane) 15.0 (ethanol)

Water as extraction solvent is not as effective as first solvent when compared to other solvents. The highest extractive yield obtained was 40.1% using ethanol as solvent.

However, according to Nyirenda et al. [103], ethanol extraction is not ideal as it extracts undesirable-coloured polar compounds which degrades the quality of CNSL. It was also shown that ethanol alone did not completely remove all the CNSL in the CNS [103]. Therefore, extraction with hexane as solvent was selected as the best solvent when compared to petroleum ether and ethanol, with a value of 38.2% [103].

It is also noted that the total extractives content obtained using two solvents extraction method was > 50wt% [10,15] which this yield has never yet been obtained using one solvent

extraction method. Thus, it is evident that one solvent is not sufficient to extract all the extractives in the CNS.

The quality of the extractives and their yield depend on the extraction method. The type and the number of solvents, the order of the solvents, the extraction duration, and the granulometry largely affect the extractives yield and the ones of the compounds of interest.

Several authors [16,82,166] have carried out extraction on CNSL using other methods than Soxhlet extraction. They include subcritical water/CO_2 extraction and accelerated solvent extraction. Table 2.3 shows the extraction yield of CNSL using subcritical water (SCW) or CO2 extraction (SC-CO_2) and accelerated solvent extraction (ASE).

Table 2.3: Extraction yield of CNSL using other methods than Soxhlet extraction (wt%)

Yuliana et al. [82]	**Yuliana et al.** [82]	**Yuliana et al.** [82]	**Yuliana et al.** [82]	**Ahmadou et al.** [166]	**Ahmadou et al.** [166]	**Paiva et al.** [16]
27.3 (SCW)	15.9 (SC-CO_2)	58.6 (Hexane-SCW)	62.5 (Methanol-SCW)	51.7 (ASE at 100 bars with water-ethanol)	49.8 (ASE at atmospheric pressure with water)	4.6 (not mentioned)

The extractives yield obtained using hexane-SCW, methanol-SCW extraction and accelerated solvent extraction are very high, when compared to Soxhlet extraction. However, none of these studies reported the real ACC yield in the CNS. The study of Ahmadou et al. [166] did study the ACC content in the extractives, but the HPLC method was calibrated using just one isomer to represent the 4 isomers of each ACC constituents.

Pre-treatment of CNS before extraction also affects the extraction yield of CNSL. Around 6.1 wt% of CNSL was extracted by soaking CNS in light petroleum for a week and then subjecting the half-processed shell to Soxhlet extraction at 40–60°C for 12 h with light petroleum as the solvent [178]. The yield increased to 25.7 wt% when CNS were macerated and re-extracted again for another 10 h. CNSL obtained consists of 19.72% cardols, 58.14% anacardic acids, 1.92% cardanols and 20.22% polymeric materials [178].

CNSL extracted for 30 h by using methanol contains 28.64% cardanols, 19.06% anacardic acids, 45.27% cardols, 1.86% b-sitosterol, 3.41% triacontane and a trace amount of polymeric materials [82].

Because there is no standardized extraction method of CNSL, there are a lot of discrepancies in the extractives yield. According to the information obtained in the literature, it is clear that one solvent is not sufficient enough to extract all CNSL in the CNS. Based on the extractive yields obtained under different operating conditions, it is insufficient to determine the optimal method for extracting ACC compounds. Therefore, it is necessary to perform ACC quantification to identify the most effective extraction method.

b) Lignocellulosic content

A few authors [6,10,15,16,179] reported the lignocellulosic content of CNS (Table 2.4).

Table 2.4: Cashew nut shells composition by different authors

Composition (%)	**Melzer et al. 2013** [6]	**Ocheja et al. 2015** [179]	**Kaur et al. 2023** [15]	**Paiva et al. 2024** [16]
Cellulose	4.9	11.50	25.5	12.78
Hemicelluloses	20.8	7.35	5.23	58.34
Lignins	9.5	7.45	14.3	24.3

The lignocellulosic composition reported in the studies were significantly different. This discrepancy is due to difference in methodologies (extraction methods, Van Soest method protocol etc.) and the source of the cashew nut shells.

c) Proximate and ultimate analysis

Unlike the lignocellulosic content analysis of CNS, the proximate and ultimate analysis of CNS was carried out by numerous authors (Table 2.5).

Table 2.5: Proximate and ultimate analysis of cashew nut shells (adapted from Melzer et al. [10]). Volatile Matter, Ash, Fixed Carbon, C, H, N, O and S in wt%, High Heating Value in MJ/kg.

Year	**2003**	**2006**	**2011**	**2011**	**2013**	**2018**	**2020**	**2023**	**2024**
Author (s)	**Das et al.**	**Tsamba et al.**	**Wilson et al.**	**Tippayawong et al.**	**Melzer et al.**	**Abrego et al.**	**Nam et al.**	**Kaur et al.**	**Paiva et al.**
	[4]	[180]	[181]	[182]	[10]	[14]	[9]	[15]	[16]
VM	77.3	81.8	84.1	79.0	84.5	81.2	76.81	84.6	86.23
Ash	1.1	1.9	1.9	5.9	1.9	2.0	5.02	1.7	1.79
FC	21.5	16.3	14	14.8	13.6	11.5	18.17	9.7	11.98
HHV	-	24.1	22.4	17.8*	25.7	22.4	20.16	23.85	23.72
C	48.7	58.3	56.0	45.7	58.1	53.7	45.7	56.56	54.65
H	7.0	7.0	6.9	3.7	7.1	7.1	3.7	7.58	7.68
N	0.4	0.7	0.44	0.3	0.5	0.4	0.2	0.63	0.65
O	43.0[a]	32.0	34.7[a]	44.6	32.4	36.8 [a]	44.6	34.13	35.23 [a]
S	-	-	-	-	-	-	-	1.1	-

[a] calculated by difference

The difference in values from authors could be explained by the origin of cashew nut shells as well as the composition of the CNSL. The high carbon content explains the high calorific value of cashew nut shells. The hydrogen and oxygen content reduces the calorific value of biomass.

d) Vitamin content

Cashew nut shells are very rich in vitamins C and A, with a value of 46.41 mg/100 g and 8.12 mg /100 g respectively, followed by vitamins B1 and B2, then vitamins D, E, K and B6 [179].

e) Protein and starch content

Defatted cashew nut shells according to Yuliana et al. and Harini et al. are cashew nut shells after extraction of phenols. Defatted cashew nut shells contain 26.17% protein and 15.98% starch [177] (62.53% [183]).

2.2.2.2 Composition of CNSL

a) Molecular content

As mentioned in the previous section, HPLC is the most suitable method to analyze and quantify the ACC compounds in the extractives. However, in the literature, none of the articles take into account all the isomers (12 ACC isomers). For instance, Chen et al. [175] did not take into account cardol 15:0 in their analysis while the study by Morais et al. [174] did not take into account the saturated compounds (15:0). Ahmadou et al. carried out HPLC method but only use one isomer to represent all 4 isomers of different degree of unsaturation [166]. Figure 2.12 shows the chromatogram of CNSL standards [175]. Table 2.6 shows the retention time and content of the ACC constituents detected in the HPLC chromatogram of two studies [174,175] .

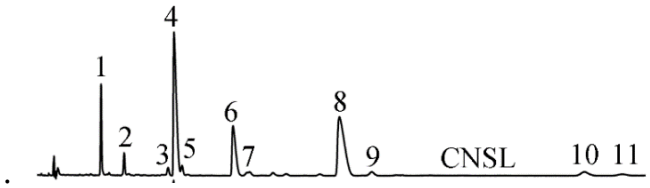

Figure 2.12: HPLC chromatogram of CNSL [175]

Table 2.6: HPLC chromatogram of CNSL [174,175]

N°	Molecule	Compound name	**Chen et al.** [175]		**Morais et al.** [174]	
			Retention time	**Content (%)**	**Retention time**	**Content (%)**
1	$C_{21}H_{30}O_2$	Cardol 15 :3	6.30	7.62	4.41	15.36
2	$C_{21}H_{32}O_2$	Cardol 15 :2	8.57	2.86	5.75	6.96
3	$C_{21}H_{34}O_2$	Cardol 15 :1	12.91	1.13	8.43	1.66
4	$C_{22}H_{30}O_3$	Anacardic acid 15 :3	13.48	34.06	7.48	28.00
5	$C_{21}H_{30}O$	Cardanol 15 :3	14.28	0.96	8.83	2.96
6	$C_{22}H_{32}O_3$	Anacardic acid 15 :2	19.31	14.63	10.35	17.77
7	$C_{21}H_{32}O$	Cardanol 15 :2	20.96	1.42	12.63	2.29
8	$C_{22}H_{34}O_3$	Anacardic acid 15 :1	29.80	32.07	15.93	17.13
9	$C_{22}H_{34}O$	Cardanol 15 :1	32.99	1.42	20.03	1.74
10	$C_{22}H_{36}O_3$	Anacardic acid 15 :0	54.01	2.31	-	-
11	$C_{22}H_{36}O$	Cardanol 15 :0	57.71	0.67	-	-
	Sum			**99.17**		**93.87**

These two studies present a concentration of ACC (anacardic acid, cardanol and cardol) > 93%. The order of the retention time of ACC differs between these two methods.

In the study of Chen et al., the anacardic acids, cardanols and cardols distribution in the extractives are 83.8%, 4.5% and 11.7% respectively, which is different from Morais et al. (67.0%, 7.4%, 25.5%). This could be explained by the difference of extraction methods applied and the source of cashew nut shells.

This section highlights the importance of the development of HPLC method for the quantification of ACC compounds in the CNSL. Without a HPLC method including full calibration of ACC isomers (12 isomers), quantification of ACC in the CNSL or CNS is impossible.

b) Proximate and ultimate analysis

Few authors [4,10,184] carried out the proximate and ultimate analysis of CNSL. Table 2.7 shows the results of three authors.

Table 2.7: Proximate and ultimate analysis of CNSL

Immediate analysis	Value
Humidity (%)	6.68 [184]
Volatile matter [wt%]	93.24 [184]
Ash [wt%]	0.06 [184]
Fixed carbon [wt%]	0.02 [184]
LHV (MJ/kg)	30.74 [184], 40.00 [4]
C [wt%]	66.23 [184], 80.00 [10]
H [wt%]	10.72 [184], 12.00 [10]
N [wt%]	0.15 [184], - [10]
O [wt%]	22.84 [184], 8.00 [10]
S [wt%]	0.36 [184],- [10]

The high content of carbon and hydrogen content suggest that CNSL has high energy output. The volatile matter of CNSL is much higher than the one of CNS, due to the composition of CNSL which are made up of phenolic compounds. Because CNSL contains mainly volatile matter, the fixed carbon is nearly zero. The range provided (30.74 MJ/kg to 40.00 MJ/kg)

reflects different conditions or methodologies in the measurement process of calorific value of CNSL.

c) Physicochemical properties

The physicochemical properties of CNSL were studied by several authors [103,185–189] (Table 2.8).

Table 2.8: Physicochemical properties of cashew nut shell liquid (CNSL)

Physicochemical properties	Values/ Observation	Ref.
Colour	Dark brown	[103,185]
Odour	Choke	[103,185]
Nature	Viscous liquid	[103,186]
Moisture (%)	6.5-6.7	[103,186]
Ash (%)	1.3-1.6	[103,186]
Specific gravity (30°C)	0.9561-0.9995	[103,190]
Refractive index (20°C)	1.52 - 1.686	[103,186]
Viscosity (mPa-s , 24°C)	105-600	[103,189]
Acid value (mg KOH/g)	112-141	[103,187,188]
Free fatty acid (%)	58-60	[103,186]
Saponification (mg KOH/g)	138-161[187]	[103,187]
Iodine value (g I_2/g)	178-188 [187]	[103,187]
pH	3-3.2 [187]	[103,187]

CNSL is commonly known as viscous liquid. Its viscosity is due to the high molecular weight of its primary constituents (anacardic acids, cardanols and cardols). The relatively acidic pH value of the CNSL, and this is probably due to the high concentration of anacardic acid in the CNSL. The free fatty acid content is significant and implies that a large portion of CNSL is composed of acids that can participate in various chemical reactions, such as esterification and polymerization. The iodine value indicates a high degree of unsaturation in the CNSL.

The boiling points of anacardic acids for the different isomers are : 474.8 °C (15:0) [191] , 492.1 °C (15:1) [192] , 496.4 °C (15:2) [193] and 519.2 °C(15:3) [194] . The boiling points of cardanols for the different isomers are : 463.1°C (15:0) [195] , 435.4 °C (15:1) [196] , 426.0 °C (15:2) [196]and -°C(15:3). The boiling points of cardols for the different isomers are : 425.5°C

(15:0) [197], -°C (15:1), 472.40 °C (15:2) [198] and 473.2 °C(15:3) [199]. To my knowledge, there is no information regarding the boiling points of cardanol 15:3 and cardol 15:0.

2.3 Pyrolysis of cashew nut shells

This section first deals with the thermal degradation of CNS, followed by the pyrolysis kinetic studies. The section ends with the products yields from the pyrolysis of CNS and of their separate components (de-oiled CNS and CNSL).

2.3.1 Thermal degradation of cashew nut shells

Several authors investigated thermal degradation of cashew nut shells [4–10,15,16,200] Among these, Melzer et al. [6,10] and Paiva et al. [16] experimented milled cashew nut shells.

Regarding CNS pyrolysis kinetics, typical TGA/DTG curves are presented in Figure 2.13 [9].

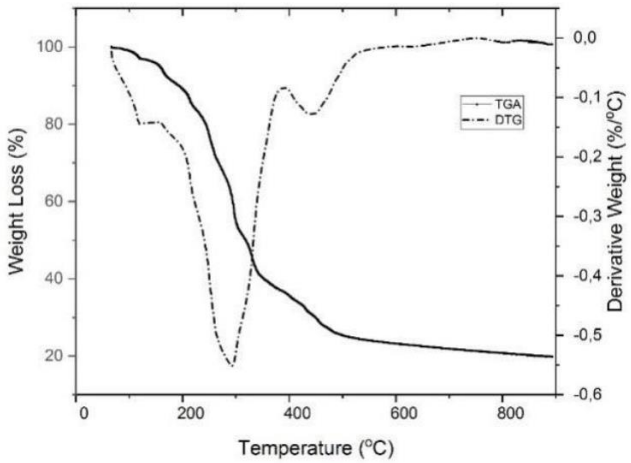

Figure 2.13: TG and dTG curves of CNS during pyrolysis [9]

A first peak is observed during the drying stage (below 200 °C) at 120 °C. This temperature corresponds both to the evaporation of moisture from the cashew nut shells and the decarboxylation of anacardic acids. The second stage consists of the breakdown of hemicellulose, cellulose and CNSL which occurred in the temperature range of 200-400 °C. During the third stage of weight loss, occurring within the temperature range of 400 to 550 °C, the process involves the degradation of intermediates products of Cashew Nut Shell Liquid (CNSL) along with the thermal degradation of lignins at a slower rate [6]. During this stage, subsequent biochar formation also takes place [16]. In general, TGA studies from the literature

show the same peak appearances, with just some temperature shifts due to different operating conditions and/or origin of cashew nut shells.

2.3.2 Kinetic studies of cashew nut shells pyrolysis

There are numerous studies on the kinetic modelling of lignocellulosic biomass like wood, but very few on extractives-containing biomass like cashew nut shells (CNS). Kinetic modelling of CNS pyrolysis involves the development of mathematical models that describe the conversion and the formation of various products under different operating conditions.

Kinetic modelling of CNS can require the deconvolution of thermogravimetric (TG) peaks, which involves separating overlapping signals to identify individual thermal reactions. This is particularly complex for CNS due to the presence of cashew nut shell liquid (CNSL).

Only two kinetic studies ([16], [8]) were carried out on pyrolysis of cashew nut shells and their components. In the study of Paiva et al., it was defined that the pyrolysis of CNS is a summative reaction of five independent reactions [16]. These reactions are attributed to the devolatilization of extractives, hemicelluloses, cellulose, primary and secondary lignins, as presented in Equation 2.15 [201,202].

$$Raw\ cashew\ nut\ shell \begin{cases} Extractives \xrightarrow{k_e} Volatiles + Char \\ Hemicelluloses \xrightarrow{k_h} Volatiles + Char \\ Cellulose \xrightarrow{k_c} Volatiles + Char \\ Primary\ lignins \xrightarrow{k_{pl}} Volatiles + Char \\ Secondary\ lignins \xrightarrow{k_{sl}} Volatiles + Char \end{cases} [16]$$

Equation 2.15

An asymmetric double sigmoidal (Asym2sig) fitting function was used to deconvolute the pyrolysis profile (dTG) of CNS (Figure 2.14) into 5 peaks, which represent the thermal degradation of five pseudo-components. This fitting function is suitable to address the asymmetric nature of the pyrolysis behavior of CNS, which was shown by its determination coefficients (R^2) of >0.99.

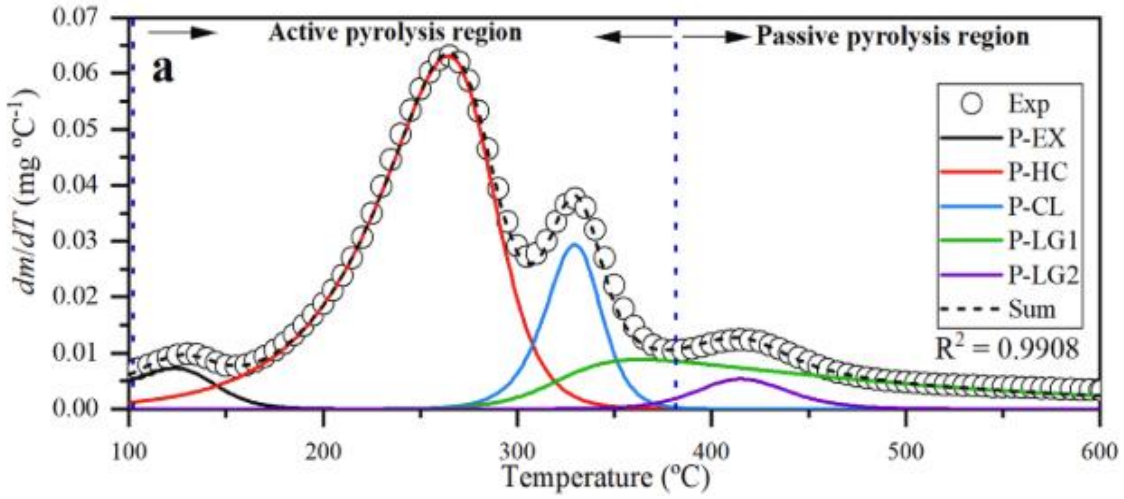

Figure 2.14: Plots of deconvoluted DTG curves (solid lines), using Asym2Sig function, against the experimental DTG curves (open circles) of raw cashew nut shells (P-EX: pseudo extractives, P-HC: pseudo hemicelluloses, P-CL: pseudo cellulose, P-LG1:pseudo primary lignins and P-LG2: pseudo secondary lignins) [16]

Conversion rate is generally described with 3 kinetics values (Activation Energy (E_a), Pre-exponential Factor (A) and Reaction model f(α)) as shown in Eq. 2.16.

$$\frac{d\alpha}{dt} = k(T)f(\alpha) = Ae^{\frac{-E_a}{RT}}f(\alpha) \qquad \textit{Equation 2.16}$$

- Activation Energy (E): This is the minimum energy required for the reactants to undergo a chemical reaction.
- Pre-exponential Factor (A): It represents the frequency of collisions between reactant molecules that result in a reaction. It is a constant that reflects the number of times reactants collide with the proper orientation and energy to react per unit time.
- Reaction Model (f(α)): This function describes the reaction mechanism, where α is the extent of conversion. The reaction model provides insights into how the reaction progresses over time and can take various forms, such as first-order, second-order, or more complex mechanisms.

Equation 2.16 shows that the rate of conversion is equivalent to a temperature-dependent reaction constant $k(T)$ multiplied by a conversion-dependent reaction model $f(\alpha)$. The temperature-dependent reaction constant is based on the Arrhenius Law. Considering non-isothermal experiments with constant heating rate, Equation 2.16 is arranged to Equation 2.17.

$$\frac{d\alpha}{dT} = \frac{1}{\beta}\frac{d\alpha}{dt} = \frac{A}{\beta}e^{\frac{-E_a}{RT}}f(\alpha) \qquad \textit{Equation 2.17}$$

The kinetic reaction of the cashew nut shells is defined as the sum of several individual kinetics i as shown in Equation 2.18.

$$\left(\frac{d\alpha}{dt}\right)_{cashew\ nut\ shells\ residues} = \sum_{i=1}^{N} c_i \left(\frac{d\alpha}{dt}\right)_i = \sum_{i=1}^{N} c_i\, A_i e^{\frac{-E_{a_i}}{RT}} f(\alpha)_i \qquad \textit{Equation 2.18}$$

Where c_i represents the mass fraction of each pseudo-component i.

The activation energy could be obtained through various model-free methods such as Friedman (FR), Flynn-Wall-Ozawa (FWO), Kissinger-Akahira-Sunose (KAS), and Starink (STK). The left-hand side of equations (Eq 2.19 to 2.22) was plotted against 1/T. The activation energy E_a is deduced from the equation for each pseudo component.

$$FR: ln\left(\frac{d\alpha}{dt}\right) = ln\left(\beta\frac{d\alpha}{dT}\right) = ln[Af(\alpha)] - \frac{E_a}{RT} \qquad \textit{Equation 2.19}$$

$$FWO: log(\beta) = log\left(\beta\frac{AE_a}{Rg(\alpha)}\right) - 2.315 - 0.4567\frac{E_a}{RT} \qquad \textit{Equation 2.20}$$

$$KAS: ln\left(\frac{\beta}{RT^2}\right) = ln\left(\frac{AR}{E_a}\right) + 0.6075 - \frac{E_a}{RT} \qquad \textit{Equation 2.21}$$

$$STK: ln\left(\frac{\beta}{T^{1.92}}\right) = Constant - 1.0008\frac{E_a}{RT} \qquad \textit{Equation 2.22}$$

The average activation energies were 63.81-88.89 kJ mol^{-1} for extractives, 94.36-102.32 kJ mol^{-1} for hemicelluloses, 123.70-133.88 kJ mol^{-1} for cellulose and 164.27-249.28 kJ mol^{-1} for primary and secondary lignins [16]. The values are smaller or similar to those found for other lignocellulosic biomass.

The reaction model was determined using integral master plots. This method involves graphically comparing experimental data with theoretical curves from seventeen classical reaction models (Table 2.9); data were taken at a conversion level of α = 0.5. According to Equation 2.23, if the experimental curve [p(x)/p(x0.5) versus α] matches one of the theoretical curves g(α)/g(0.5), the corresponding reaction model is considered the most plausible.

$$\frac{g(\alpha)}{g(0.5)} = \frac{p(x)}{p(x_{0.5})} \qquad \textit{Equation 2.23}$$

g(0.5) refers to the integral form of the reaction model at α = 0.5, and p(x0.5) refers to the approximate function (with $x = E_a/RT_{0.5}$).

Table 2.9: Algebraic expressions of the most frequent reaction models used to describe the kinetics of solid-state reactions [16].

Model	Mechanism	*g(α)*	*f(α)*
		Nucleation Models	
P2	Power law	$\alpha^{1/2}$	$2\alpha^{1/2}$
P3	Power law	$\alpha^{1/3}$	$3\alpha^{2/3}$
P4	Power law	$\alpha^{1/4}$	$4\alpha^{3/4}$
P2/3	Power law	$\alpha^{3/2}$	$2/3\alpha^{-1/2}$
A2	Avrami-Erofeev	$\left[-\ln(1-\alpha)\right]^{1/2}$	$2(1-\alpha)[-\ln(1-\alpha)]^{1/2}$
A3	Avrami-Erofeev	$\left[-\ln(1-\alpha)\right]^{1/3}$	$3(1-\alpha)[-\ln(1-\alpha)]^{2/3}$
A4	Avrami-Erofeev	$\left[-\ln(1-\alpha)\right]^{1/4}$	$4(1-\alpha)[-\ln(1-\alpha)]^{3/4}$
		Reaction Order Models	
F1	First-Order Reaction	$-\ln(1-\alpha)$	$1-\alpha$
F2	Second-Order Reaction	$(1-\alpha)^{-1}-1$	$(1-\alpha)^2$
F3	Third-Order Reaction	$(1/2)\left[(1-\alpha)^{-2}-1\right]$	$(1-\alpha)^3$
Fn	n-Order Reaction	$\left[1-(1-\alpha)^{1-n}\right]/(1-n)$	$(1-\alpha)^n$
		Geometrical Contraction Models	
R2	Contracting cylinder	$1-(1-\alpha)^{1/2}$	$2(1-\alpha)^{1/2}$
R3	Contracting sphere	$1-(1-\alpha)^{1/3}$	$3(1-\alpha)^{2/3}$
		Diffusion Models	
D1	One-dimensional diffusion	α^2	$1/2\alpha^{-1}$
D2	Two-dimensional diffusion	$(1-\alpha)\ln(1-\alpha)+\alpha$	$[-\ln(1-\alpha)]^{-1}$
D3	Three-dimensional diffusion	$\left[1-(1-\alpha)^{1/3}\right]^2$	$3/2(1-\alpha)^{2/3}\left[1-(1-\alpha)^{1/3}\right]^{-1}$
D4	Ginstling-Brounshtein	$1-(2/3)\alpha-(1-\alpha)^{2/3}$	$3\left[2\left((1-\alpha)^{-1/3}-1\right)\right]^{-1}$

The devolatilization of pseudo extractives (P-EX) and pseudo hemicelluloses (P-HC) during the pyrolysis of cashew nutshell residues is best described by a second-order reaction model, F2 = $(1 - \alpha)^2$ [16], consistent with existing literature [203]. The devolatilization of pseudo cellulose (P-CL) is well explained by the Avrami-Erofeev nucleation reaction models, specifically type A2 and A3, which involve the growth of nuclei [16]. Published studies on pseudo cellulose devolatilization also support the nucleation reaction models [204,205]. The devolatilization reactions of pseudo-primary lignins (P-LG1) and pseudo-secondary lignins (P-LG2) aligned with order-based reaction models [16].

The pre-exponential factor is deducted by the kinetic compensation effect. The kinetic compensation effect states that there is a linear relationship among Arrhenius parameters (activation energy and pre-exponential factor) in thermally induced solid-state reactions (Equation 2.24).

$$\ln (A)_i = aE_{ai} + b \qquad \textit{Equation 2.24}$$

in which a and b are compensation parameters, whereas i is the assumed and tested reaction model $g(\alpha)$, which is able to characterize the pyrolysis process.

The estimates of pre-exponential factors of the pseudo-components were 2.78×10^{10} min^{-1} for pseudo extractives (P-EX), 4.25×10^{8} min^{-1} for pseudo hemicelluloses (P-HC), 8.33×10^{9} min^{-1} for pseudo cellulose (P-CL), 6.89×10^{16} min^{-1} for pseudo primary lignins (P-LG1), and 3.89×10^{11} min^{-1} for pseudo secondary lignins (P-LG2). The value of the pre-exponential factor indicates the type of chemical reaction during pyrolysis. A value $\leq 10^{9} min^{-1}$ suggests a surface chemical reaction whereas a value of $>10^{9}$ min^{-1} indicates a simple reaction.

Therefore, the devolatilization of pseudo hemicelluloses (P-HC) and pseudo cellulose (P-CL) were considered surface chemical reactions. In contrast, the devolatilization of pseudo lignins (P-LG) and pseudo extractives (P-EX) was considered a simpler chemical reaction.

Although the kinetics study carried out by Paiva et al. has successful determined the kinetic parameters of CNS pyrolysis, the designation of deconvoluted peaks to the pseudo components was not totally correct. This is because generally, the main degradation peak of extractives CNSL overlaps with the degradation peak of hemicellulose. The degradation of extractives in the CNS does not stop at decarboxylation phase (which is shown by the P-EX peak at around 130°C). On top of that, lignins degradation is supposed to take place along with the degradation of other macromolecules (hemicelluloses and cellulose) but at a much lower mass loss rate. Despite this error, it is worth adopting the methods used by Paiva et al. to define the pyrolysis kinetics parameters with a correct peak deconvolution.

2.3.3 Pyrolysis products

A few authors paid attention on identification and quantification of gas and condensates from CNS pyrolysis. Results are commonly presented in terms of products yield, gas and condensates composition. Several types of reactors have been used for this purpose: simple batch reactor [13,14], fixed bed [6,10], packed vacuum pyrolysis unit [4], screw reactor [2], and glass tubular

reactor [15] and a bubbling fluidized bed reactor [206]. Temperatures between 400 and 600°C were generally investigated in such studies.

2.3.3.1 Pyrolysis product yields

The yields of char, condensates and gas obtained during CNS pyrolysis [14] is depicted in Figure 2.15.

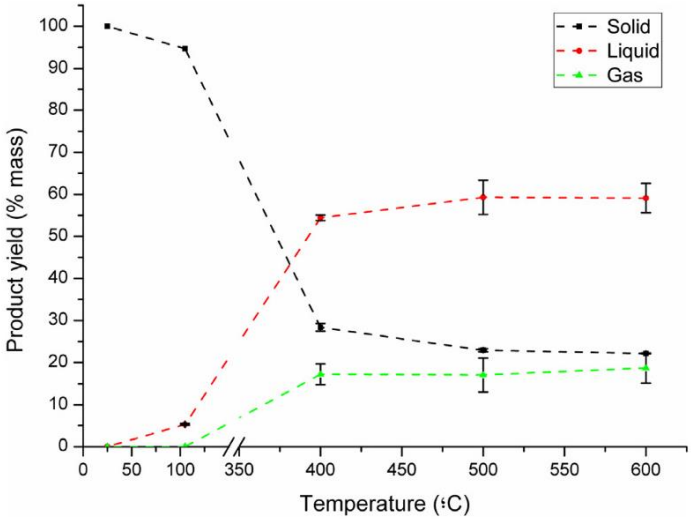

Figure 2.15: Product distribution from CNS pyrolysis from the study of Abrego et al. [14]

The study of Abrego et al. showed that the temperature does not change the product distribution significantly [14]. The char yield obtained was below 30% between 400 and 600°C. The gas yield slight increases with the temperature.

Slow pyrolysis of de-oiled CNS and CNS was conducted at temperatures ranging from 300 to 550 °C by Kaur et al. (Figure 2.16) [15] .

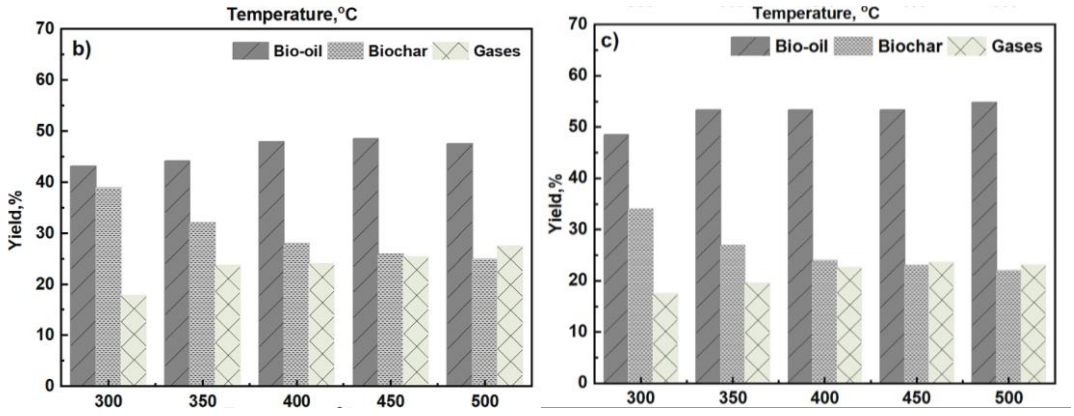

Figure 2.16: Product distribution from de-oiled CNS (left) and CNS pyrolysis (right) [15]

The highest bio-oil (condensates) yields were 48.6 wt% at 450 °C for de-oiled CNS and 54.9 wt% at 500 °C for CNS. The yield of condensates increased with temperature, driven by the enhanced degradation of biomass components. However, beyond the optimal temperature, condensates yield began to decrease due to secondary cracking and the extensive breakdown of the biomass structure, which led to a higher production of permanent gases [15]. A similar study was carried out by Melzer et al. [6,10], showing that at 500°C, the de-oiled CNS has a lower condensates yield (42.1 wt%) when compared to CNS (61.9 wt%), therefore coherent to the results of Kaur et al. CNSL pyrolysis contributes mainly condensates (82.0 wt%) in the pyrolysis products [6,10].

From the studies above, the products yield of CNS pyrolysis is not too different from the ones of wood generally found in the literature despite the high concentration of extractives.

2.3.3.2 Pyrolysis permanent gas composition

The permanent gas composition of CNS, CNSL and de-oiled CNS pyrolysis is shown in Table 2.10.

Table 2.10: Permanent gas composition of CNS, CNSL and de-oiled CNS pyrolysis (wt%)

Gas yields (wt%)	**CNS** [6,10] **500 °C**	**CNS** [14] **500 °C**	**CNSL** [6,10] **500 °C**	**De-oiled CNS** [6,10] **500 °C**
H_2	0.04	0.09	0.03	0.03
CH_4	0.44	2.57	0.39	0.92
C_2H_4	0.30	0.13	0.64	0.25
C_2H_6	0.34	0.55	0.59	0.18
CO	2.71	2.08	0.26	6.40
CO_2	9.68	11.65	2.62	10.01
Total gas	13.51	17.07	4.53	17.79

The permanent gas issued from CNS is mainly composed of CO_2 and CO. CO_2 is the main gas, representing 68-72% of the total gas mass. CO_2 is produced from the hemicelluloses and lignins degradation and the decarboxylation of anacardic acids into cardanol.

According to Melzer et al. [6,10], the pyrolysis of CNSL contributes to a production of 4.53% gas. CO_2 accounts for up to 58% of the gas, followed by the light hydrocarbons (CH_4, C_2H_4, C_2H_6) which accounts 36 wt% of the permanent gas composition. The high percentage of CO_2

suggests significant decarboxylation reactions during the pyrolysis process. The presence of light hydrocarbons indicates thermal cracking of larger organic molecules within the CNSL.

2.3.3.3 Pyrolysis condensates composition

The composition of CNS pyrolysis condensates has been rarely studied, except from Melzer et al. and Kaur et al. The interpretation of condensates composition can either be carried out with GC-MS, either quantitatively (by mass) or qualitatively (by the peak area percentage in chromatogram) if no calibration curves exist.

a) Quantitative analysis of condensates

The tar distribution in the CNS and CNS pyrolysis condensates at 500 °C carried out by Melzer et al is shown in Table 2.11.

Table 2.11: Tar distribution in CNS and CNSL pyrolysis condensates at 500°C (mg/g biomass) [6,10]

Tar (mg/g)	CNS	CNSL
Alcohols	6.1	0.0
Aldehydes/ketones	13.0	0.0
Acids	30.1	1.0
Furans	4.3	0.0
N-aromatics	2.0	2.4
Sugars	2.4	0.0
Phenols	5.9	7.3
Guaiacols	0.2	0.0
PAHs	0.4	0.4
Total	64.5	11.1

The quantification of tars in the CNS pyrolysis condensates requires an adapted GC-MS method (type of column, temperature of injection etc.). This is why most biomass pyrolysis studies use qualitative analysis to identify the tars in the condensates.

During the CNS and CNSL pyrolysis (500°C) carried out by Melzer et al., 619 mg/g of CNS pyrolysis condensates and 820 mg/g CNSL pyrolysis condensates were obtained (Table 2.10). This means that at 500°C, 10.4 % of the condensates was quantified in the case of CNS pyrolysis (1.3 % in the case of CNSL pyrolysis) despite the calibration of 65 chemical compounds in the study of Melzer et al. [10]. This is because the GC-MS method applied

was more adapted to pyrolysis condensates from lignocellulosic biomass, thus there are CNSL derived compounds that could not be quantified. Therefore, other more adapted analytical method such as HPLC is required to better analyze these compounds.

b) Qualitative analysis of condensates

The qualitative analysis of de-oiled CNS and CNS pyrolysis condensates showed that the chromatogram is dominated by phenolics. The phenolics peak area percentage is lower in the case of de-oiled CNS than the one of CNS (59.55% and 70.96% respectively) [15].

The phenolics present were phenol, p-Cresol, 4-ethylphenol, Cardanol 15:0, 2-methylphenol and 3-methylphenol [15]. Other phenolics such as phenol-3-cyclohexyl and phenol-3-ethyl were detected [6,10]. Among these phenolics, Cardanol 15:0 is the major phenolic present [92], [94] with an area percentage of 24.72 and 24.98% respectively [94].

The explanation of the presence of several compounds is presented as follows:

- Phenolics

Phenol and p-Cresol originate from 2-methoxyphenol (guaiacol). Guaiacol and syringol which are both monomeric units of lignins undergo demethylation to form catechol and methane, as well as demethoxylation to produce phenol and carbon dioxide [125], [126].

Phenol, guaiacol, syringol and catechol could be produced by different mechanisms. They include cleaving of -OH functional group connected to the aliphatic side chain, breaking of the alkyl side chain, aryl ether and the linkage between aromatic rings which takes place when temperature increases [127]. Phenol can also be produced by the breakdown of lignins.

- Carbonyls and furans

Carbonyls and furans are decomposition products of cellulose and hemicelluloses. The breakdown of β-1,4glycosidic linkage forms levoglucosan as intermediates as well as furans. The furans present in both condensates of de-oiled CNS and CNS pyrolysis were: 2,5-dimethylfuran, furfural, 2,3-dihydrobenzofuran [6] and 2-methylbenzofuran[15] . Benzofurans are usually produced from the breakdown of β -5' moieties of lignins. The carbonyls include esters, aldehydes, carboxylic acids and ketones. In the case of de-oiled CNS and CNS, the area percentage of carbonyls account up to 14.5% and 16.2%

respectively [15]. m-Cresyl acetate is the major carbonyl in the condensates of de-oiled CNS (6.28%) and CNS (6.15%) [15].

- N-containing compounds

N-containing compounds such as aliphatic or aromatic amines and N-containing heterocyclics could also be formed. N-containing heterocyclics are generated by combination of N-containing monomers and carbonyls through the rearrangement reactions of Maillard and Madori [210].

- Linear hydrocarbons

Linear hydrocarbons such as 1-decene and 2-tridecene could be formed by the cleavage of the double bonds of the alkyl chains of the ACC constituents [15] or radical chain scission processes [211].

2.4 Thermal degradation of ACC constituents

Based on published works, this section aims to describe the state of art on the thermal degradation mechanisms of ACC.

2.4.1 Thermal degradation of anacardic acids

The thermal degradation of ACC first commences with the thermal degradation of anacardic acids. Anacardic acids degrade by **decarboxylation** which results in the production of cardanols and CO_2. Decarboxylation takes place between 150 and 250°C according to the study of Coulibaly et al. [12] (Figure 2.17). However, this temperature range depends on the operating conditions of the TG experiments (heating rate, sample mass).

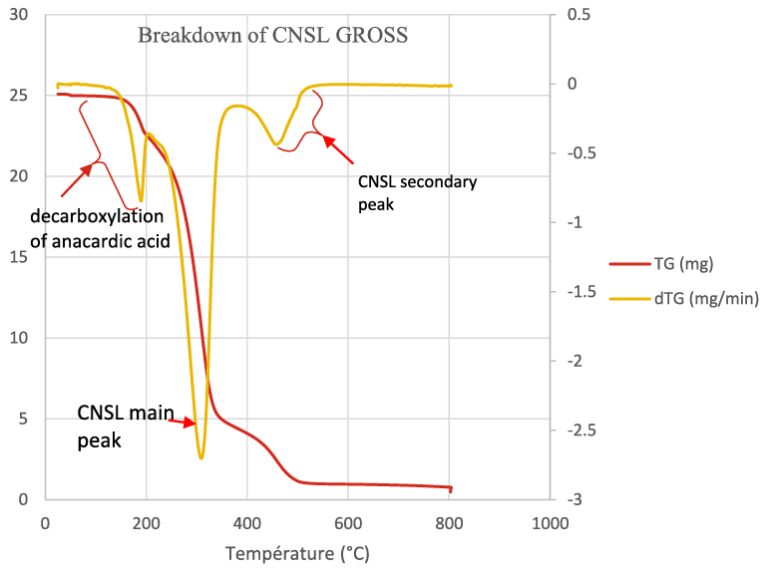

Figure 2.17: TG and dTG curve of CNSL [12]

Because anacardic acids undergo decarboxylation at a lower temperature than their boiling point (boiling temperature range of all anacardic acid isomers : 472-519°C), anacardic acids undergo this reaction at liquid phase. The cardanols produced are also in liquid phase (Equation 2.25).

$$Anacardic\ acid_{liq.} \rightarrow Cardanol_{liq} + {CO_2}_{gas} \qquad \textit{Equation 2.25}$$

Mass loss during decarboxylation reaction of anacardic acids originates from the volatilization of CO_2.

2.4.2 Thermal degradation of cardanols and cardols

Once the anacardic acids have been decarboxylated, only the cardanols and cardols remain as ACC. The primary weight loss peak for CNSL pyrolysis is prominent at 320 °C [12] (Figure 2.17). An additional peak observed at 460 °C may be attributed to the complete decomposition of polymeric intermediates [10] or secondary degradation of CNSL [12].

There is not many information on the thermal degradation of anacardic acids and cardols when compared to cardanols and cardanol-based polymers.

Cardanol 15:0 (or Hydrogenated cardanol) undergoes a one-step degradation from 200 to 320°C during thermal-oxidative treatment [212] (Figure 2.18).

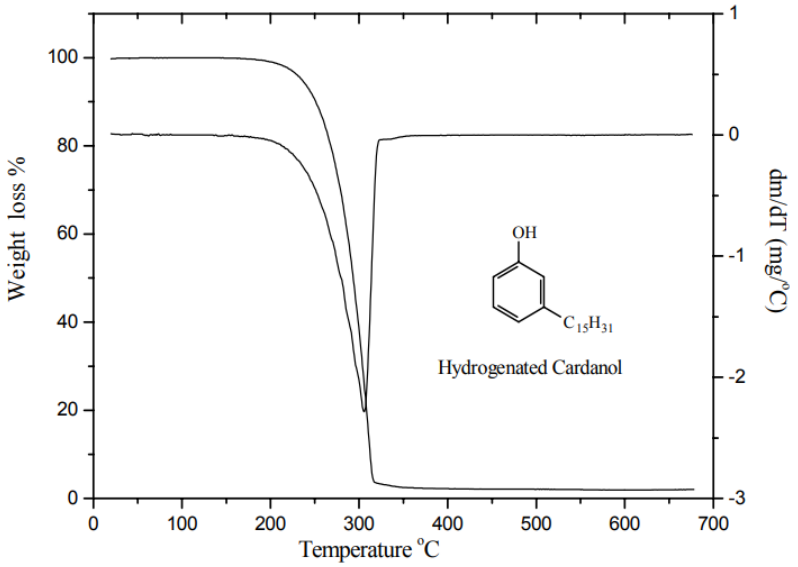

Figure 2.18: TG and dTG curve of hydrogenated cardanol (Cardanol 15:0) at 10°C/min under air atmosphere [212]

Hydrogenation of cardanols could take place during pyrolysis [92] using hydrogen and catalysts such as copper chromite, nickel, palladium or platinum [171].

During the heat treatment of cardanols and cardols, these large (>C20) and multi-functional molecules (phenol + alkene group) can undergo different types of reactions: The two possible reactions that cardanols and cardols can undergo during thermal degradation are: polymerization and devolatilization.

Polymerization reactions of cardanols and cardols

Polymerization is a process by which monomers are linked to form a big polymer molecule (Equation 2.26).

$$nM \rightarrow -M-M-M-M-M-M-M-M- \qquad \textit{Equation 2.26}$$

Monomer Polymer

There are two modes of polymerization: chain growth polymerization and step growth polymerization.

Step growth polymerization is the process in which bi-functional or multifunctional monomers like ACC constituents react to form first dimers, then trimers, longer oligomers and eventually long chain polymers [213] This type of polymerization is also known as

condensation polymerization. According to Murthy et al. [214], cardanol can be polymerized by condensation with aldehydes.

Chain growth polymerization is the process of repeated addition of monomers that possess double or triple bonds to form polymers [215]. It is also known as addition polymerization.

According to Voirin et al. [216], polymerization of CNSL is said to take place when it is heated to 200°C and above.

Murthy et al. [214] explained that, cardanols can undergo chain growth polymerization using the side chain unsaturation. Rodrigues et al. [217] described that thermal oligomerization of cardanols at 140°C takes place at internal double bond (monoene, diene) and vinyl bond (triene). An oligomerization reaction is a chemical process where monomers react with each other to form oligomers, which are molecules composed of a few (typically 2 to 10) repeating units of the monomers. Cardanols can undergo thermal oligomerization with or without catalyst (Figure 2.19) [217]. Thermal oligomerization studies of cardanols at 140°C indicated that dimer was the main oligomer that was formed [217]. A higher temperature could lead to the formation of more complex polymers than dimers.

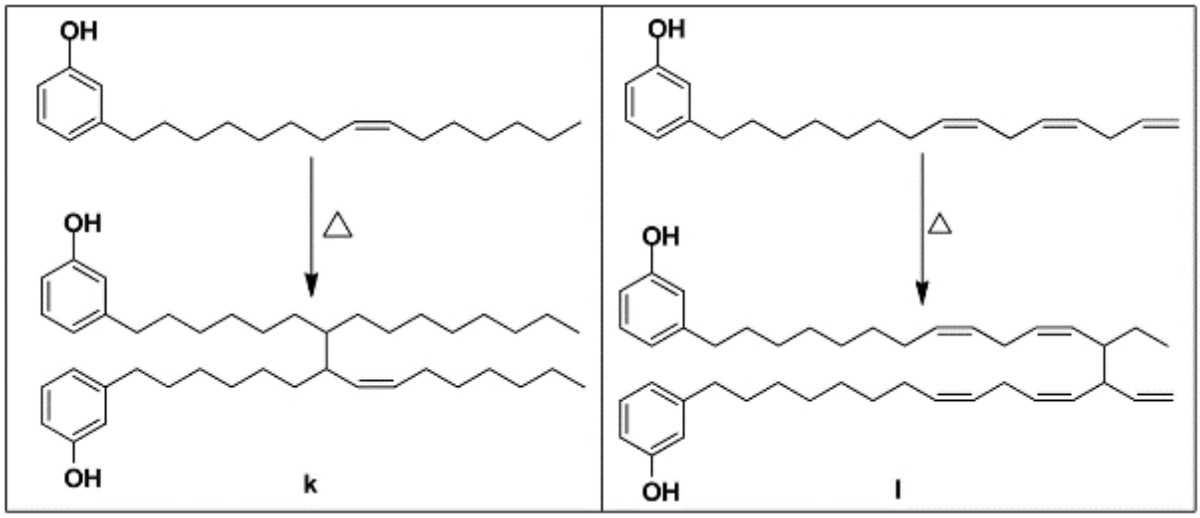

Figure 2.19: Step growth polymerization (thermal oligomerization) of cardanol [217]

Kiratitanavit et al. [218] showed in their work, that cardanols-based polymers have higher thermal stability than cardanol monomers (Figure 2.20), which therefore require a higher temperature to crack. Cardanol polymers (produced by thermal oxidative polymerization) first undergo decomposition (rupture) of the unsaturated aliphatic side chains, followed by the decomposition of -OH entities and C-O-C linkages [218]. This could mean that in any cardanol-

based polymers, the unsaturated aliphatic side chains undergo thermal decomposition first before other functional groups and carbon linkages.

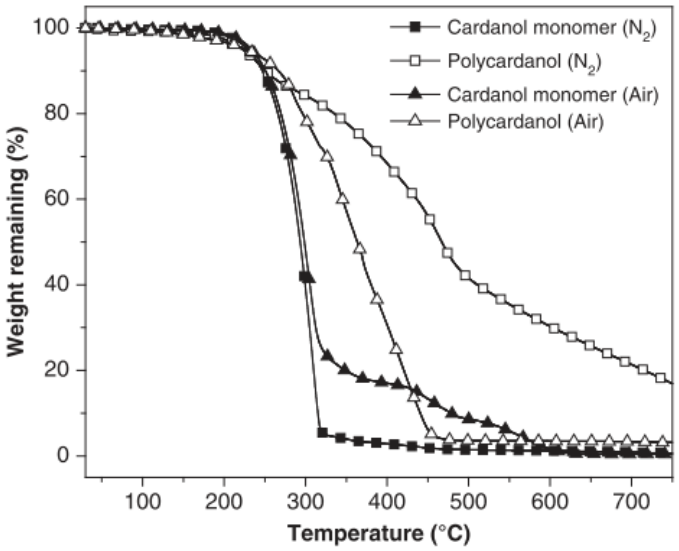

Figure 2.20: TG curves of cardanol monomers and polycardanols (under N_2 and air atmosphere) 20°C/min [218]

With the information collected from the literature, it is clear that cardanols **first undergo polymerization to form cardanol-based polymers**. At higher temperature these polymers **then thermally degrade** through devolatilization and/or depolymerization reactions.

Despite the fact that there is no information regarding the thermal degradation of cardols in the literature, the polymerization reactions of cardols could be quite similar to the ones of cardanols. This is because the sole difference between cardanols and cardols is that cardols contain one additional hydroxyl group (one at ortho position and the other at the para position) when compared to cardanols.

If polymerization of cardanols or/and cardols takes place during the TG experiments, heavier molecules are produced and there is no volatilization of molecules. Therefore, no mass loss should be observed during this reaction.

Devolatilization reactions of cardanols and cardols

Cardanols and cardols are big molecules, which are therefore difficult to vaporize, and which under the effect of heat can undergo devolatilization reactions, generating fragments of lighter molecules, which volatilize easily.

By referring to the study on the thermal degradation of a simpler alkylphenol than cardanols and cardols − cresols (a methyl substituted phenol) and the previous pyrolysis studies on CNSL in the literature, the devolatilization reactions of cardanols and cardols are hypothesized.

The two possible devolatilization reactions of cardanols and cardols are: dealkylation [219–221] and the rupture of aliphatic side chain [10].

a. **Dealkylation** refers to the removal of alkyl group from the alkylphenol. It requires generally a catalyst. The study of Jones and Neuworth showed that thermal cracking of alkylphenols without catalyst produced phenol as primary products [221]. This is supported by the fact that the phenyl group exerts an inductive effect (-I), meaning it pulls electron density towards itself through the sigma bond [222], making it electron-withdrawing. In contrast, the alkyl group exhibits a +I inductive effect [223], donating electron density. As a result, the bond between the phenyl and alkyl groups becomes more likely to break due to the opposing effects of electron withdrawal by phenol and electron donation by the alkyl group.In the case of cardanols, its dealkylation produces a phenol and a hydrocarbon whereas dealkylation of cardol produces a resorcinol and a hydrocarbon (Figure 2.21).

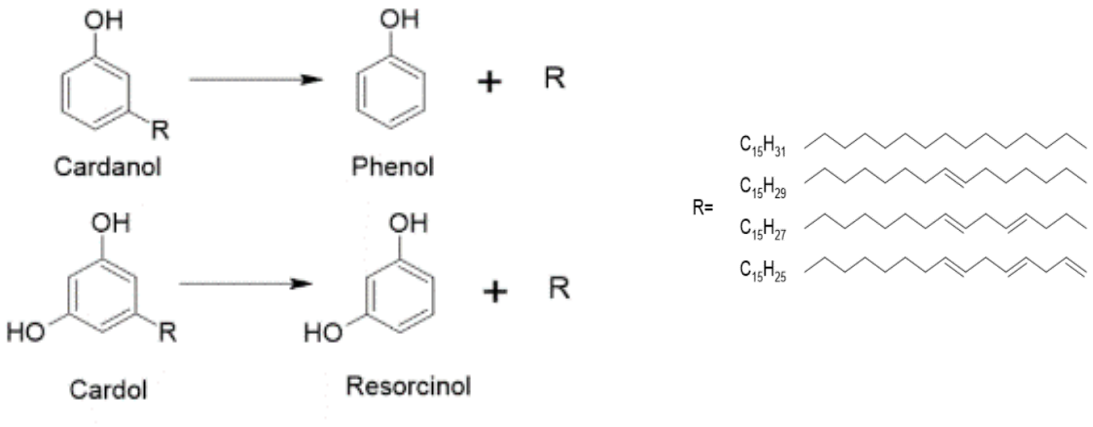

Figure 2.21: Dealkylation of cardanol and cardol

It is interesting to note that, although resorcinol has a boiling point of 277°C, its thermal decomposition only takes place at a temperature higher than > 650°C [224]. Phenol also thermally decomposes at relatively high temperature, which is shown by its low conversion rate (<10%) during a pyrolysis at 550°C [225].

b. The **rupture of aliphatic side chain** refers to the breaking or cleavage of carbon-carbon (C-C) or carbon-hydrogen (C-H) within the aliphatic side chain of a molecule. This reaction results in hydrocarbons with different carbon numbers.

In the study of Melzer et al., the presence of linear hydrocarbons in the CNSL pyrolysis condensates (for example 1-decene and 2-tridecene) confirms the presence of cleavage of double bonds of the side chains on the alkylphenols [6].

The rupture of aliphatic side chain depends on the position of the double bonds. Taking the dienes as example, conjugated dienes are more stable than non-conjugated (isolated and cumulated dienes) due to factors such as delocalization of charge through resonance and hybridization energy [226]. The high level of double bonds in the aliphatic side chain facilitates degradation [227].

Devolatilization reactions could result in the production of lighter molecules which could undergo **phase changes** if the temperature is higher than their boiling points. Depending on the temperature and the pression, the aliphatic chain produced during the thermal degradation of cardanols and cardols changes its phase (liquid or gaseous). Generally, saturated and unsaturated aliphatic chains have similar boiling points. The aliphatic chains (saturated and unsaturated) that could volatilize at a designated temperature can be determined by Figure 2.22.

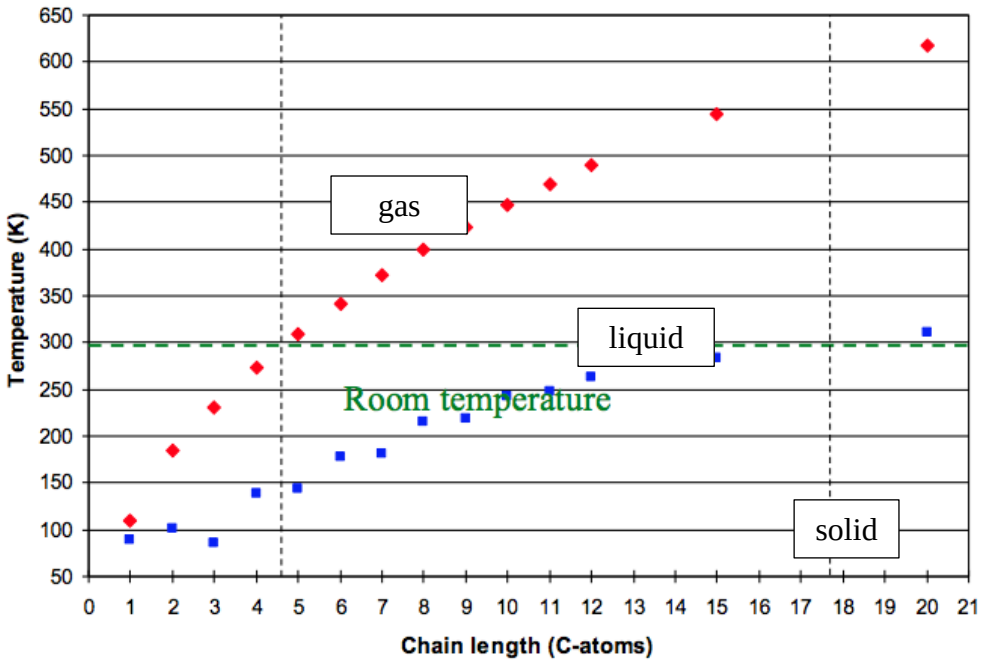

Figure 2.22: Variation of boiling (red) and melting point (blue) of alkanes with different chain lengths [228]

If devolatilization of cardanols or/and cardols take place, mass loss in TG experiments could be observed due to the volatilization of molecules.

To conclude, the **3 main reactions** of the ACC thermal degradation mechanisms are:

a) **Decarboxylation of anacardic acids** ;

b) **Polymerization and devolatilization of cardanols and cardols** ;

c) **Thermal degradation of cardanols and cardols based polymers**.

2.5 Scientific positioning and objectives

The final section of this chapter is dedicated to outlining the positioning and the objectives of this thesis.

2.5.1 Positioning

This thesis is part of 2 development projects in West Africa, funded by i) the Agence Française de Développement (AFD) through the AgroGazelec project (CZZ 2604.01 Z) and ii) the European Union and the Agence Française de Développement (AFD) through the BioStar Project (FOOD/2019/410-794) in the frame of DeSIRA initiative, focusing on energy recovery from agri-food residues. Several biomasses are concerned by these projects, but cashew nuts are common to both. Agrogazelec project aims to establish two electricity generation units in West Africa using CNS gasification technology. A demonstration plant has been installed in Benin and is waiting for commissioning. Biostar project focuses on the combustion of CNS to generate heat. Prototypes have been recently installed in Burkina Faso and Senegal to produce hot water to feed mango driers. Additionally, prototypes have also been designed to produce steam by combustion for the need of the cashew processing.

Despite these two promising projects, there remain significant gaps in understanding the full potential of CNS for energy production. These gaps include the comprehension of the biomass composition and its thermochemical behavior.

To start with, previous research on cashew nut shells characterization has been primarily concentrated on the lignocellulosic composition, specifically focusing on hemicelluloses, cellulose, and lignins. However, there is a notable absence of standardized methods for extracting extractives, leading to a limited understanding of CNS composition. The

identification and quantification method of anacardic acids, cardanols and cardols (ACC) compounds in the extractives require proper development by taking into account all the isomers (12 isomers).

With regard to the CNS pyrolysis, various authors have conducted thermogravimetric studies within the temperature range of 400-700°C, primarily emphasizing the degradation temperatures of macromolecules [4–10]. Only few studies paid attention to the degradation temperatures of the CNSL [6,7,10–12]. The effect of CNSL on the pyrolytic behavior of cashew nut shells has never been studied except by Melzer et al.[6,10]. No one have really been able to adequately explain the peaks observed in the TG of CNS or CNSL.

CNS pyrolysis was investigated using lab scale reactors (400-600°C) [2,4,6,13–16] to study the product yield and composition. However, there is always a lack of comprehension on the condensates composition due to the analytical methods applied. The analytical method either lacks the possibility of quantification, or the method applied is not suitable for the chemical compounds of interest, i.e ACC. For instance, in the study of Melzer et al., the GC-MS method could not quantify ACC constituents due to the peak coelutions. The quantification of ACC constituents in the condensates was not included in previous studies.

Moreover, the literature lacks investigations into the conversion of gas derived from cashew nut shells pyrolysis. The effect of high temperature (> 600 °C) on the cracking of molecules has only been studied by Das et al. (600°C) and Moreira et al. (700°C) [4,17]. Both studies did not quantify the chemical compounds in the condensates.

While some studies have explored gasification of cashew nut shells, the focus has primarily been on the gasification of char [182,229–233] or combustion [234], leaving a significant gap in understanding the broader aspects of CNS pyrolysis gas conversion.

In summary, the current state of research on cashew nut shells reveals substantial gaps in the understanding of the degradation of CNS and their extractives. Addressing these gaps will contribute significantly to advancing knowledge in the field.

2.5.2 Objectives

In conjunction with the two projects mentioned previously (Agrogazelec and Biostar), the aim of this thesis is to provide further insights into the thermochemical behavior of cashew nut shells, in order to optimize their energy valorization. Therefore, this research focuses on

studying the pyrolysis and gas conversion, which are crucial steps in both thermochemical conversion process: combustion and gasification.

The scientific objectives of the thesis are as follows:

1. To determine the detailed chemical composition of cashew nut shells (CNS) and of cashew nut shell liquid (CNSL), which involves the development of analytical methods.
2. To study the pyrolysis of CNS, focusing on both the kinetics and the quantification of resulting products.
3. To investigate the thermal degradation mechanisms of ACC.
4. To study the conversion of CNS pyrolysis gas through thermal cracking and catalytic cracking over a char bed.

Based on experimental results, this research aims to provide insights into the utilization and improved valorization of cashew nut shells (CNS) as a sustainable alternative to fossil fuels for energy production, particularly for semi-industrial units in Africa. By promoting the use of CNS as an energy source, this approach can contribute to reducing air and ground pollution, as well as decreasing dependency on unreliable energy supply systems that are common in many parts of Africa.

CHAPTER 3

Materials and methods

3. Material and methods

This chapter provides a detailed overview of the materials, equipment, and methodologies employed throughout this thesis.

The first section presents a discussion on the source and preparation of the biomass used in this study, focusing on CNS as the primary biomass of interest, alongside beech wood chips, which serve as a reference for lignocellulosic biomass.

The second section of this chapter will describe the materials and the methodologies carried out to characterize the biomass (proximate analysis, ultimate analysis, extractives content, lower heating value, lignocellulosic, protein and starch content).

In the third section, experimental reactors are presented. They include a micro thermogravimetric analyzer (microTG) which allows the study of pyrolysis kinetics and mechanisms of CNS and their components. It was also used to study the thermal degradation mechanisms of ACC (anacardic acids, cardanols and cardols). Next, a pyrolysis and tar conversion (PyTar) reactor was used to study the influence of the extractive content on the decomposition of CNS during various thermochemical reactions (pyrolysis, thermal/ catalytic cracking). The section ends with a discussion on the precautions and the repeatability of the PyTar reactor experiments.

The fourth section describes the equipment used to characterize the permanent gas and the different fractions of the condensates (tar, ACC, water) obtained from the microTG and PyTar reactor experiments.

The last part presents the definitions and calculations of the main products yield (char, condensates and gas).

The description of the carbonization furnace used to produce cashew nut shells char is presented in the Appendices A3.1. The char produced was used to study the catalytic cracking of CNS pyrolysis gas.

3.1 Preparation of cashew nut shells

Cashew nut shells (CNS) (Figure 3.1) were supplied by a cashew nut processing company in Bobo-Dioulasso (ANATRANS) in 2020. CNS were produced from the steaming of raw cashew

nuts in an autoclave to weaken the outer shells and remove the kernels from them. It is proven in a study [235] that steaming does not affect the composition of CNSL in the CNS.



Figure 3.1: Cashew nut shells

In order to ensure the homogeneity of the sample, CNS were selected according to a quartering method (ISO 14488:2007) used by Alakangas et al. [236] (Figure 3.2). A random sack of 25 kg CNS was selected. The CNS were mixed together and divided into four equal parts. Two opposite quarters were mixed as a heap and divided into four equal parts again. The same process was carried out until the desired CNS mass was obtained.

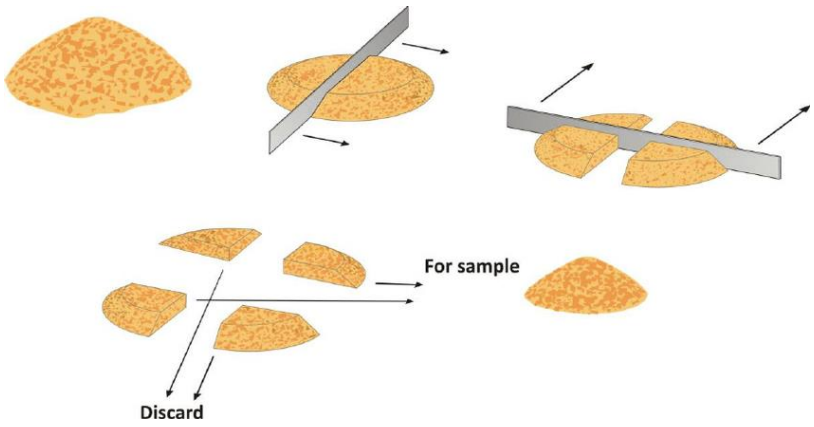

Figure 3.2: Quartering method of biomass [236]

Depending on the experimental results obtained, we decide to either use ground CNS or quartered CNS. For the production of CNS char for catalytic cracking, the CNS were pyrolyzed in their initial size.

Ground CNS were prepared by first freezing the CNS overnight at -80°C before the grinding process. This is to increase the hardness of the shells and facilitate the milling process. It is also to prevent extractives oozing out of the shells. The CNS were then ground the next day to small particle sizes using a laboratory scale mill (Retsch Ultra Centrifugal Mill) fitted with a 1 mm mesh sieve. Because CNS contain high amount of extractives, the CNS tend to agglomerate and form little particles of 2-3 mm diameter.

Ground CNS were used both for the extraction of the cashew nut shells extractives, as well as for the microTG and the PyTar (Pyrolysis and Tar conversion reactor) experiments.

Quartered CNS were prepared by cutting each cashew nut shell into quarters with a pruning shear. Each quarterly cut CNS has a diameter around 1-2 cm. The CNS of this granulometry was used as sample for the extractions and PyTar experiments.

Once processed, both ground and quartered CNS were stored in airtight containers in a cool, dark area.

Moreover, local **beech wood chips** (1-2 cm) were utilized as a lignocellulosic reference material with low extractives content (<5%).

3.2 Characterization techniques of cashew nut shells (CNS)

3.2.1 Ultimate and proximate analysis

All these analyses were conducted on milled biomass with a granulometry <1 mm.

Ultimate analysis was performed using a Vario Macro Cube Elemental analyzer according to the norm ASTM D5373 and NF EN ISO 16948 for biomass samples on fresh basis. The results were calculated on dry basis. The oxygen content was calculated by difference (Equation 3.1):

$$O\% = 100\% - \%C - \%H - \%N - \%ash \qquad \textit{Equation 3.1}$$

Proximate analysis of CNS was carried out in a muffle furnace according to NF EN ISO 18122 for ash content (%ash), NF EN ISO 18123 for volatile matter content (%volatile matter), NF EN ISO 18134-3 for moisture content (% moisture). Fixed carbon (%FC) was calculated by difference (Equation 3.2).

$$\%FC = 100\% - \%volatile\ matter - \%ash - \%moisture \qquad \textit{Equation 3.2}$$

The Lower Heating Value (LHV) of the CNS was determined using a bomb calorimeter 1108 (Parr Instrument, Parr-6200) according to the NF EN ISO 18125 standard.

3.2.2 Extractives content

The determination of extractives content in the CNS was carried out using Soxhlet extraction.

Soxhlet extraction of CNS was applied with two objectives: a) to determine the yield and composition of extractives; b) to produce extractives and solid residues for future experiments on individual CNS component.

This extraction method was inspired by DIN12602 soxhlet extraction method. It is a liquid-solid extraction that consists of a condenser, a thimble, a Soxhlet extractor with a distillation path and a round bottom flask to collect the extractives as shown in Figure 3.3. The extractions were carried out using a 34*100 mm cellulose thimble (Whatman) and with one solvent each time.

Different solvents were tested for the extraction of CNSL (hexane, ethanol, acetone, and water). The solvents used can be polar or non-polar depending on the target of the extracted compounds. Although water can also be used to extract CNSL, this method is less applied because the recovery of products via rotavapor is more difficult.

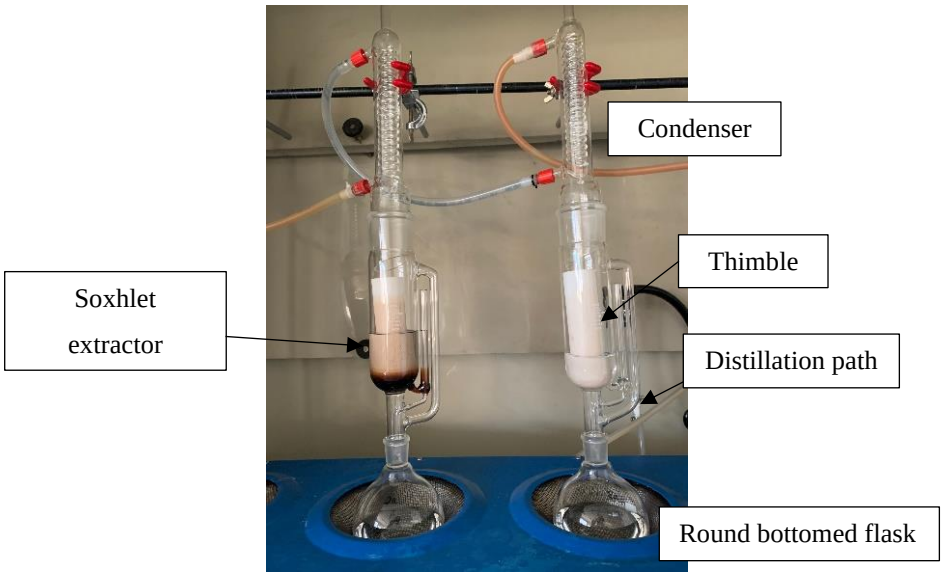

Figure 3.3: Soxhlet extraction

The protocol of Soxhlet extraction was optimized during this study and is detailed as follows.

a) Protocol of Soxhlet extraction

Before each extraction, the cellulose thimble was dried in an oven at 105°C for 6 hours. Other glassware required during the extraction such as round bottomed flask and Soxhlet extractor were also dried before each extraction. This will prevent error in establishing the mass balance.

After 6 hours, the Soxhlet extractor, the cellulose thimble and the round bottom flask were put in a desiccator to prevent humidity absorption as well as to cool the items to ambient temperature. When temperature was cooled down, the cellulose thimble along with the sample was weighed. Around 20 g of CNS were used during each extraction. The CNS were not pre-dried before extraction to avoid any decarboxylation of anacardic acids in the extractives. Some cotton was inserted into the thimble in order to prevent sample flowing out the thimble during extraction process.

For each extraction, the mass of the round bottomed flask, the cellulose thimble, the sample and the cotton were weighed. A volume of around 300 mL of solvent was then added in the round bottomed flask and the flask was weighed.

The mass fraction of extractives was calculated by measuring the weight of extractives collected in the round bottomed flask after the evaporation of solvent, and the content was calculated on dry biomass basis. The mass balance was verified for each extraction by adding the mass of solid residue and the mass of extractives, which the sum was compared to the mass of initial biomass.

b) Determination of water content

The water content in each extractive was determined by Karl Fischer method (Mettler Toledo V20) according to the ASTM E203 standard before eliminating the solvent. The program applied was PYRACE as water content in the extractives is <10%. The extractive was then evaporated using a Buchi Rotavapor at 40°C, according to the optimal pressure of evaporation of the solvent.

c) Identification and quantification of ACC constituents

After solvent elimination, the identification and the quantification of ACC constituents in the extractive were carried out using a High-Performance Liquid Chromatography coupled with UV (HPLC/UV) (Figure 3.4). The HPLC method was developed by taking into account all 12 compounds (3*4 ACC isomers) during HPLC calibration. A supelcosil LC-18 column (4.6 mm ; granulation 25 cm ; 5µm) was used to detect the ACC components.

The temperature of the column was set at 30°C. The mobile phase used was acetonitrile: water: acetic acid with a volume ratio of 80:20:1. The elution rate of the mobile phase was set at 1.80 mL/min with an injection volume of 20 µL. The absorbance was monitored at 280 nm by a UV detector. Each analysis sample was prepared by dissolving 25 mg of sample in 5 mL of acetonitrile.



Figure 3.4: High-Performance Liquid Chromatography coupled with UV

3.2.3 Determination of macromolecular composition

The macromolecular composition of biomass studied include starch, hemicelluloses, cellulose, lignin and protein contents.

a) Starch content

Van Soest method used generally to determine the lignocellulosic content in a biomass consists of a pre-washing step to remove the extractives. It includes using enzymes to remove protein and starch in the biomass. Usually, the mass of starch removed by the enzymes is neglected during the determination of lignocellulosic content. However, in this study, efforts were put to analyze all possible components in the CNS.

The starch content was therefore determined by weighing the starch removed by α-amylase, following the method suggested by Van Soest [237] before analyzing the lignocellulosic content.

b) Lignocellulosic content

The analysis of lignocellulosic content (hemicelluloses, cellulose and lignins) was carried out using Van Soest method with a Fibersac analyzer [237,238]. This method determines Neutral Detergent Fiber (NDF), Acid Detergent Fiber (ADF) and Acid Detergent Lignin (ADL). NDF is theoretically the sum of cellulose, hemicelluloses and lignins. ADF is the sum of cellulose and lignins. ADL is the organic residue obtained by 72% sulphuric acid attack on the ADF. In our study, the difference between NDF and ADF contents was used as an approximation of hemicelluloses whereas the difference between ADF and ADL contents was used an approximation of the cellulose (according to Van Soest). The lignins content was approximated by ADL content.

To summarize the protocol of the lignocellulosic analysis: the biomass sample was pretreated, by the attack of the neutral detergent solution. The insoluble residue obtained after filtration and washing was dried to constant weight. Then the residue was hydrolyzed by the acid detergent solution, filtered and washed. The residue obtained was treated with the 72% sulfuric acid solution. After filtration and washing, the residue was again dried, weighed, mineralized at 550°C then weighed.

c) Protein content

In order to determine the protein content in a biomass, the nitrogen content was first determined using Vario Macro Cube Elemental analyzer according to the norm ASTM D5373 and NF EN ISO 16948 explained in Chapter 3.2.1.

The protein content was then calculated by multiplying the nitrogen content of biomass with the nitrogen-to-protein factor (Jones's factor) of 6.25.

3.3 Thermochemical studies of biomass

Two types of reactors were used to investigate CNS thermochemical behavior.

First, a thermogravimetric analyzer (TGA) was used to investigate the pyrolysis kinetics of CNS, extractives and solid residues. It was also used to study the thermal decomposition of ACC constituents.

Secondly, a fixed bed pyrolysis and tar conversion (PyTar) reactor was used to study the products issued from the pyrolysis of CNS and their components, as well as the conversion of CNS pyrolysis gas.

3.3.1 Description and experimental procedure of thermogravimetric analyzer

A thermogravimetric analyzer (Mettler Toledo TGA 2) was used (Figure 3.5) to measure the mass loss of a sample put in an alumina crucible during heating.

To mitigate any potential limitations of internal heat and mass transfer, the CNS samples were meticulously ground and sieved through a 1 mm mesh sieve. Regarding extractives, samples were homogeneously mixed and weighed with precision using a Pasteur pipette. Less than 10 mg of samples were used for each test. These experiments were carried out using an alumina crucible of 150µL.

However, for the study of the ACC thermal degradation mechanisms, a higher sample mass (160 mg) was employed to obtain sufficient products for analysis. For this an alumina crucible of 900µL was used.



Figure 3.5: Thermogravimetric analyzer

During the thermogravimetric analyses, nitrogen was used as inert carrier gas at 40 ml/min.

The temperature program applied was as follows: (i) from 25 ◦C to 125 °C at 5 °C/min, (ii) 125 °C for 30 min (drying) ; (iii) from 125 °C to 500 °C at different heating rates, 1-25 °C/min. The lower heating rate of 1°C/min was specifically chosen to ensure a purely chemical regime by minimizing thermal gradients and allowing for more controlled and uniform reaction conditions. This careful control helps in accurately studying the intrinsic chemical reactions without interference from physical phenomena such as heat and mass transfer. In contrast, a

higher heating rate (10°C/min and 25°C/min) was used to observe the behavior under more typical, industrial-like conditions, providing a comprehensive understanding of the material's performance across different thermal scenarios.

The program called StarE Software was used for data acquisition of the sample mass. It allows to trace the TG signals (mass loss of sample) during the TG experiments as well as the dTG signals (mass loss derivative).

3.3.2 Description and experimental procedure of tar conversion reactor

The pyrolysis and tar conversion reactor (PyTar) built by BioWooEB research unit, includes 3 zones: a pyrolysis zone to generate pyrolysis gas, a cracking zone in which the conversion of pyrolysis gas occurs and a condensation system. The condensation system allows the recovery of the condensates, in the same time allowing the gas to pass through the microGC for analysis.

This reactor was already used by Milhé [106] to study the thermal and catalytic cracking of wood issued pyrolysis gas. It was slightly modified during this thesis by improving its insulation and the configuration of the condensation system (see Chapter 3.3.2.1(c)).

This reactor was used to investigate either pyrolysis alone or conversion of pyrolysis gas.

3.3.2.1 Pyrolysis and tar conversion reactor (PyTar)

The description of the pyrolysis and tar conversion reactor (PyTar) (Figure 3.6) (pyrolysis and cracking zone) and the condensation system are detailed as follows.

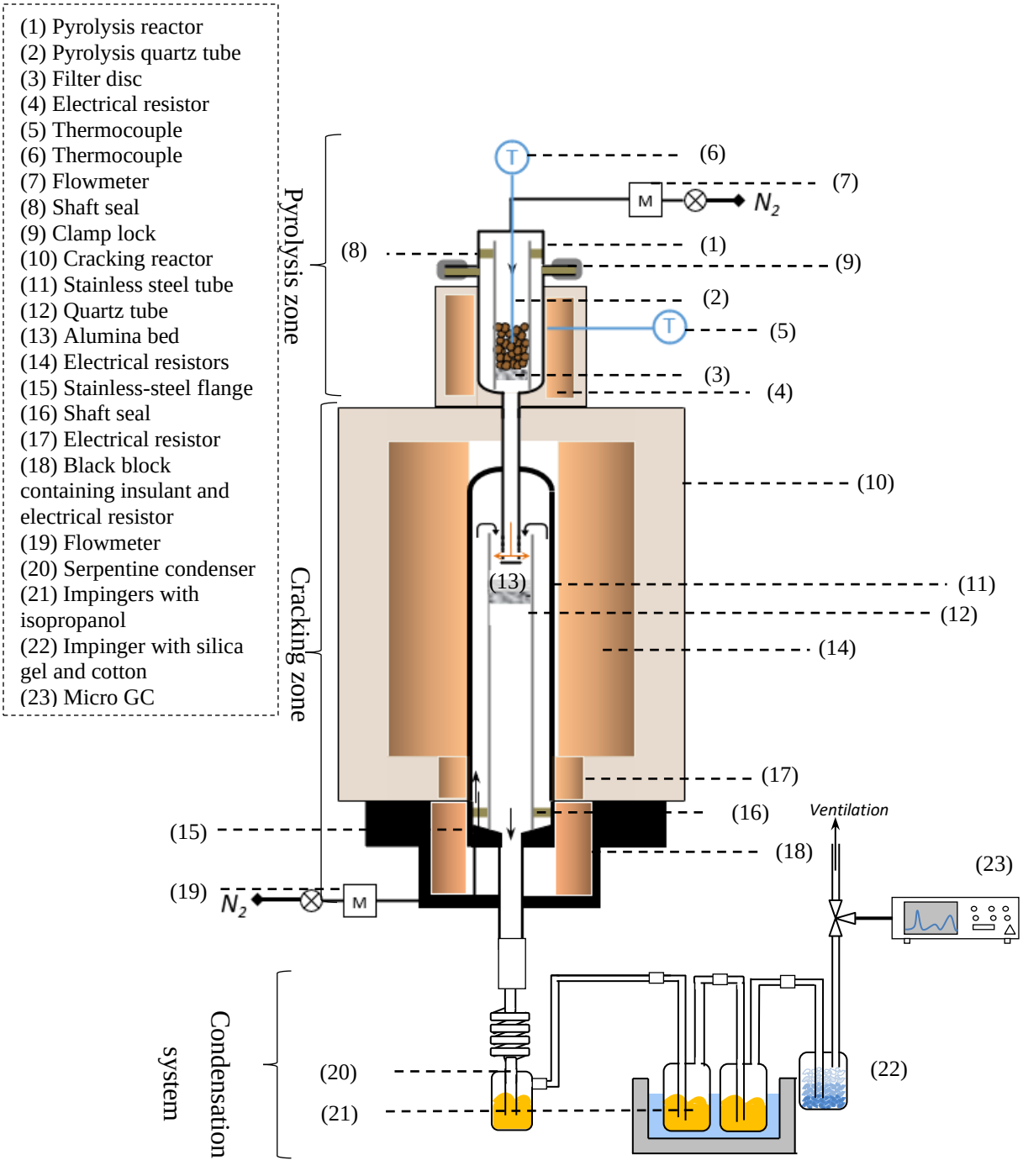

Figure 3.6: Pyrolysis and tar conversion reactor (PyTar)

a) Pyrolysis zone

The pyrolysis reactor (1) consists of a quartz tube (2) with an internal diameter of 26 mm and a height of 230 mm. The quartz tube has a filter disc (3) situated 4 cm from the end of the tube in order to place the sample. The filter disc has a porosity of 2 microns. It is enveloped by a stainless-steel tubular enclosure of 40 mm internal diameter. The quartz tube was heated to desired temperature at a fixed heating rate of 20°C/min with the help of a 500

W spiral electrical resistor (4). The average measured heating rate of the sample was at 25°C/min in the pyrolysis tube.

The heating was controlled by a regulator connected to a thermocouple (5) in contact with the pyrolysis reactor. A thermocouple (6) inserted from the top of the reactor was used to measure the temperature in the sample. The gas enters the pyrolysis reactor was controlled by a mass flowmeter Brooks 5850S (7) calibrated for a maximum flow of 500 NmL/min. To ensure that there was no leak from the pyrolysis reactor, the quartz tube was held by a shaft seal (8), whereas a lip seal and a clamp lock (9) were used to close the reactor lid.

b) Cracking zone

The cracking zone of the reactor consists in a tubular quartz tube (12) of 26 mm i.d. inserted in a 36 mm i.d. stainless steel tube (11). For pyrolysis and thermal cracking experiments, a 3 cm alumina bed (13) was put on top on the filter disc of the cracking tube in order to homogenize the atmosphere (better distribution of gases) in the tube. All the system was located in a heated oven with 10 electrical resistors (14). Tubes of different diameters can be inserted in the furnace. The residence time at the transfer line before entering the cracking zone is 0.5 s. The pyrolysis gas passes through a quartz tube which temperature was maintained at a temperature above gas condensation. The reactor rests on a removable stainless-steel flange (15) in bottom of the enclosure held by a shaft seal (16). An electrical resistor located at the bottom of the enclosure (17) makes it possible to limit the vertical temperature gradient in the reactor and guarantees an isothermal zone sufficiently long. A black block (18) containing insulant and electrical resistor set at 300°C for all experiments to ensure that there was no condensation of heavy molecules at the exit of the reactor.

A Brooks 5850S mass flow meter (19) calibrated for a maximum flow rate of 1000 NmL/min allows to inject nitrogen through the lower stainless-steel flange. The nitrogen thus injected was preheated when rising in the annular space between the stainless tube and the quartz tube. The gas flow from pyrolysis reactor then mixes with the nitrogen before entering in the conversion quartz tube.

In order to ensure a homogeneous mixture of the two gas streams, the end of the tube leading the pyrolysis gas was equipped with 4 holes of 5 mm diameter. The pyrolysis gas was thus injected horizontally into the cracking reactor. All of the gases pass through the reactor and were directed towards the condensation system.

The complete system (including the reactor system, condensation system and the microGC) is shown in Figure 3.7.



Figure 3.7: Fixed bed reactor system connected to condensation system and microGC

c) Condensation system

The gas at the outlet of the reactor passes through the condensation system. A small fraction of the gas forms condensates forms some deposits on the interior of the flange and in the cracking reactor. The mass of deposits on the cracking reactor was negligeable. The deposits on the flange could not be measured because the stainless-steel flange is too heavy to obtain a good precision of the mass.

Different configurations of condensation system were tested in order to trap at best the condensates which allows better quantification. The total amount of isopropanol used should not exceed 40 mL in order to prevent excess dilution of condensates. The

condensation system is composed of a serpentine condenser (with or without isopropanol) (20), and 2 impingers (21) connected in series in order to trap all the condensates. Both impingers were filled with some isopropanol (around 15 mL of isopropanol in each gas washing bottle). The impinger(s) were kept in a bath at -20°C to condense the majority of the heavier compounds. Then, the gas passes through a third impinger (22) filled with silica gel and some cotton to remove the last traces of water vapor, and absorb any leftover condensates. In certain operating conditions, the impinger containing silica gel and cotton trapped a high percentage of condensates, which hindered the analysis of this fraction trapped.

Thus, the different system configurations were tested (Table 3.1):

Table 3.1: Different configurations of condensation system

Configuration	**Serpentine condenser with or without isopropanol**	**2 impingers**	**3 impingers**	**Electrostatic filter (at ambient temperature)**	**Impinger with silica gel and cotton**
1	with	X			X
2	without	X			X
3	without	X		X	X
4	without		X		X

To sum up, configuration 4 turned out to trap best quantifiable condensates. Configuration 3 with electrostatic filter was not successful as the rinsing of the system with isopropanol leads to excessive dilution of the condensates, and hinders the quantification of chemical compounds.

Next to the condensation system, permanent gas was analyzed continuously throughout the experiment via microGC (23). The condensates collected were weighed and analyzed later on using HPLC and GC-MS. The char in the reactor was weighed. The analysis of the pyrolysis products is detailed in Chapter 3.5.

3.3.2.2 Experimental procedure of a typical experiment run

Experiments were carried out with CNS, ACC-free CNS, ACC, and wood, following the same experimental procedure, described below. CNS particles (diameter < 1 mm) were used for the experiments because according to pre-liminary experiments, quartered CNS hinder the repeatability of the experiments. Wood chips (1–2 cm) were also used in this study as reference biomass. Around 4.5 g of sample was used for the tests.

The masses of both ACC and ACC-free CNS samples were chosen according to their perspective concentrations in the CNS:

- Around 1.9 g of ACC (liquid) was placed in a crucible centered in the pyrolysis reactor;
- Around 2.6 g of ACC free CNS.

Each experiment was repeated at least 3 times to obtain the average yields.

The different steps of an experiment were:

- Setting the cooling bath at -20°C, which takes around 2.5-3 hrs;
- Heating the cracking zone at desired temperature (400-900°C at 50°C/min);
- Weighing the condensation system (serpentine condenser and gas impingers).
- Putting the sample in the pyrolysis reactor.
- Flushing the reactor with nitrogen to ensure an inert atmosphere. This process takes around 15-30 minutes.
- Starting the data acquisition of the microGC.
- Starting the data acquisition of the temperature and the gas flow rates.
- Setting the temperature in the pyrolysis reactor to the desired temperature (400-500 °C).

Pressure drop through the reactor was measured with a manometer, in order to check the absence of plugging.

The end of the experiment was defined when no gas production was measured. A criterion was chosen in which all gas concentration (except N_2) should be below 1/100 of their maximum value during the test.

At the end of the experiment the system was cooled down under a nitrogen flow.

The condensation system was then taken out from the system to be weighed. The condensates were mixed and collected from the different glassware (serpentine condenser, impingers). If

there were stubborn deposits on the glassware, acetone was used to rinse and to recover the condensates. The mass of acetone was weighed.

Char was taken out and weighed in order to measure the mass of char.

The tube in the cracking reactor and the pyrolysis tube was cleaned using an air supplied muffle oven at 700°C after each experiment.

3.3.2.3 Repeatability and precautions of experiments

There are several precautions that must be taken during each experiment:

1. The homogeneity of biomass is improved by using smaller granulometry of biomass.
2. A leak test is carried out by measuring the flow rate using a mobile flowmeter as well as checking the gas composition when flushing the system with nitrogen.
3. The leap seal of the pyrolysis reactor, the shaft seals that holds the pyrolysis tube and the cracking tube, the o-ring seal in between the flange and the cracking tube have to be replaced once there is a slight loose contact.
4. The reconditioning and recalibration of microGC have to be carried out once the peaks in the chromatogram start to get closer to each other.
5. The identification of ACC compounds in the condensates are verified not only with the elution time of chemical compounds, but also compared with the peak spectra of the standards.

Despite the numerous precautions taken, it was not possible to calculate a precise uncertainty value. Thus, several repetitions were carried out for an experiment in which the errors observed were generally less than 5%. A higher error was observed especially when increasing the reaction temperature.

3.4 Analysis of pyrolysis/cracking products

3.4.1 Permanent gas

Permanent gas was continuously injected and analyzed by a microGC (VARIAN CP 4900) during each pyrolysis experiment. The system was equipped with two columns (MolSieve 5Å and PoraplotQ) which used different carrier gas. The MolSieve 5Å column allowed the measurement of CO, N_2, O_2, H_2, CH_4 using argon as the carrier gas whereas the PoraplotQ column measured CO_2, CH_4, C_2H_6, C_2H_4, and C_2H_2 using helium as the carrier gas. It allows to sample the flow of dry gases approximately every 80 seconds.

The volume percentage of the gases was thus determined during each experiment. Mass flow rate of each permanent gas will be detailed in Chapter 3.5.

3.4.2 Condensates

The composition of condensates was divided into 3 fractions: water, tar and ACC constituents. ACC constituents were distinguished from tars as they are specific components of the CNS.

3.4.2.1 Water content

Water content in the condensates was measured using the Karl Fischer method (Mettler Toledo V20) according to the ASTM E203 standard. As the condensates were trapped in isopropanol, a different titration solvent was used (Hydranal composite 5) and a different analysis method was applied in the apparatus program (PYR). 3 repetitions were carried out to determine the mass fraction of water present in the condensates. The presented values were the average of the three results. The fraction of water in the condensates ω_{H2O} was calculated with Equation 3.3.

$$\omega_{H_2O}(g/g\ condensates) = \%_{H_2O} \times m_{condensates} \qquad \textit{Equation 3.3}$$

3.4.2.2 Tar composition

Tars were analyzed by an Agilent 6980 gas chromatograph (Agilent DB1701 capillary column of dimension 60 m* 0.25mm* 0.25µm), coupled to a mass spectrometer (Agilent 5975) (GC-MS). Helium was used as a carrier gas with a constant flow rate of 1.9 mL/min.

The database contains the calibration of 85 compounds. The analyzes were carried out according to 2 modes, split and splitless. For split mode, a 10:1 ratio was applied with a first rise in temperature from 45°C to 120°C at 3°C/min then up to 270°C at 20°C/min. A similar temperature rise program was applied in splitless mode, with a dwell time of 60 minutes at 270°C.

The transfer line was maintained at 270°C. The acquisition of the mass spectrum was done by a quadrupole with an ionization energy of 70eV. The temperature of the quadrupole was 150°C and that of the ion source of 230°C. For the preparation of the samples, the condensates collected after each pyrolysis experiment were stored in the fridge at 5°C, then filtered using a 45µm micro-filter Milex-Gx), and mixed with the internal standards. 1 mL of condensates was mixed with 100 µL of internal standard solution. In some cases, when the tar concentration is high, condensates had to be diluted. In this case, the condensates were diluted by 10 (100 µL of internal standard solution, 900 µL of acetone and 100 µL of condensates).

For identification, the mass spectrum of the unknown compound was compared with the base of NIST data. The comparison was performed in full scan mode, including all ions with a mass/charge ratio (m/z) between 35 and 500. Quantification was performed in SIM mode (Selected Ion Monitoring) from the majority ion of each compound, which increases the sensitivity compared to full scan mode.

The different tars analyzed by GC-MS during this study are presented in the Appendices A3.2.

3.4.2.3 ACC composition

ACC in the condensates were analyzed using the same HPLC method stated in Chapter 3.2.2. However, as the condensates did not contain only ACC compounds, a supplementary step was required during the determination of ACC compounds in the chromatogram. The peak spectra of each ACC isomers detected were verified to the ones of standards.

3.5 Definitions and calculations

a) Char yield

A known mass of sample, m_{sample}, was introduced into the reactor before each experiment. The amount of residual char in the reactor m_{char} was determined by weighing at the end of the experiment, once the reactor has cooled. Char yield η_{char} was calculated using Equation 3.4:

$$\eta_{char} = \frac{m_{char}}{m_{sample}} \qquad \textit{Equation 3.4}$$

In the case of PyTar reactor experiments, coke deposits on the inside wall of the cracking reactor were not taken into account because they are negligible under our operating conditions (< 2 mg).

b) Permanent gas flow rate and yield

During the experiments, the flow of gases produced varied over the duration experiments. At each analysis of the microGC, the molar concentration of each gas [i](t) at the outlet of the reactor was known. Since the nitrogen flow was constant, it was used as a tracer to determine the molar flow Qi(t) of each gas analyzed according to Equation 3.5:

$$\dot{Q}_i = \sum_i \frac{\dot{Q}_{N_2}}{y_i} \qquad \textit{Equation 3.5}$$

Q_{gaz}: flow rate of gas

$\dot{Q}_{N_2}$: flow rate of nitrogen gas

y_i : mass fraction of gas i in the pyrolysis gas

The sampling frequency of the microGC depends on the time required for method equilibration before each analysis (around 80 seconds). As we only had access to the concentration values at given times, we suppose that $[i]$ varies linearly between two analyses. The mass of each gas i produced during an experiment, m_i, was then calculated by integrating the instantaneous flow rate values obtained according to the trapezium method (Equation 3.6):

$$m_i = M_i \left[\sum_{t_1}^{t_f} Q_i(t_n)(t_{n-1}) - \frac{[Q_i(t_n)-Q_i(t_{n-1})]\times(t_n-t_{n-1})}{2}\right] \qquad \textit{Equation 3.6}$$

Where M_i is the molar mass of gas i and t_f is the duration of an experiment.

The overall yield of permanent gases η_{gas} was finally obtained according to equation 3.7:

$$\eta_{gas} = \frac{\sum m_i}{m_{sample}} \qquad \textit{Equation 3.7}$$

c) <u>Condensates yield</u>

Condensates were collected by the condensation system during sampling, weighed and analyzed in the lab in order to quantify tar, water and ACC contents. The condensates yield $\eta_{condensates}$ was calculated as follows (Equation 3.8).

$$\eta_{condensates} = \frac{m_{condensates}}{m_{sample}} \qquad \textit{Equation 3.8}$$

The mass of the condensates was determined by difference with the mass of char and permanent gas (Equation 3.9). This is because a higher error was observed in the weighing of condensates in the condensation system (impingers and serpentine condenser) between the repetitions. Moreover, some condensates deposits in the reactor could not be measured (i.e. deposits on the exit flange of the reactor).

$$m_{condensates} = m_{sample} - m_{gas} - m_{char} \qquad \textit{Equation 3.9}$$

Note that additional definitions and calculations will be introduced and detailed in Chapter 4-6.

CHAPTER 4

Cashew nut shells composition: Development of analytical methods and study of CNS composition

4. Cashew nut shells composition: Development of analytical methods and study of CNS composition

Reviewing the literature reveals gaps in the composition of cashew nut shells (CNS), particularly concerning the extractives. Most existing studies have focused predominantly on the lignocellulosic content (hemicelluloses, cellulose, and lignin), with little attention given to other constituents such as proteins, tannins, and other extractives. Moreover, there is no established standard method for the extraction of CNS extractives, nor is there a specific analytical method to identify and quantify all isomers of anacardic acid (ACC), cardanol, and cardol—the key constituents of CNSL.

Improving the analysis of CNS composition is crucial to better understand the influence of extractive content on the thermochemical behavior of CNS. Therefore, this chapter encompasses various aspects of the characterization of cashew nut shells.

This chapter begins by presenting the chemical properties of cashew nut shells, covering proximate and ultimate analysis, lignocellulosic, protein, starch, extractives and tannin content.

The analysis of the extractives in the CNS is divided into several sections. The first part consists of the optimization of extraction method for ACC recovery. This is followed by the development of multiple solvent extraction method for determination of extractives content in the CNS. Finally, the third section details the development of a HPLC method for quantifying all 12 ACC isomers with varying degrees of unsaturation. Together, these studies provide a comprehensive understanding of the physico-chemical properties of CNSL and the extractives content of CNS.

This chapter ends with a summary on the composition of cashew nut shells.

4.1 CNS proximate and ultimate analysis

The proximate and ultimate analysis of cashew nut shells is shown in Table 4.1. All analyses were carried out using milled CNS (<1 mm), with at least two replicates.

Table 4.1 : Proximate and ultimate analysis of cashew nut shells

	Parameters	
Proximate (dry basis, db)	Humidity (%)	6.19
	Ash (% db)	2.21
	Volatile matter (% db)	82.95
	Fixed carbon (% db)*	14.84
*Calculated by difference : Fixed carbon(%) =100%-Humidity(%)-Ash(%)-Volatile matter(%)		
Ultimate (dry ash free basis, daf)	H (% daf)	6.24
	C (% daf)	56.07
	N (% daf)	0.39
	O (% daf) **	37.30
**Calculated by difference : O%=100%-H%-C%-N%		
	LHV on anhydrous (MJ/kg)	23.60

Since the water content in CNS received is low, drying is not required prior any thermochemical conversion process. When compared to wood chips (1.2%) [239], the ash content of CNS is slightly higher.

The LHV of CNS is higher than the LHV of classical woody biomass. It is due to the presence of CNSL which has a high calorific value (36 MJ/kg).

The volatile matter content of CNS is similar to that of the wood chips (83.7%) regardless of the high extractives content (around 40%) [239].

The elemental composition of CNS showed higher carbon content (56%) than the wood (49%) [239]. The difference of the carbon content was offset by the oxygen content. Hydrogen and nitrogen content were similar for wood chips (7.2% and 0.1% respectively) [239] and CNS (6.24% and 0.36% respectively).

4.2 Molecular composition of CNS

In this section, the lignocellulosic, proteins, starch, extractives and tannin contents of CNS are presented.

4.2.1 Lignocellulosic content

The hemicelluloses, cellulose and lignins contents of cashew nut shells are shown in Table 4.2.

Table 4.2: Hemicelluloses, cellulose and lignins content of cashew nut shells (%db)

	Hemicelluloses	**Cellulose**	**Lignins**
Lignocellulosic content (%db)	8	14	5

A comparison of lignocellulosic content with other studies is challenging, as the methods used for analysis are generally not standardized or consistent across studies. For instance, the values from Melzer et al. [6,10] cannot be compared as the extraction procedures were different. In his study, water and petroleum ether extractions were carried out to eliminate the extractives before carrying out the lignocellulosic content analysis. Whereas, in our study, neutral detergent solution was used to eliminate the extractives before the analysis.

Among the literature, the values obtained in this work (hemicelluloses, cellulose and lignins content) are only in agreement with those obtained by Ocheja et al. [179] who used the same Van Soest method.

4.2.2 Protein and starch content

Proteins, which are found in seed biomass, have a variety of enzymatic, structural and functional roles in the seed cell (photosynthesis, biosynthesis, transport, immunity, etc.) [240]. They are macromolecules of different nitrogen containing amino acids. They are characterized by both an acid group (carboxylic -COOH) and an amine group ($-NH_2$) [241].

Starch is a natural energy reserve of polysaccharides in plants which is mainly composed of two glucose polymers, which are amylose and amylopectin. The distribution of these two polymers depends on the biomass species [10]. Starch is highly volatile (about 90%) and consists, depending on the amylose/amylopectin ratio, of around 53% C, 6% H and 38% O [10].

Starch and protein contents in the CNS measured in this study were quite low, about 2 wt% for each, compared to those in the cashew kernel, respectively, 60.7 wt% [242], and 21.3 wt%

[243]. Their content is negligeable when compared to the extractives content extracted during the lignocellulosic content analysis.

4.2.3 Extractives content

The first step of the characterization study consists of the optimization of extraction method for ACC constituents recovery. Then, the development of multiple solvent extraction method for determination of extractives content in the CNS was detailed. The section is followed by the description on the development of HPLC method to quantify all 12 ACC isomers of different degrees of unsaturation. The last section presents the extractives content in the CNS.

4.2.3.1 Optimization of extraction method for ACC recovery

The main objective of this part of the study is to optimize the extraction of pure ACC, allowing for precise determination of their composition in the CNS. The optimization process began by selecting the most suitable solvent for ACC extraction which gives the optimal yield. After identifying the optimal solvent, further optimization was performed through parametric testing, which involved varying factors such as the biomass granulometry and extraction duration. To ensure the reliability of the results, each extraction was conducted at least twice, ensuring repeatability and consistency in the results.

a) Optimal solvent for ACC extraction

Table 4.3 presents the yield of extractives obtained with different solvents over the extraction times for a single extraction. The solvents used included water (extracted over 24 hours), acetone (extracted over 6 hours), hexane (extracted over 6 hours), and ethanol (extracted over 6 hours). The extractives yield, expressed as weight percent (%wt), depends on the solvent and extraction duration.

Table 4.3 Extractives yield with single solvent extraction (wt%)

	Water 24 h	**Acetone 6 h**	**Hexane 6 h**	**Ethanol 6 h**
Extractives yield (wt%)	26.9	41.4	43.7	32.3

The results show that the choice of solvent influences the yield of extractives obtained from the sample. Hexane and acetone exhibit higher efficiency in extracting extractives compared to water and ethanol within the same duration of 6 hours. Hexane, a nonpolar solvent,

demonstrates the highest extraction yield (43.7%), followed closely by acetone (41.4%). Ethanol, a polar solvent, achieves a moderate extraction yield (32.3%), while water, also polar but less aggressive, produces the lowest yield over a longer extraction time (26.9%).

Although hexane exhibits the highest yield, acetone was chosen due to its versatility in dissolving both polar and nonpolar compounds. The higher volatility of acetone compared to hexane makes it easier to evaporate using a rotavapor, reducing the risk of overheating the extractives in the round-bottomed flask during recovery. This is particularly important because anacardic acids are thermolabile and degrade easily when exposed to excessive heat.

Thus, in the following studies, only acetone was used to study the influence of granulometry and extraction duration on the extractive yield.

b) Influence of granulometry on extractive yield

The extractions were carried out over a duration of 12 h on both milled cashew nut shells and quartered cashew nut shells, using acetone as solvent. The extractive yields of cashew nut shells with different granulometry are presented in Table 4.4.

Table 4.4: Influence of cashew nut shells granulometry on extractives yield (%)

	Extraction duration	**Solid residue (%)**	**Extractive (%)**	**Sum (extractive and solid residue) (%)**	**Water content (%)**
Milled cashew nut shells	12 h	57.0	44.5	101.5	0.77
Quartered cashew nut shells	12 h	70.0	33.0	103.0	0.66
No biomass	12 h	-	-	-	0.33

Milled cashew nut shells yield a higher percentage of extractives (44.5%) compared to quartered shells (33%). The difference can be attributed to a better accessibility of the solvent to the solid matrix of the shells when milled. Both cases resulted in a sum slightly above 100%, which could be due to experimental uncertainties (variations in solvent evaporation).

When comparing table 4.4 to 4.3, it is also observed that an extraction of 12 h produces a higher yield than a 6-h period for milled cashew nut shells.

For the extraction without biomass, it is observed that 0.33% of water content is attributable to the acetone solvent.

c) Influence of extraction duration on extractive yield

To study the influence of extraction duration on extractives yields, extractions were performed on quartered cashew nut shells with durations of 30 and 50 hours. Table 4.5 presents the results of the extraction of quartered cashew nut shells with varying extraction duration.

Table 4.5: Influence of extraction duration on extractives yield (%)

	Extraction duration	**Solid residue (%)**	**Extractives (%)**	**Sum (extractives and solid residue) (%)**	**Water content (%)**
Quartered cashew nut shells	30 h	62.5	33.5	96.0	0.64
	50 h	68.0	34.0	102.0	0.78

The percentage of extractives remains relatively consistent at around 33.5% to 34.0% across the different extraction durations (30 hours and 50 hours) when compared to the yield at 12 h extraction duration (33.0%) (Table 4.4). This indicates that the extraction process reaches a plateau at around 12 h, after which further extraction time does not increase the yield of extractives.

From the results above, it is concluded that an extraction duration of 12 h with acetone as solvent is optimal in terms of cashew nut shell extractives quantity.

4.2.3.2 Development of multiple solvent extraction method for determination of extractives content in the CNS

The extractives removed during the pre-washing step of Van Soest method contained components beyond CNSL, starch and protein. This was confirmed by the non-closed mass balance: CNSL yield using acetone as solvent : 41.4 wt% ; lignocellulosic contents: 27 wt% ; starch: 2 wt% ; and proteins: 2 wt%.

As a result, 28 wt% were unidentified components in the CNS.

Therefore, a multiple-solvent extraction method was developed to enhance the recovery of extractives from the CNS.

The extraction process began with the use of a polar organic solvent, acetone, identified as the optimal solvent for CNSL extraction. Following this, a non-polar organic solvent, hexane, was employed to remove any remaining fatty materials from the biomass. Finally, to extract any residual components, water, a highly polar solvent, was used as the last step in the extraction process.

The extraction duration for acetone and hexane was set to 12 h as this was found to be optimal. However, for water extraction, the duration was doubled (24 h) because water is significantly less volatile than acetone and hexane.

The same Soxhlet protocol extraction was carried out. However, between each extraction, in order to carry out this multiple solvent extraction, the solid residue had to be dried until constant mass in an oven to remove the remaining solvent. The oven temperature was set according to boiling temperature of the solvent used (60°C for acetone and hexane extractions; 100°C for water extraction). The dried solid residue was weighed each time and used for the following extraction. The extractive was collected in a round bottomed-flask at the end of the extraction.

The extraction process is summarized in Figure 4.1. Acetone, hexane and water extractives were obtained through this successive triple solvent extraction. The solid fractions resulting from each extraction are generally named ACC-free CNS, de-oiled CNS and extractive-free CNS.

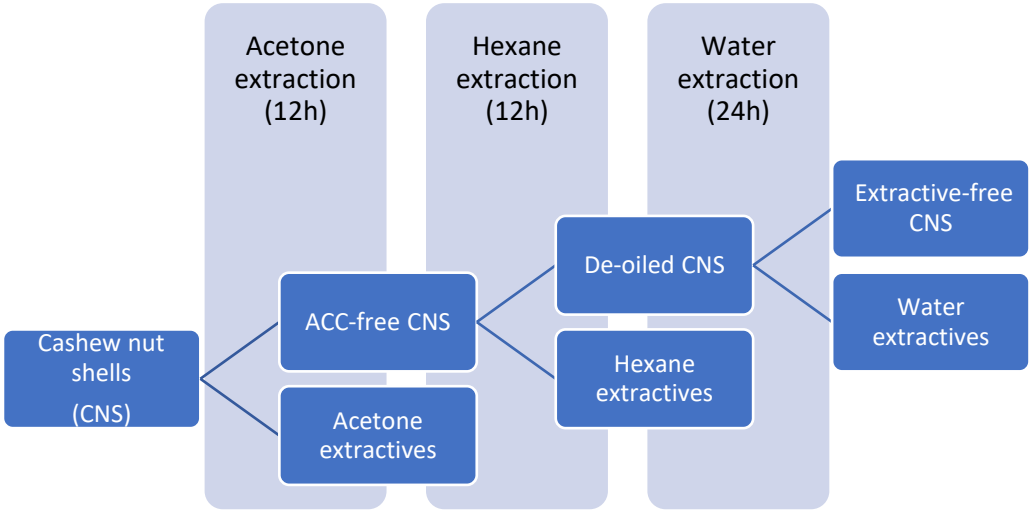

Figure 4.1: Successive triple solvent extraction process

4.2.3.3 Development of HPLC method for ACC quantification

The objective of this study was to develop an analytical method to accurately quantify all ACC isomers present in the extractives of CNS. The ability to quantify these ACC isomers enables a detailed investigation into the behavior and evolution of each isomer during the thermal degradation of CNS.

Previous studies conducted at CIRAD indicated that approximately 70 wt% of CNSL was composed of unknown constituents. However, two more recent studies [174,175] achieved higher detection rates using HPLC, with 93-95% of the ACC identified in the CNSL.

The standards initially available in our lab included anacardic acid 15:0, 15:3, cardanol, and cardol. However, these standards did not fully represent the complete CNSL constituents, as they accounted for only 4 out of the 12 ACC isomer standards needed for comprehensive analysis.

Using the calibration curve of a single isomer cannot accurately represent other isomers. Oiram Filho et al. showed that the calibration curves are specific to each unsaturated compound, as shown in Figure 4.2 for anacardic acids [173]. Thus, to quantify all 12 isomers, it is necessary to use all 12 to calibrate the HPLC method.

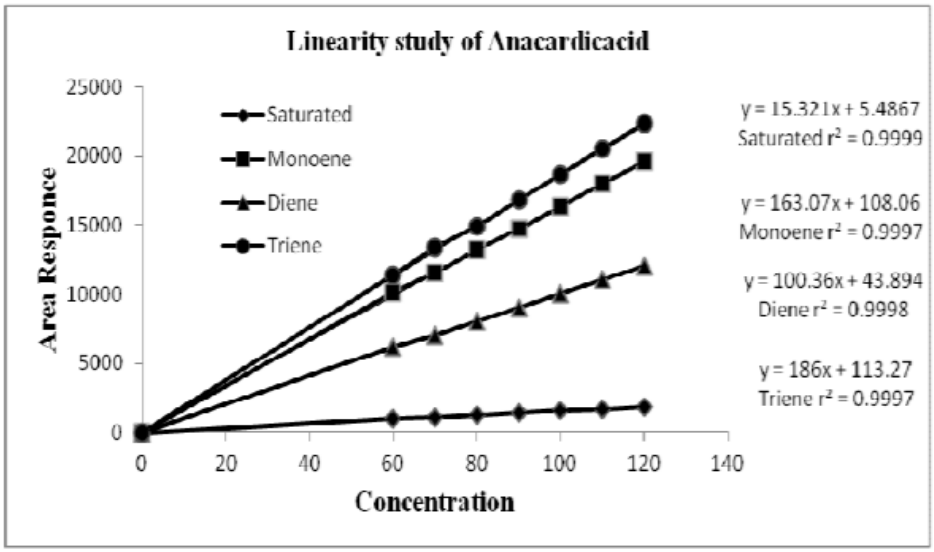

Figure 4.2: Calibration curve of anacardic acids 15:0, 15:1, 15:2, et 15:3.

Therefore, HPLC calibration was carried out with the whole standards (12 ACC isomers in total) [235]. The standards were purchased from Bertin Technologies and Sigma Aldrich. The

calibration ranges were prepared with mono-compound solutions ranging from 0.025 to 0.5 mg/L [235].

The detailed protocol of this HPLC method is presented in Chapter 3.2.2. The HPLC chromatogram of the mixture of these 12 ACC isomers is depicted in Figure 4.3.

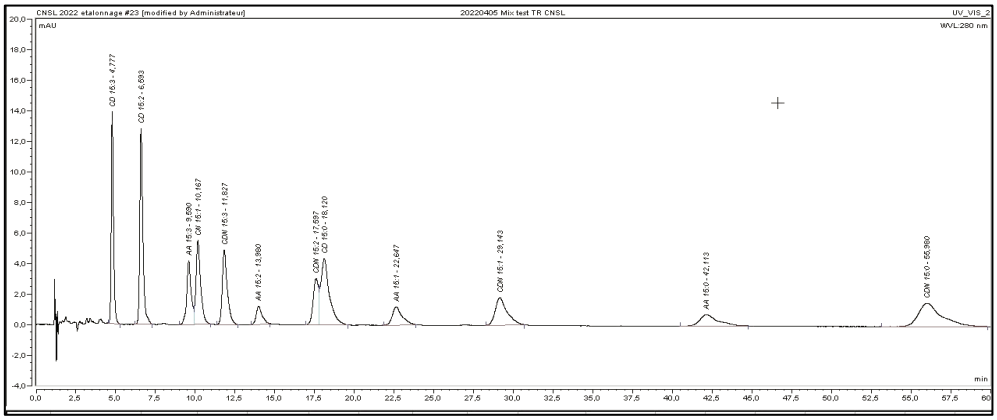

Figure 4.3: HPLC chromatogram of the mixture of 12 ACC isomers

From Figure 4.3, it is observed that all ACC isomers were separated from each other except in the case of Anacardic acid 15:3 and Cardol 15:1 as well as Cardanol 15:2 and Cardol 15:0, where peaks elution were observed. Despite the peaks coelution, they did not hinder the quantification of pyrolysis condensates because the peaks were finely separated from each other. Table 4.6 shows the retention time of the 12 ACC isomers.

Table 4.6: Retention times of all ACC isomers (min)

Chemical compound	**Retention time (min)**
Cardol 15 :3	4.7
Cardol 15 :2	6.6
Anacardic acid 15 :3	9.6
Cardol 15 :1	10.2
Cardanol 15 :3	11.9
Anacardic acid 15 :2	14.1
Cardanol 15 :2	17.7
Cardol 15 :0	18.2
Anacardic acid 15 :1	22.8
Cardanol 15 :1	29.3
Anacardic acid 15 :0	42.4
Cardanol 15 :0	56.1

It is observed that with the LC18 column, in the case of anacardic acid, cardanol and cardol isomers, the peak retention time in chromatography is influenced by the degree of unsaturation in the molecule. The more unsaturated compounds have a shorter retention time than a less unsaturated compound. This is because unsaturated compounds are less polar and they tend to elute faster in reversed-phase chromatography. Therefore, increase unsaturation decreases retention time.

Apart from the retention time, the UV spectrum (Figure 4.4 and 4.5) of the ACC isomers peak is a supplementary indicator to confirm the identification as in some condensates, there could be presence of other chemical compounds near the retention peak of a certain isomer. In general, anacardic acids, cardanols and cardols isomers have each distinctive peak spectrum. However, among the same group of isomers (e.g. Anacardic acid 15:3, 15:2, 15:1 and 15:0) (Figure 4.4), all isomers share the same maximum absorbance.

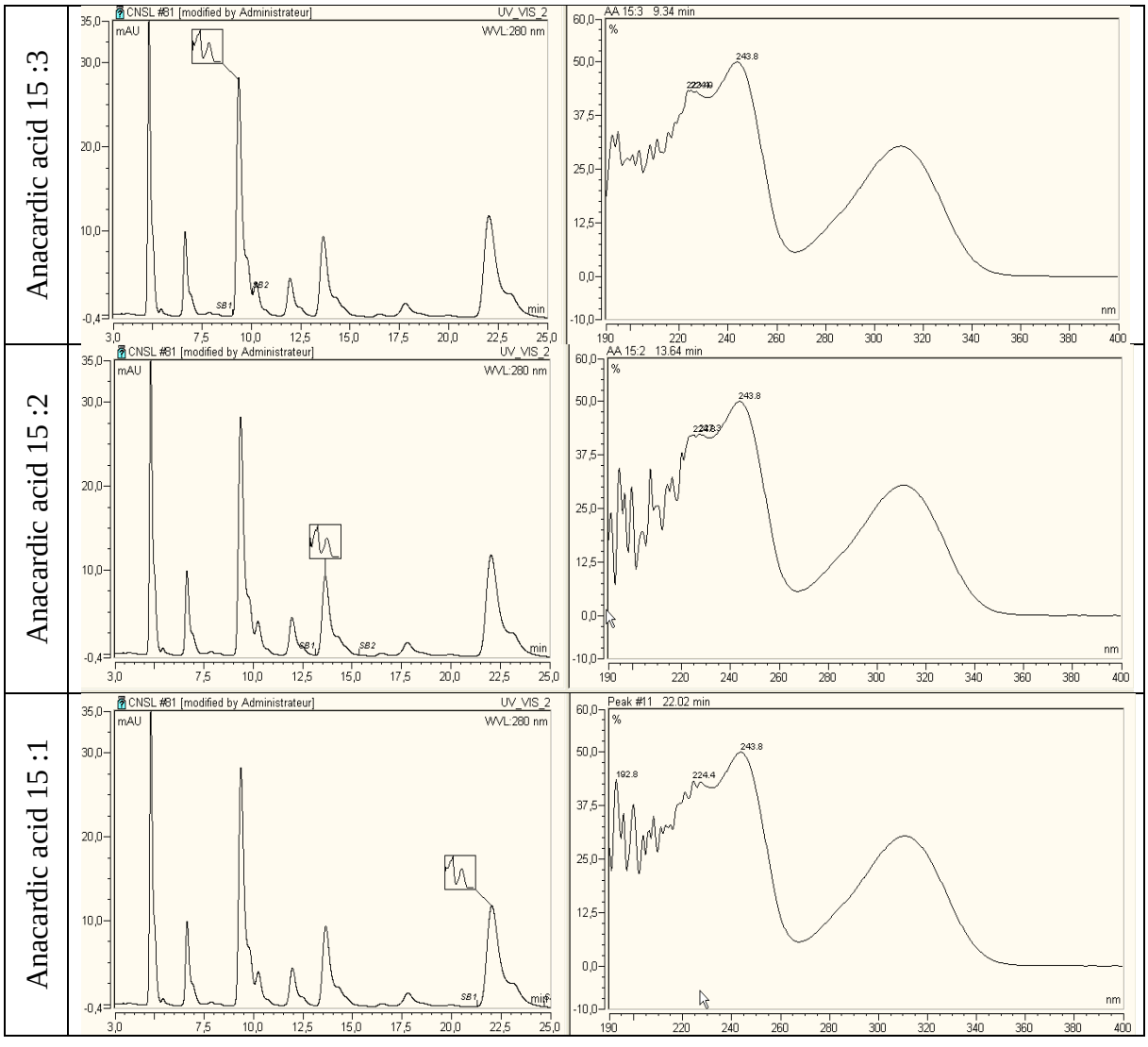

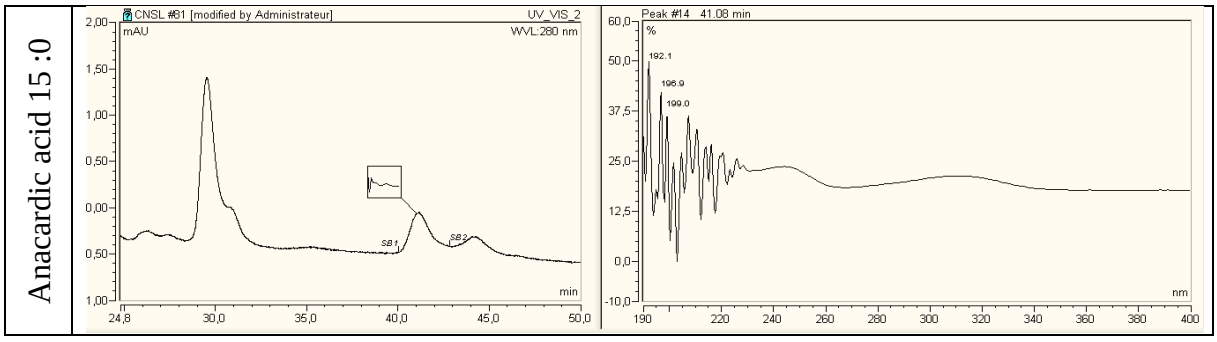

Figure 4.4: Chromatogram (left) and spectra (right) of anacardic acid isomers (Anacardic acid 15:3, 15:2, 15:1 and 15:0)

From Figure 4.4, two main peaks are observed. The first main peak is situated around 243.5-243.8 nm for all anacardic acids isomers. In the case of anacardic acid 15:0, the amplitude of the first peak is weaker than other anacardic acid isomers. This is because there is less anacardic acid 15:0 in the extractives. The second peak of the spectrum distinguishes anacardic acids easily from cardanols and cardols because it is situated at 310 nm, whereas cardanols and cardols both have the second peak at around 274 nm (Figure 4.5).

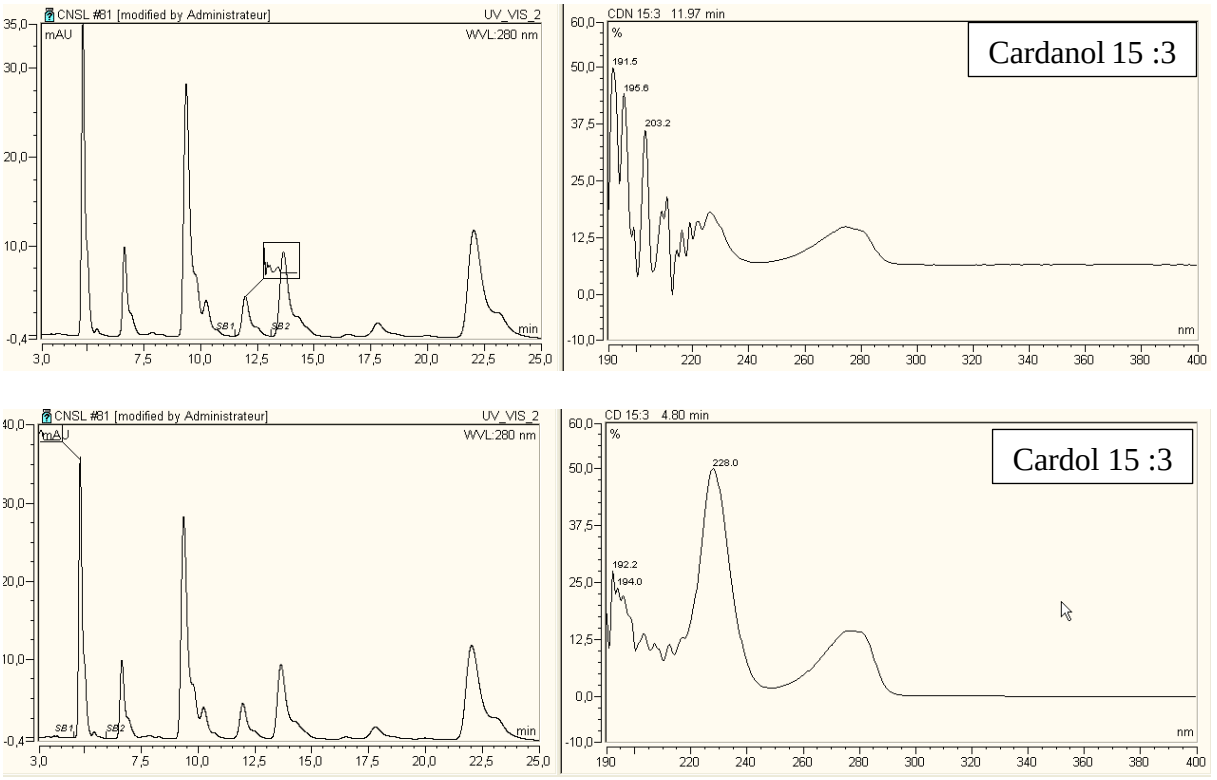

Figure 4.5: Chromatograms and spectra of cardanol 15:3 and cardol 15:3

The main difference of the spectra of cardanol and cardol isomers is the first main peak in the spectra (Figure 4.5). Cardol isomers has a first main peak at 227.5 nm whereas cardanol isomers

has a peak at the same temperature but with a much weaker amplitude. Both cardanol and cardol isomers have an absorbance peak at 276 nm.

With the peak spectra, it helps to confirm the presence of ACC isomers in the sample, giving more affirmation to the results obtained.

4.2.3.4 Determination of extractives content in CNS

The application of successive triple solvent extraction method made it possible to obtain the yields of different extractives.

Based on the replicates, the mass percentages of each extractive in the CNS were :

- 41-43% for acetone extractives
- 2.1-2.6% for hexane extractives
- 16-19 % for water extractives

The yield of solid residue obtained was 42.7–42.9%. This resulted in a total mass balance in the range 102-107%. The total mass balance surpassed 100% because the solvent extraction was not totally completed. It is impossible to remove all solvent in the solid residue after each extraction as the ACC constituents risk being decarboxylated. Water as extraction solvent is also difficult to evaporate completely even with very low pression. This is because water creates easily hydrogen bonds which are hard to break.

The acetone extractives were dark brown and viscous, whereas the hexane extractives were light yellow and less viscous. The water extractives after solvent evaporation presented as solid brown residues. The presence of foam-like product during the solvent evaporation (water) suggests the possible presence of tannins among the water extractives.

All these three extractives were analyzed by HPLC using the novel method developed, in order to identify and quantify the 12 chemical compounds of the ACC. ACC were only detected in the acetone and hexane extractives. No ACC were detected in the water extractives. Figure 4.6 and 4.7 show the HPLC chromatogram of acetone and hexane extractives respectively.

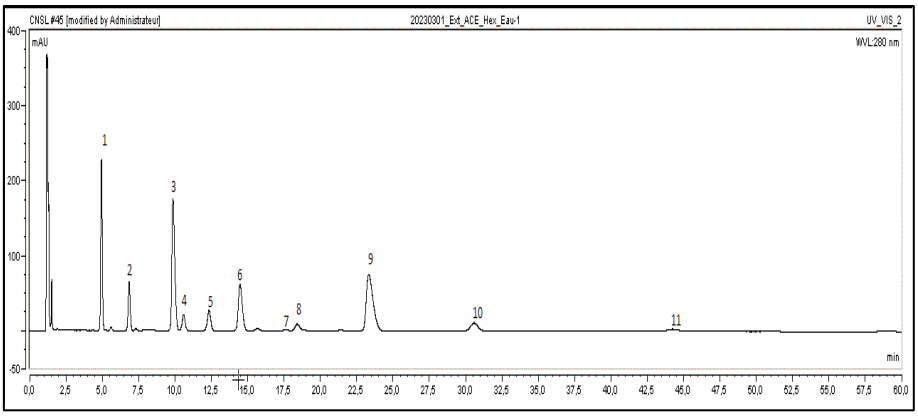

Figure 4.6: HPLC chromatogram of acetone extractives (1: Cardol 15:3, 2: Cardol 15:2, 3: Anacardic acid 15:3, 4: Cardol 15:1, 5: Cardanol 15:3, 6:Anacardic acid 15:2, 7: Cardanol 15:2, 8: Cardol 15:0, 9: Anacardic acid 15:1, 10: Cardanol 15:1, 11: Anacardic acid 15:0)

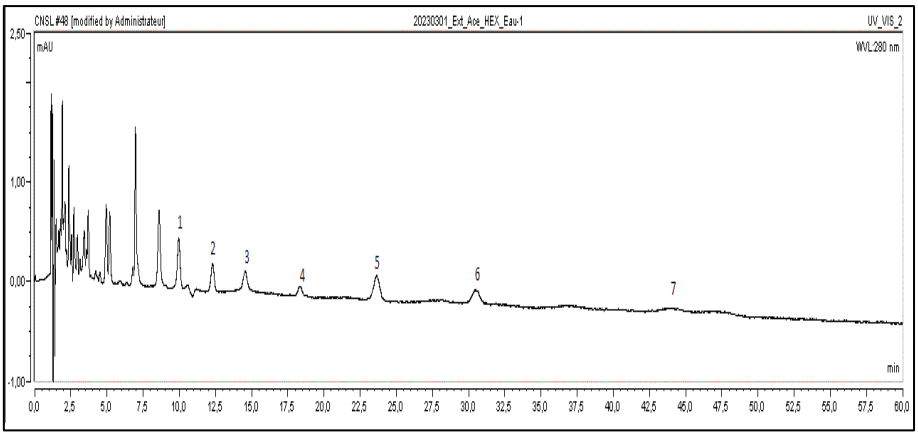

Figure 4.7: HPLC chromatogram of hexane extractives (1: Anacardic acid 15:3, 2: Cardanol 15:3, 3:Anacardic acid 15:2, 4: Cardol 15:0, 5: Anacardic acid 15:1, 6: Cardanol 15:1, 7: Anacardic acid 15:0)

In terms of quality, in the acetone extractives (Figure 4.6), all ACC isomers were present except for Cardanol 15:0, which its quantity was below the limit of quantification.

In the case of hexane extractives (Figure 4.7), there are less ACC isomers, only 7 out of 12 isomers: Anacardic acid 15:3, Cardanol 15:3, Anacardic acid 15:2, Cardol 15:0, Anacardic acid 15:1, Cardanol 15:1, and Anacardic acid 15:0.

The percentage of ACC in the extractives was then quantified using the calibration curves. 99% of the total ACC was found in the acetone extractives, less than 1% was detected in the hexane extractives.

A total of 94 wt% of the acetone extractives consisted of ACC, accounting for 39.84 wt% of the total weight of the CNS. The remaining 6% of the acetone extractives could not be analyzed,

but it is suspected to be 2-methylcardol or other minor compounds. In contrast, 3.4 wt% of the hexane extractives were identified as ACC, representing only 0.08 wt% of the CNS weight. The unidentified components in the hexane extractives are likely to be lipids.

The detailed yields of each unsaturated compounds are given in Table 4.7.

Table 4.7: Distribution of ACC constituents in acetone extractives (wt%)

Compounds	Percentage (wt%)
Anacardic acid 15:0	2.56
Anacardic acid 15:1	29.06
Anacardic acid 15:2	22.65
Anacardic acid 15:3	21.15
Cardanol 15:0	0
Cardanol 15:1	3.42
Cardanol 15:2	0.43
Cardanol 15:3	3.42
Cardol 15:0	1.92
Cardol 15:1	2.78
Cardol 15:2	2.99
Cardol 15:3	9.62

According to this table 4.7, anacardic acids were the most abundant of the three main constituents detected (75.4%) in the acetone extractives, around 10 times more than cardanols (7.3%) and 4 times more than cardols (17.3%). The monoene anacardic acid (15:1) represented the highest yield among the different anacardic acid isomers. The saturated forms of anacardic acid, cardanol and cardol were less present in the acetone extractives.

The proximate and ultimate analysis of acetone extractives was carried out and presented in Table 4.8.

Table 4.8 : Proximate and ultimate analysis of acetone extractives

	Parameters	
Proximate (dry basis, db)	Humidity (%)	0.54
	Ash (% db)	1.55
	Volatile matter (% db)	98.8
Ultimate (dry ash free basis, daf)	H (% daf)	9.30
	C (% daf)	72.15
	N (% daf)	0.29
	O (% daf) **	18.26
	**Calculated by difference : O%=100%-H%-C%-N%	
	LHV on anhydrous (MJ/kg)	36.62

The acetone extractives in the CNS have a very low moisture content, despite the pre-treatment of CNS with vapor to fragilize the shells. This is ideal for the combustion process, as humidity decreases the energy efficiency of the CNSL.

Surprisingly, there is some ash in the acetone extractives (1.5%), in which its value is slightly lower than the one of CNS (2.21%). The extractives have a high volatile matter content, which leads to high reactivity and rapid combustion.

The high carbon content explains the high calorific value of acetone extractives (36.62 MJ/kg).

4.2.4 Tannin content in water extractives

In the previous section, the presence of foam-like product during the water evaporation (from the third extraction step) suggests the possible presence of tannins among the water extractives. To confirm this, Ferric (and Ferrous) test was employed to detect them. These tests allows the distinction between condensed and hydrolysable tannins, which have different structures [244].

Condensed tannins, also known as proanthocyanidins, are polymers of flavonoid units. Hydrolyzable tannins are esters of a sugar (usually glucose) with phenolic acids. They contain a polyol core, usually a carbohydrate, to which phenolic acids could be linked by ester bonds [245].

Pizzi (2004) highlighted that condensed tannins produce a green-black color, while hydrolysable tannins yield blue-black products. This test relies on the interactions between phenolics and iron salts, resulting in a blue, green-black, or grey product [246].

The examined water extractives displayed as a blue-black solution (Figure 4.8), leading to the conclusion that the detected phenolics were indeed hydrolysable tannins. This means that, in the CNS, the phenolic acids such as anacardic acids form tannins through the linkage to a sugar.

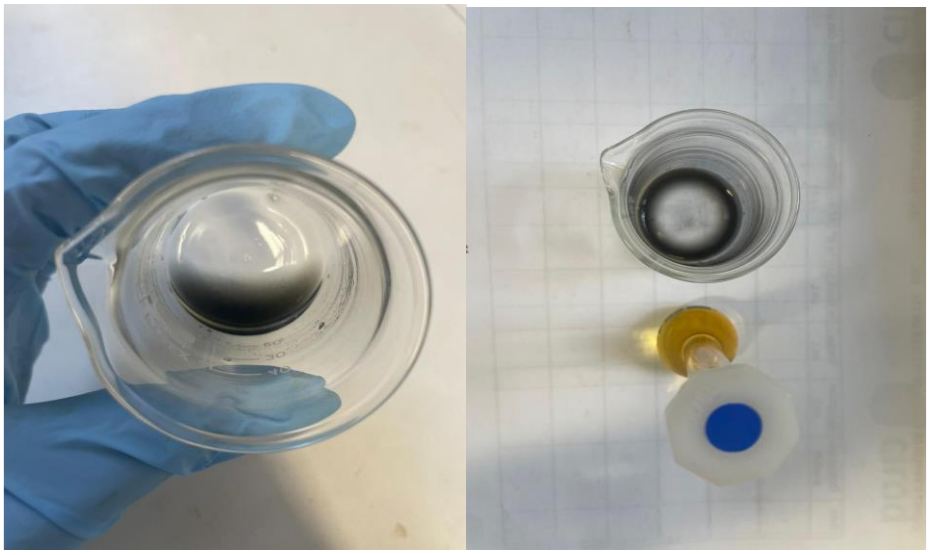

Figure 4.8: Ferric chloride test

Hydrolysable tannins could either be gallic acid esters or ellagic acid esters. Gallic acid esters are composed of multiple galloyl (gallic acid-derived) group esterified to a central core, usually glucose. On the other hands, ellagic acid esters are formed from the oxidative coupling of galloyl groups to form ellagic acid units.

The dTG of water extractives displayed a degradation peak at 225 °C, followed by another wide peak at around 300 °C. This curve suggests the presence of tannins, which primarily decompose within the range 150-350 °C [247].

The presence of tannins was also confirmed by the significant yield of char during pyrolysis, i.e., 39.1 wt%, similar to the one of Acacia dealbata bark tannin (44 wt%) [248].

To further investigate the type of molecules in the tannins, analytical methods for identifying tannins compounds could be developed. Potential analytical techniques include high-performance liquid chromatography (HPLC), liquid chromatography-mass spectrometry, nuclear magnetic resonance (NMR) spectroscopy.

4.3 Summary: Composition of cashew nut shells

The determination of lignocellulosic content (hemicellulose, cellulose and lignin), protein, starch and extractives (acetone, hexane and water extractives) allowed us to characterize finely the cashew nut shells. The composition of CNS is clearly illustrated in a pie chart (Figure 4.9), providing a visual representation of these components.

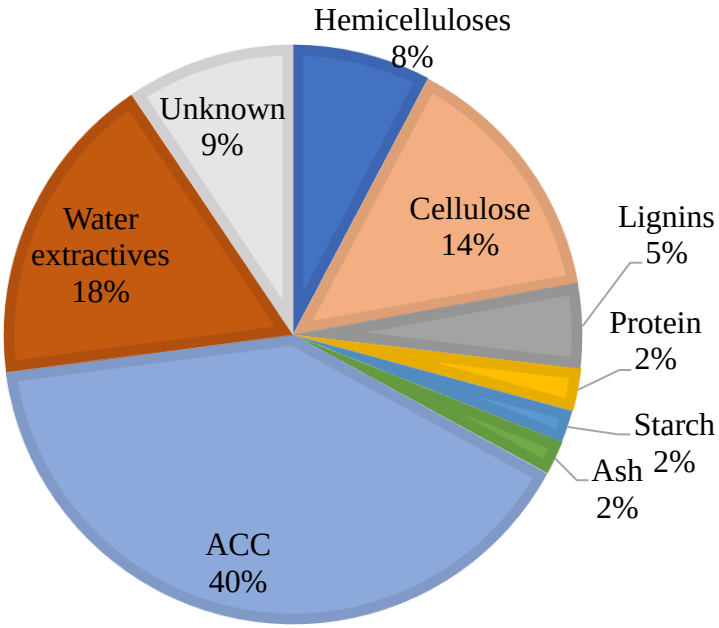

Figure 4.9: Composition of cashew nut shells (dry basis)

The hemicelluloses, cellulose and lignins contents CNS were respectively, 8 wt%, 14 wt% and 5 wt% (dry basis). The lignocellulosic content was low compared to lignocellulosic biomass, mainly due to the presence of extractives in the CNS. However, on an extractive-free basis, CNS had a higher hemicellulose and lower cellulose content than other lignocellulosic biomasses such as wood. The starch, protein and ash content were 2% respectively.

With the optimization of extraction method and the development of HPLC method, acetone which is a polar aprotic solvent was chosen to extract the ACC constituents. A successive triple solvent extraction was carried out to recovery all extractives in the CNS. Acetone extractives were used to remove most ACC (99%), hexane to remove remaining fatty materials and water to remove other possible extractives.

The ACC constituents in the extractives were identified, considering all 12 ACC isomers. The majority of the ACC was found in the acetone extractives, comprising up to 40 wt% of the CNS. Further analysis of the CNS and the thermal degradation curve of the water extractives indicated the potential presence of tannins, accounting for 18 wt% of the CNS in addition to the ACC content. Together, these extractives represent 58 wt% of the CNS.

To the best of our knowledge, this is the first characterization of CNS including protein and starch content as well as the exhaustive extraction and identification of ACC content. However, the pie chart shows that despite the more comprehensive characterization, 9% of substances in the cashew nut shells still could not be identified. These 9% substances could be soluble carbohydrates, lipids (fats and oils), soluble minerals, organic acids and the minor CNSL constituents: 2-methylcardols.

The breakthrough in ACC identification has paved the way for a detailed investigation into their conversion during pyrolysis and thermal/catalytic cracking, which will be studied in the next chapters.

Note that in the following chapters in this thesis, acetone extractives are assumed to be ACC, as they contained 99% of the ACC constituents in the CNS. The solid residue left after removal of ACC from CNS by extraction is named ACC-free CNS.

CHAPTER 5

Pyrolysis of cashew nut shells

5. Pyrolysis of cashew nut shells

In this chapter, we explore the pyrolysis of cashew nut shells (CNS) and of their components, ACC-free CNS (solid fraction) and ACC (extractives). Particular attention was given to understanding the thermal degradation of the main constituents of cashew nut shell liquid (CNSL): anacardic acids, cardanols, and cardols (ACC).

The pyrolysis study starts with the investigation of the pyrolysis kinetics of CNS, ACC-free CNS and ACC, using a micro thermogravimetric analyzer (micro-TG).

The second section delves deeper into the comprehension of thermochemical conversion of ACC during CNS pyrolysis.

The final section investigates the pyrolysis products from CNS, ACC-free CNS, and ACC using the pyrolysis and tar cracking reactor (PyTar), as well as the influence of temperature on CNS and ACC pyrolysis products distribution.

The last section presents a summary on the principal results obtained in this chapter.

5.1 Pyrolysis kinetics

Objective of this study was to identify the temperatures at which CNS, ACC-free CNS, and ACC degrade, as well as to pinpoint the major degradation events. The study was carried out using a micro thermogravimetric analyzer (microTG). This study also explores the potential synergistic effects between the ACC and the ACC-free CNS within CNS during pyrolysis.

5.1.1 Pyrolysis of CNS, ACC-free CNS and ACC

Experiments were carried out with 10 mg of CNS, 5.8 mg of ACC-free CNS and 4.2 mg ACC. Mass samples of ACC-free CNS and ACC were determined based on their precise proportions in a CNS (58% and 42% respectively). The dTG graphs in Figure 5.1 trace the mass loss rate (mg/s) of the different samples between 150 °C and 500 °C. The heating rate chosen was 10 °C/min, as it is close to the one in the lab scale reactor experiment used also in this work.

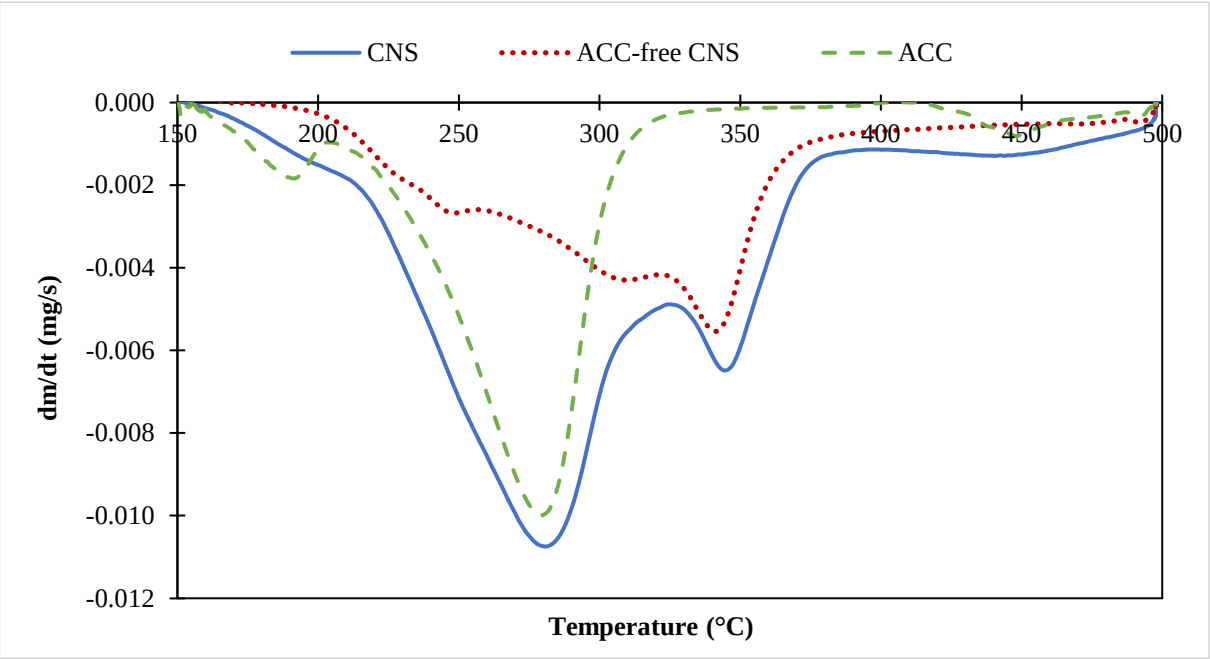

Figure 5.1: dTG curves of CNS (10 mg), ACC-free CNS (5.8 mg) and ACC (4.2 mg), 10°C/min

In the case of **CNS**, a major loss peak appeared at 282 °C. This was due to the decomposition of hemicelluloses and ACC, whereas the peak at 345 °C was due to the decomposition of cellulose [6,9,14]. The last peak at 444°C was due to at least two types of degradation. One consists of lignins degradation which occurs from 150 °C to 500 °C. The other consists of the degradation of polymeric intermediates of ACC [6], which could be shown by the last dTG peak of ACC at 450°C (Figure 5.1). The char yield obtained at the end of the TG analysis was 25.8 wt% (dry basis).

The dTG of **ACC-free CNS** showed a succession of three peaks. The first peak at 246°C was due to the residual extractives (water extractives) that could not be extracted by acetone. The second and the third peaks were due to both hemicelluloses and cellulose degradation. 35.5 wt% of char residue was left at the end of the experiment, logically higher than that left by CNS, which contain ACC. Lignins degradation takes place simultaneously with the degradation of water extractives, hemicelluloses and cellulose degradation.

In the case of **ACC**, the first peak at 192°C was caused by decarboxylation of anacardic acids into cardanols according to scheme in Figure 5.2 [178,249,250]. The dTG curve showed a large degradation peak at 280 °C. This is due to the main thermal degradation and/or evaporation of

the ACC constituents [6]. As mentioned previously in Chapter 2, the peak at 450 °C was said due to decomposition of polymeric intermediates of the ACC [6].

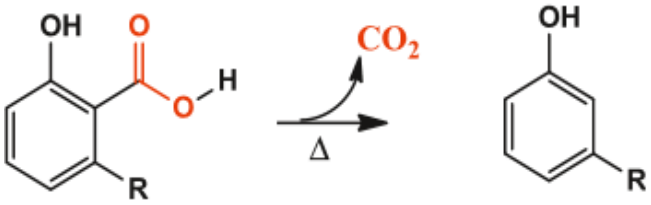

Anacardic acid → Cardanol + CO_2

Figure 5.2: Decarboxylation reaction of anacardic acid [250]

Comparison of ACC and CNS dTG showed that the maximum mass loss occurred at around the same temperature in both curves. This means that the **ACC do not affect the hemicelluloses degradation temperature of CNS** during CNS pyrolysis. However, the comparison of ACC-free CNS and CNS dTG showed that the cellulose degradation peak of ACC-free CNS (342°C) is lower than the one of CNS (345°C). This could mean that ACC increase the thermal degradation temperature of cellulose in the CNS.

The degradation temperatures of the different components of ACC-free CNS (water extractives, hemicelluloses, cellulose and lignins) and ACC (ACC and their polymeric intermediates) are summarized in Table 5.1.

Table 5.1 ACC-free CNS and ACC components and their degradation temperatures

	ACC-free CNS	**ACC**
First peak	246°C degradation of water extractives and lignins	192°C decarboxylation of anacardic acids
Second peak	310°C degradation of hemicelluloses and lignins	280°C degradation of ACC
Third peak	342°C degradation of cellulose and lignins	450°C degradation of polymeric intermediates derived from ACC

Then, occurrence of synergistic effect between the ACC-free CNS and ACC was investigated. The synergistic effect of two components in a biomass refers to the interaction(s) between these components during thermal degradation or chemical reactions, resulting in behavior that differs from what would be expected based on the individual contributions of each component.

Therefore, the sum of the dTG of ACC-free CNS (5.8 mg) and ACC (4.2 mg) was plotted and compared to that of CNS (10 mg) (Figure 5.3).

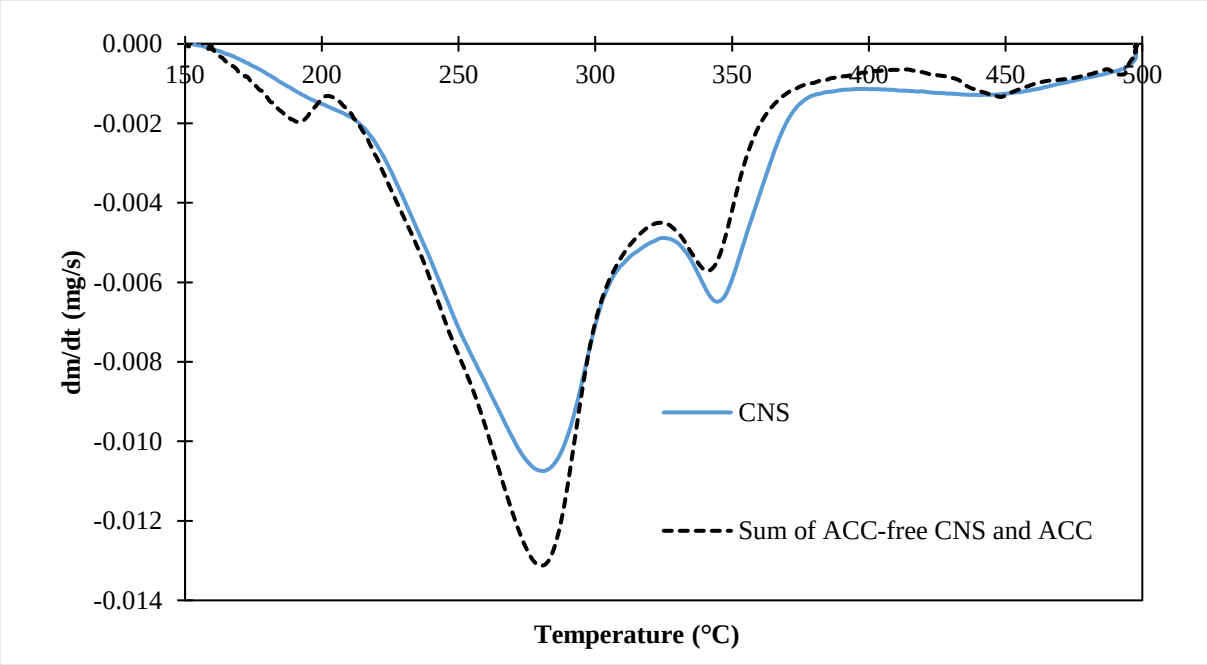

Figure 5.3: dTG curves of CNS and of sum of ACC-free CNS and ACC (10 °C/min)

The peak of the curve (282°C) obtained by addition of ACC-free CNS and ACC (Figure 5.3) is higher than that of CNS and the difference in question is 0.002 mg/s. This means that there is no additivity kinetics of ACC-free CNS and ACC during pyrolysis. This also suggests the existence of intermolecular interactions that limit the conversion of the solid matrix and/or the extractives in the CNS during pyrolysis. This could be explained by the ACC (main components of CNSL) situating in the glandular cells or cavities (interstitial spaces) between the inner shell and the other shell of CNS, which limits the thermal degradation of ACC. The CNSL therefore evaporates with more facility when being pyrolyzed alone.

5.1.2 Limitation of CNS kinetic studies

During our experiments we observed a limitation of CNS pyrolysis kinetic due to the presence of ACC.

Pyrolysis experiments were carried out with CNS using different sample masses (2.5, 5 and 10 mg) at a very low heating rate (1°C/min) (Figure 5.4).

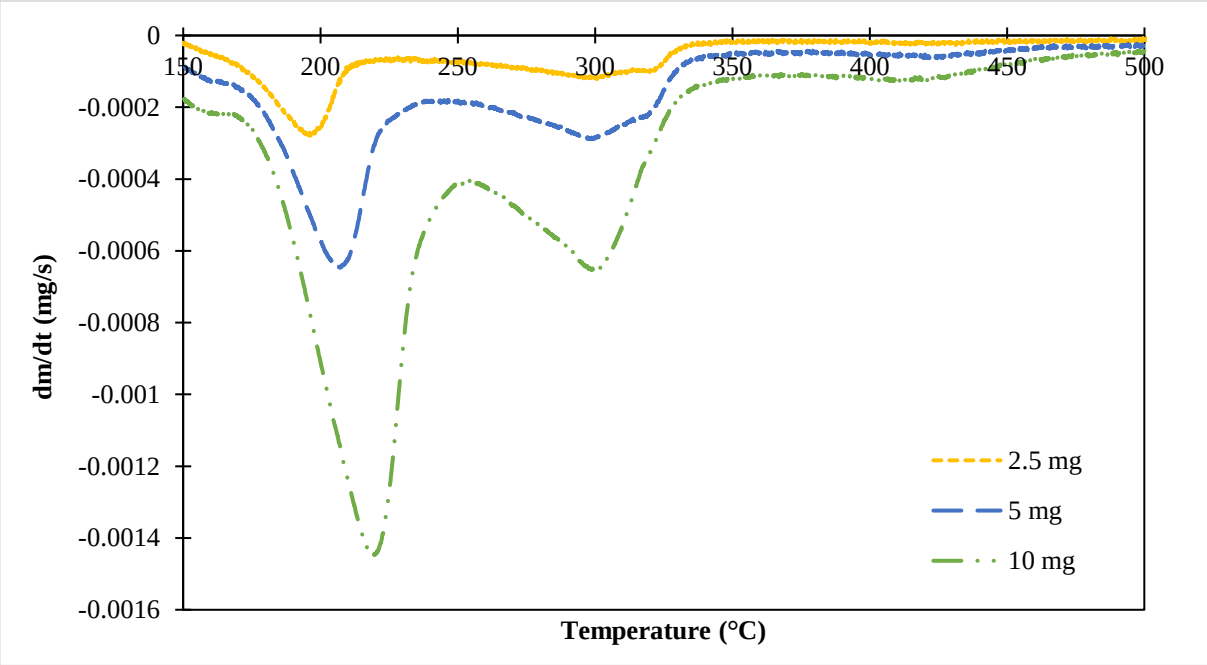

Figure 5.4: dTG curves of CNS with different sample masses 2.5, 5 and 10 mg (1 °C/min)

A notable shift (11-12 °C) occurred in the primary peak (between 199 and 219 °C) for sample mass from 2.5 to 10 mg, caused by the degradation of hemicellulose and ACC. This shift is due to the thermal inertia due to the increasing extractive content in the CNS. Such thermal inertia because of the extractives was also observed by Melzer et al. [6].

Almost no shift in the cellulose degradation peak (298-300 °C) was observed. This is because most of the ACC have already thermal degraded at this heating rate before the cellulose degradation [2].

In conclusion, the TGA experiments revealed that kinetic regime was not achievable as the mass of extractives ACC influences the kinetics of CNS pyrolysis, even at 1°C/min and with 2.5 mg mass sample. Note that same experiments carried out with ACC-free CNS have clearly shown a kinetic regime of pyrolysis without influence of the mass sample.

These results show that homogeneous kinetic models are not suitable for CNS pyrolysis in TGA reactors. Heterogeneous or multi-component models, which consider the distinct behaviors of individual biomass components (pseudo-components) and their interactions, are required to provide a more accurate representation of pyrolysis kinetics.

5.2 ACC thermal degradation mechanisms

The degradation mechanisms of ACC during pyrolysis remains unexplained despite several TG studies on ACC in the literature. In this study, we address this gap by investigating the behavior of ACC isomers as pyrolysis temperature increases, using the High-Performance Liquid Chromatography (HPLC) method specifically developed during this thesis to identify and quantify these isomers.

This study utilizes TG analysis, with the process being interrupted at selected temperatures to analyze the remaining products (residual ACC) in the crucible.

The interpretation of the results obtained from ACC conversion was aided by the state of art on ACC thermal degradation (see Chapter 2.4.2).

The work was divided into 2 main parts:

- Selection of temperature ranges for the analysis of ACC conversion products (Chapter 5.2.1); To investigate the thermochemical conversion of ACC, several temperature ranges were selected using a micro thermogravimetric analyzer.
- Analysis of ACC conversion residues at various temperatures (Chapter 5.2.2 and 5.2.3); The composition of ACC conversion residues generated at different temperatures was investigated. HPLC analysis was conducted on the residual ACC to determine their composition and to propose the degradation mechanisms of ACC.

5.2.1 Selection of temperatures for analysis of ACC conversion products

ACC samples were initially heated to 600°C at a minimal heating rate of 1°C/min to accurately identify the degradation temperatures for which significant mass losses have been observed. This slow heating rate was deliberately chosen to allow sufficient time for molecular reactions to take place within the ACC. A sample mass of 160 mg was selected to ensure enough residual material remained in the crucible for subsequent HPLC analysis and ACC quantification. A larger crucible with a capacity of 900 µL was employed to accommodate the sample, and a lid was used to cover the crucible in order to avoid liquid splash. Using a sample mass greater than 160 mg was avoided to prevent product overflow during heat treatment.

The TG and dTG curves of the pyrolysis of 160 mg ACC at 1°C/min are shown in Figure 5.5.

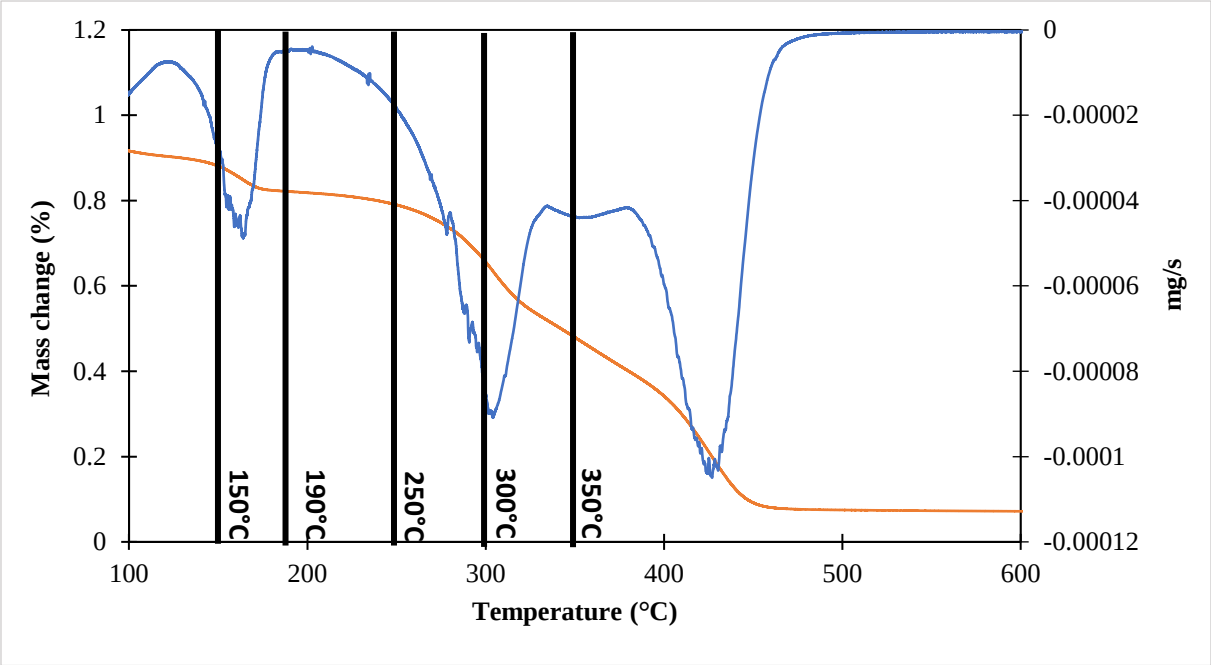

Figure 5.5: TG and dTG curves of ACC (160 mg and 1°C/min)

The first peak observed at 163°C is due to the decarboxylation of anacardic acids, as supported by existing literature. The second (304°C) and third (427°C) peaks are partially superposed. The second and the third peaks can be associated to the thermal degradation of cardanols and/or cardols as well as of their degradation products. The char yield obtained at the end of the experiment was 7 wt%.

While the degradation temperatures of ACC were determined, the complete degradation mechanisms could not be elucidated based solely on these temperatures. As previously stated, the primary objective of this study was to characterize the phenomena occurring at each degradation peak. To further investigate the thermochemical behavior of each ACC constituent, the evolution of these components during pyrolysis was studied. Thermogravimetric (TG) analyses were conducted, and the experiment was halted at specific temperatures (150°C, 190°C, 250°C, 300°C, and 350°C) to analyze the residual ACC in the crucible (HPLC analyses after solubilization of residual ACC in acetonitrile).

A temperature of 150°C was selected as it corresponds to the moment when decarboxylation of anacardic acids takes place. The temperature of 190°C was chosen to represent the end of the decarboxylation process. A temperature of 250°C was then chosen as it corresponds to the initial phase of the second degradation. 300°C was selected as it corresponds to the maximum mass loss during the second degradation, while 350°C was chosen to signify the completion of this second degradation process.

Beyond 350°C, the residual ACC products in the crucible could not be analyzed by HPLC/UV as they present as insoluble solids in acetonitrile.

5.2.2 Analysis of ACC conversion residues at various temperatures

The ACC residues left in the crucible after each experiment were analyzed and quantified using the same HPLC/UV method used for the pyrolysis experiments. 25 mg of sample was diluted in 5 mL of acetonitrile before sample injection in the HPLC. GC-MS is only adapted to residues produced at a temperature above its injection temperature (270°C) because the residues may undergo further thermal decomposition. Therefore, HPLC/UV method was prioritized in this study.

Figure 5.6 shows the composition of residual ACC products in the crucible at different final temperatures (25, 150, 190, 250, 300 and 350°C). The residual ACC products in the crucible were quantified in terms of: **ACC** (anacardic acids, cardanols and cardols) and **non-volatile products in the crucible**. These non-volatile products correspond to non-HPLC quantified chemical compounds, including char. The composition of residual ACC products and the mass loss is represented in g/g ACC (in reference to the initial mass 160 mg).

The graph (Figure 5.6) shows the evolution of mass of liquid ACC (green) and of each ACC constituents (anacardic acids, cardanols and cardols) with the pyrolysis temperature. The evolution of the residual sample mass (%) in the crucible is presented by the orange curve.

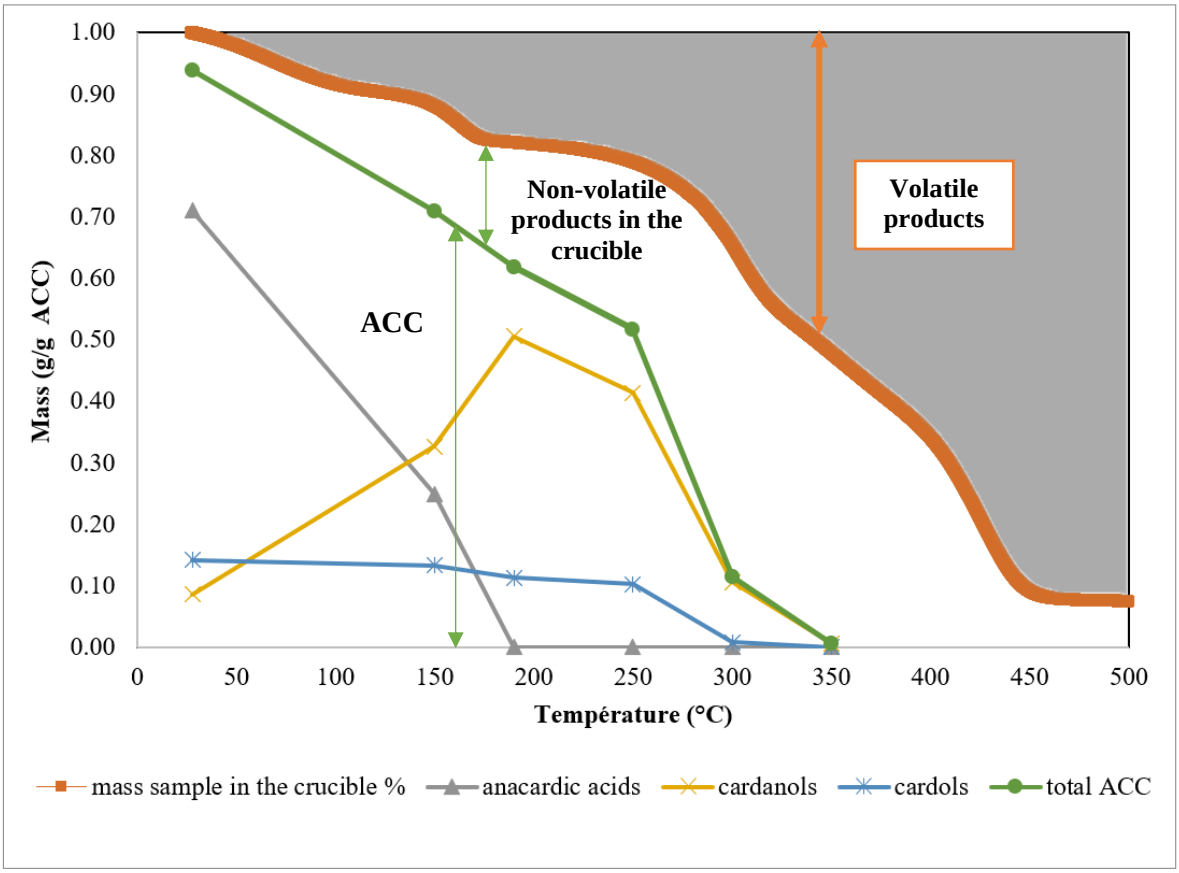

Figure 5.6: Composition of ACC residual products in the crucible (g/g ACC)

Following this orange curve it is possible to consider that this figure (Figure 5.6) is divided into two parts. The upper part of the orange curve (shaded area) represents the volatile products issued from the heat treatment. As these products volatilize, a mass loss within the crucible occurs. Below the orange curve represents the evolution of the residual liquid ACC products (ACC and non-volatile products) in the crucible.

For the following sections, the analyses of ACC residual products are structured around the distinct phases corresponding to the different peaks observed in the dTG analysis of ACC (Figure 5.7).

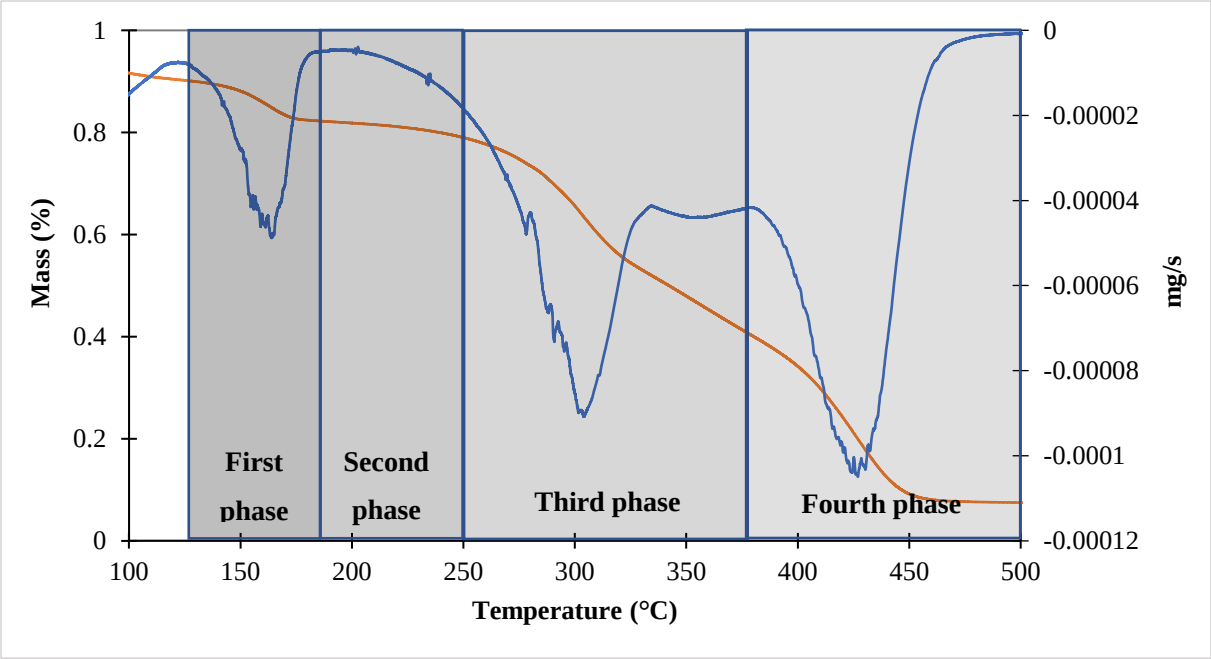

Figure 5.7: Temperature phases selected for ACC conversion analysis

The interpretation of the results of ACC conversion begins by describing the initial phase of ACC (before degradation), in which ACC have not yet undergone any thermal treatment. Following this, the first phase, corresponding to the first peak observed between 125°C and 190°C, is analyzed in detail. The discussion then moves to the second phase, a transition phase between the first and the second peak, in the temperature range of 190°C to 250°C. The subsequent phase (third phase), spanning 250°C to 385°C, focuses on the reactions associated with the second peak. Finally, the last phase (fourth phase) addresses the main phenomena occurring during the third peak and extends the analysis to the complete degradation of ACC.

a) <u>Before degradation</u>

Before any heat treatment, ACC used was composed of 71% of anacardic acids, 9% of cardanols, 14% of cardols and 6% of unknowns (unidentified compounds of ACC). The ACC distribution is slightly different than the one analyzed during the characterization of CNS (Chapter 4). This is due to the long period of storage of the CNS sample used for this experiment, which caused some alterations to the ACC distribution.

Up to 125°C, the evolution of the composition of ACC was not analyzed. A light mass loss was observed, which can be due to the drying of ACC and some prior decarboxylation of anacardic acids.

b) First phase (125 - 190°C)

The composition of ACC residual products in the crucible during first phase (125-190°C) is depicted in Figure 5.8. The first phase studied corresponds to the first degradation peak of ACC dTG (Figure 5.7).

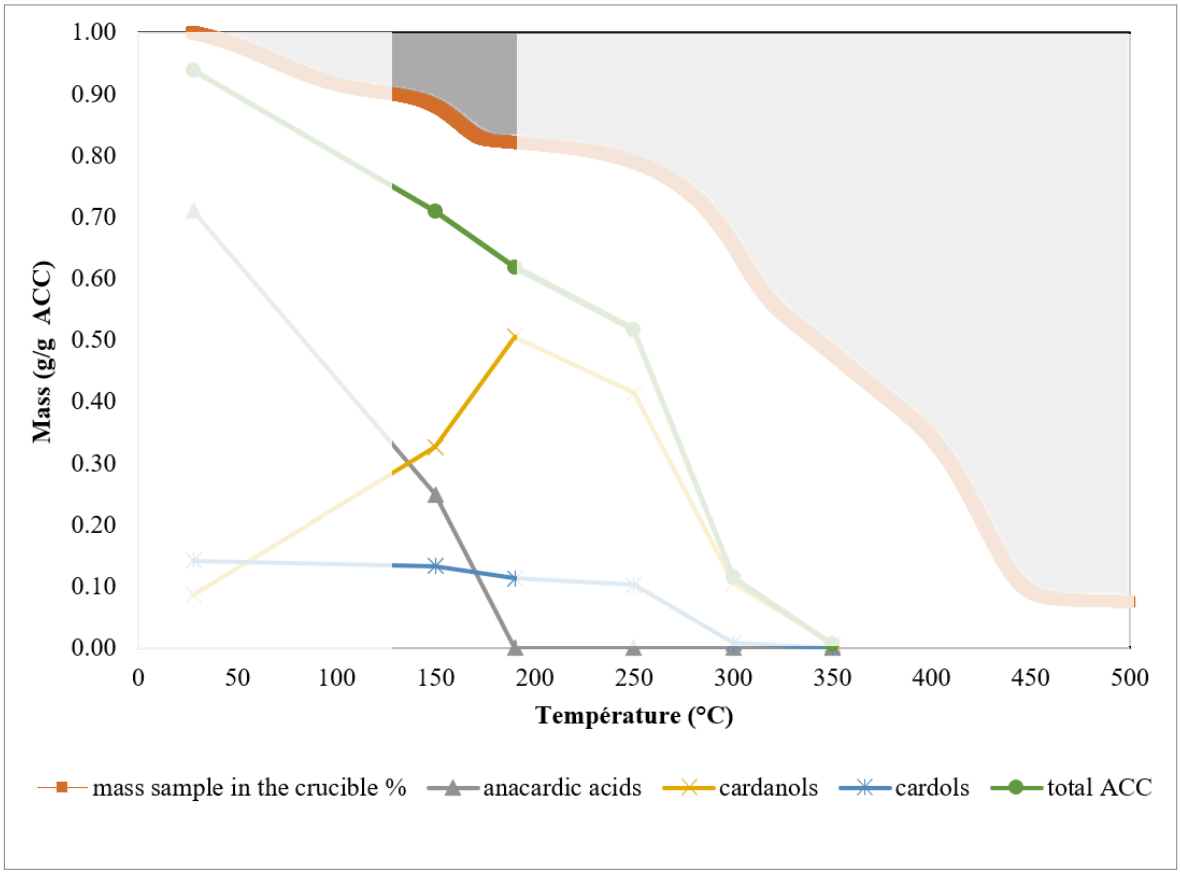

Figure 5.8: Composition of ACC residual products in the crucible during first phase (g/g ACC)

Between 125 and 190°C, decarboxylation of anacardic acids takes places. At 190°C, there is no more anacardic acid in the crucible, showing that all anacardic acids have decarboxylated. If only decarboxylation had taken place in this range of temperature (125-190°C), the mass loss (observed following the orange curve) would be due solely to the volatilization of CO_2.

In order to determine if there are other reactions than decarboxylation during this temperature range, the productions of CO_2 and cardanols were calculated and compared to their experimental values.

The CO_2 (Equation 5.1) and the cardanols (Equation 5.2) produced by decarboxylation were calculated using the mass of anacardic acids decarboxylated during the experiment.

$$m_{CO2} = M_{CO2} \times m_{AA} / M_{AA} \qquad \textit{Equation 5.1}$$

$$m_{CDN} = M_{CDN} \times m_{AA} / M_{AA} \qquad \textit{Equation 5.2}$$

With m_{CO2}, m_{CDN} *and* m_{AA} : mass of CO_2 ,cardanols and anacardic acids respectively (g/g ACC)

M_{CO2}, M_{CDN} *and* M_{AA} : molar mass of CO_2, cardanols and anacardic acids respectively (g/mol)

The calculations above results in the production of 0.09 g/g ACC of CO_2 and 0.62 g/g ACC of cardanols.

The cardanols produced by decarboxylation experimentally was determined by subtracting the cardanols quantity in the ACC residual products (quantity of cardanols after decarboxylation) at 190°C (0.51 g/g ACC) with the initial quantity of cardanols (0.09 g/g ACC). This accounts to 0.42 g/g ACC of cardanols produced during the TG studies.

The volatiles produced is deduced by the mass loss of ACC at 190°C (1.00 g/g ACC - 0.82g/g ACC= 0.18 g/g ACC).

With the calculations, two mass balances on the decarboxylation of anacardic acids obtained experimentally and theoretically are depicted in Figure 5.9.

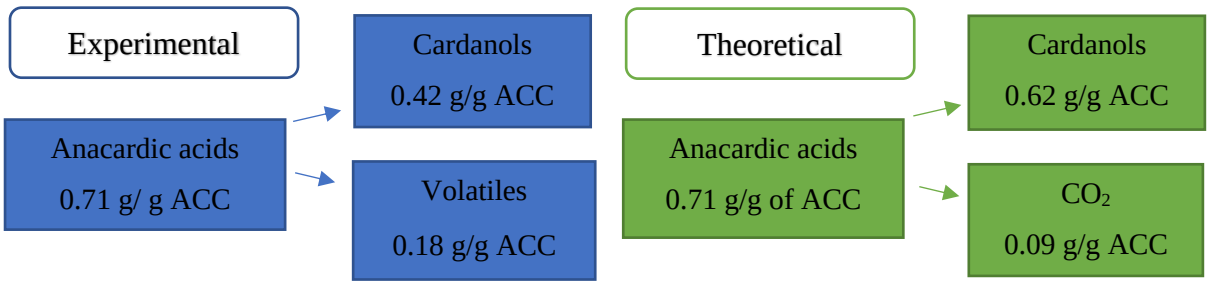

Figure 5.9: Experimental and theoretical value of mass balance of decarboxylation of anacardic acids (g/g of ACC)

According to this calculation, only 0.42 g/g ACC of cardanols were produced instead of 0.62 g/g ACC of cardanols (theoretical value). This means that 32% of the cardanols produced through decarboxylation undergo other reactions. This contradicts all literature which mentioned that the first degradation is solely due to the decarboxylation of anacardic acids. There were also volatiles that were not issued by decarboxylation reaction (shown by the mass loss on the orange curve). Indeed, the mass of volatiles (0.18 g/g ACC) obtained

by experiment is twice that the CO_2 produced theoretically (0.09 g/g ACC). This means that devolatilization of cardanols take place.

The devolatilization of cardanols could produce phenols and aliphatic chain products. Thus, the possible volatile products emitted during this temperature range include phenols which have a boiling point of 181°C and light hydrocarbons with carbon numbers C<11 which could be produced by the devolatilization of cardanols, as well as CO_2 produced by decarboxylation of anacardic acids.

Given by the quantity increase of non-volatile products in the crucible (gap between orange and green curves), this shows that polymerization of cardanols also takes place simultaneously with the decarboxylation reaction of anacardic acids and the devolatilization of cardanols.

The polymerization temperature of cardanols (125-190°C) during these experiments is coherent to the one of literature which states thermal oligomerization of cardanols takes place at 140°C [216] A precise polymerization temperature of cardanols could be determined if more intermediate points between this temperature were studied.

The mass of cardols remained relatively constant. This means that no thermal degradation of cardols take place during this temperature range.

c) Second phase (190°C-250°C)

This temperature range corresponds to the transition phase between the first and the second peak observed in Figure 5.7. The composition of ACC residual products in the crucible during second phase (g/g ACC) is presented in Figure 5.10.

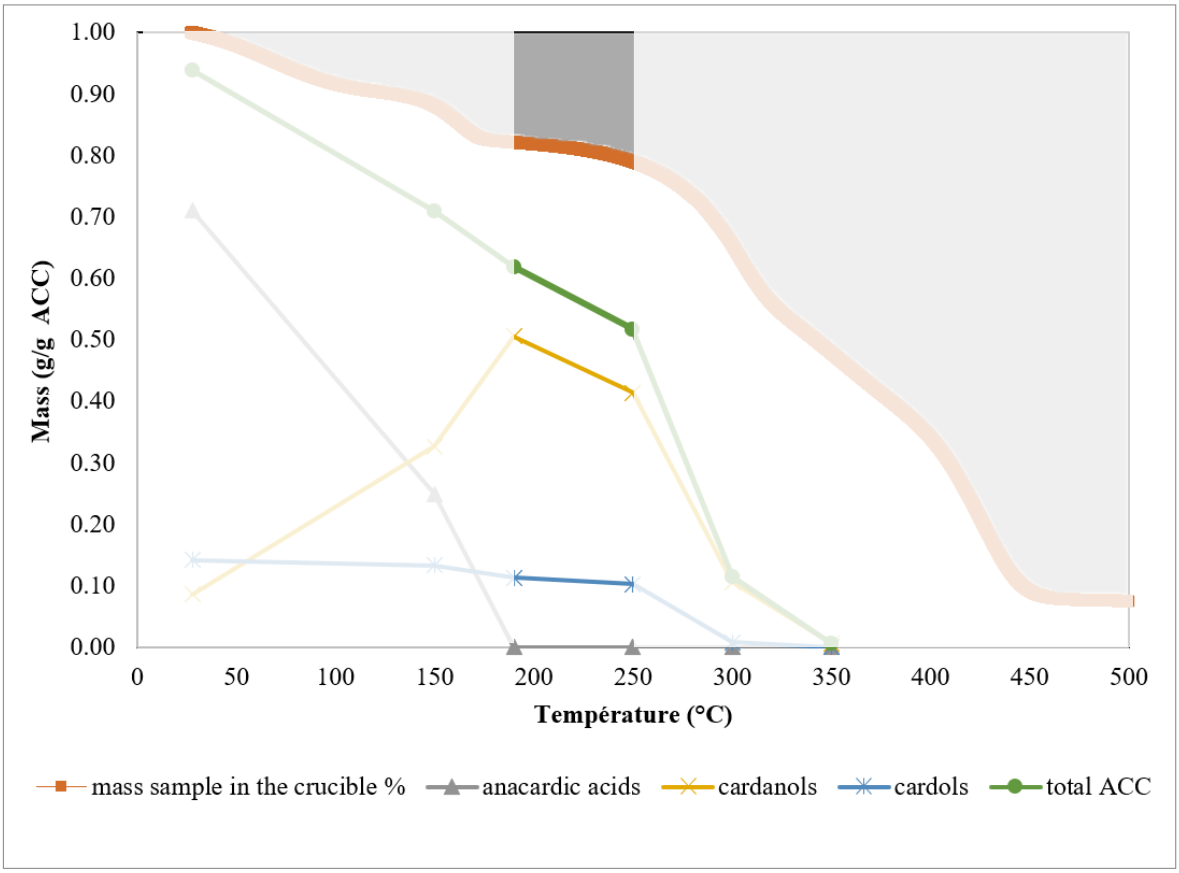

Figure 5.10: Composition of ACC residual products in the crucible during second phase (g/g ACC)

Between 190°C and 250°C, the mass of cardols still remained relatively constant (0.01 g/g ACC difference) whereas the mass of cardanols decreases significantly (0.10 g/g ACC difference). There is almost no mass loss during this temperature range. This means that almost no volatiles are produced. This indicates that, during this range of temperature, only the polymerization of cardanols takes place.

d) Third phase (250°C-385°C)

This temperature range corresponds to the second degradation peak observed in Figure 5.7. The composition of ACC residual products in the crucible during the third phase is depicted in Figure 5.11.

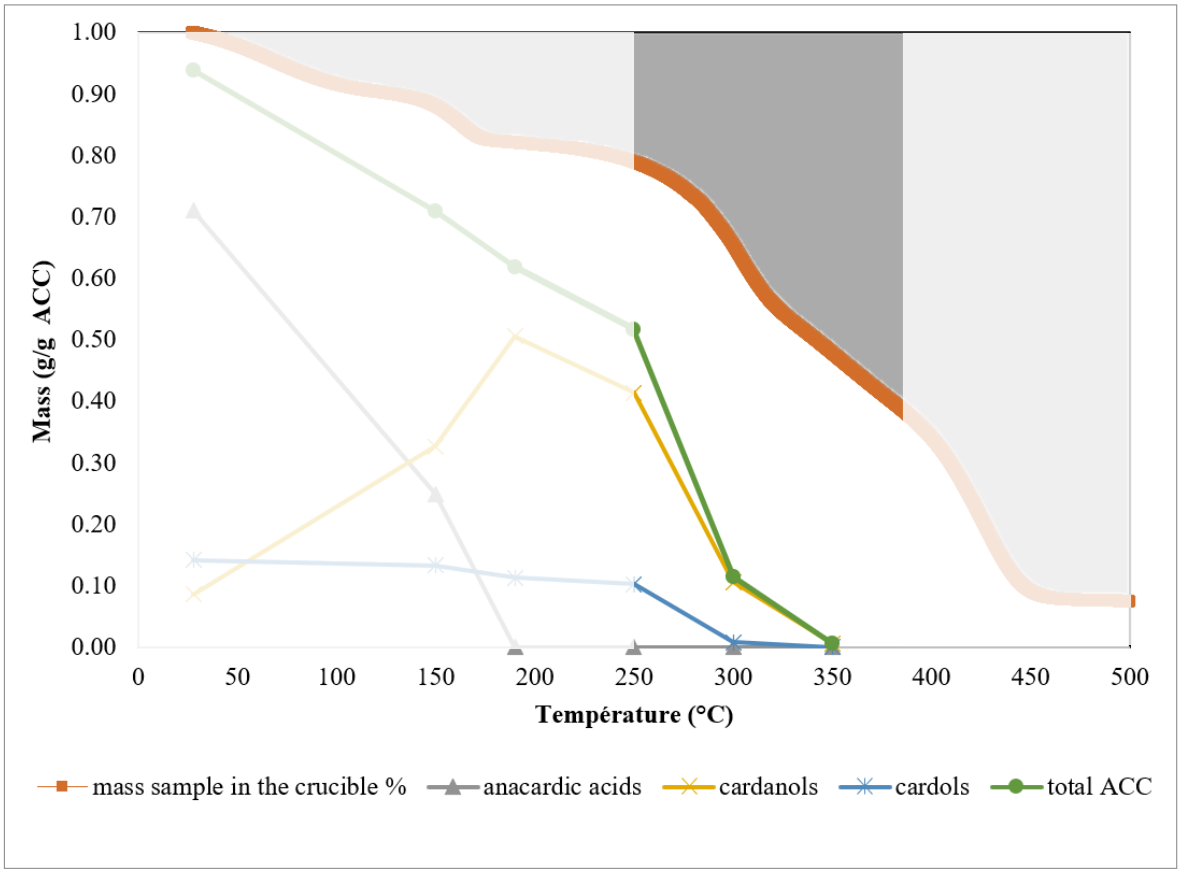

Figure 5.11: Composition of ACC residual products in the crucible during third phase (g/g ACC)

During this phase, all the cardols and cardanols disappear completely, and are no longer present in the crucible for the analyses of the liquid, carried out after 300°C and 350°C respectively.

A huge decline of the mass of cardanols is observed. This is due to the polymerization and the devolatilization of cardanols.

The mass of cardols which was relatively constant from 25°C to 250°C also decreases during this phase. Between 250°C and 300°C, the mass of cardols decreases from 0.10 g/g ACC to almost no cardols (0.01 g/g ACC). This means that polymerization and devolatilization reactions of cardols take place during this temperature range (250-300°C). As mentioned in Chapter 5.2.1, the devolatilization of cardols could lead to the formation of resorcinol which volatilizes at a temperature above 277°C.

Between 300 and 350°C, a decrease in the non-volatile products in the crucible was observed. At 300°C, there are 0.51 g/g ACC of non-volatile products whereas at 350°C

there are 0.41g/g ACC of volatile products. The decrease could be explained by the thermal degradation of cardanols and cardols-based polymers.

At 350°C, all of the cardanols and cardols are absent in the crucible. This means that all cardanols and cardols have converted through polymerization and devolatilization reactions.

e) Fourth phase (>385°C)

This temperature range corresponds to the third degradation peak observed in Figure 5.7. The composition of ACC residual products in the crucible during this last phase is shown in Figure 5.12.

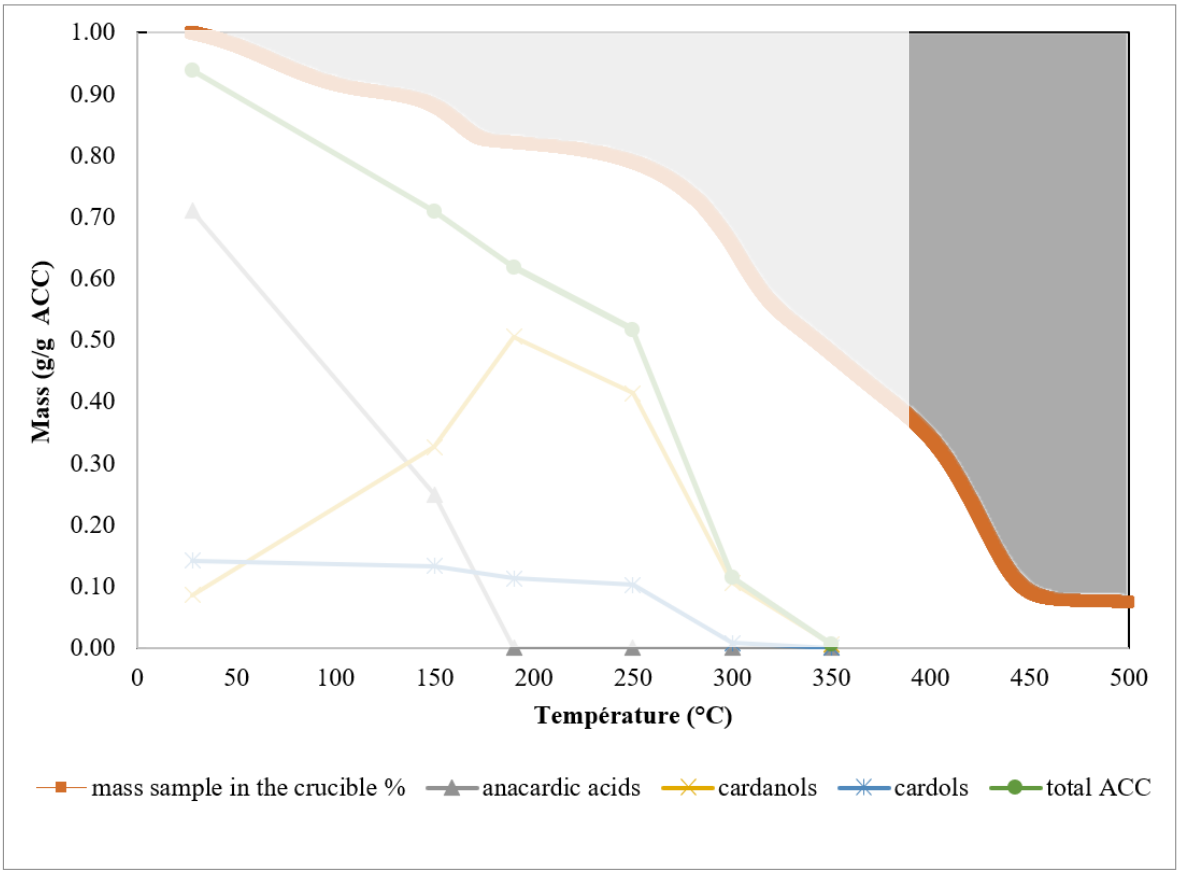

Figure 5.12: Composition of ACC residual products in the crucible during fourth phase (g/g ACC)

Despite the absence of ACC in the crucible, the mass of sample continues to decrease. This means that at this temperature range, thermal degradation reactions of cardanol based polymers and cardol based polymers take place.

The thermal degradation of polymers takes place until 450°C. At 500°C, only char was left in the crucible and its yield was 7.4 wt%. This means that a pyrolysis of ACC at 500°C generates 92.6 wt% volatiles.

With all the interpretation made on the results obtained, a table summarizing the ACC degradation mechanisms is presented (Table 5.2). It includes the reaction(s) that take place during the different degradation phases, the volatile products and the residual products in the crucible.

Table 5.2: ACC degradation mechanisms and their degradation products

	First phase	**Second phase**	**Third phase**	**Fourth phase**
T(°C)	125-190°C	190-250°C	250°C-385°C	>385°C
Reactions	Decarboxylation of anacardic acids + Polymerization and devolatilization of cardanols	Polymerization of cardanols	Polymerization and devolatilization of cardanols and cardols Thermal degradation of cardanols and cardols based polymers	Thermal degradation of cardanols and cardols based polymers
Volatiles	CO_2 Devolatilization products (phenol, aliphatic chain C<11, etc.)	none	Devolatilization products (resorcinol, phenol, aliphatic chains C<15, etc.)	Devolatilization products (resorcinol, phenol, aliphatic chains C<15, etc.)
Residual products in the crucible	Cardanol based polymers Devolatilization products (phenol, aliphatic chains C⩾ 11, etc.)	Cardanol based polymers	Cardanol and cardol based polymers Devolatilization products (resorcinol, aliphatic chains C⩾ 15, etc.)	Cardanol and cardol based polymers Char Devolatilization products (aliphatic chains C⩾15, etc.)

From this study, it is confirmed that the ACC degradation mechanisms is divided into several main reactions:

- **decarboxylation of anacardic acids**,
- **polymerization of cardanols and cardols versus devolatilization of cardanols and cardols**
- **thermal degradation of cardanol and cardol-based polymers**.

It is important to highlight that no study on ACC degradation mechanisms has been as comprehensive as what has just been presented. The novelty in the information obtained could be useful for other studies such as ACC kinetic modelling, ACC polymerization etc.

From the ACC conversion studies, it is understood that the thermal degradation of cardanol and cardol based polymers, during the fourth phase originates from the polymerization of cardanols and cardols during the third phase.

During this third phase, two main reactions take place during the ACC degradation: polymerization and devolatilization reactions. It is possible that there is a competition between these two reactions. This competition conditions the thermal degradation of polymers during the third degradation.

Therefore, additional experiments were required to investigate this competition. For this, TGA pyrolysis of ACC were carried out using different sample mass (5, 10, 20, 40, 80 and 160 mg) at 1°C/min (Figure 5.13).

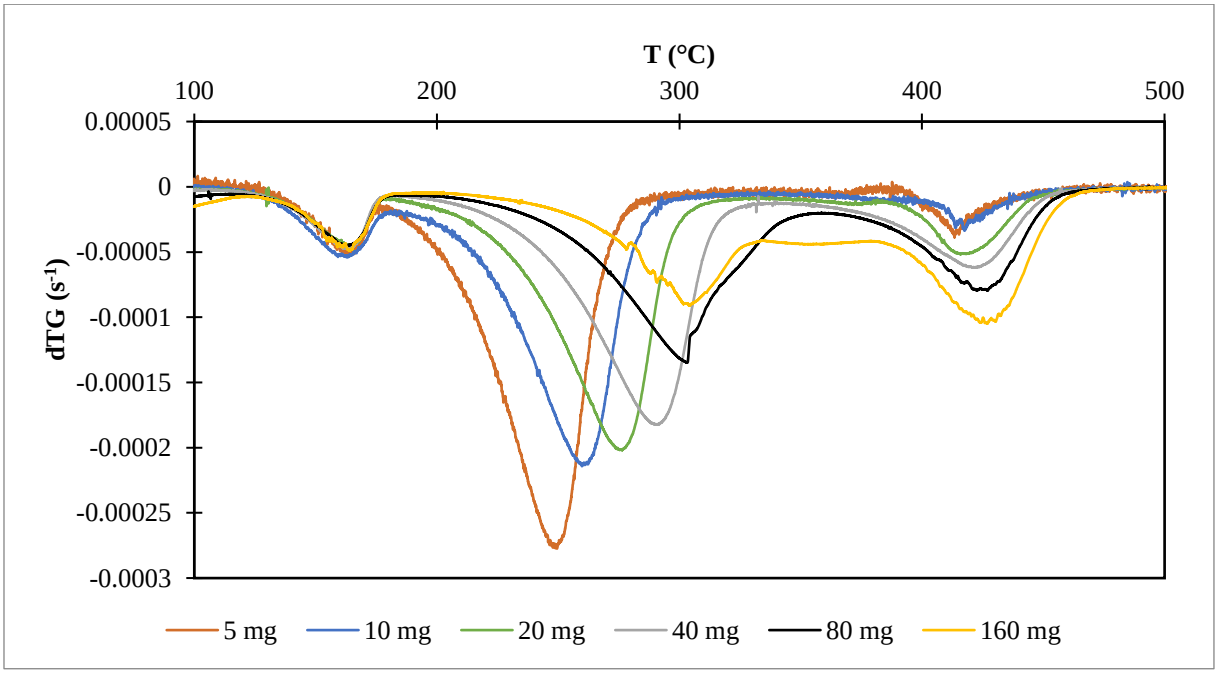

Figure 5.13: dTG curves of ACC at different sample mass (5, 10, 20, 40, 80 and 160 mg) at 1°C/min (dimensionless mass)

According to Figure 5.13, it is observed that each increase in sample mass results in a lower second peak amplitude and a higher third peak amplitude.

The sum of areas of the second and third peaks observed in this dTG (Figure 5.13) was determined. For this, a fitting function called Asy2Sig was used to deconvolute the dTG peaks into three individual peaks. The areas of the 3 peaks were determined (%). Results of this calculation are presented Table 5.3.

Table 5.3: Areas of ACC degradation peaks (%)

Sample mass (mg)	First peak	Second peak	Third peak	Sum of second and third peak
5	34%	40%	27%	**67%**
10	12%	78%	10%	**87%**
20	9%	76%	14%	**90%**
40	9%	65%	26%	**91%**
80	10%	57%	33%	**90%**
160	10%	43%	47%	**90%**

For sample mass of 10 -160 mg, the sum of area of second and third peak becomes relatively constant (87%-91%) (Table 5.3). This confirms that the third degradation is conditioned by the second degradation for sample masses between 10 mg and 160 mg.

Depending on the sample mass, the second degradation is either dominated by polymerization reactions or devolatilization reactions:

When the mass of sample in the crucible is substantial, the second degradation is dominated by polymerization reactions, there will be less devolatilization reactions. Consequently, there will be less mass loss (smaller peak area %) during the second degradation. This leads to more thermal degradation reactions of cardanol-based polymers and cardol-based polymers during the third degradation because more polymers were formed during the second degradation. This results in higher mass loss (higher peak area %) during the third degradation.

When the mass of sample in the crucible is low, the second degradation is dominated by devolatilization reactions, there will be less polymerization reactions of cardanols and cardols. This results in higher mass loss (higher peak area %) during the second degradation and less formation of polymers. Therefore, there will be less thermal degradation of cardanol and cardol-based polymers, which leads to less peak area % during third degradation.

From the results obtained in Table 5.3, it is observed that for sample masses between 10 and 160 mg, the increase in sample mass decreases the second peak area % and increases the third peak area %. This concludes that a higher sample mass favorizes the polymerization reactions during the second degradation while lower sample mass favorizes the devolatilization reactions during the second degradation.

This phenomenon observed could be explained as follows:

When a large sample is used, the gas-liquid surface contact area decreases while the thickness of the liquid layer in the crucible increases. This leads to increased intermolecular interactions, promoting polymerization reactions of cardanols and cardols. Conversely, when a small sample is taken, the gas-liquid surface contact increases and the liquid layer becomes thinner, which facilitates the release of volatile products and favors intramolecular reactions, favorizing devolatilization reactions of cardanols and cardols.

Based on the results, this phenomenon appears to be applicable only to ACC mass samples ranging from 10 to 160 mg. The thermochemical behavior of the 5 mg sample differs from the others, indicating the need for further studies to better understand this competitive behavior of polymerization and devolatilization reactions. Analysis or characterization of these polymers and/or volatile products formed during polymerization or/and devolatilization could help validate the explanation of this phenomenon of competition.

5.2.3 Evolution of each ACC isomers at different temperatures

In this section, we present the evolution of each isomer (15:0, 15:1, 15:2 and 15:3) with the temperature. The mass of ACC isomers remaining in the crucible after each experiment is presented g/g ACC (Figure 5.14).

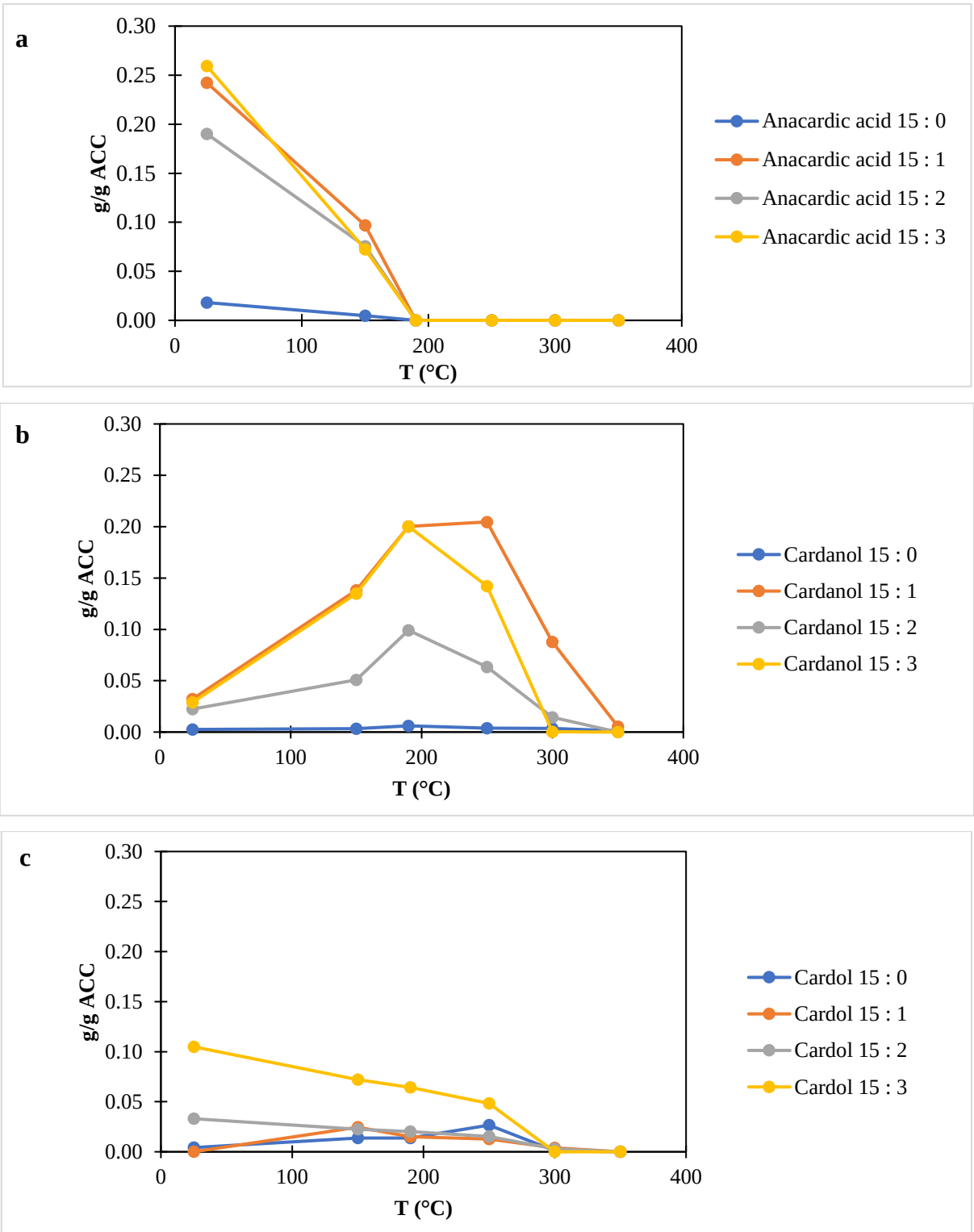

Figure 5.14: Mass of anacardic acids (a), cardanols (b) and cardols (c) isomers during pyrolysis at different temperatures (25, 150, 190, 250, 300 and 350°C) (g/g ACC)

Beyond 190°C, none of the anacardic acids isomers was present anymore in the crucible (Figure 5.14 (a)). Anacardic acid 15:3, which is the most abundant anacardic acids, shows the highest mass loss at 190°C than other isomers during decarboxylation. This is probably due to its degree

of unsaturation which is higher than other isomers, which makes it more reactive than other isomers which have lesser double bonds (monoene, diene for example).

According to Figure 5.14(b), the quantity of cardanols increases while the anacardic acids decarboxylated. A maximum production yield (0.20 g/g ACC) is shown at 190°C for all cardanol isomers except for cardanol 15:1. It is clear that the maximum percentage of the different cardanols are correlated with those of the initial anacardic acids in the following order: 15:3 > 15:1 > 15:2 > 15:0. The yield of cardanol 15:1 increases between 190 and 250°C. At 300°C, its quantity is significant (0.09 g/g ACC) when compared to other isomers. This could be due to : a) cardanol 15:1 degrades slower than other cardanol isomers, b) cardanol 15:1 is formed through the rupture of double bonds in cardanol 15:3 and 15:2 [251]. At 350°C, only a very small quantity of cardanol 15:0 (0.01g/g ACC) and 15:1 (0.05g/g ACC) remained.

Overall, the concentrations of cardols (Figure 5.14(c)) only decrease with the rise in temperature, indicating that there is no anacardic acid or cardanols transforming into cardols. Two interesting peaks were observed: cardol 15:1, which increases at 150°C, and cardol 15:0, which increases at 250°C. This could be due to hydrogenation reactions of other cardol isomers.

The interpretation of the mass evolution of ACC isomers with temperature shows that the thermal degradation of ACC constituents as a combination of many complex thermochemical reactions. The rupture of the double bonds of the ACC aliphatic chains that take place during thermal degradation could not be mastered without a proper analytical method.

5.3 Products from CNS pyrolysis

This section deals with the compositions and yields of the products derived the pyrolysis of CNS (char, condensates, and permanent gas).

Experiments were conducted using the pyrolysis and tar cracking reactor (PyTar) described in Chapter 3. This reactor enables pyrolysis tests to be carried out under controlled conditions and allows the collection all the products (char, condensates and gases) before analyzing them individually.

The pyrolysis experiments were carried out on CNS, ACC-free CNS and ACC. Wood chips were also investigated as a reference to lignocellulosic biomass. In these experiments, around 4.5 g of sample mass was used for both CNS and wood chips. 1.9 g of ACC and 2.6 g of ACC-

free CNS were used as they represent their respective mass proportion within CNS. The ACC sample was carefully placed in a crucible using a Pasteur pipette. The N_2 flow rate in the pyrolysis zone and the cracking zone were set at 30L/h and 6L/h respectively. The pyrolysis temperature was set at 400 °C because the majority of volatiles are emitted below 400°C during the CNS pyrolysis (Figure 5.15).

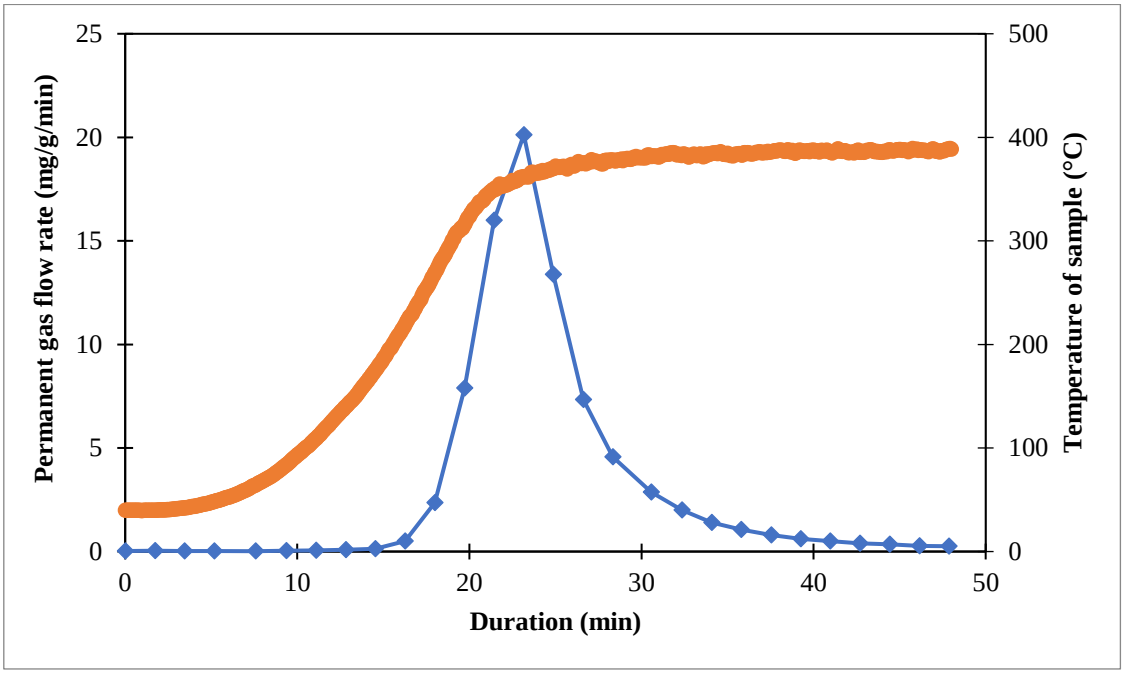

Figure 5.15: Evolution of permanent gas flow rate (blue) of CNS pyrolysis (400°C, 25°C/min) and of pyrolysis temperature (orange) with time

5.3.1 Pyrolysis products yield

At the end of each experiment, the char was weighed. Permanent gases were analyzed and quantified, and the condensates recovered were collected and analyzed using HPLC/UV and GC-MS. By taking into account the mass of condensates recovered in the condensation system, the mass balances closed between 88-98%. The mass balance was not complete due to deposits of condensates in the flange and outlet pipe of the reactor, for which weighing was impossible. Consequently, the condensates yield of these experiments was calculated by difference, considering the measured mass of char and permanent gas.

The yield of main products and the composition of the condensates resulting from the pyrolysis of CNS, ACC-free CNS, ACC and wood chips at 400 °C are presented in Figure 5.16. The yields were calculated on dry and ash-free basis. The fraction of condensates was composed of ACC constituents, quantified tar, water and unknown and presented in the form of pie charts.

Although ACC constituents are also tars, we distinguish the difference between tars and ACC constituents in this study. The quantified tar corresponds to tars which could be determined quantitatively with our GC-MS method.

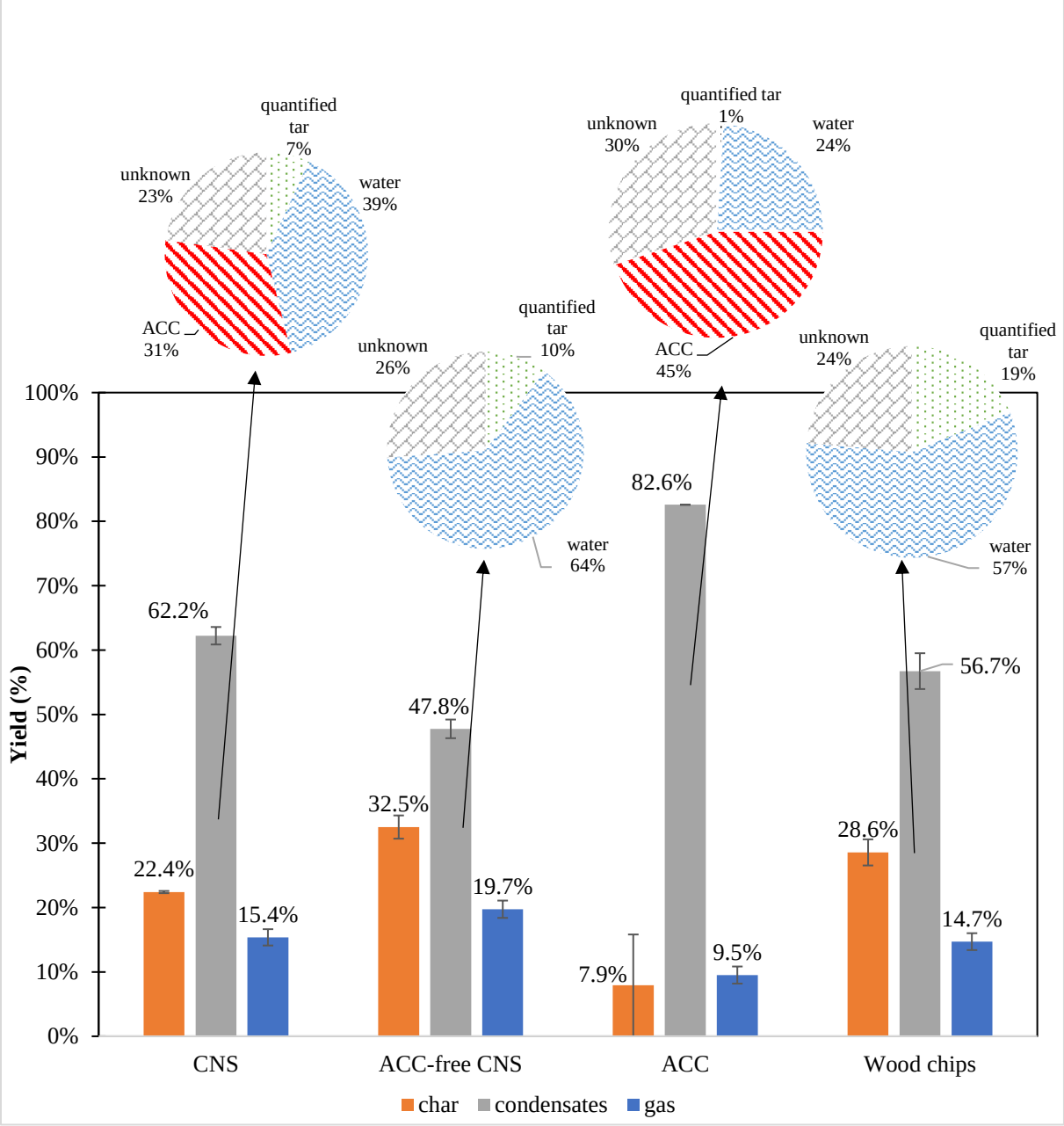

Figure 5.16: Yield of main products of pyrolysis of CNS, ACC-free CNS, ACC, and wood chips at 400 °C (dry and ash-free basis) (%), and composition of condensates (pie charts).

According to the figure, the gas production of CNS pyrolysis is mainly contributed by ACC-free CNS. If we calculate the gas yields of ACC and ACC-free CNS respectively (by taking into their mass proportions in the CNS), the gas contributed by ACC-free CNS (11.4%) is much higher than the one of ACC (4.0%).

By comparing pyrolysis of CNS and wood chips, there is no significant difference in the gas yields despite the large amount of ACC constituents in the CNS. As mentioned just previously, the gas production of CNS is mainly contributed by ACC-free CNS and not ACC. However, a slightly higher condensates yield is observed from CNS pyrolysis than wood chips pyrolysis. This could be explained by the breakdown of extractives (ACC and tannins) which form condensates, on top the lignocellulosic content. In terms of char yields, the difference is significant with a 6 % increase in the case of wood chips, due to the higher presence of lignins.

Focusing on CNS related samples (CNS, ACC-free CNS, and ACC), it is clear that the yield of condensates increases with an increase in the concentration of ACC constituents at the expense of the gas yield. ACC also produce char during pyrolysis and its yield account up to 7.9 wt%, which is less than the char yield via ACC-free CNS pyrolysis (32.5wt%).

From this figure 5.16, ACC conversion was calculated to 52% during CNS pyrolysis and 61% during pyrolysis of ACC alone. However, during the study of ACC thermal degradation using TGA reactor, all ACC converted at 350°C. The fact that there are still ACC in the condensates shows the competition of ACC evaporation with their polymerization and devolatilization reactions.

The lower ACC conversion during CNS pyrolysis than during ACC pyrolysis observed is in accordance with Chapter 5.1.1 where it is explained that the existence of intermolecular interactions limits the conversion of ACC when embedded in the solid matrix.

The percentages of tars in the CNS (7%) and ACC- free CNS (10%) pyrolysis condensates were significantly lower than in the wood chips (19%). Only 1% of tars was found during ACC pyrolysis condensates. In fact, we highlight here a difficulty in analyzing the products (tars) issued from the ACC pyrolysis. It appears that the tars issued from ACC pyrolysis are not the same than the tars issued from pyrolysis of a lignocellulosic biomass.

The water content in the condensates was higher in the case of ACC-free CNS and wood chips, as cellulose and hemicelluloses are known to produce water during pyrolysis [110]. This is also the reason why the water content was higher in the CNS pyrolysis condensates (39%) than in the ACC pyrolysis condensates (24%).

The GC-MS method applied was initially adapted to quantify tars that are usually issued from the pyrolysis of lignocellulosic biomass, which therefore hinders the quantification of tars issued from CNS, which only contains 27% lignocellulosic fraction. However, the analytical

methods applied (HPLC for ACC, GC-MS for Tar and Karl Fischer for water) enabled the identification and quantification of approximately 70-77% of the total condensates for pyrolyses at 400°C, which is rather satisfactory as results.

5.3.2 Permanent gas composition

To assess the contribution of ACC to gas production during CNS pyrolysis, the distribution of gases was analyzed and compared to that of CNS and of wood chips. Table 5.4 shows the production of permanent gases during pyrolysis of CNS, ACC-free CNS, ACC and wood chips at 400 °C. To ease comparison, the quantities of gas produced are expressed per gram of equivalent CNS (mg/g CNS) considering an average ACC ratio of 42 %.

Table 5.4: Distribution of permanent gases (mg/g CNS) in the pyrolysis gas (CNS, ACC-free CNS, ACC and wood chips) at 400 °C.

mg/g sample	**CNS**	**ACC-free CNS**	**ACC**	**Wood chips**
	mg/g CNS	mg/g CNS	mg/g CNS	mg/g wood chips
CO_2	123.6	86.7	35.2	92.6
CO	23.9	22.1	0.6	46.7
Remaining gas (H_2, CH_4, C_2H_2, C_2H_4 and C_2H_6)	6.2	5.7	4.2	7.7

In all cases, the permanent gas produced was mainly composed of CO_2 and CO. The formation of CO_2 during wood pyrolysis is explained by the degradation of hemicelluloses and cellulose [14]. In CNS, part of the CO_2 produced is due to the decarboxylation of anacardic acids to produce cardanols [14]. This explains the higher production of CO_2 in the CNS permanent gas than in the wood chips and also why CO_2 production from ACC-free CNS pyrolysis is lower than the one of CNS. In the case of ACC pyrolysis, mainly CO_2 (88% of permanent gas) is produced. If we add the CO_2 production from ACC-free CNS and ACC considering their proportion in the CNS, it logically corresponds to the one of CNS. This means that there is no intermolecular reactions between the CO_2 produced by ACC and by ACC-free CNS. Considering the hypothesis that ACC constituents in the CNS volatilize freely, i.e., with no restriction from solid matrix, they can potentially contribute up to 28% (35.2 mg/g CNS / 123.6 mg/g CNS) of the total CO_2 produced during CNS pyrolysis.

5.3.3 Condensates composition

The composition of condensates was investigated, focusing on the distributions of the ACC and the tars. The ACC distribution consists of all the 12 ACC isomers, analyzed and quantified using HPLC. The tars include only quantifiable tars using our current GC-MS method.

5.3.3.1 ACC constituents

The distribution of ACC constituents in the CNS and ACC pyrolysis condensates is presented in Table 5.5. The quantity of ACC constituents in ACC pyrolysis condensates is calculated per gram of equivalent CNS (mg/g CNS) by taking into account an average ACC ratio in CNS of 42 %.

Table 5.5: Distribution of anacardic acids, cardanols and cardols (ACC) in the CNS and ACC pyrolysis condensates (mg/g CNS) at 400 °C.

	ACC constituents in CNS before pyrolysis **mg /g CNS**	**ACC constituents in <u>CNS pyrolysis</u> condensates mg/g CNS**	**ACC constituents in <u>ACC pyrolysis</u> condensates mg/g CNS**
Anacardic acid 15:0	10.2	0	0
Anacardic acid 15:1	115.8	0	0
Anacardic acid 15:2	90.2	0	0
Anacardic acid 15:3	84.3	0	0
Cardanol 15:0	0.00	16.5	15.6
Cardanol 15:1	13.6	98.8	80.6
Cardanol 15:2	1.70	39.5	32.3
Cardanol 15:3	13.6	38.8	24.8
Cardol 15:0	7.7	0	0
Cardol 15:1	11.1	0	0
Cardol 15:2	11.9	0	0
Cardol 15:3	38.3	0	0
Total anacardic acids	300.5 (75.4%)	0	0
Total cardanols	28.9 (7.3%)	193.6	153.3
Total cardols	69.0 (17.3%)	0	0
Total ACC	**398.4**	**193.6**	**153.3**

Before undergoing pyrolysis, the distribution of ACC constituents in the CNS was 75.4 wt% anacardic acids, 7.3 wt% cardanols and 17.3 wt% cardols.

Following the pyrolysis of both CNS and ACC at 400 °C, only cardanols, represented by the presence of all four isomers, were identified among the ACC constituents of the condensates. This means that the cardanols in condensates came from either their evaporation or the thermal degradation of polymers formed during pyrolysis.

Table 5.5 shows that more cardanols were produced by CNS pyrolysis (193.6 mg/g CNS) than by ACC pyrolysis (153.3 mg/g CNS). This is because when ACC is pyrolyzed alone, the cardanols and cardols have more contact surface between them, which facilitates polymerization reactions. Therefore, ACC pyrolysis produces less cardanols in the condensates. The production of cardanol 15:1 was the highest among other cardanols in both condensates (CNS and ACC pyrolysis). This observation is coherent to the ACC pyrolysis results in 5.2.3, where the production of cardanol 15:1 is the highest among other isomers. As mentioned previously in Chapter 5.2.2, the production of cardanol 15:1 can be due to the rupture of double bonds of other cardanol isomers [251]. The production of cardanol 15:1 is relevant with the high initial quantity of anacardic acid 15:1, which forms cardanol 15:1 during decarboxylation.

At 400 °C, all cardols were converted during CNS and ACC pyrolysis through devolatilization and polymerization reactions. The fact that all cardols were totally converted first before cardanols during ACC pyrolysis was also observed during the study of thermal degradation of ACC Chapter 5.2.2. This could be explained by the extra hydroxyl group possessed by cardols, which make cardols more reactive than cardanols.

The number of moles of anacardic acids isomers that reacted during pyrolysis was compared with the number of moles of cardanol isomers produced during pyrolysis (Table 5.6).

Table 5.6: Anacardic acids in CNS ($n_{AA\ before\ pyrolysis}$) and Cardanols produced during pyrolysis ($n_{CDN\ produced\ during\ pyrolysis}$) at 400°C (mmol/g).

	$n_{AA\ before\ pyrolysis}$ (mmol/g of CNS)	$n_{CDN\ produced\ during\ pyrolysis}$ (mmol/g of CNS)	
		CNS pyrolysis	ACC pyrolysis
Saturated (15:0)	0.029	0.055	0.051
Monoene (15:1)	0.335	0.286	0.224
Diene (15:2)	0.262	0.128	0.103
Triene (15:3)	0.246	0.086	0.038

Having a look at the unsaturated anacardic acids (15:1,15:2 and 15:3), there are less cardanols produced during the pyrolysis than anacardic acids decarboxylated. This confirms that cardanols 15:1, 15:2 and 15:3, which are produced by the decarboxylation of anacardic acids subsequently undergo further thermal reaction through either devolatilization reactions into lighter chemical compounds or possible polymerization reactions.

Very few cardanol 15:3 was produced during pyrolysis because it certainly underwent significant polymerisation reaction during pyrolysis compared to other unsaturated compounds. Indeed, this least saturated cardanol with three double bonds is more reactive to polymerization reactions than the other isomers [30].

From this table 5.6 it is observed that ACC pyrolysis produces less cardanols than in the case of CNS. This is because when pyrolysis ACC alone, the cardanols and cardols have more contact surface between them, which facilitates polymerization reactions.

5.3.3.2 Tars

In the previous section, we quantified the remaining ACC constituents in the pyrolysis condensates using HPLC/UV.

This section focuses on the quantification of tars in the pyrolysis condensates.

GC-MS method was used to quantify 85 chemical compounds in the condensates commonly found in lignocellulosic condensates from pyrolysis.

A comparison on the mass of quantified tars among CNS, ACC-free CNS, ACC and wood chips pyrolysis condensates is presented (mg/g sample) in Figure 5.17. The chemical compounds in the pyrolysis condensates are categorized by chemical families: alcohols, aldehydes and ketones, acids, sugars, anisoles, guaiacols, furans, N-aromatics, aromatics, phenols and PAH (Polycyclic Aromatic Hydrocarbon).

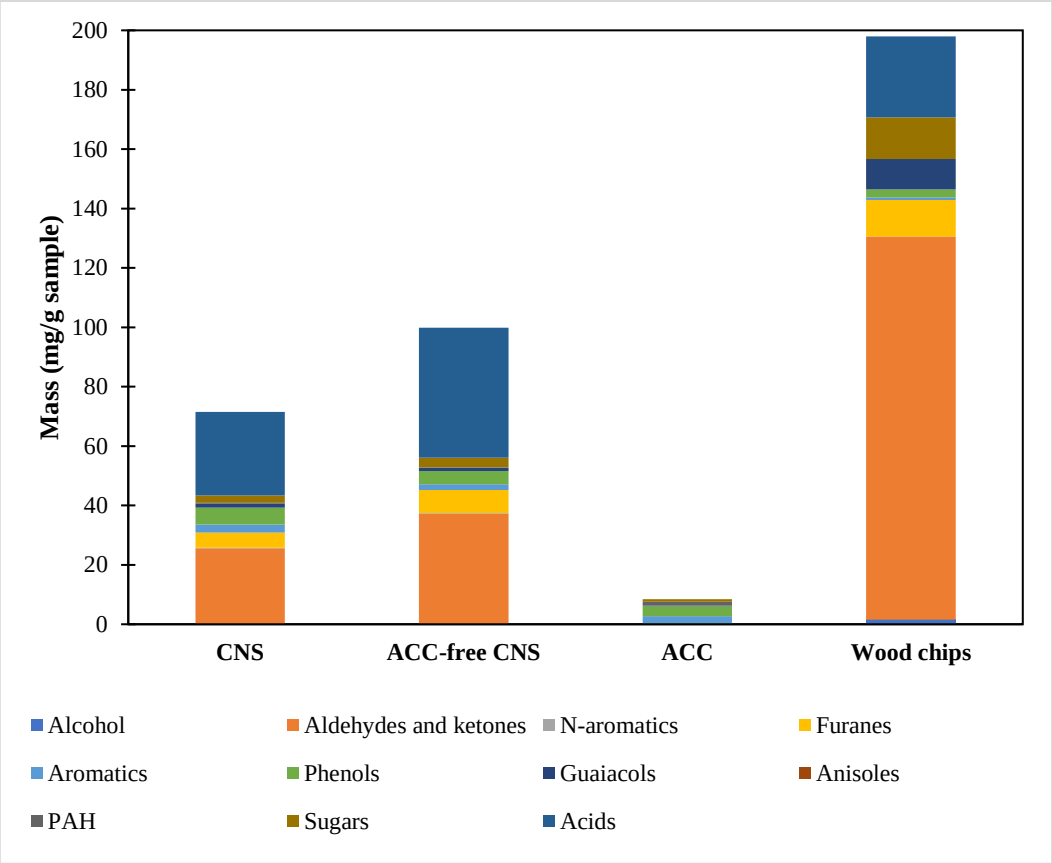

Figure 5.17: Mass of quantified tars by chemical families formed during pyrolysis at 400°C (mg/g sample)

The distributions of quantified tars are similar in the case of CNS and ACC-free CNS pyrolysis. The main chemical families found in both condensates are acids and ketones. The quantified acids present were acetic acid and propionic acid. The quantified ketones include 1-hydroxy-2-propanone, 2-cyclopenten-1-one, 3-methyl-2-cyclopenten-1-one, 1-hydroxy-2-butanone, 3-methyl-1,2-cyclopentandione, 1-acetyloxy-2-propanone and cyclopentanone. In the case of wood chips pyrolysis, the same ketones were present in the condensates. The formation of ketones is due to the decomposition of cellulose and hemicelluloses.

The difference between wood chips vs. CNS related samples was the presence of aldehydes (formaldehyde, acetaldehyde and glycolaldehyde) in the wood chips pyrolysis condensates. It is interesting to note that CNS related samples do not form these aldehydes even though aldehydes are mainly issued from macromolecules (hemicelluloses, cellulose and lignins) degradation. Aldehydes and ketones are the main chemical families (66%) quantified in wood chips pyrolysis.

In the case of ACC, the mass distribution of quantified tars is much different than the other samples. The two main chemical families present in the ACC pyrolysis condensates were phenols and aromatics.

56% of the quantified tars in the ACC pyrolysis condensates are made up of phenols. The mass distribution of quantified tars in the case of ACC is distinct when compared to other samples (CNS, ACC-free CNS and wood chips). The phenols present include, phenol, 2-methylphenol, Phenol-3-methyl+Phenol-4-methyl, 3,4-dimethylphenol, 2,4-dimethylphenol, 1-napthalenol, 2-napthalenol and hydroquinone. All these phenols are also present in other samples (CNS, ACC-free CNS and wood chips).

Apart from phenols, the main chemical family found in the ACC pyrolysis condensates are the aromatics. They account up to 40% among the quantified tars. The aromatics include benzene, toluene, ethylbenzene, (m+p) xylene, O-xylene, styrene, indene, 2-methyindene. These aromatics are tertiary tars (light phenols) that are issued from the thermal degradation of primary and secondary tars (heavier phenols).

5.3.3.3 Qualitative analysis of ACC pyrolysis condensates

The tars quantified in the ACC pyrolysis condensates only represented 1% of the total condensates. Therefore, qualitative analysis was carried out to identify other chemical compounds in the ACC pyrolysis condensates.

The qualitative analysis was carried out using MassHunter Unknown Analysis-deconvolution method. Deconvolution method was used to separate the mass spectra of the GC-MS chromatogram, which allows us to identify and quantify individual compounds even when they co-elute (appear together) during the chromatographic separation. The deconvolution method calculates the area of each individual compounds identified.

The list of chemical compounds in ACC pyrolysis condensates with a peak area percentage >1% is presented in Table 5.7. The chemical compounds are presented in the decreasing order of peak area percentage (%).

Table 5.7 : Major chemical compounds in ACC pyrolysis condensates characterized by GC-MS

Chemical compounds	Retention time (min)	Peak area percentage (%)	Match factor (%)
ACC constituents			
Cardanol 15 :1	78.83	33.21	66.84
Cardanol C17 :2	79.20	6.12	68.85
Cardanol 15 :0	71.31	5.80	75.69
Cardol C15 :2	94.43	1.86	74.19
Cardol C15 :1	93.41	1.79	87.26
Cardanol C17 :1	83.56	1.59	95.08
Cardanol C13 :0	74.44	1.37	97.58
Cardanol C17 :2	76.05	1.09	85.00
Other chemical compounds			
Acetoin	7.29	21.68	78.76
Acetic acid, 4-methylphenyl ester	73.28	5.80	75.69
Spiro[2.4]heptane, 1,2,4,5-tetramethyl-6-methylene-	79.89	1.33	79.90

According to Table 5.7, the main chemical compounds detected through the qualitative analysis were cardanols and cardols of different aliphatic chain lengths (C13, C15 and C17). They account up to 53% of the total area.

Unlike the analysis of condensates by HPLC (see Chapter 5.3.3.1), GC-MS did not detect cardanols 15:2 and 15:3. This could be explained by the devolatilization reactions of these unsaturated cardanols that take place within the GC-MS injection chamber (270°C).

Surprisingly, this qualitative analysis detected cardol C15:2 and C15:1 which both were not detected by HPLC. This is because the concentrations of both chemical compounds were much below the detection limit of HPLC. Another explanation is that they were formed inside the GC-MS injection chamber by devolatilization reactions.

Among the ACC constituents, Cardanol 15:1 has the maximum peak area percentage (33.21%), followed by Cardanol C17:2 (6.12%) and Cardanol 15:0 (5.80%). As mentioned previously, Cardanol 15:1 is produced by the decarboxylation of anacardic acid 15 :1 but could also be produced by devolatilization [251] of other cardanol isomers, thermal degradation of polymers and evaporation. Cardanol C13:0 could result from the thermal rupture of the aliphatic side chains [252] of Cardanol 15:1 but also from the thermal degradation of cardanol-based polymers. Cardanol C17:1 and C17:2 could be produced by the thermal degradation of cardanol based polymers.

It is interesting to note that, the fact that there were cardanols with C17 and C13 aliphatic chains in the condensates could mean that thermal oligomerization of cardanols took place and formed dimers with C30 aliphatic chains. And when these dimers undergo thermal degradation, they break into C17 and C13 molecules. This is in accordance with the study of Rodrigues et al where dimer was the main oligomer that was formed during thermal oligomerization of cardanols [217].

Cardol 15:1 and Cardol 15:2 were also present in the ACC pyrolysis condensates. This could be due to thermal degradation of cardol-based polymers, rupture of aliphatic side chains of other cardol isomers or evaporation.

Acetoin, acetic acid, 4-methylphenyl ester and Spiro[2.4]heptane, 1,2,4,5-tetramethyl-6-methylene could be products of polymerization and devolatilization reactions. Their formation could not be explained due to the complex chemical reactions involved in their synthesis and requires further studies.

5.3.4 Influence of temperature on pyrolysis products

The pyrolysis temperature studied was 400°C, 450°C and 500°C. Although as mentioned previously, that most volatile matters are released before 400°C using PyTar reactor, TG studies showed that the degradation of ACC continues up to 450°C or even 500°C, depending on the operating condition (mass, heating rate etc.). Furthermore, the selected temperatures of 400°C, 450°C, and 500°C are optimal for studying the pyrolysis of CNS because they cover the critical range where major biomass components decompose, providing insights into the thermal behavior and product distribution. The sample masses of CNS and ACC were the same than in previous study (4.5 and 1.9 g respectively). The N_2 flow rate in the pyrolysis zone and the cracking zone were set at 30 L/h and 16.39 L/h respectively.

The yield of char, condensates and gas obtained was determined.

In both cases, CNS and ACC, the char, condensates and gas yields remained constant for the pyrolysis at the 3 temperatures. As there is no influence of temperature (400°C – 500°C) on the pyrolysis gas yield (condensates and gas) of both CNS and ACC, 400°C was confirmed a right choice as the pyrolysis temperature for the study of conversion of pyrolysis gas (Chapter 6).

5.3.4.1 Permanent gas

The composition of pyrolysis gas obtained during the pyrolysis of CNS and ACC was determined (Figure 5.18). C_2H_2 is not presented in the results as its percentage is negligeable (0%) when compared to other permanent gases.

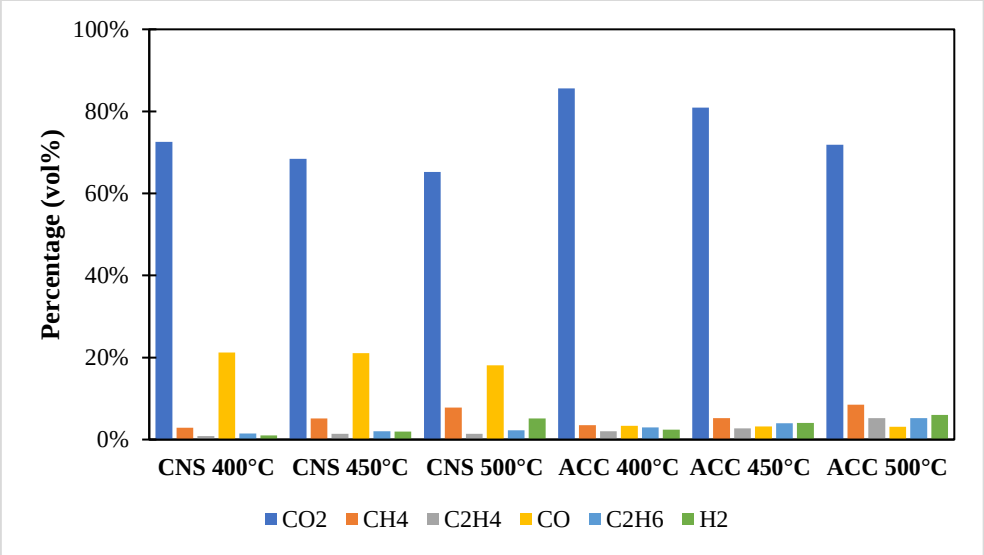

Figure 5.18: Pyrolysis gas composition of CNS and ACC (400, 450 and 500°C)

Although the pyrolysis products yields were constant in both CNS and ACC pyrolysis when varying the temperature, the CO_2 and CO percentages slightly decrease with the pyrolysis temperature. As the temperature increases beyond 400°C, the majority of oxygen containing groups such as cellulose, lignins, hemicelluloses and most ACC have already decomposed, therefore less CO_2 and CO are produced with the increasing temperature.

A particularity was observed when studying the total gas flow rate during ACC pyrolysis at 500°C, in which a secondary peak of gas production was clearly observed (Figure 5.19).

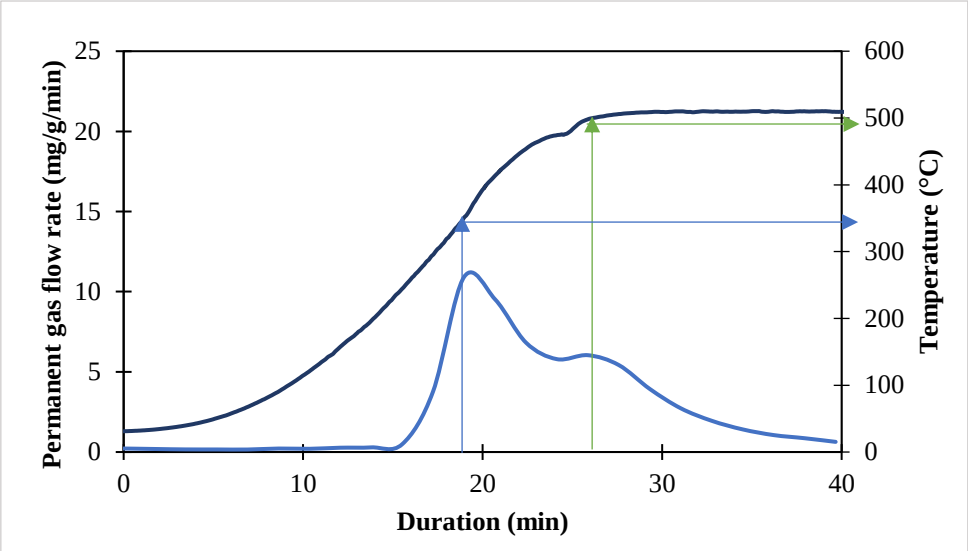

Figure 5.19: Permanent gas flow rate (blue) and pyrolysis temperature (black) of ACC pyrolysis at 500°C

The first peak in the figure (357°C) corresponds to the first gas production, which is due to the thermal degradation of ACC.

Based on this figure 5.19, it is confirmed that secondary reactions of pyrolysis take place during ACC pyrolysis at 500°C, producing CO, C_2H_2, C_2H_4, C_2H_6, CH_4 and H_2. This is in accordance with the third degradation peak observed at 427°C in previous section (Figure 5.7) attributed to the thermal degradation of cardanol based and cardol based polymers.

5.3.4.2 Condensates

In terms of condensates, when the pyrolysis temperature increases, the ACC content decreases. This is logic because a higher temperature facilitates the thermal degradation of ACC. Unlike at 400°C, where all cardanol isomers were present (see 5.3.3.1), at 450°C and 500°C, only cardanol 15:1 was present in the pyrolysis condensates. A higher pyrolysis temperature could promote polymerization reactions of the more unsaturated cardanols. The tars quantified were very little in terms of quantity (<5 wt% of sample) as the GC-MS method used was more adapted for lignocellulosic biomass. There was no obvious correlation between the water content and the pyrolysis temperature in both CNS and ACC pyrolysis.

5.3.4.3 Char

The char produced by ACC pyrolysis (Figure 5.20) showed a porous, fibrous and somewhat shiny surface compared to CNS and other lignocellulosic biomass char. The shiny appearance of the char could be due to the partial graphitization of the carbon during pyrolysis. The porous and fibrous structure of the char is likely a result of polymer cracking during ACC degradation.

As the polymers thermally degrade, volatile compounds are released and diffuse outward, contributing to the formation of the porous structure. This shiny, porous and fibrous characteristic of ACC char was not observed in CNS char.

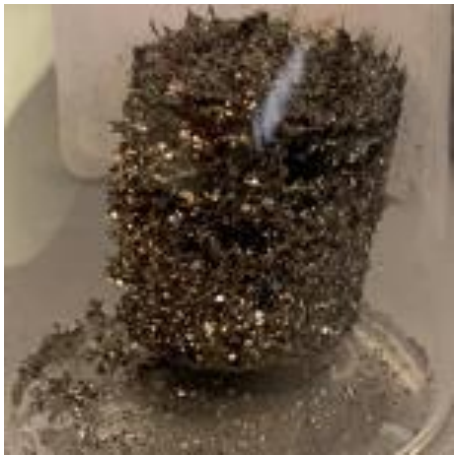

Figure 5.20: ACC-derived char produced by pyrolysis at 500°C

Given the unique structural characteristics observed in ACC-derived char, further studies could be carried out to gain a deeper understanding of its formation and properties. Techniques such as Raman spectroscopy, X-ray diffraction (XRD), and scanning electron microscopy (SEM) could be employed to analyze the char's structure, degree of graphitization, surface morphology, and elemental composition.

5.4 Summary

Pyrolysis of CNS, of ACC and of their individual constituents was investigated using both a micro-TG and a lab-scale fixed bed reactor.

DTG on ACC and ACC-free CNS allowed us to separate and identify temperature peaks of successively decarboxylation of anacardic acid, degradation of ACC, and degradation of polymeric intermediates derived from ACC, as well as classical peaks of hemicelluloses, cellulose and lignins degradation.

The study highlighted the occurrence of intermolecular interactions between the solid matrix and the extractives within the CNS during pyrolysis at 400°C: the solid matrix hinders the conversion of ACC, resulting in 52% of ACC conversion rate rather than 61% when pyrolyzing ACC alone.

Kinetics study using microTG reactor highlighted a limitation: chemical regime was not achievable due to presence of ACC even considering a very low mass and minimal heating rate.

Products from CNS pyrolysis at 400°C have been thoroughly characterized and the composition is summarized in the pie chart below (Figure 5.21). It was shown that ACC mainly contribute to the formation of condensates and CO_2 during CNS pyrolysis at 400 °C.

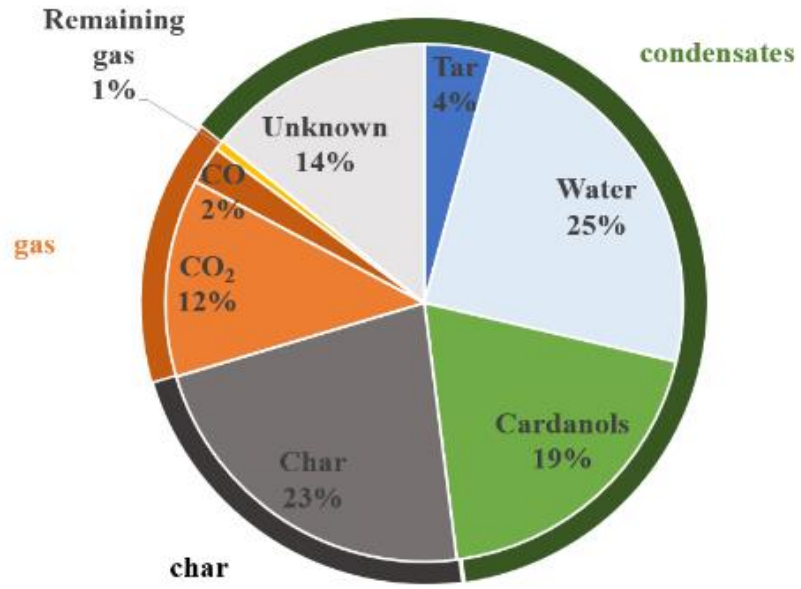

Figure 5.21: Distribution of the products of CNS pyrolysis at 400 °C (dry ash free basis)

Particular attention was paid to the thermal degradation of ACC leading to a series of mechanisms which is summarized in Figure 5.22.

Initially, anacardic acids in the ACC undergo decarboxylation (around 125-190°C), producing cardanols and CO_2.

Then, polymerization of cardanols takes place (around 190-250°C).

Next, in the temperature range of 250-385°C, several competing reactions take place: polymerization of cardanols and cardols to form cardanol based and cardol based polymers, devolatilization of cardanols and cardols, as well as evaporation of cardanols. Thermal cracking of cardanol and cardol based polymers also starts to take place. It is noted that high concentration of ACC favorizes polymerization reactions due to increased intermolecular interactions.

And finally (T°>385°C), the polymers formed during these processes undergo further thermal degradation, leading to secondary gas production. These polymers may undergo depolymerization, as indicated by the presence of cardanols with C17 and C13 aliphatic chains in the ACC pyrolysis condensates. The degradation of the polymers contributes to the formation of char towards the end of the pyrolysis reactions.

Future research should prioritize the investigation of polymers formation and degradation to provide further validation and refinement of the proposed mechanisms.

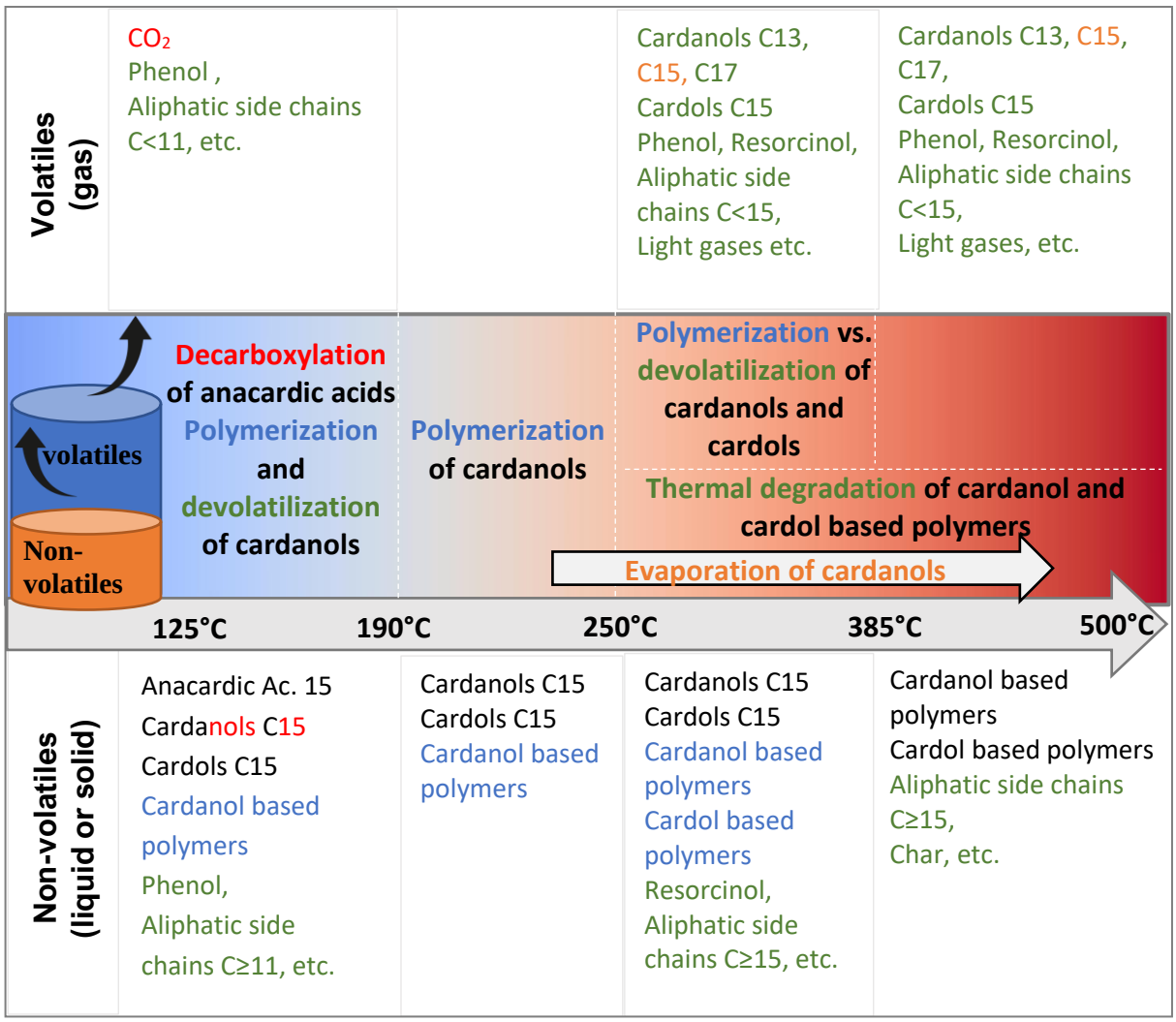

Figure 5.22 : ACC degradation mechanisms and products during CNS pyrolysis, initial products (black), decarboxylation products (red), polymerization products (blue), thermal degradation and devolatilization products (green),evaporation products (orange)

CHAPTER 6

Cracking of CNS pyrolysis gas

6. Cracking of CNS pyrolysis gas

In the previous chapter, we have comprehensively examined the pyrolysis of cashew nut shells (CNS) and their individual components. Building on this foundation, the present chapter focuses on the conversion of CNS pyrolysis gas under several operating conditions. This investigation centers on two primary pyrolysis gas cracking reactions that occur during thermochemical conversion processes: thermal and catalytic cracking. The aim of the study is to contribute information regarding the conversion of pyrolysis gas, in order to limit the formation of condensates (tars), and optimize the production of combustible gas such as CO and H_2 in industrial applications.

We first investigated the thermal cracking products derived from CNS pyrolysis gas and compared the results to a lignocellulosic biomass reference (wood chips), with a focus on the behavior on each CNS components (ACC and ACC-free CNS). The study was followed by investigating the influence of temperature on the thermal cracking of CNS pyrolysis gas.

For catalytic cracking, we utilized char derived from CNS produced at 910°C as catalyst and investigated the catalytic cracking at 600°C.

The experimental work was conducted using the same pyrolysis and tar cracking reactor (PyTar) as employed in the previous pyrolysis studies (Chapter 5).

This chapter is structured as follows:

- The first section provides definitions of the terms and the calculations applied in these experiments.
- Section 2 presents the results of thermal cracking experiments of CNS pyrolysis gas.
- The third section deals with the influence of temperature on the distribution of thermal cracking products from CNS pyrolysis gas.
- Lastly, this chapter presents the catalytic cracking experiments of CNS pyrolysis gas using CNS char as catalyst.

By exploring these reactions under controlled conditions, we aim to gain deeper insights into the mechanisms and optimization strategies for the efficient conversion of CNS pyrolysis gas in thermochemical conversion processes such as gasification.

6.1 Definition and calculations

In this section, we outline the key parameters and calculations used to describe and analyze the cracking experiments. We focus on the conversion rate of organic condensates, temperature profiles within the cracking zone, gas residence times, and the variation (production or consumption) of each constituent during cracking.

6.1.1 Conversion rate of organic condensates

We consider as a first approach the following global reaction scheme to represent the cracking of pyrolysis gas (Equation 6.1).

Organic condensates → Permanent gas *Equation 6.1*

The conversion rate of organic condensates (X_{craq}) is defined as (Equation 6.2):

$$X_{craq} = 1 - \frac{m_{cond\ craq}}{m_{cond\ pyro}} \qquad \textit{Equation 6.2}$$

In which $m_{cond\ craq}$ is the mass of water-free condensates remaining after the cracking of pyrolysis gas, and $m_{cond,\ pyro}$ is the mass of water-free condensates produced by the pyrolysis.

6.1.2 Temperature profile in the cracking zone

In order to adjust the nitrogen flow rate to obtain the desired residence time of the experiment, the length of the isothermal zone first had to be identified. The temperature profiles were measured for different reaction control temperatures (600°C, 800°C and 1000°C) from the exit of the pyrolysis zone (Figure 6.1).

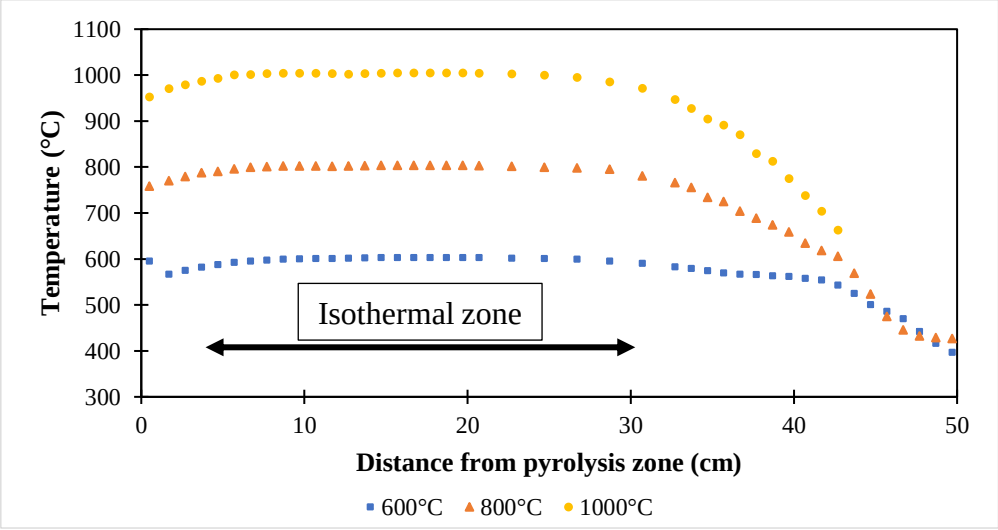

Figure 6.1: Temperature profiles of cracking zone

From this figure, we considered an isothermal zone of 25 cm: from 5 to 30 cm. This value was used to calculate the residence time of all experiments.

6.1.3 Residence time of thermal cracking experiments

In order to improve the homogeneity of temperature in the cracking zone and ensure quick gas preheating [31], a 3 cm inert alumina bed was added on the top of the cracking tube, just next to injection of the pyrolysis zone (Figure 6.2). According to the study of Huchon et al., the alumina bed does not have a catalytic effect [31].

The total residence time of the experiment is the sum of the residence time in the zone a) that is filled with 3 cm of alumina (3 cm) and in the zone b), free (22 cm).

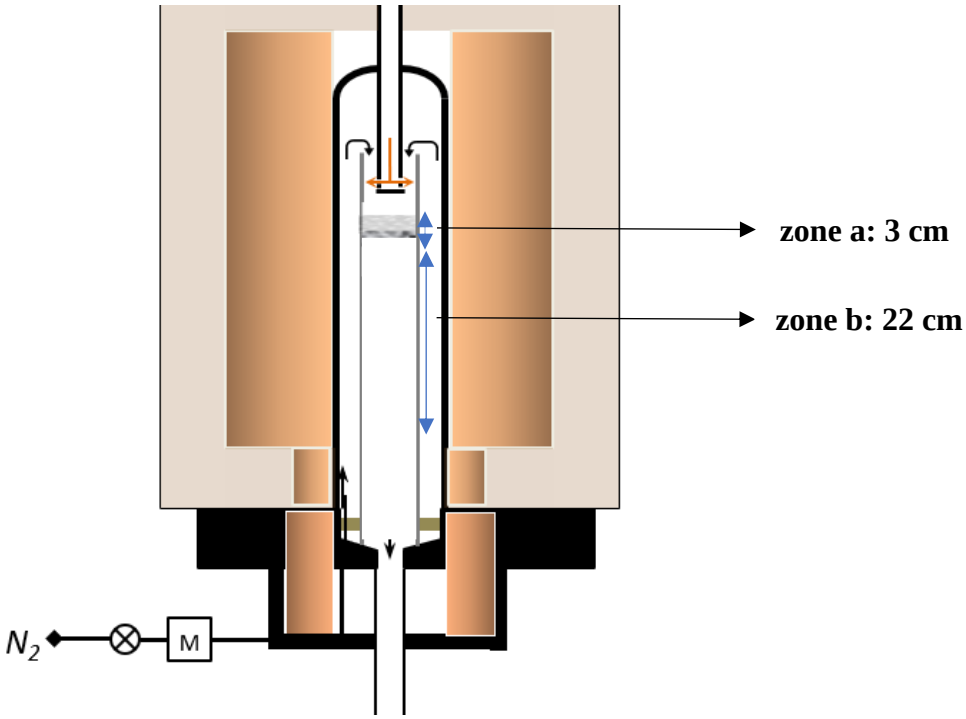

Figure 6.2: Cracking zone

The residence time was calculated using the equations below (Equation 6.3 and 6.4).

$$\text{Residence time (s)} = \frac{\text{Length of reaction zone (m)}}{\text{Gas velocity (ms}^{-1})} \qquad \textit{Equation 6.3}$$

with

$$\text{Gas velocity (ms}^{-1}) = \frac{\text{Real gas flow rate (m}^3\text{s}^{-1})}{\text{Surface (m}^2) \times \text{Porosity}} \qquad \textit{Equation 6.4}$$

The porosity of the alumina bed was calculated using the water beaker method (Equation 6.5). This method involves measuring the volume of water filled till it covers the surface of the bed.

$$\varepsilon = \frac{\text{Volume of water needed to fill the pores of the bed}}{\text{Volume of alumina bed}} \qquad \textit{Equation 6.5}$$

With this method, we obtained a value of **0.69** for the porosity of the alumina bed.

6.1.4 Variation of constituent mass during thermal cracking

The calculation of the mass variation (production or consumption) of a constituent *i* during thermal cracking is shown in Equation 6.6.

$$\text{Variation(mg/g pyrolysis gas)} = \frac{m_i^{after\ cracking} - m_i^{before\ cracking}}{\text{m}_{pyro}} \qquad \textit{Equation 6.6}$$

Which

$m_i^{before\ cracking}$ refers to the mass of constituent *i* before cracking. It was calculated from the total gas mass of the cracking experiment and the mass concentration of *i* in the pyrolysis gas measured during reference pyrolysis experiment at 400°C

$m_i^{after\ cracking}$ refers to the mass of constituent *i* obtained after cracking

m_{pyro} refers to the mass of pyrolysis gas of the cracking experiment, that is equal to gas mass after cracking.

A positive value of variation means a production of constituent *i* in the cracked gas compared to its quantity in the pyrolysis gas, whereas a negative value means consumption.

6.2 Thermal cracking of CNS pyrolysis gas

The cracking temperature was selected to 800°C as recommended by previous study [106] for achieving a desirable conversion rate with pyrolysis gas from wood. For this study, a cracking tube of 16 mm i.d. was used. The residence time applied in these experiments was 2.5 s. For this, the nitrogen flow rate in the cracking zone Q_{N_2}'' was fixed at 16.39 L/h.

The operating conditions in the pyrolysis zone for the cracking experiments was the same as the pyrolysis experiments in Chapter 5. Thus, the pyrolysis temperature was fixed at 400°C, with a heating rate of 20°C/min. The nitrogen flow rate in the pyrolysis zone Q_{N_2}' was maintained at 30 L/h. The sample mass used was 4.5 g for CNS or wood chips. The sample

mass of ACC and ACC-free CNS were 2.6 g and 1.9 g respectively to their mass distribution in the CNS.

6.2.1 Conversion and product distribution

The reported results are the average derived from at least two tests, each repeatable within a difference in the conversion rate lower than ± 5%. The mass balance ranges from 88% to 93%, indicating high recovery across the experiments.

The conversion rate of organic condensates after the thermal cracking of pyrolysis gas (CNS, ACC, ACC-free CNS and wood chips) was calculated and presented in Figure 6.3.

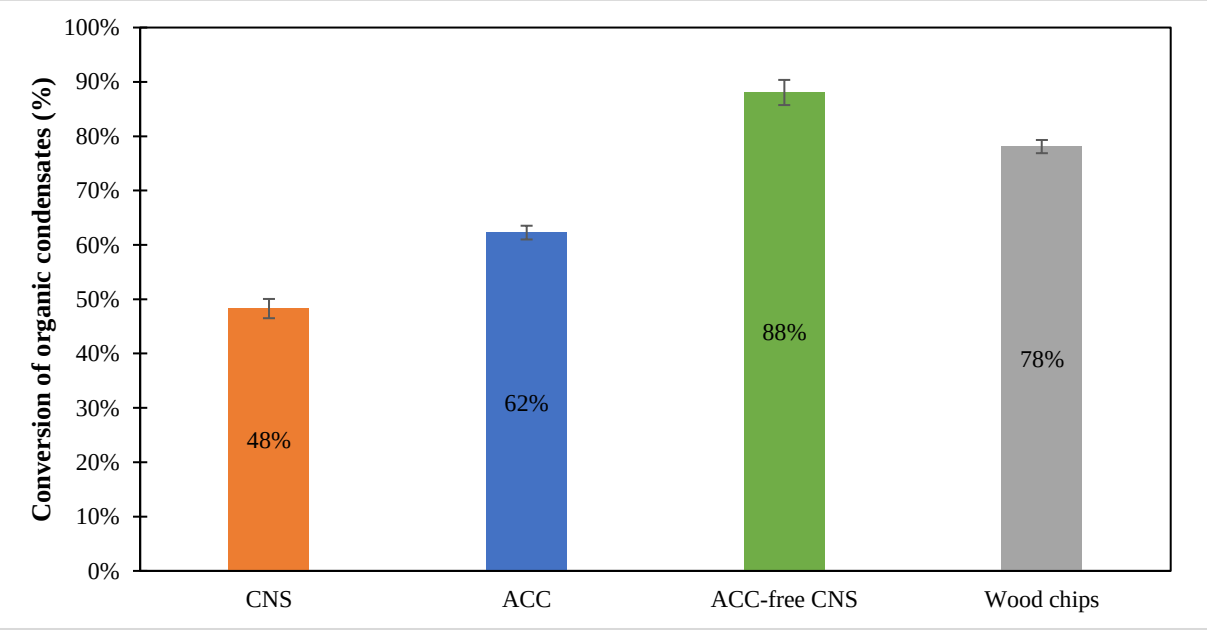

Figure 6.3: Conversion rate of organic condensates via thermal cracking (800°C) of CNS, ACC, ACC-free CNS and wood chips pyrolysis gas in %

Figure 6.3 shows that experiments with ACC-containing samples (CNS and ACC) have lower conversion rates compared to ACC-free samples (ACC-free CNS and wood chips). This difference is explained by the presence of extractives in CNS (ACC), which form more stable condensates that are more resistant to thermal degradation than lignocellulosic derived condensates.

By comparing the conversion rate of CNS experiments and those of CNS components (ACC and ACC-free CNS), it is observed that cracking is more efficient when the CNS components

pyrolysis gases were cracked individually. This could be explained by intermolecular interactions of pyrolysis gas issued from ACC and ACC-free CNS which form more thermally stable condensates during CNS experiments.

The product distribution in the gas: condensates (water-free), permanent gas and water for each experiment (% of pyrolysis gas mass) is shown in Figure 6.4. The maximum error for water and permanent gas yields were +/-2% respectively. The error of the condensates yield is presented by the sum of error of water and permanent gas yields.

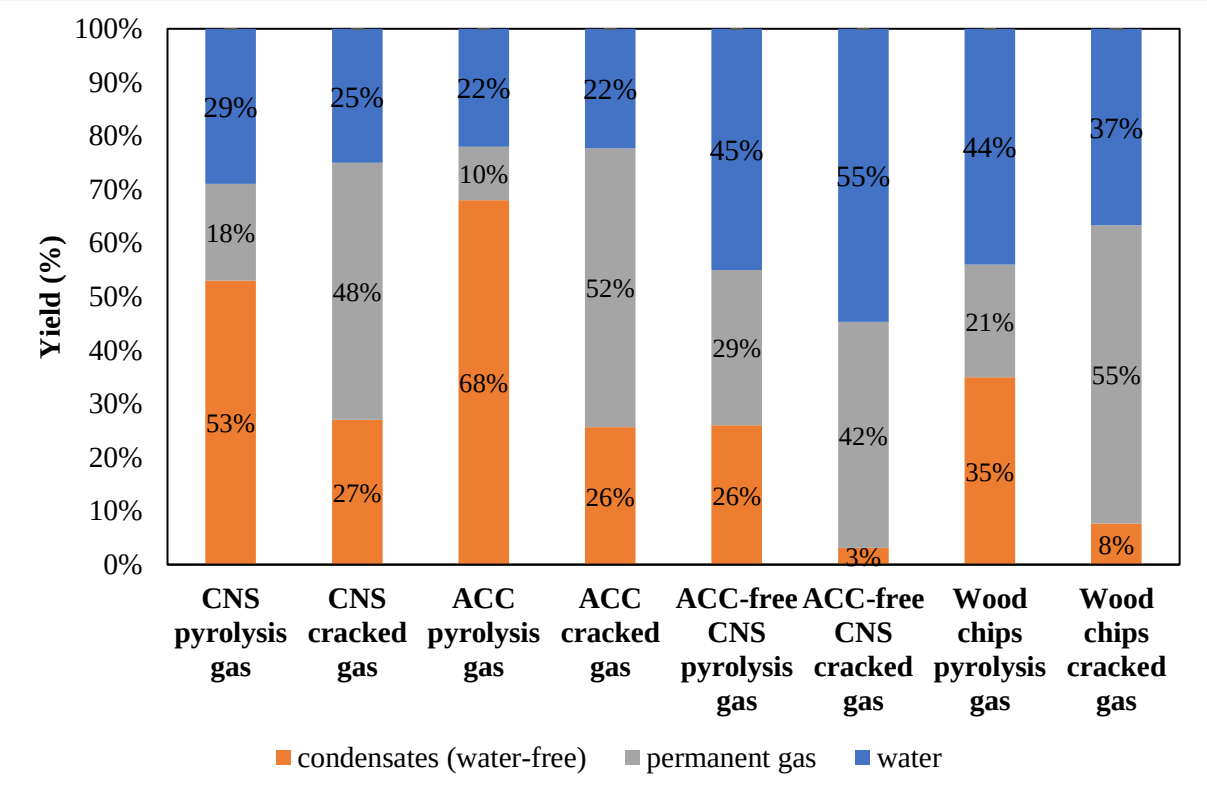

Figure 6.4: Distribution of condensates (water-free), permanent gas, and water before and after cracking at 800°C (CNS, ACC, ACC-free CNS and wood chips) in % of pyrolysis gas mass

For all samples (CNS, ACC, ACC-free CNS and wood chips), thermal cracking at 800°C decreases **the proportion of condensates** to less than 27% while proportionally increasing the share of permanent gas in the pyrolysis gas (maximum 55%).

It is also noteworthy that thermal degradation of extractive-containing biomass (CNS and ACC) generates less water compared to the extractive-free biomass (wood chips and ACC-free CNS).

6.2.2 Permanent gas composition

In order to understand how cracking reactions change the composition of pyrolysis gas, the mass variation (mg/g pyrolysis gas) of the individual permanent gas constituents due to the thermal cracking was determined (Figure 6.5).

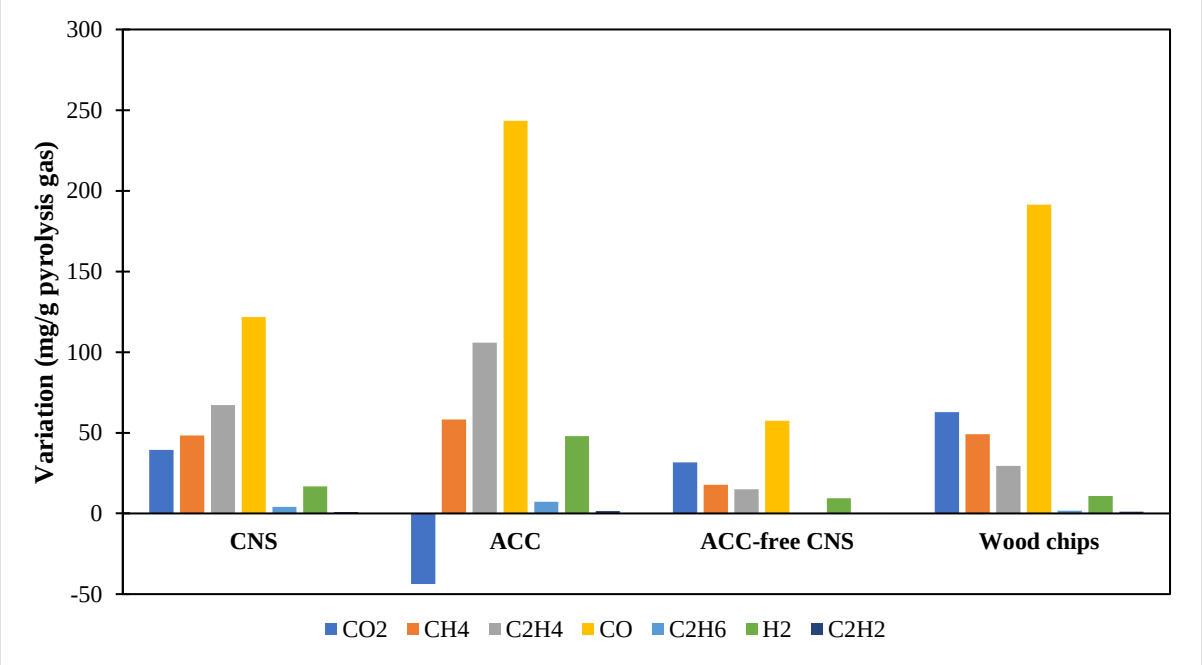

Figure 6.5: Variation of individual permanent gas (CNS, ACC, ACC-free CNS and wood chips experiments, 800°C) in mg/g pyrolysis gas

In all cases, thermal cracking reactions favor the formation of CO, which shows the highest production among the gases. Experiments with ACC show higher CO production (243 mg/g pyrolysis gas) than with ACC-free CNS (58 mg/g pyrolysis gas). This suggests that during the thermal cracking of CNS pyrolysis gas, ACC contribute indirectly to the production of CO.

Moreover, the presence of ACC seems to favor the production of H_2, CH_4 and C_2H_4, higher during CNS and ACC experiments as compared to those with ACC-free CNS.

In terms of CO_2, all experiments showed similar production except the one with ACC alone where a consumption was measured.

6.2.3 Condensates composition

Using the GC-MS method, the quantity of tars in the condensates before and after cracking of pyrolysis gas (CNS, ACC, ACC-free CNS and wood chips) was determined (Table 6.1). Although the GC-MS method only quantify 85 chemical compounds, it still allowed us to relatively compare the composition of quantified tars between the experiments.

Table 6.1: Quantified tars in the condensates before and after cracking of pyrolysis gas (CNS and wood chips) (mg/g pyrolysis gas)

Tars	***CNS***		***ACC***		***ACC-free CNS***		***Wood chips***	
	Before cracking	After cracking	Before cracking	After cracking	Before cracking	After cracking	Before cracking	After cracking
Primary tars	43.4	0.9	1.1	0.1	61.4	1.2	120.4	0.4
Secondary tars	4.0	1.0	2.9	0.1	2.9	0.5	1.6	0.7
Tertiary tars	2.1	49.2	3.3	43.6	1.5	14.0	0.5	22.0
Total quantified tars	49.5	51.1	7.3	43.8	65.8	15.7	122.5	23.1
ACC	224.7	-	377.3	-	-	-	-	-

The table shows that for all samples except for ACC experiments (CNS, ACC-free CNS and wood chips), the total quantified tars issued from pyrolysis (before cracking) were dominated by primary tars. After cracking, these primary tars thermally converted into tertiary tars. Almost no primary tars were left in the condensates, as at elevated temperature they were converted into tertiary tars. However, for ACC experiments, almost no tars were detected in the pyrolysis gas (7.3 mg/g pyrolysis gas). One reason is that the GC-MS method has been developed for lignocellulosic-derived tars and seems less adapted to ACC-derived tars.

Before cracking, condensates of CNS and ACC pyrolysis gas contained ACC at concentrations of 224.7 mg/g and 377.3 mg/g respectively, which were composed only of cardanols. After cracking, no ACC was detected in the condensates. This means that at 800°C, all ACC transformed into their degradation products in the cracking zone.

Since most of the quantified tars were tertiary tars in the cracked gas, we focused on studying the composition of these tertiary tars. Figure 6.6 shows the main tertiary tars quantified in the condensates after thermal cracking of pyrolysis gas. The results are presented in terms of variation before and after thermal cracking (mg/g pyrolysis gas).

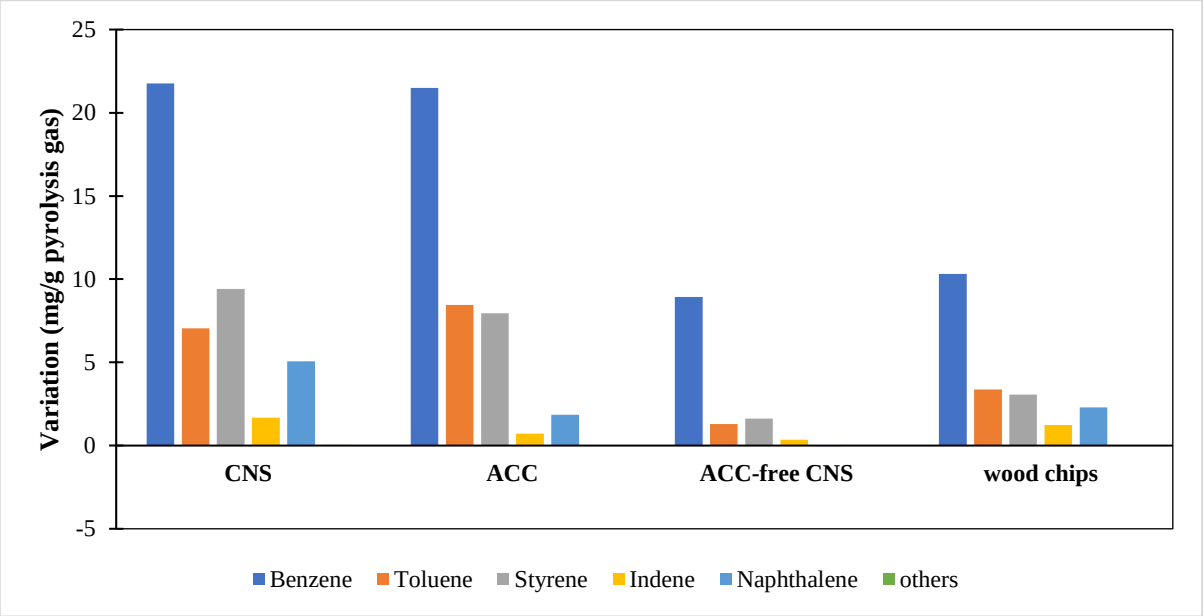

Figure 6.6: Variation of main tertiary tars in the condensates (CNS, ACC, ACC-free CNS and wood chips experiments, 800°C) in mg/g pyrolysis gas

The main tertiary tars produced were the same in all samples: benzene, toluene, styrene, indene and naphthalene. Their formation in the CNS and ACC experiments was due to the cracking reactions of ACC and their polymers, and of primary and secondary tars. Whereas in the ACC-free CNS and wood chips experiments, the formation of tertiary tars was mainly due to the conversion of primary tars and secondary tars.

The quantified tertiary tars were dominated by benzene in all experiments (CNS, ACC, ACC-free CNS and wood chips). Indeed, benzene is known to very stable, and refractory to thermal cracking at 900°C [253] . On the other hand, its formation is known to result from the cracking of larger aromatic compounds. Demethylation (hydrogenolysis) of ethylbenzene and toluene forms benzene [254] .

The formation of toluene in the CNS and ACC cracked gas was higher than the one in ACC-free CNS and wood chips. Toluene in CNS cracking experiments could be explained by 2 sources: a) the cracking of residual cardanols formed during pyrolysis as well as their thermal degradation products (polymers, phenolics, etc.) due to ACC, and b) the cracking of lignocellulosic derived components.

An example of the formation of styrene in the experiments could be explained by the dehydrogenation of ethylbenzene [255] whereas indene could be formed by the cracking of naphthalene [256] .

The production of naphthalene in most of the experiments could be explained by the conversion of phenol during thermal cracking [31,257]. Naphthalene can also be produced by demethylation reactions of 1-naphthalene methyl and 2-naphthalene-methyl [31]. But the absence of production in ACC-free CNS experiments is not explained.

6.3 Influence of temperature on thermal cracking of CNS pyrolysis gas

The thermal cracking of CNS pyrolysis gas produced at 400 °C was studied at different temperatures: 600 °C, 800 °C and 900 °C. The residence time applied in these experiments was 2.5 s. A cracking tube of 16 mm i.d. was used.

In order to obtain the same residence time for all experiments, the nitrogen flow rate in the cracking zone was calculated and adjusted according to the temperature applied. The cracking zone flow rate of the experiments were 27.0 L/h at 600°C, 16.4 L/h at 800°C and 12.4 L/h at 900°C.

The results are presented in the following sections, first in terms of conversion and product distribution, and lastly the permanent gas and condensates compositions.

6.3.1 Conversion and product distribution

The conversion rates of organic condensates were calculated for different cracking temperatures (600, 800 and 900°C) and are presented in Figure 6.7.

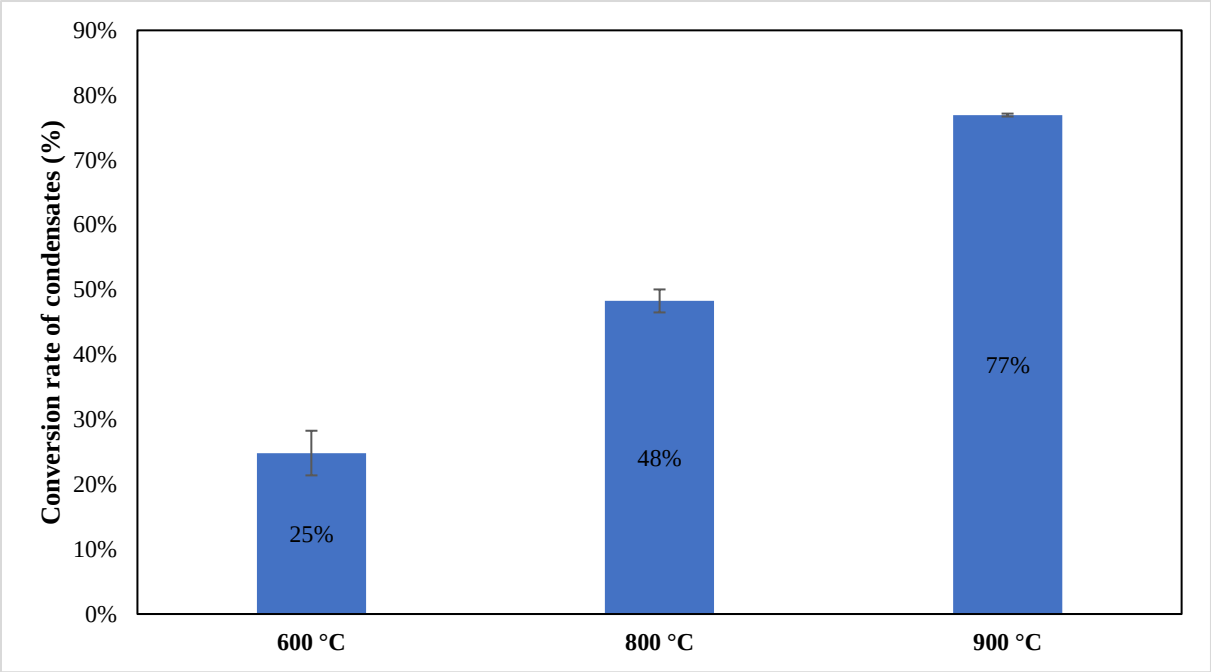

Figure 6.7: Conversion rate of organic condensates via thermal cracking (800°C) of CNS pyrolysis gas at 3 different temperatures (600,800 and 900°C) in %

The figure demonstrates a strong positive correlation between temperature and the conversion rate of organic condensates, with an increase from 25% at 600°C to 77% at 900°C.

The product distribution of condensates (water-free), permanent gas, and water before and after cracking for 3 temperatures (600,800 and 900°C) was determined and is shown in Figure 6.8. The maximum error for water and permanent gas yields were +/-2% respectively.

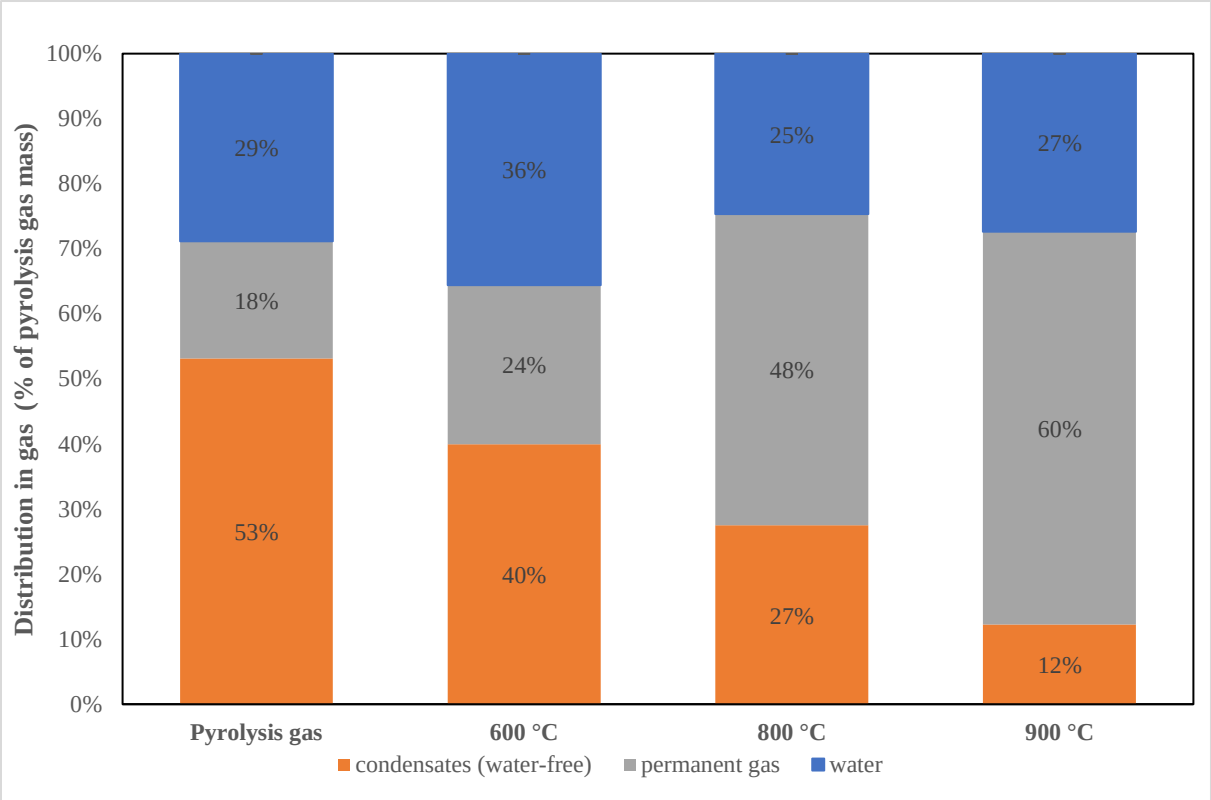

Figure 6.8: Distribution of condensates (water-free), permanent gas, and water before and after cracking for 3 temperatures (600, 800 and 900°C) in % of pyrolysis gas mass

The percentage of condensates decreases with the temperature as the cracking of heavy molecules is known to be improved at higher temperatures. This results in the increase of the percentage of permanent gas with the cracking temperature.

A water production due to cracking was measured only at 600°C. It can result from reactions involving oxygen-containing functional groups present in the hydrocarbons. This includes hydroxyl (-OH) [258] or carboxyl (-COOH) groups [259], which are present in the lignocellulosic fraction, tannins and the ACC compounds. Cardanols and cardols both contain hydroxyl groups.

At 800 and 900°C, the water content is similar before and after cracking. During these temperatures, water production due to thermal cracking can be compensated by reactions such as water-gas shift reaction.

6.3.2 Permanent gas composition

The effect of temperature on the variation of the mass of permanent gas was investigated. The results are depicted in Figure 6.9, which illustrates the variation in percentage of individual permanent gas components: CO_2, CH_4, C_2H_4, CO, C_2H_6, and H_2.

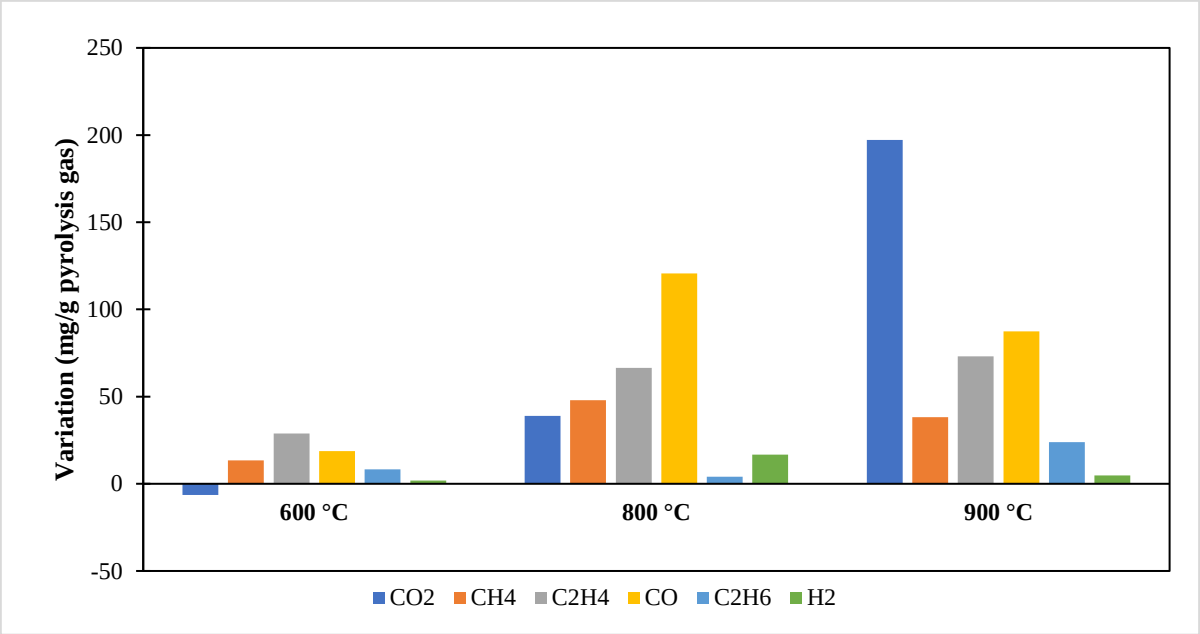

Figure 6.9: Variation of individual permanent gas (600,800 and 900°C) in mg/g pyrolysis gas

As the temperature increases from 600°C to 900°C, there is a significant shift towards the production of gas, particularly CO_2. The increase in production of CO_2 can be attributed to water gas shift reaction, despite the rise in CO mass from 600 to 800°C, which can be produced by other reactions.

Regarding carbon monoxide (CO), its production initially rises, increasing by 19 mg/g pyrolysis gas at 600°C and reaching a peak of 121 mg/g pyrolysis gas at 800°C. The observed decrease in CO concentration beyond 800°C suggests that the water-gas shift reaction is becoming more dominant, converting CO into CO_2 and H_2 as the temperature approaches 900°C.

The percentage of CH_4 which increases between 600°C and 800°C could be explained by the cracking of heavier hydrocarbons such as aromatics, C_2H_6 etc. The decrease in the mass of CH_4 as the temperature increases from 800°C to 900°C is not significant enough to be discussed.

The C_2H_4 increases with the temperature could be explained by the cracking of other heavier hydrocarbons.

According to the figure 6.9, temperature does not have much influence on the production of H_2 in the CNS cracked gas when compared to other permanent gases.

6.3.3 Condensates composition

The quantified tars, determined using the GC-MS method, are presented by tars groups (primary, secondary and tertiary tars) in mg/g of pyrolysis gas (Figure 6.10).

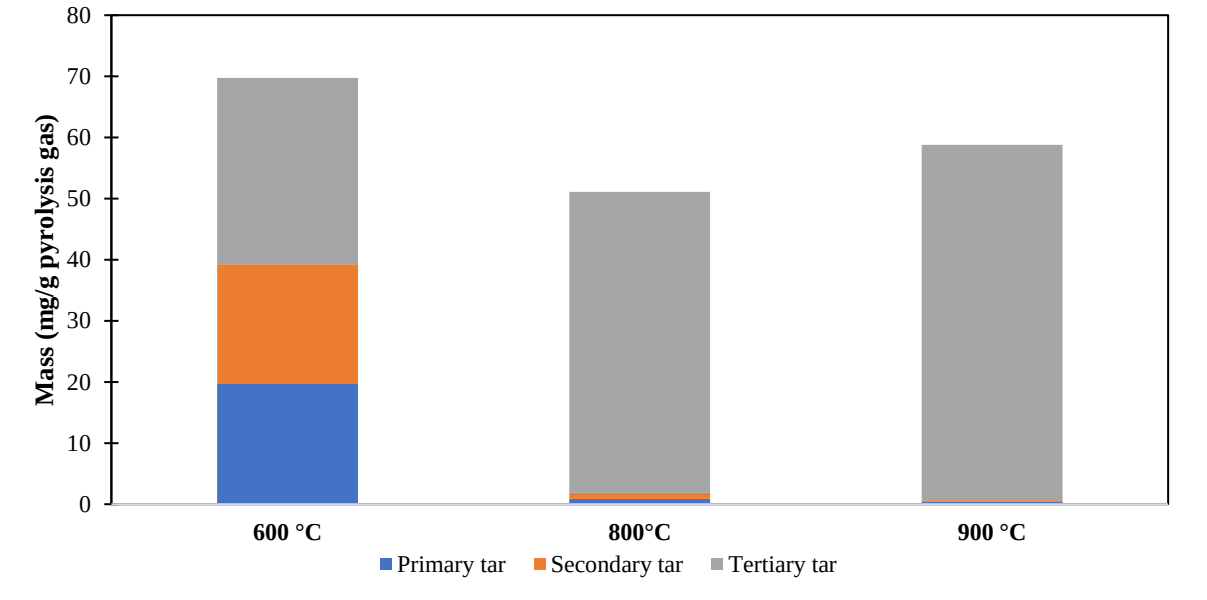

Figure 6.10: Tars distribution (by group) of thermal cracking of CNS pyrolysis gas (600,800, and 900°C) in mg/g of pyrolysis gas

Temperature has a significant impact on primary tars, causing them to undergo rapid conversion into secondary tars, tertiary tars and permanent gases. After thermal cracking at 600°C, tertiary tars are dominant and the fractions of primary and secondary tars are more or less equal. The dominance of tertiary tars is significant beyond 800°C, as they account for more than 95% of total tars This means that beyond 800°C, most heavy tars are already converted to light molecules.

Figure 6.11 shows the main tertiary tars after thermal cracking of CNS pyrolysis gas (600, 800 and 900°C). The results are presented in terms of variation (mg/g pyrolysis gas).

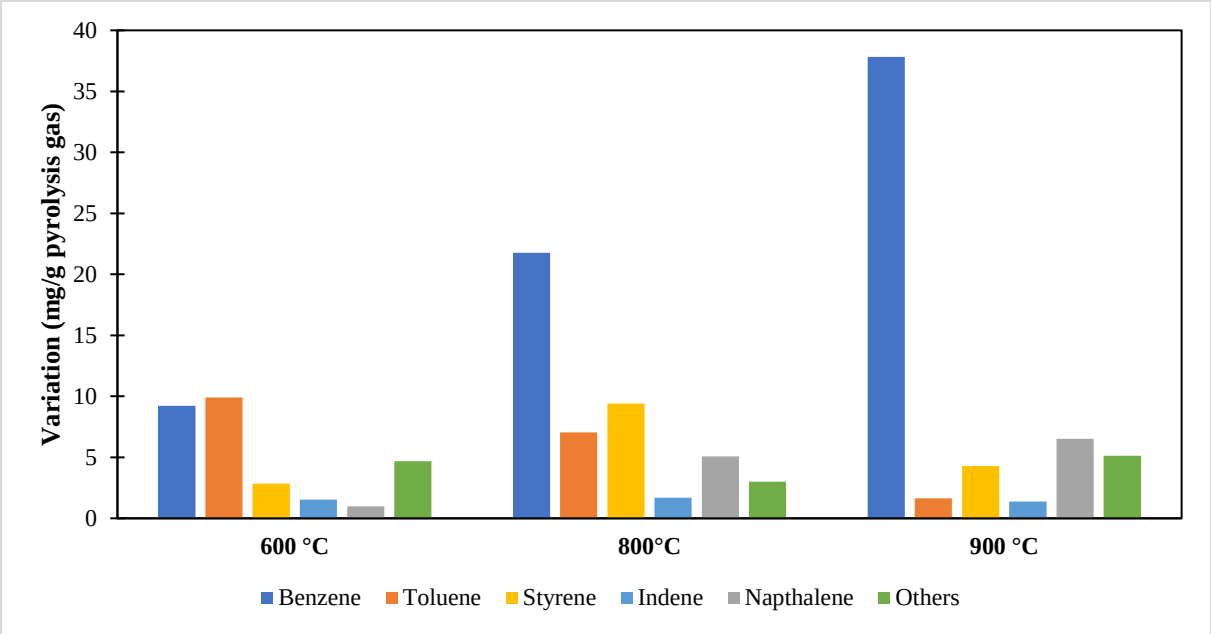

Figure 6.11: Variation of main tertiary tars in the condensates of CNS cracked gas for 3 temperatures (600,800 and 900°C) in mg/g of pyrolysis gas

The figure clearly confirms the high impact of temperature on the production of benzene due to cracking of primary and secondary tars. This increase was also observed in the study of Arayedh, where the quantity of benzene increased between 850°C and 900°C [260] and the study of Yu et al. between 700 and 900°C [261] during pyrolysis of wood.

The increasing production of naphthalene with the cracking temperature is also in accordance with other studies carried out with wood [261].

The production of toluene decreases with the temperature increase. This is because toluene decomposes into other smaller compounds or converts into other aromatic hydrocarbons such as benzene. This was also observed in the study of Arayedh et al., in which the conversion of toluene passed from 4.4% at 750°C to 64.5% at 900°C [260] and the study of Yu et al. [261].

The percentages of indene and other quantified tertiary tars remain relatively constant with the temperature increase. The formation of styrene is favorized from 600 to 800°C. Beyond 800°C the concentration of styrene decreases.

6.4 Catalytic cracking of CNS pyrolysis gas

With the aim to measure the impact of the char bed (catalytic cracking) on the conversion of pyrolysis gas, the operating conditions of 600°C and 2.5 s were chosen. The choice of

temperature was inspired by Milhé's study [106], which studied the catalytic cracking of wood pyrolysis gas.

Note that the CNS thermal cracking experiment at 600°C did not have the same nitrogen flow rate in the cracking zone and cracking tube diameter than the study in Chapter 6.3. For this study, 26 mm i.d. of cracking tube was used.

The methodology including char preparation and operating conditions is given in Appendices 6.1.

Cracking over a char bed was compared to thermal cracking at 600°C.

The resulting distribution of condensates (water-free), permanent gas, and water from both the thermal cracking and catalytic cracking of CNS and ACC pyrolysis gas were compared to those from their pyrolysis gas (reference experiment at 400°C), as shown in Figure 6.12. The maximum error for water and permanent gas yields were +/-2% respectively.

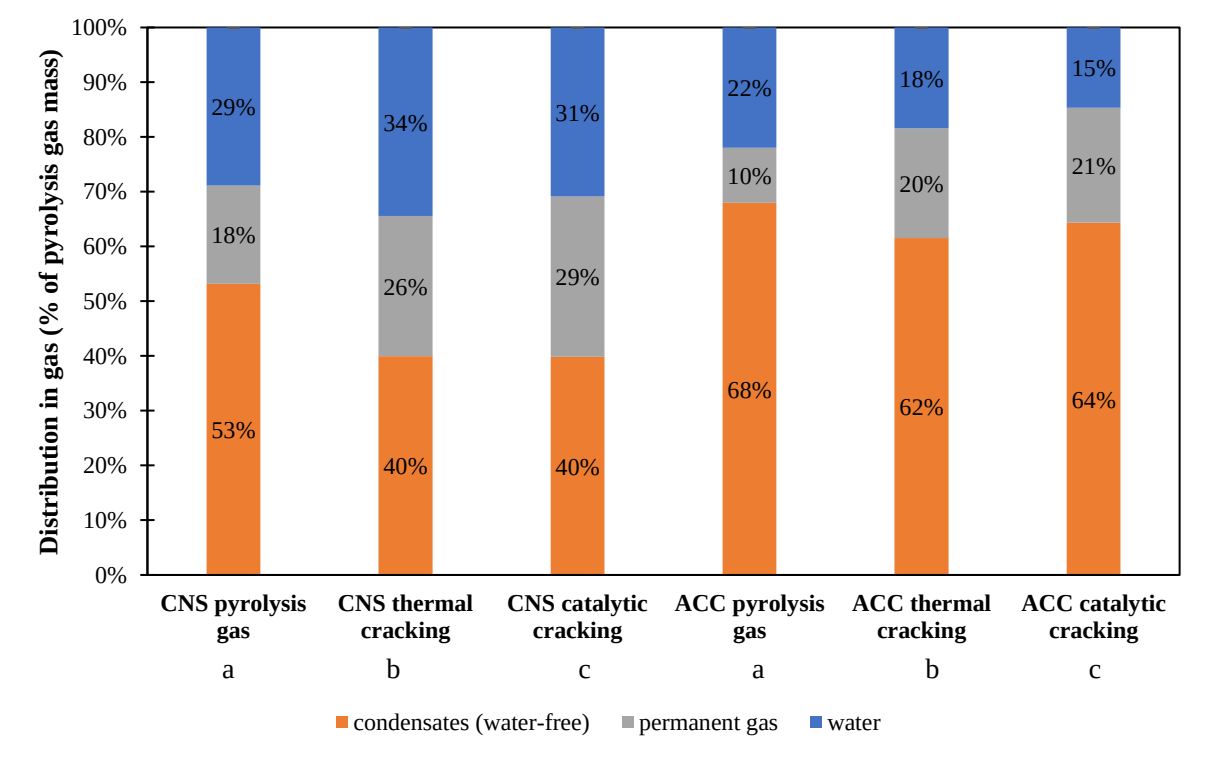

Figure 6.12: Distribution of pyrolysis gas (400°C) (a) and cracked gas of CNS (b) and ACC (c) (thermal and catalytic cracking at 600°C) in % of pyrolysis gas mass

From this figure it appears clearly that in our operating conditions CNS char at 600°C does not provide any additional catalytic effect on the cracking of heavy condensates from CNS pyrolysis beyond what is achieved through thermal cracking alone.

Through both CNS thermal cracking and catalytic cracking, the conversion rate of organic condensates (water-free) obtained was 25%, whereas in the case of ACC, the rate of conversion of organic condensates were 9 and 6% respectively. This is different form the catalytic cracking of wood pyrolysis gas at 600°C which increased the conversion rates of condensates by 21% compared to thermal cracking [106] .

Higher temperatures have to be investigated to observe and measure the catalytic effect of CNS char on pyrolysis gas cracking.

The gas productions of the cracked gas (thermal and catalytic cracking) of CNS and ACC were also measured and compared (Figure 6.13).

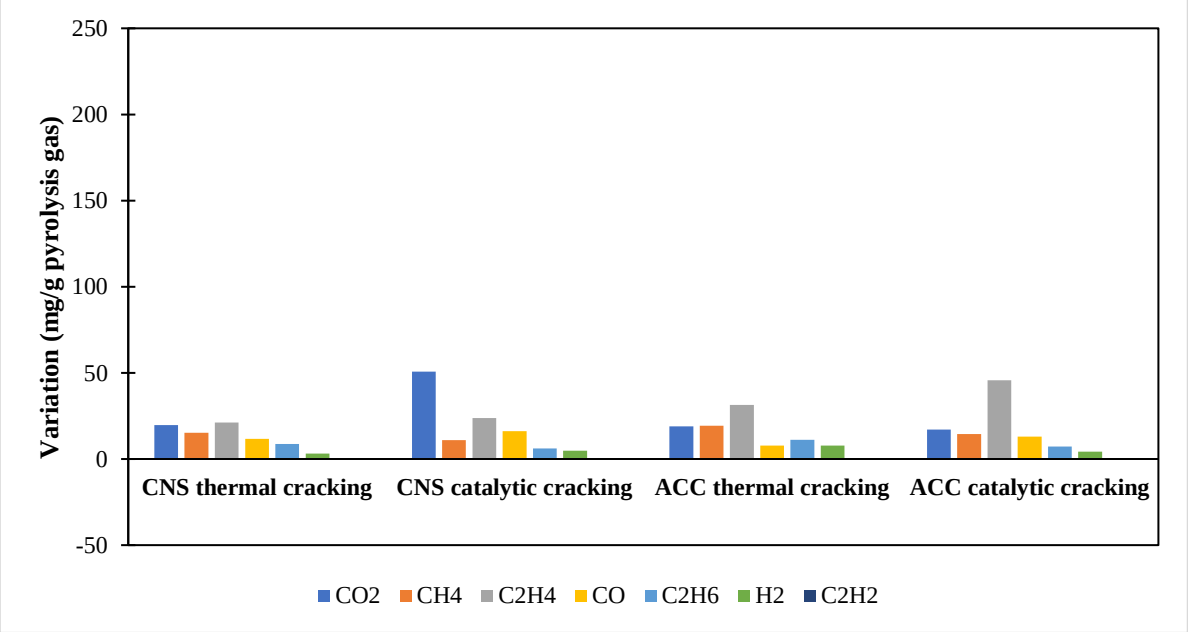

Figure 6.13: Variation of permanent gas in the CNS and ACC cracked gas (thermal and catalytic cracking) at 600°C in mg/g of pyrolysis gas

No significant difference exists in the permanent gases production, confirming that CNS char has no impact on cracking of CNS pyrolysis gas at 600°C.

6.5 Conclusion

In this chapter, experiments on thermal cracking of pyrolysis gas were conducted on various samples, including CNS, ACC-free CNS, ACC, and wood chips. The conversion rates of organic condensates of ACC-containing samples (CNS and ACC) experiments were lower than the one of ACC-free samples (ACC-free CNS and wood chips). This is explained by the presence of ACC which are more resistant to thermal degradation.

ACC contribute also to the formation of tertiary tars (benzene, toluene, naphthalene, indene and styrene) in the CNS cracked gas.

Regarding impact of temperature, the conversion rate of condensates increased from 25% to 77% when it increased from 600°C to 900°C. This results in a rise of CO_2 production due to intensification of cracking reactions which were seemingly accentuated by the water-gas shift reactions.

Furthermore, the catalytic cracking over a char bed of CNS and ACC pyrolysis gas at 600°C showed no improvement in condensates conversion when compared to thermal cracking. Therefore, higher catalytic temperatures should be investigated.

Conclusions and perspectives

Conclusions and perspectives

This PhD research was carried out in conjunction with two projects: AgroGazelec and Biostar, both of which share the common objective of effectively valorizing Cashew Nut Shells (CNS), specifically through thermochemical conversion processes (gasification and combustion) to meet the energy needs of small and medium-sized enterprises (SMEs) in West Africa. Consequently, this work focused on the pyrolysis of CNS and the conversion of pyrolysis gas, which are critical steps in all thermochemical processes.

The scientific objectives were to determine the detailed composition of CNS and to investigate their pyrolysis behavior, particularly focusing on the thermal degradation mechanisms of the primary constituents of Cashew Nut Shell Liquid (CNSL)—Anacardic acids, Cardanols, and Cardols (ACC).

Achieving these objectives first required the development of analytical methods. These included optimized extraction processes for ACC recovery and determination of extractives content, as well as the establishment of a High-Performance Liquid Chromatography (HPLC) method to quantify the 12 ACC isomers in the CNSL.

An experimental study was conducted at two different scales, utilizing both a micro-thermogravimetric analyzer (microTG) and a fixed bed pyrolysis and tar conversion reactor (PyTar). By integrating the results from these two experimental setups with existing literature, a deeper understanding of the thermochemical behavior of ACC during pyrolysis, as well as the conversion of pyrolysis gas, was achieved.

With the analytical methods developed, a more comprehensive characterization of CNS was achieved, identifying 91% of its components. Results revealed an extractive content of 58 wt%, with ACC constituting 40 wt% and tannin 18 wt%. Protein and starch were both quantified at 2%.

Thermal degradation studies using microTG allowed us to identify key thermal degradation events for ACC and ACC-free CNS, revealing distinct stages for ACC decarboxylation, ACC and their polymeric intermediates degradations, as well as classical peaks of hemicelluloses, cellulose and lignins degradation.

Pyrolysis of CNS at 400°C in the PyTar reactor yielded 23% char, 62% condensates, and 15% gas. The condensates were composed of: 39% water, 31% cardanols, and 7% quantified tars. During this study, ACC in CNS were found to primarily contribute to condensates and CO_2

formation. The solid fraction of CNS (ACC-free CNS) appeared to hinder the conversion of ACC during CNS pyrolysis, resulting in 52% of ACC conversion rate rather than 61% when pyrolyzing ACC alone.

From this work, it was understood that the degradation of ACC during CNS pyrolysis occurs through a series of successive reactions:

- First, anacardic acids undergo decarboxylation (around 125-190°C), producing cardanols and CO_2.
- Then, polymerization of cardanols takes place (around 190-250°C).
- This reaction is followed by several competing reactions: polymerization of cardanols and cardols to form cardanol based and cardol based polymers, devolatilization of cardanols and cardols, as well as evaporation of cardanols (around 250-385°C).
- The cardanol based and cardol based polymers formed during these processes then undergo further thermal degradation.

Thermal cracking experiments at 800°C revealed that ACC form more stable condensates resistant to thermal degradation compared to the lignocellulosic components of CNS. This was shown by the condensates conversion rate of ACC experiments (62%) which was lower than during ACC-free experiments (88%). Additionally, ACC favor tertiary tar formation during the thermal cracking of pyrolysis gas.

Regarding the influence of temperature on the thermal cracking of CNS pyrolysis gas, the conversion rate of condensates increased from 25% to 48% and then to 77% as the cracking temperature rose from 600°C to 800°C and finally to 900°C.

This PhD research has delivered notable results in advancing the understanding of CNS, covering its chemical composition, the thermal degradation mechanisms of ACC, and their behavior during pyrolysis and thermal cracking. Further studies could be carried out to deepen the exploration of CNS thermochemical behavior.

Therefore, regarding CNS characterization, future research could focus on a more detailed investigation of the specific molecular composition of tannins in the CNS and the 9% unidentified components in the CNS.

Concerning the thermochemical behavior of ACC, it would be relevant to analyze the types of polymers formed during ACC pyrolysis and to investigate the mechanisms of heat-induced polymerization of cardanols and cardols. Additionally, more intermediate temperature points

could be examined in the degradation process to precisely identify the onset of each reaction—decarboxylation, devolatilization, polymerization, and polymer cracking—providing deeper insights into ACC behavior.

A more in-depth study could be conducted to identify parameters that promote cracking reactions while reducing polymerization. This is particularly relevant because cracking reduces the production of condensates, especially tars, which are undesirable in pyrolysis products. Such an approach could offer valuable insights for optimizing industrial reactors to minimize tars formation during thermochemical processes.

Additionally, it would be worthwhile to investigate the role of other extractives such as tannins, wax, resins etc.

Regarding pyrolysis gas conversion over a char bed, exploring temperatures above 600°C is recommended to better quantify the catalytic effect of CNS char. Furthermore, coupling of pyrolysis with other thermochemical reactions could play a crucial role in optimizing industrial processes, enhancing efficiency, and reducing unwanted by-products.

References

References

[1] N. Nguyen, Producing countries in Africa strive to increase cashew nuts production and export, (2022). https://vihaba.global/2022/03/03/cashew-nut-production-in-africa/ (accessed December 8, 2022).

[2] J.-P. Tagutchou, P. Naquin, Caracterisation et traitement thermochimique des coques d'anacarde en vue de leur valorisation énergetique dans les procédés de transformation artisanale de noix de cajou, Déchets Sciences et Techniques 62 (2012). https://doi.org/10.4267/dechets-sciences-techniques.2722.

[3] X. Li, D. Chen, V.J. Carrión, D. Revillini, S. Yin, Y. Dong, T. Zhang, X. Wang, M. Delgado-Baquerizo, Acidification suppresses the natural capacity of soil microbiome to fight pathogenic Fusarium infections, Nat Commun 14 (2023) 5090. https://doi.org/10.1038/s41467-023-40810-z.

[4] P. Das, A. Ganesh, Bio-oil from pyrolysis of cashew nut shell-a near fuel, Biomass Bioenergy 25 (2003) 113–117. https://doi.org/https://doi.org/10.1016/S0961-9534(02)00182-4.

[5] R. Muthu Dineshkumar, K.M. Meera Sheriffa Begum, A. Ramanathan, Comprehensive characterization of cashew nutshell for biomass gasification, Mater Today Proc 46 (2019) 9837–9843. https://doi.org/10.1016/j.matpr.2020.10.932.

[6] M. Melzer, J. Blin, A. Bensakhria, J. Valette, F. Broust, Pyrolysis of extractive rich agroindustrial residues, J Anal Appl Pyrolysis 104 (2013) 448–460. https://doi.org/10.1016/j.jaap.2013.05.027.

[7] S. Sabana Prabha, Potty V.P, Thermal stability of CNSL by TGA and HPTLC, International Journal of Biotechnology and Biochemistry 7 (2011).

[8] A.J. Tsamba, W. Yang, W. Blasiak, Pyrolysis characteristics and global kinetics of coconut and cashew nut shells, Fuel Processing Technology 87 (2006) 523–530. https://doi.org/10.1016/j.fuproc.2005.12.002.

[9] N.H. Nam, K.D. Anh, L.G.T. Truc, T.A. Ha, V.T.T. Ha, Pyrolysis of cashew nut shell: A parametric study, Vietnam Journal of Chemistry 58 (2020) 506–511. https://doi.org/10.1002/vjch.202000015.

[10] Melzer M, Energetic valorisation of agricultural by-products in the sub-Saharan zone: Biomass pre-conditioning via flash pyrolysis., University of Technology of Compiègne, 2013.

[11] F. Bastos, M. Tubino, The Use of the Liquid from Cashew Nut Shells as an Antioxidant in Biodiesel, J Braz Chem Soc (2016). https://doi.org/10.21577/0103-5053.20160223.

[12] A. Coulibaly, M.K. Sako, D. Soro, S. Sidibé, R. Yohan, Valuation of cashew nut shell for the production of biofuel, Energy Reports 8 (2022) 691–707. https://doi.org/10.1016/j.egyr.2022.07.090.

[13] R. Moreira, R. dos Reis Orsini, J.M. Vaz, J.C. Penteado, E. V. Spinacé, Production of Biochar, Bio-Oil and Synthesis Gas from Cashew Nut Shell by Slow Pyrolysis, Waste Biomass Valorization 8 (2017) 217–224. https://doi.org/10.1007/s12649-016-9569-2.

[14] J. Ábrego, D. Plaza, F. Luño, M. Atienza-Martínez, G. Gea, Pyrolysis of cashew nutshells: Characterization of products and energy balance, Energy 158 (2018) 72–80. https://doi.org/10.1016/j.energy.2018.06.011.

[15] R. Kaur, V. Tarun Kumar, B.B. Krishna, T. Bhaskar, Characterization of slow pyrolysis products from three different cashew wastes, Bioresour Technol 376 (2023). https://doi.org/10.1016/j.biortech.2023.128859.

[16] E.M. de Paiva, A.L.A. Mattos, J.C.G. da Silva, G.D. Mumbach, S. Arias, J.G.A. Pacheco, M. Di Domenico, J.L.F. Alves, E.S. de Brito, Pyrolysis of cashew nutshell residues for bioenergy and renewable chemicals: Kinetics, thermodynamics, and volatile products, J Anal Appl Pyrolysis 177 (2024). https://doi.org/10.1016/j.jaap.2023.106303.

[17] R. Moreira, R. dos Reis Orsini, J.M. Vaz, J.C. Penteado, E. V. Spinacé, Production of Biochar, Bio-Oil and Synthesis Gas from Cashew Nut Shell by Slow Pyrolysis, Waste Biomass Valorization 8 (2017) 217–224. https://doi.org/10.1007/s12649-016-9569-2.

[18] D. Auditor, Cashews: slight increase in global production, 2022.

[19] TechnoServe, Cashew Shells: from Waste to Energy & Profit, 2020. https://www.technoserve.org/blog/turning-waste-products-into-profit/ (accessed December 8, 2022).

[20] M.C. Lubi, E.T. Thachil, Cashew nut shell liquid (CNSL) - a versatile monomer for polymer synthesis, Des Monomers Polym 3 (2000) 123–153. https://doi.org/10.1163/156855500300142834.

[21] Y. Shi, P.C.J. Kamer, D.J. Cole-Hamilton, Synthesis of pharmaceutical drugs from cardanol derived from cashew nut shell liquid, Green Chemistry 21 (2019) 1043–1053. https://doi.org/10.1039/C8GC03823F.

[22] S. Caillol, Cardanol: A promising building block for biobased polymers and additives, Elsevier (2018) 26–32. https://doi.org/10.1016/j.cogsc.2018.05.002ï.

[23] M. Sawadogo, S. Tchini Tanoh, S. Sidibé, N. Kpai, I. Tankoano, Cleaner production in Burkina Faso: Case study of fuel briquettes made from cashew industry waste, J Clean Prod 195 (2018) 1047–1056. https://doi.org/10.1016/j.jclepro.2018.05.261.

[24] K.M. Kouadio, F. Alhassane, A.N. Verdier, K.T. Arsène, Sustainable Thermochemical Valorization of Cashew Nut Waste in West Africa: Experimental Study and Evaluation of the Energy Potential in Côte d'Ivoire, International Journal of Renewable Energy Research (2020). https://doi.org/10.20508/ijrer.v10i3.11106.g8016.

[25] African Energy Commission, Programme on Bioenergy Monitoring and Reporting, (n.d.).

[26] J. Blin, BioStar, Bioenergy for SMEs in West Africa, (n.d.). https://www.biostar-afrique.org/en/about/background (accessed July 3, 2024).

[27] Y. Sokona, Y. Mulugetta, H. Gujba, Widening energy access in Africa: Towards energy transition, Energy Policy 47 (2012) 3–10. https://doi.org/10.1016/j.enpol.2012.03.040.

[28] The Climate Reality Project, Mobilizing clean energy to address energy poverty in West Africa, (2023).

[29] A.I. Osman, Z.Y. Lai, M. Farghali, C.L. Yiin, A.M. Elgarahy, A. Hammad, I. Ihara, A.S. Al-Fatesh, D.W. Rooney, P.-S. Yap, Optimizing biomass pathways to bioenergy and biochar application in electricity generation, biodiesel production, and biohydrogen production, Environ Chem Lett 21 (2023) 2639–2705. https://doi.org/10.1007/s10311-023-01613-2.

[30] X.H. Pham, Oxidative pyrolysis of biomass pellets in a fixed bed, 2018.

[31] V. Huchon, Épuration d'un gaz de synthèse à travers un lit fixe de charbon, Université de Montpellier, 2021.

[32] V.P. Soudham, Biochemical conversion of biomass to biofuels : pretreatment-detoxification-hydrolysis-fermentation, Umeå universitet, 2015.

[33] A. Garba, Biomass Conversion Technologies for Bioenergy Generation: An Introduction, in: Biotechnological Applications of Biomass, IntechOpen, 2021. https://doi.org/10.5772/intechopen.93669.

[34] Ö. Tezer, N. Karabağ, A. Öngen, C.Ö. Çolpan, A. Ayol, Biomass gasification for sustainable energy production: A review, Int J Hydrogen Energy (2022). https://doi.org/10.1016/j.ijhydene.2022.02.158.

[35] M. Cortazar, L. Santamaria, G. Lopez, J. Alvarez, L. Zhang, R. Wang, X. Bi, M. Olazar, A comprehensive review of primary strategies for tar removal in biomass gasification, Energy Convers Manag 276 (2023) 116496. https://doi.org/10.1016/j.enconman.2022.116496.

[36] F. Wang, Y. Zhang, X. Zeng, J. Yue, G. Zhang, D. Hu, M. Haruna Adamu, X. Lai, G. Xu, Insight into tar thermal cracking and catalytic cracking by char: Characteristics and kinetics, Fuel 326 (2022). https://doi.org/10.1016/j.fuel.2022.124929.

[37] K. Sivabalan, S. Hassan, H. Ya, J. Pasupuleti, A review on the characteristic of biomass and classification of bioenergy through direct combustion and gasification as an alternative power supply, J Phys Conf Ser 1831 (2021) 012033. https://doi.org/10.1088/1742-6596/1831/1/012033.

[38] Legifrance, Code de l'énergie - Article L211-2, (2023). https://www.legifrance.gouv.fr/codes/article_lc/LEGIARTI000043213358 (accessed November 27, 2024).

[39] K.N. Yogalakshmi, T. Poornima Devi, P. Sivashanmugam, S. Kavitha, R. Yukesh Kannah, Sunita Varjani, S. AdishKumar, Gopalakrishnan Kumar, J. Rajesh Banu, Lignocellulosic biomass-based pyrolysis: A comprehensive review, Chemosphere 286 (2022). https://doi.org/10.1016/j.chemosphere.2021.131824.

[40] S. Wang, G. Dai, H. Yang, Z. Luo, Lignocellulosic biomass pyrolysis mechanism: A state-of-the-art review, Prog Energy Combust Sci 62 (2017) 33–86. https://doi.org/10.1016/j.pecs.2017.05.004.

[41] D. Fengel, G. Wegener, eds., Wood, DE GRUYTER, 1983. https://doi.org/10.1515/9783110839654.

[42] H.F. Zobel, A.M. Stephen, Hemicelluloses: Structure and Properties., in: Food Polysaccharides and Their Applications, 2006: pp. 279–310.

[43] R. Kaur, B.B. Krishna, A. Kumar, T. Bhaskar, Biomass Pyrolysis, Encyclopedia of Sustainable Technologies (2024) 252–265. https://doi.org/10.1016/B978-0-323-90386-8.00031-0.

[44] A. Gregory, G.P. Bolwell, Hemicelluloses, in: A. Gregory, G. Pqul Bolwell (Eds.), Comprehensive Natural Products Chemistry, Elsevier, 1999: pp. 599–615. https://doi.org/10.1016/B978-0-08-091283-7.00084-9.

[45] M.A. O'Neill, W.S. York, The Composition and Structure of Plant Primary Cell Walls, in: Annual Plant Reviews Online, Wiley, 2018: pp. 1–54. https://doi.org/10.1002/9781119312994.apr0067.

[46] R.K. Rajaonarivony, Micronisation par voie sèche de biomasses lignocellulosiques natives et torréfiées pour une application poudre-carburant, SupAgro, 2020.

[47] P.F.H. Harmsen, W. Huijgen, L. Bermudez, R. Bakker, Literature review of physical and chemical pretreatment processes for lignocellulosic biomass, 2010.

[48] A.T.W.M. Hendriks, G. Zeeman, Pretreatments to enhance the digestibility of lignocellulosic biomass, Bioresour Technol 100 (2009) 10–18. https://doi.org/10.1016/J.BIORTECH.2008.05.027.

[49] B. Prieur, M. Meub, M. Wittemann, R. Klein, S. Bellayer, G. Fontaine, S. Bourbigot, Phosphorylation of lignin: characterization and investigation of the thermal decomposition, RSC Adv 7 (2017) 16866–16877. https://doi.org/10.1039/C7RA00295E.

[50] J.F. Araneda, I.W. Burton, M. Paleologou, S.D. Riegel, M.C. Leclerc, Analysis of lignins using P benchtop NMR spectroscopy: quantitative assessment of substructures and

comparison to high-field NMR, Can J Chem 100 (2022) 799–808. https://doi.org/10.1139/cjc-2022-0041.

[51] B.M. Jenkins, L.L. Baxter, T.R. Miles, T.R. Miles, Combustion properties of biomass, Fuel Processing Technology 54 (1998) 17–46. https://doi.org/10.1016/S0378-3820(97)00059-3.

[52] F.J. Maathuis, Physiological functions of mineral macronutrients, Curr Opin Plant Biol 12 (2009) 250–258. https://doi.org/10.1016/j.pbi.2009.04.003.

[53] J.A. Lacey, J.E. Aston, V.S. Thompson, Wear Properties of Ash Minerals in Biomass, Front Energy Res 6 (2018). https://doi.org/10.3389/fenrg.2018.00119.

[54] S.K. Gupta, T.F. Wall, R.A. Creelman, R.P. Gupta, Ash fusion temperatures and the transformations of coal ash particles to slag, Fuel Processing Technology 56 (1998) 33–43. https://doi.org/10.1016/S0378-3820(97)00090-8.

[55] M.B. Pecha, M. Garcia-Perez, Pyrolysis of lignocellulosic biomass: oil, char, and gas, in: Bioenergy, Elsevier, 2020: pp. 581–619. https://doi.org/10.1016/B978-0-12-815497-7.00029-4.

[56] X.-J. Guo, S.-R. Wang, K.-G. Wang, L. Qian, L. Zhong-Yang, Influence of extractives on mechanism of biomass pyrolysis, J Fuel Chem Technol 38 (2010) 42–46. https://doi.org/https://doi.org/10.1016/S1872-5813(10)60019-9.

[57] A. Kallioinen, A. Vaari, M. Rättö, J. Konn, M. Siika-Aho, L. Viikari, Effects of bacterial treatments on wood extractives, J Biotechnol 103 (2003) 67–76. https://doi.org/10.1016/S0168-1656(03)00051-8.

[58] P.E.A. Debiagi, C. Pecchi, G. Gentile, A. Frassoldati, A. Cuoci, T. Faravelli, E. Ranzi, Extractives Extend the Applicability of Multistep Kinetic Scheme of Biomass Pyrolysis, Energy & Fuels 29 (2015) 6544–6555. https://doi.org/10.1021/acs.energyfuels.5b01753.

[59] A. Oasmaa, E. Kuoppala, S. Gust, Y. Solantausta, Fast Pyrolysis of Forestry Residue. 1. Effect of Extractives on Phase Separation of Pyrolysis Liquids, Energy & Fuels 17 (2003) 1–12. https://doi.org/10.1021/ef020088x.

[60] M.J. Taherzadeh, R. Eklund, L. Gustafsson, C. Niklasson, G. Lidén, Characterization and Fermentation of Dilute-Acid Hydrolyzates from Wood, Ind Eng Chem Res 36 (1997) 4659–4665. https://doi.org/10.1021/ie9700831.

[61] A. Demirbaş, Thermochemical Conversion of Biomass to Liquid Products in the Aqueous Medium, Energy Sources 27 (2005) 1235–1243. https://doi.org/10.1080/009083190519357.

[62] C. Di Blasi, C. Branca, A. Galgano, Biomass Screening for the Production of Furfural via Thermal Decomposition, Ind Eng Chem Res 49 (2010) 2658–2671. https://doi.org/10.1021/ie901731u.

[63] H. Rabemanolontsoa, S. Saka, Comparative study on chemical composition of various biomass species, RSC Adv 3 (2013) 3946. https://doi.org/10.1039/c3ra22958k.

[64] T. Qu, W. Guo, L. Shen, J. Xiao, K. Zhao, Experimental Study of Biomass Pyrolysis Based on Three Major Components: Hemicellulose, Cellulose, and Lignin, Ind Eng Chem Res 50 (2011) 10424–10433. https://doi.org/10.1021/ie1025453.

[65] E. Alakangas, Biomass and agricultural residues for energy generation, Fuel Flexible Energy Generation: Solid, Liquid and Gaseous Fuels (2016) 59–96. https://doi.org/10.1016/B978-1-78242-378-2.00003-1.

[66] Y.-H. Kiang, Basic properties of fuels, biomass, refuse derived fuels, wastes, biosludge, and biocarbons, Fuel Property Estimation and Combustion Process Characterization (2018) 41–65. https://doi.org/10.1016/B978-0-12-813473-3.00003-9.

[67] C. Telmo, J. Lousada, N. Moreira, Proximate analysis, backwards stepwise regression between gross calorific value, ultimate and chemical analysis of wood, Bioresour Technol 101 (2010) 3808–3815. https://doi.org/10.1016/j.biortech.2010.01.021.

[68] A. Demirbaş, Calculation of higher heating values of biomass fuels, Fuel 76 (1997) 431–434. https://doi.org/10.1016/S0016-2361(97)85520-2.

[69] S.A. Channiwala, P.P. Parikh, A unified correlation for estimating HHV of solid, liquid and gaseous fuels, Fuel 81 (2002) 1051–1063. https://doi.org/10.1016/S0016-2361(01)00131-4.

[70] Y. Kato, R. Enomoto, M. Akazawa, Y. Kojima, Characterization of Japanese cedar bio-oil produced using a bench-scale auger pyrolyzer, Springerplus 5 (2016) 177. https://doi.org/10.1186/s40064-016-1848-7.

[71] B.M. Jenkins, J.M. Ebeling, Correlation of physical and chemical properties of terrestrial biomass with covnersion, (1985).

[72] P.R. BONELLI, Slow Pyrolysis of Nutshells: Characterization of Derived Chars and of Process Kinetics, Energy Sources 25 (2003) 767–778. https://doi.org/10.1080/00908310390207819.

[73] C.A. Jose Antonio SuÁrez, Thermochemical Properties of Cuban Biomass, Energy Sources 22 (2000) 851–857. https://doi.org/10.1080/00908310051128156.

[74] A. Tortosa Masia, B. Buhre, R. Gupta, T. Wall, Characterising ash of biomass and waste, Fuel Processing Technology (2007) 1–11.

[75] N.N. Oliveira, C.G. Mothé, M.G. Mothé, L.G. de Oliveira, Cashew nut and cashew apple: a scientific and technological monitoring worldwide review, J Food Sci Technol 57 (2020) 12–21. https://doi.org/10.1007/s13197-019-04051-7.

[76] A.D. Berry, S.A. Sargent, Cashew apple and nut (Anacardium occidentale L.), 2011.

[77] Nation Master, Cashew Nuts Production, (2020). https://www.nationmaster.com/nmx/ranking/cashew-nuts-production (accessed August 9, 2022).

[78] S.G. De Lima, C.M. Feitosa, A.M.G.L. Cito, J.M. Moita Neto, J.A.D. Lopes, A.S. Leite, M.C. Brito, S.M.M. Dantas, A.A.C. Melo Cavalcante, Effects of immature cashew nut-shell liquid (Anacardium occidentale) against oxidative damage in Saccharomyces cerevisiae and inhibition of acetylcholinesterase activity, Genetics and Molecular Research 7 (2008) 806–818. https://doi.org/10.4238/vol7-3gmr473.

[79] Eric Gaba, File:Cashew Brazil fruit 1.jpg, Wikimedia Commons (2005).

[80] Service N'Kalô, Bulletin sur le Marché de l'Anacarde, 2023.

[81] S. Caillol, The future of cardanol as small giant for biobased aromatic polymers and additives, Eur Polym J 193 (2023). https://doi.org/10.1016/j.eurpolymj.2023.112096.

[82] M. Yuliana, N.Y. Tran-Thi, Y.H. Ju, Effect of extraction methods on characteristic and composition of Indonesian cashew nut shell liquid, Ind Crops Prod 35 (2012) 230–236. https://doi.org/10.1016/j.indcrop.2011.07.007.

[83] M.L. Adekanbi, T.T. Olugasa, Utilizing cashew nut shell liquid for the sustainable production of biodiesel: A comprehensive review, Cleaner Chemical Engineering 4 (2022) 100085. https://doi.org/10.1016/j.clce.2022.100085.

[84] C.S. Tamiello-Rosa, T.M. Cantu-Jungles, M. Iacomini, L.M.C. Cordeiro, Pectins from cashew apple fruit (Anacardium occidentale): Extraction and chemical characterization, Carbohydr Res 483 (2019). https://doi.org/10.1016/j.carres.2019.107752.

[85] de l'Industrie et de l'Artisanat du B.F. Ministère du Commerce, Le Guide de la Transformation de l'Anacarde au Burkina Faso: Projet d'appui à la commercialisation de mangue séchée et de noix de cajou transformée, 2017.

[86] A. Kozubek, J.H. Tyman, Resorcinolic lipids, the natural non-isoprenoid phenolic amphiphiles and their biological activity, Chem Rev 99 (1999) 1–26.

[87] L.J. Cruz Reina, D.D. Durán-Aranguren, L.F. Forero-Rojas, L.F. Tarapuez-Viveros, D. Durán-Sequeda, C. Carazzone, R. Sierra, Chemical composition and bioactive compounds of cashew (Anacardium occidentale) apple juice and bagasse from Colombian varieties, Heliyon 8 (2022). https://doi.org/10.1016/j.heliyon.2022.e09528.

[88] A.G. Mathew, H.A.B. Parpia, Polyphenols of cashew kernel testa, J Food Sci (1970).

[89] J. Trox, V. Vadivel, W. Vetter, W. Stuetz, D.R. Kammerer, R. Carle, V. Scherbaum, U. Gola, D. Nohr, H.K. Biesalski, Catechin and epicatechin in testa and their association with bioactive compounds in kernels of cashew nut (Anacardium occidentale L.), Food Chem 128 (2011) 1094–1099. https://doi.org/10.1016/j.foodchem.2011.04.018.

[90] P. Anilkumar, Cashew nut shell liquid: A goldfield for functional materials, Springer International Publishing, 2017. https://doi.org/10.1007/978-3-319-47455-7.

[91] A.I. Rahobinirina, M.F. Rakotondramanga, A. Berlioz-Barbier, E. Métay, V. Ramanandraibe, M. Lemaire, Valorization of Madagascar's CNSL via the synthesis of one advanced intermediate (3-Pentadecylcyclohexanone), Tetrahedron Lett 58 (2017) 2284–2289. https://doi.org/10.1016/J.TETLET.2017.04.093.

[92] C. Sahin, L. Magomedova, T.A.M. Ferreira, J. Liu, J. Tiefenbach, P.S. Alves, F.J.G. Queiroz, A.S. de Oliveira, M. Bhattacharyya, J. Grouleff, P.C.N. Nogueira, E.R. Silveira, D.C. Moreira, J.R.S. de A. Leite, G.D. Brand, D. Uehling, G. Poda, H. Krause, C.L. Cummins, L.A.S. Romeiro, Phenolic Lipids Derived from Cashew Nut Shell Liquid to Treat Metabolic Diseases, J Med Chem 65 (2022) 1961–1978. https://doi.org/10.1021/acs.jmedchem.1c01542.

[93] E. Uliassi, A.S. de Oliveira, L. de Camargo Nascente, L.A.S. Romeiro, M.L. Bolognesi, Cashew Nut Shell Liquid (CNSL) as a Source of Drugs for Alzheimer's Disease, Molecules 26 (2021) 5441. https://doi.org/10.3390/molecules26185441.

[94] N. de O. Souza, D.A. Cunha, N. de S. Rodrigues, A.L. Pereira, E.J.T. Medeiros, A. de A. Pinheiro, M.A. de Vasconcelos, L.G. do Nascimento Neto, T.T. Bezerra, S.E. Mazzetto, D. Lomonaco, E.H. Teixeira, V. de P.A. Saboia, Cashew nut shell liquids: Antimicrobial compounds in prevention and control of the oral biofilms, Arch Oral Biol 133 (2022) 105299. https://doi.org/10.1016/j.archoralbio.2021.105299.

[95] S.K. Sanjeeva, M.P. Pinto, M.M. Narayanan, G.M. Kini, C.B. Nair, P.V. SubbaRao, P.K. Pullela, S. Ramamoorthy, C.J. Barrow, Distilled technical cashew nut shell liquid (DT-CNSL) as an effective biofuel and additive to stabilize triglyceride biofuels in diesel, Renew Energy 71 (2014) 81–88. https://doi.org/10.1016/j.renene.2014.05.024.

[96] A. Velmurugan, M. Loganathan, E.J. Gunasekaran, Experimental investigations on combustion, performance and emission characteristics of thermal cracked cashew nut shell liquid (TC-CNSL)–diesel blends in a diesel engine, Fuel 132 (2014) 236–245. https://doi.org/10.1016/j.fuel.2014.04.060.

[97] S. Vedharaj, R. Vallinayagam, W.M. Yang, C.G. Saravanan, W.L. Roberts, Synthesis and utilization of catalytically cracked cashew nut shell liquid in a diesel engine, Exp Therm Fluid Sci 70 (2016) 316–324. https://doi.org/10.1016/j.expthermflusci.2015.09.026.

[98] V. Thanigaivelan, M. Loganathan, M. Vikneswaran, S. Venkatramanan, M. Manickam, Effect of hydrogen and ethanol addition in cashew nut shell liquid biodiesel operated direct injection (DI) diesel engine, Int J Hydrogen Energy 47 (2022) 5111–5129. https://doi.org/10.1016/j.ijhydene.2021.11.128.

[99] F.J.N. Maia, F.W.P. Ribeiro, J.H.G. Rangel, D. Lomonaco, F.M.T. Luna, P. de Lima-Neto, A.N. Correia, S.E. Mazzetto, Evaluation of antioxidant action by electrochemical and accelerated oxidation experiments of phenolic compounds derived from cashew nut shell liquid, Ind Crops Prod 67 (2015) 281–286. https://doi.org/10.1016/j.indcrop.2015.01.034.

[100] W.I. Eke, E. Ituen, L. Yuanhua, O. Akaranta, Laboratory evaluation of modified cashew nut shell liquid as oilfield wax inhibitors and flow improvers for waxy crude oils,

Upstream Oil and Gas Technology 8 (2022). https://doi.org/10.1016/j.upstre.2022.100068.

[101] S. Masood, F. Zafar, N. Nishat, Green flame retardant material from cashew nut shell liquid, in: Applications of Advanced Green Materials, Elsevier, 2021: pp. 663–679. https://doi.org/10.1016/b978-0-12-820484-9.00025-8.

[102] L. Nambela, L. V. Haule, Q.A. Mgani, Anacardic acid isolated form cashew nut shells liquid: precursor for synthesis of anthraquinone dyes, Cleaner Chemical Engineering (2022) 100056. https://doi.org/10.1016/j.clce.2022.100056.

[103] J. Nyirenda, K. Zombe, G. Kalaba, C. Siabbamba, I. Mukela, Exhaustive valorization of cashew nut shell waste as a potential bioresource material, Sci Rep 11 (2021). https://doi.org/10.1038/s41598-021-91571-y.

[104] S.K. Kyei, W.I. Eke, R.D. Nagre, I. Mensah, O. Akaranta, A comprehensive review on waste valorization of cashew nutshell liquid: Sustainable development and industrial applications, Cleaner Waste Systems 6 (2023). https://doi.org/10.1016/j.clwas.2023.100116.

[105] T. Wang, X. Cao, M. Chen, Y. Lou, H. Wang, Q. Yang, H. Pan, Y. Zhuge, Effects of Soil Acidification on Bacterial and Fungal Communities in the Jiaodong Peninsula, Northern China, Agronomy 12 (2022) 927. https://doi.org/10.3390/agronomy12040927.

[106] M. Milhé, Pyrolyse de plaquettes forestières en lit continu, Université de Perpignan Via Domitia, 2013.

[107] R.J. Evans, T.A. Milne, Molecular characterization of the pyrolysis of biomass. 2. Applications, Energy & Fuels 1 (1987) 311–319. https://doi.org/10.1021/ef00004a001.

[108] M. Garcia-Perez, A. Chaala, H. Pakdel, D. Kretschmer, C. Roy, Characterization of bio-oils in chemical families, Biomass Bioenergy 31 (2007) 222–242. https://doi.org/10.1016/j.biombioe.2006.02.006.

[109] H. Yang, B. Huan, Y. Chen, Y. Gao, J. Li, H. Chen, Biomass-Based Pyrolytic Polygeneration System for Bamboo Industry Waste: Evolution of the Char Structure and the Pyrolysis Mechanism, Energy and Fuels 30 (2016) 6430–6439. https://doi.org/10.1021/acs.energyfuels.6b00732.

[110] F.X. Collard, J. Blin, A review on pyrolysis of biomass constituents: Mechanisms and composition of the products obtained from the conversion of cellulose, hemicelluloses and lignin, Renewable and Sustainable Energy Reviews 38 (2014) 594–608. https://doi.org/10.1016/j.rser.2014.06.013.

[111] C.A. Mullen, A.A. Boateng, Characterization of water insoluble solids isolated from various biomass fast pyrolysis oils, J Anal Appl Pyrolysis 90 (2011) 197–203. https://doi.org/10.1016/j.jaap.2010.12.004.

[112] M. Garcia-Perez, A. Chaala, H. Pakdel, D. Kretschmer, C. Roy, Characterization of bio-oils in chemical families, Biomass Bioenergy 31 (2007) 222–242. https://doi.org/10.1016/j.biombioe.2006.02.006.

[113] M. Van de Velden, J. Baeyens, A. Brems, B. Janssens, R. Dewil, Fundamentals, kinetics and endothermicity of the biomass pyrolysis reaction, Renew Energy 35 (2010) 232–242. https://doi.org/10.1016/j.renene.2009.04.019.

[114] M.C. Blanco López, C.G. Blanco, A. Martínez-Alonso, J.M.D. Tascón, Composition of gases released during olive stones pyrolysis, J Anal Appl Pyrolysis 65 (2002) 313–322. https://doi.org/10.1016/S0165-2370(02)00008-6.

[115] E. Jakab, O. Faix, F. Till, T. Székely, Thermogravimetry/mass spectrometry study of six lignins within the scope of an international round robin test, J Anal Appl Pyrolysis 35 (1995) 167–179. https://doi.org/10.1016/0165-2370(95)00907-7.

[116] P. Morf, P. Hasler, T. Nussbaumer, Mechanisms and kinetics of homogeneous secondary reactions of tar from continuous pyrolysis of wood chips, Fuel 81 (2002) 843–853. https://doi.org/10.1016/S0016-2361(01)00216-2.

[117] L. Wei, S. Xu, L. Zhang, H. Zhang, C. Liu, H. Zhu, S. Liu, Characteristics of fast pyrolysis of biomass in a free fall reactor, Fuel Processing Technology 87 (2006) 863–871. https://doi.org/10.1016/j.fuproc.2006.06.002.

[118] R.J. Evans, T.A. Milne, Molecular characterization of the pyrolysis of biomass, Energy & Fuels 1 (1987) 123–137. https://doi.org/10.1021/ef00002a001.

[119] D. Neves, H. Thunman, A. Matos, L. Tarelho, A. Gómez-Barea, Characterization and prediction of biomass pyrolysis products, Prog Energy Combust Sci 37 (2011) 611–630. https://doi.org/10.1016/j.pecs.2011.01.001.

[120] F.X. Collard, J. Blin, A. Bensakhria, J. Valette, Influence of impregnated metal on the pyrolysis conversion of biomass constituents, J Anal Appl Pyrolysis 95 (2012) 213–226. https://doi.org/10.1016/j.jaap.2012.02.009.

[121] J.J.M. Orfão, F.J.A. Antunes, J.L. Figueiredo, Pyrolysis kinetics of lignocellulosic materials—three independent reactions model, Fuel 78 (1999) 349–358. https://doi.org/10.1016/S0016-2361(98)00156-2.

[122] J.A. Caballero, J.A. Conesa, R. Font, A. Marcilla, Pyrolysis kinetics of almond shells and olive stones considering their organic fractions, J Anal Appl Pyrolysis 42 (1997) 159–175. https://doi.org/10.1016/S0165-2370(97)00015-6.

[123] J. Piskorz, D. Radlein, D.S. Scott, On the mechanism of the rapid pyrolysis of cellulose, Elsevier Science Publishers B.V, 1986.

[124] H. Yang, R. Yan, H. Chen, D.H. Lee, C. Zheng, Characteristics of hemicellulose, cellulose and lignin pyrolysis, Fuel 86 (2007) 1781–1788. https://doi.org/10.1016/j.fuel.2006.12.013.

[125] S.D. Stefanidis, K.G. Kalogiannis, E.F. Iliopoulou, C.M. Michailof, P.A. Pilavachi, A.A. Lappas, A study of lignocellulosic biomass pyrolysis via the pyrolysis of cellulose, hemicellulose and lignin, J Anal Appl Pyrolysis 105 (2014) 143–150. https://doi.org/10.1016/j.jaap.2013.10.013.

[126] R.D. Singh, J. Banerjee, S. Sasmal, J. Muir, A. Arora, High xylan recovery using two stage alkali pre-treatment process from high lignin biomass and its valorisation to xylooligosaccharides of low degree of polymerisation, Bioresour Technol 256 (2018) 110–117. https://doi.org/10.1016/j.biortech.2018.02.009.

[127] L. Dai, Y. Wang, Y. Liu, C. He, R. Ruan, Z. Yu, L. Jiang, Z. Zeng, Q. Wu, A review on selective production of value-added chemicals via catalytic pyrolysis of lignocellulosic biomass, Science of the Total Environment 749 (2020). https://doi.org/10.1016/j.scitotenv.2020.142386.

[128] P. de Wild, Biomass pyrolysis for chemicals, Rijksuniversiteit Groningen, 2011.

[129] Y. Peng, S. Wu, The structural and thermal characteristics of wheat straw hemicellulose, J Anal Appl Pyrolysis 88 (2010) 134–139. https://doi.org/10.1016/j.jaap.2010.03.006.

[130] J.M. Heikkinen, J.C. Hordijk, W. de Jong, H. Spliethoff, Thermogravimetry as a tool to classify waste components to be used for energy generation, J Anal Appl Pyrolysis 71 (2004) 883–900. https://doi.org/10.1016/j.jaap.2003.12.001.

[131] M.G. Grønli, G. Várhegyi, C. di Blasi, Thermogravimetric analysis and devolatilization kinetics of wood, Ind Eng Chem Res 41 (2002) 4201–4208. https://doi.org/10.1021/ie0201157.

[132] WANG Gang, Li-Wen, Xue-Qin-Zhao, Yi-Yue-Chao, Li-Bao-Qiang, Thermogravimetric behaviors of biomass&prime|chemical components under air or syngas, Journal of Fuel Chemistry and Technology 37 (2009) 170–176.

[133] J. Hamada, A. Pétrissans, F. Mothe, J. Ruelle, M. Pétrissans, P. Gérardin, Intraspecific variation of European oak wood thermal stability according to radial position, Wood Sci Technol 51 (2017) 785–794. https://doi.org/10.1007/s00226-017-0910-0.

[134] M. Poletto, A.J. Zattera, M.M.C. Forte, R.M.C. Santana, Thermal decomposition of wood: Influence of wood components and cellulose crystallite size, Bioresour Technol 109 (2012) 148–153. https://doi.org/10.1016/j.biortech.2011.11.122.

[135] Y. Chen, M.A. Tshabalala, J. Gao, N.M. Stark, Y. Fan, R.E. Ibach, Thermal behavior of extracted and delignified pine wood flour, Thermochim Acta 591 (2014) 40–44. https://doi.org/10.1016/j.tca.2014.06.012.

[136] A.N. Shebani, A.J. van Reenen, M. Meincken, The effect of wood extractives on the thermal stability of different wood-LLDPE composites, Thermochim Acta 481 (2009) 52–56. https://doi.org/10.1016/J.TCA.2008.10.008.

[137] A.N. Shebani, A.J. van Reenen, M. Meincken, The effect of wood extractives on the thermal stability of different wood species, Thermochim Acta 471 (2008) 43–50. https://doi.org/10.1016/j.tca.2008.02.020.

[138] M. Poletto, Effect of extractive content on the thermal stability of two wood species from Brazil, Maderas: Ciencia y Tecnologia 18 (2016) 435–442. https://doi.org/10.4067/S0718-221X2016005000039.

[139] P. Jusner, S. Barbini, S. Schiehser, M. Bacher, E. Schwaiger, A. Potthast, T. Rosenau, Impact of residual extractives on the thermal stability of softwood Kraft pulp, Cellulose 29 (2022) 8797–8810. https://doi.org/10.1007/s10570-022-04807-z.

[140] Y. Peng, X. Tang, R. Xuan, L. Wang, L. Dai, L. Zhang, F. Liao, H. Li, X. Li, Y. Shen, Y. Su, H. Wang, Analysis of pyrolysis behaviors of biomass extractives via non-linear stepwise heating program based on Gaussian multi-peak fitting of differential thermogravimetric curve, Thermochim Acta 702 (2021) 178976. https://doi.org/10.1016/J.TCA.2021.178976.

[141] D.G. Lima, V.C.D. Soares, E.B. Ribeiro, D.A. Carvalho, É.C.V. Cardoso, F.C. Rassi, K.C. Mundim, J.C. Rubim, P.A.Z. Suarez, Diesel-like fuel obtained by pyrolysis of vegetable oils, J Anal Appl Pyrolysis 71 (2004) 987–996. https://doi.org/10.1016/J.JAAP.2003.12.008.

[142] E. Ranzi, A. Cuoci, T. Faravelli, A. Frassoldati, G. Migliavacca, S. Pierucci, S. Sommariva, Chemical Kinetics of Biomass Pyrolysis, Energy & Fuels 22 (2008) 4292–4300. https://doi.org/10.1021/ef800551t.

[143] E. Ranzi, P.E.A. Debiagi, A. Frassoldati, Mathematical Modeling of Fast Biomass Pyrolysis and Bio-Oil Formation. Note I: Kinetic Mechanism of Biomass Pyrolysis, ACS Sustain Chem Eng 5 (2017) 2867–2881. https://doi.org/10.1021/acssuschemeng.6b03096.

[144] V. Krevelen, Graphical-statistical method for the study of structure and reaction processes of coal, Fuel 29 (1950) 269–284. https://api.semanticscholar.org/CorpusID:208705483.

[145] A.G.W. Bradbury, Y. Sakai, F. Shafizadeh, A kinetic model for pyrolysis of cellulose, J Appl Polym Sci 23 (1979) 3271–3280. https://doi.org/10.1002/app.1979.070231112.

[146] J. Lédé, Cellulose pyrolysis kinetics: An historical review on the existence and role of intermediate active cellulose, J Anal Appl Pyrolysis 94 (2012) 17–32. https://doi.org/10.1016/j.jaap.2011.12.019.

[147] G. Varhegyi, E. Jakab, M.J. Antal, Is the Broido-Shafizadeh Model for Cellulose Pyrolysis True?, Energy & Fuels 8 (1994) 1345–1352. https://doi.org/10.1021/ef00048a025.

[148] C. Branca, C. Di Blasi, C. Mango, I. Hrablay, Products and Kinetics of Glucomannan Pyrolysis, Ind Eng Chem Res 52 (2013) 5030–5039. https://doi.org/10.1021/ie400155x.

[149] D. Shen, W. Jin, J. Hu, R. Xiao, K. Luo, An overview on fast pyrolysis of the main constituents in lignocellulosic biomass to valued-added chemicals: Structures, pathways and interactions, Renewable and Sustainable Energy Reviews 51 (2015) 761–774. https://doi.org/10.1016/j.rser.2015.06.054.

[150] X. Zhou, W. Li, R. Mabon, L.J. Broadbelt, Inside Back Cover: A Critical Review on Hemicellulose Pyrolysis (Energy Technol. 1/2017), Energy Technology 5 (2017) 217–217. https://doi.org/10.1002/ente.201600396.

[151] T. Faravelli, A. Frassoldati, G. Migliavacca, E. Ranzi, Detailed kinetic modeling of the thermal degradation of lignins, Biomass Bioenergy 34 (2010) 290–301. https://doi.org/10.1016/j.biombioe.2009.10.018.

[152] C. Deng, W. Song, Z. Chai, S. Guo, Z. Zhu, Characteristics of Tar Thermal Cracking and Catalytic Conversion during Circulating Fluidized Bed Char Gasification, Energy & Fuels 34 (2020) 142–149. https://doi.org/10.1021/acs.energyfuels.9b03346.

[153] J.J. Bolívar Caballero, I.N. Zaini, W. Yang, Reforming processes for syngas production: A mini-review on the current status, challenges, and prospects for biomass conversion to fuels, Applications in Energy and Combustion Science 10 (2022) 100064. https://doi.org/10.1016/j.jaecs.2022.100064.

[154] W. Song, C. Deng, S. Guo, Effect of Steam on the Tar Reforming during Circulating Fluidized Bed Char Gasification, ACS Omega 6 (2021) 11192–11198. https://doi.org/10.1021/acsomega.0c05861.

[155] Y.K. Kim, J. Il Park, D. Jung, J. Miyawaki, S.H. Yoon, I. Mochida, Low-temperature catalytic conversion of lignite: 3. Tar reforming using the supported potassium carbonate, Journal of Industrial and Engineering Chemistry 20 (2014) 9–12. https://doi.org/10.1016/J.JIEC.2013.04.003.

[156] Y. Gao, H. Xie, Z. Yu, M. Qin, Z. Wu, P. Wang, X. Zhao, S. Zhang, Two-Stage Dry Reforming Process for Biomass Gasification: Product Characteristics and Energy Analysis, Energies (Basel) 16 (2023) 4783. https://doi.org/10.3390/en16124783.

[157] B. De Caprariis, C. Bassano, P. Deiana, V. Palma, A. Petrullo, M. Scarsella, P. De Filippis, Carbon Dioxide Reforming of Tar During Biomass Gasification, Chem Eng Trans 37 (2014) 97–102.

[158] M. Hervy, Valorisation de chars issus de pyrogazéification de biomasse pour la purification de syngas: lien entre propriétés physico-chimiques, procédé de fonctionnalisation et efficacité du traitement, Université de Toulouse/ Mines d'Albi, 2014.

[159] Z. Abu El-Rub, E.A. Bramer, G. Brem, Review of Catalysts for Tar Elimination in Biomass Gasification Processes, Ind Eng Chem Res 43 (2004) 6911–6919. https://doi.org/10.1021/ie0498403.

[160] C. Deng, W. Song, Z. Chai, S. Guo, Z. Zhu, Characteristics of Tar Thermal Cracking and Catalytic Conversion during Circulating Fluidized Bed Char Gasification, Energy and Fuels 34 (2020) 142–149. https://doi.org/10.1021/acs.energyfuels.9b03346.

[161] T.S. Gandhi, B.Z. Dholakiya, M.R. Patel, Extraction protocol for isolation of CNSL by using protic and aprotic solvents from cashew nut and study of their physico-chemical parameter, Polish Journal of Chemical Technology 15 (2013) 24–27. https://doi.org/10.2478/pjct-2013-0062.

[162] M.T.S. Trevisan, B. Pfundstein, R. Haubner, G. Würtele, B. Spiegelhalder, H. Bartsch, R.W. Owen, Characterization of alkyl phenols in cashew (Anacardium occidentale) products and assay of their antioxidant capacity, Food and Chemical Toxicology 44 (2006) 188–197. https://doi.org/10.1016/j.fct.2005.06.012.

[163] S. Rwahwire, B. Tomkova, A.P. Periyasamy, B.M. Kale, Green thermoset reinforced biocomposites, in: Green Composites for Automotive Applications, Elsevier, 2018: pp. 61–80. https://doi.org/10.1016/B978-0-08-102177-4.00003-3.

[164] R.N. Patel, S. Bandyopadhyay, A. Ganesh, Extraction of cashew (Anacardium occidentale) nut shell liquid using supercritical carbon dioxide, Bioresour Technol 97 (2006) 847–853. https://doi.org/10.1016/j.biortech.2005.04.009.

[165] R.K. Jain, S. Kumar, Development of a cashew nut sheller, J Food Eng 32 (1997) 339–345. https://doi.org/10.1016/S0260-8774(97)00020-4.

[166] A. Ahmadou, E. Tardan, J. Valette, A. Napoli, N. Durand, D. Montet, Improvement of extraction methods of Malian Cashew nut shell liquid-siftdesk, SDRP Journal of Earth Sciences & Environmental Studies (2022) 121–130. https://doi.org/10.25177/JESES.6.1.RA.10782.

[167] R.L. Smith, R.M. Malaluan, W.B. Setianto, H. Inomata, K. Arai, Separation of cashew (Anacardium occidentale L.) nut shell liquid with supercritical carbon dioxide, Bioresour Technol 88 (2003) 1–7. https://doi.org/10.1016/S0960-8524(02)00271-7.

[168] P.H. Gedam, P.S. Sampathkumaran, Cashew nut shell liquid: Extraction, chemistry and applications, 1986.

[169] Risfaheri, T. Tedja Irawadi, M. Anwar Nur, I. Sailah, Isolation of cardanol from cashew nut shell liquid usinf the vacuum distillation method, 2009.

[170] J.P.A. Feitosa, F.H.A. Rodrigues, F.C.F. França, J.R.R. Souza, N.M.P.S. Ricardo, Autor para correspondência: Comparison Between Physico-Chemical Properties of the Technical Cashew Nut Shell Liquid (CNSL) and those Natural Extracted from Solvent and Pressing, n.d.

[171] M.R. Patel, B.Z. Dholakiya, T. Gandhi, M. Patel, B. Kumar Dholakiya, Studies on effect of various solvents on extraction of cashew nut shell liquid (CNSL) and isolation of major phenolic constituents from extracted CNSL, 2012. http://scholarsresearchlibrary.com/archive.html.

[172] T.S. Gandhi, B.Z. Dholakiya, M.R. Patel, Extraction protocol for isolation of CNSL by using protic and aprotic solvents from cashew nut and study of their physico-chemical parameter, Polish Journal of Chemical Technology 15 (2013) 24–27. https://doi.org/10.2478/pjct-2013-0062.

[173] F. Oiram Filho, D.B. Alcântra, T.H.S. Rodrigues, L.M. Alexandre Silva, E. De Oliveira Silva, G.J. Zocolo, E.S. De Brito, Development and Validation of a Reversed Phase HPLC Method for Determination of Anacardic Acids in Cashew (Anacardium occidentale) Nut Shell Liquid, J Chromatogr Sci 56 (2018) 300–306. https://doi.org/10.1093/chromsci/bmx111.

[174] S.M. Morais, K.A. Silva, H. Araujo, I.G.P. Vieira, D.R. Alves, R.O.S. Fontenelle, A.M.S. Silva, Anacardic acid constituents from cashew nut shell liquid: NMR characterization and the effect of unsaturation on its biological activities, Pharmaceuticals 10 (2017). https://doi.org/10.3390/ph10010031.

[175] J. Chen, G. Wu, S. Huo, Z. Kong, Synthesis and Characterization of Curing Reaction of Epoxy Resin Obtained from Anacardic Acids, Chemistry and Industry of Forest Products 40 (2020) 41–46. https://doi.org/10.3969/j.issn.0253-2417.2020.04.006.

[176] M. Yuliana, C.T. Truong, L.H. Huynh, Q.P. Ho, Y.H. Ju, Isolation and characterization of protein isolated from defatted cashew nut shell: Influence of pH and NaCl on solubility and functional properties, LWT - Food Science and Technology 55 (2014) 621–626. https://doi.org/10.1016/J.LWT.2013.10.022.

[177] M. Yuliana, L.H. Huynh, Q.P. Ho, C.T. Truong, Y.H. Ju, Defatted cashew nut shell starch as renewable polymeric material: Isolation and characterization, Carbohydr Polym 87 (2012) 2576–2581. https://doi.org/10.1016/J.CARBPOL.2011.11.044.

[178] J.H.P. Tyman, R.A. Johnson, M. Muir, R. Rokhgar, The Extraction of Natural Cashew Nut-Shell Liquid From the Cashew Nut (Anacardium occidentale), 66 (1989) 553–557. https://doi.org/10.1007/BF02885447.

[179] J.O. Ocheja, B.C. Lablabe, H.G.E. Oguche, G.O. Usman, Vitamin Composition and Fibre Fractions of Cashew Nut Shell: Implication for Animal Nutrition, Pakistan Journal of Nutrition 14 (2015) 252–254. https://doi.org/10.3923/pjn.2015.252.254.

[180] A.J. Tsamba, W. Yang, W. Blasiak, Pyrolysis characteristics and global kinetics of coconut and cashew nut shells, Fuel Processing Technology 87 (2006) 523–530. https://doi.org/10.1016/j.fuproc.2005.12.002.

[181] L. Wilson, W. Yang, W. Blasiak, G.R. John, C.F. Mhilu, Thermal characterization of tropical biomass feedstocks, in: Energy Convers Manag, Elsevier Ltd, 2011: pp. 191–198. https://doi.org/10.1016/j.enconman.2010.06.058.

[182] N. Tippayawong, C. Chaichana, A. Promwangkwa, P. Rerkkriangkrai, Gasification of cashew nut shells for thermal application in local food processing factory, Energy for Sustainable Development 15 (2011) 69–72. https://doi.org/10.1016/j.esd.2010.10.001.

[183] K. Harini, C. Chandra Mohan, K. Ramya, S. Karthikeyan, M. Sukumar, Effect of Punica granatum peel extracts on antimicrobial properties in Walnut shell cellulose reinforced Bio-thermoplastic starch films from cashew nut shells, Carbohydr Polym 184 (2018) 231–242. https://doi.org/10.1016/j.carbpol.2017.12.072.

[184] A.H. Fombu, A.E. Ochonogor, O.E. Olayide, Characterization of Cashew Nut Shell Pyrolysis Liquid: As a Source of Sustainable Energy and a Precursor in many Chemical Industries, IOP Conf Ser Earth Environ Sci 1178 (2023) 012013. https://doi.org/10.1088/1755-1315/1178/1/012013.

[185] P.A. Idah, S.M. Imonologie, Extraction and Characterization of Cashew Nut (Anacardium Occidentale) Oil and Cashew Shell Liquid Oil, Academic Research International 5 (2014) 50–54.

[186] T.F. Akinhanmi, V.N. Atasie, P.O. Akintokun, Chemical Composition and Physicochemical Properties of Cashew nut (Anacardium occidentale) oil and Cashew Nut Shell Liauid, Journal of Agricultural, Food and Environmental Sciences 2 (2008).

[187] S.S. Achi, O.M. Myina, Preliminary Investigation of Kaduna-Grown Cashew Nutshell Liquid as a Natural Precursor for Dyestuffs, Pigments and Binders for Leather Finishing, Nigerian Journal of Chemical Research 16 (2014).

[188] P.A. Mahanwar, D.D. Kale, Effect of cashew nut shell liquid (CNSL) on properties of phenolic resins, J Appl Polym Sci 61 (1996) 2107–2111. https://doi.org/10.1002/(SICI)1097-4628(19960919)61:12<2107::AID-APP8>3.0.CO;2-E.

[189] F.H.A. Rodrigues, F.C.F. França, J.R.R. Souza, N.M.P.S. Ricardo, J.P.A. Feitosa, Comparison between physico-chemical properties of the technical Cashew Nut Shell Liquid (CNSL) and those natural extracted from solvent and pressing, Polímeros 21 (2011) 156–160. https://doi.org/10.1590/S0104-14282011005000028.

[190] A.N. Mohrammed, Development of High Performance Cashew Nut Shell Liquid (CNSL) Based Surface Coatings Cross Linked with Styrene and Methyl Methacrylate, Jomo Kenyatta University of Agriculture and Technology, 2015.

[191] ChemSrc, Anacardic acid, (2024). https://www.chemsrc.com/en/cas/16611-84-0_1109645.html (accessed November 27, 2024).

[192] ChemSrc, Ginkgolic acid C15:1, (2024). https://www.chemsrc.com/en/cas/22910-60-7_830478.html (accessed November 27, 2024).

[193] ChemSrc, 2-(14-hydroxypentadeca-7,9-dien-5-yl)benzoic acid, (2024). https://www.chemsrc.com/en/cas/103904-74-1_1049048.html (accessed November 27, 2024).

[194] ChemSrc, Anacardic acid triene, (2024). https://www.chemsrc.com/en/cas/103904-73-0_1049047.html (accessed November 27, 2024).

[195] ChemSrc, 4-methyl-5-pentadecylresorcinol, (2024). https://www.chemsrc.com/en/cas/16737-83-0_1028937.html (accessed November 27, 2024).

[196] ChemSrc, Cardanol diene, (2024). https://www.chemsrc.com/en/cas/51546-63-5_717363.html (accessed November 27, 2024).

[197] ChemSrc, Adipostatin A, (2024). https://www.chemsrc.com/en/cas/3158-56-3_32722.html (accessed November 27, 2024).

[198] Biosynth, Cardanol diene, (n.d.). https://www.biosynth.com/p/BCA54663/51546-63-5-cardanol-diene (accessed November 27, 2024).

[199] ChemSrc, Cardol triene, (2024). https://www.chemsrc.com/en/cas/79473-24-8_265022.html (accessed November 27, 2024).

[200] A.J. Tsamba, W. Yang, W. Blasiak, M.A. Wójtowicz, Cashew nut shells pyrolysis: Individual gas evolution rates and yields, Energy and Fuels 21 (2007) 2357–2362. https://doi.org/10.1021/ef0604792.

[201] G.D. Mumbach, J.L.F. Alves, J.C.G. da Silva, M. Di Domenico, C. Marangoni, R.A.F. Machado, A. Bolzan, Investigation on prospective bioenergy from pyrolysis of butia seed waste using TGA-FTIR: Assessment of kinetic triplet, thermodynamic parameters and evolved volatiles, Renew Energy 191 (2022) 238–250. https://doi.org/10.1016/j.renene.2022.03.159.

[202] J.C.G. da Silva, J.G. de Albuquerque, W.V. de A. Galdino, R.F. de Sena, S.L.F. Andersen, Single-step and multi-step thermokinetic study – Deconvolution method as a simple pathway for describe properly the biomass pyrolysis for energy conversion, Energy Convers Manag 209 (2020) 112653. https://doi.org/10.1016/j.enconman.2020.112653.

[203] J.C.G. da Silva, J.G. de Albuquerque, W.V. de A. Galdino, R.F. de Sena, S.L.F. Andersen, Single-step and multi-step thermokinetic study – Deconvolution method as a simple pathway for describe properly the biomass pyrolysis for energy conversion, Energy Convers Manag 209 (2020) 112653. https://doi.org/10.1016/j.enconman.2020.112653.

[204] V. Mamleev, S. Bourbigot, J. Yvon, Kinetic analysis of the thermal decomposition of cellulose: The main step of mass loss, J Anal Appl Pyrolysis 80 (2007) 151–165. https://doi.org/10.1016/j.jaap.2007.01.013.

[205] D. Zhang, R. Pan, R. Chen, X. Xu, Pyrolysis Characteristics and Reaction Mechanisms of Pine Needles, Appl Biochem Biotechnol 189 (2019) 1056–1083. https://doi.org/10.1007/s12010-019-03057-3.

[206] T. Anh Vo, J. Kim, H. Tae Hwang, S.S. Kim, Fast pyrolysis of cashew nut shells in a bubbling fluidized bed reactor for producing high-heating value bio-oil using dolomite as a catalyst and carbon capture sorbent, Fuel 364 (2024). https://doi.org/10.1016/j.fuel.2024.131024.

[207] S. Wang, G. Dai, H. Yang, Z. Luo, Lignocellulosic biomass pyrolysis mechanism: A state-of-the-art review, Prog Energy Combust Sci 62 (2017) 33–86. https://doi.org/10.1016/j.pecs.2017.05.004.

[208] X. Lu, X. Gu, A review on lignin pyrolysis: pyrolytic behavior, mechanism, and relevant upgrading for improving process efficiency, Biotechnology for Biofuels and Bioproducts 15 (2022) 106. https://doi.org/10.1186/s13068-022-02203-0.

[209] H. Wang, M. Tucker, Y. Ji, Recent Development in Chemical Depolymerization of Lignin: A Review, Journal of Applied Chemistry 2013 (2013) 1–9. https://doi.org/10.1155/2013/838645.

[210] A. Kumar, B. Biswas, R. Kaur, B.B. Krishna, B. Thallada, Predicting the decomposition mechanism of Loktak biomass using Py-GC/MS, Environ Technol Innov 23 (2021) 101735. https://doi.org/10.1016/j.eti.2021.101735.

[211] P. Olivares-Carrillo, J. Quesada-Medina, Thermal decomposition of fatty acid chains during the supercritical methanol transesterification of soybean oil to biodiesel, J Supercrit Fluids 72 (2012) 52–58. https://doi.org/10.1016/j.supflu.2012.08.012.

[212] A.A.S. Lopes, E.A. Carneiro, M.A.S. Rios, J.J.H. Filho, J.O.B. Carioca, G.G. Barros, S.E. Mazzetto, Study of antioxidant property of a thiophosphorated compound derived from cashew nut shell liquid in hydrogenated naphthenics oils, Brazilian Journal of Chemical Engineering 25 (2008) 119–127. https://doi.org/10.1590/S0104-66322008000100013.

[213] V. Moody, H.L. Needles, Fiber Theory and Formation, Tufted Carpet (2004) 3–21. https://doi.org/10.1016/B978-188420799-0.50002-6.

[214] B.G.K. Murthy, M.C. Menon, J.S. Agarwal, S.H. Zaheer, -, Paint Manuf 31 (1961) 47–50.

[215] T.A. Saleh, Polymer science and polymerization methods toward hybrid materials, Polymer Hybrid Materials and Nanocomposites (2021) 59–103. https://doi.org/10.1016/B978-0-12-813294-4.00004-2.

[216] C. Voirin, S. Caillol, N. V. Sadavarte, B. V. Tawade, B. Boutevin, P.P. Wadgaonkar, Functionalization of cardanol: Towards biobased polymers and additives, Polym Chem 5 (2014) 3142–3162. https://doi.org/10.1039/c3py01194a.

[217] F.A. Helder Rodrigues, J.R. Roberto Souza, F.F. Célio França, N.M. P S Ricardo, J.P. A Feitosa, Thermal Oligomerisation of Cardanol, (2006). http://www.e-polymers.org.

[218] W. Kiratitanavit, S. Ravichandran, Z. Xia, J. Kumar, R. Nagarajan, Thermally stable polymers of cardanol as char-forming additives for polypropylene, J Renew Mater 1 (2013) 289–301. https://doi.org/10.7569/JRM.2013.634126.

[219] R. Nakai, On the thermal decomposition of cresols, Bull Chem Soc Jpn 5 (1930) 136–157. https://doi.org/10.1246/bcsj.5.136.

[220] S. Li, B. Lu, Y. Wang, X. Lin, H. Zhang, Dealkylation of alkylphenols in phenol oil on acid zeolites, J Anal Appl Pyrolysis 179 (2024). https://doi.org/10.1016/j.jaap.2024.106470.

[221] B.W. Jones, M.B. Neuworth, Thermal Cracking of Alkyl Phenols - Mechanism of Dealkylation, Ind Eng Chem 44 (1952) 2872–2876. https://doi.org/10.1021/ie50516a034.

[222] P.D. Shelley, T.J. Bannan, S.D. Worrall, M.R. Alfarra, U.K. Krieger, C.J. Percival, A. Garforth, D. Topping, Measured solid state and subcooled liquid vapour pressures of nitroaromatics using Knudsen effusion mass spectrometry, Atmos Chem Phys 20 (2020) 8293–8314. https://doi.org/10.5194/acp-20-8293-2020.

[223] R.J. Ouellette, J.D. Rawn, Aromatic Compounds, in: Principles of Organic Chemistry, Elsevier, 2015: pp. 133–162. https://doi.org/10.1016/B978-0-12-802444-7.00005-7.

[224] H. Yang, Y. Furutani, S. Kudo, J. Hayashi, K. Norinaga, Experimental investigation of thermal decomposition of dihydroxybenzene isomers: Catechol, hydroquinone, and resorcinol, J Anal Appl Pyrolysis 120 (2016) 321–329. https://doi.org/10.1016/j.jaap.2016.05.019.

[225] H. Yang, J. Jiang, B. Zhang, P. Xu, Experimental study on light volatile products from thermal decomposition of lignin monomer model compounds: effect of temperature, residence time and methoxyl group, RSC Adv 11 (2021) 37067–37082. https://doi.org/10.1039/D1RA06743E.

[226] M.S.U. Department of Chemistry, Dienes, (2013). https://www2.chemistry.msu.edu/faculty/reusch/VirtTxtJml/addene2.htm#dien1 (accessed December 12, 2024).

[227] H. Vaskova, M. Buckova, Thermal Degradation of Vegetable Oils: Spectroscopic Measurement and Analysis, Procedia Eng 100 (2015) 630–635. https://doi.org/10.1016/j.proeng.2015.01.414.

[228] Alkanes and alkenes, (n.d.). https://chemistryclinic.co.uk/alkanes-and-alkenes/ (accessed August 12, 2024).

[229] A. Diedhiou, A. Bensakhria, L.G. Ndiaye, A. Khelfa, O. Sock, Study of cashew nut shells Valorisation by gasification, Chem Eng Trans 39 (2014) 1171–1176. https://doi.org/10.3303/CET1439196.

[230] H.N. Nguyen, D.A. Khuong, T.T.H. Vu, T.N. Mai, T. Tsubota, V.B. Tran, J. Blin, L. Van De Steene, Kinetic and structural changes during gasification of cashew nut shell char particles, Environ Prog Sustain Energy 40 (2021). https://doi.org/10.1002/ep.13580.

[231] M.V. Ramanan, E. Lakshmanan, R. Sethumadhavan, S. Renganarayanan, Modeling and experimental validation of cashew nut shell char gasification adopting chemical equilibrium approach, Energy and Fuels 22 (2008) 2070–2078. https://doi.org/10.1021/ef700467x.

[232] S. Singh Siwal, Q. Zhang, C. Sun, S. Thakur, V. Kumar Gupta, V. Kumar Thakur, Energy production from steam gasification processes and parameters that contemplate in biomass gasifier – A review, Bioresour Technol 297 (2020). https://doi.org/10.1016/j.biortech.2019.122481.

[233] M. Venkata Ramanan, E. Lakshmanan, R. Sethumadhavan, S. Renganarayanan, Performance prediction and validation of equilibrium modeling for gasification of cashew nut shell char, Brazilian Journal of Chemical Engineering 25 (2008) 585–601. https://doi.org/10.1590/s0104-66322008000300016.

[234] F.L. Moreira, G.R. dos Santos, R. dos S. Araújo, M.L.M. de Oliveira, F.S.Á. Cavalcante, D.S. Serra, Combustion of pellets produced from corn straw and cashew nut shell in residential and industrial scenarios: Chemical, thermal and emission analyses, Waste Management & Research: The Journal for a Sustainable Circular Economy 41 (2023) 1486–1495. https://doi.org/10.1177/0734242X221135518.

[235] C. Lanvin, J. Valette, K.W.Y. Chung, J. Blin, L. Van de Steene, A new method to quantify CNSL from Cashew Nut Shells and its major constituents: anacardic acids, cardanols and cardols (ACC), (n.d.).

[236] E. Alakangas, Quality guidelines of wood fuels in Finland, 2015. https://doi.org/10.13140/RG.2.1.3290.3127.

[237] P.J. Van Soest, J.B. Robertson, B.A. Lewis, Methods for Dietary Fiber, Neutral Detergent Fiber, and Nonstarch Polysaccharides in Relation to Animal Nutrition, J Dairy Sci 74 (1991) 3583–3597. https://doi.org/10.3168/jds.S0022-0302(91)78551-2.

[238] P.J. Van Soest, Development of a Comprehensive System of Feed Analyses and Its Application to Forages, J Anim Sci 26 (1967) 119–128.

[239] E. Daouk, L. Van De Steene, F. Paviet, E. Martin, J. Valette, S. Salvador, Oxidative pyrolysis of wood chips and of wood pellets in a downdraft continuous fixed bed reactor, 196 (2017) 408–418. https://doi.org/10.1016/j.fuel.2017.02.012.

[240] F. Rasheed, J. Markgren, M. Hedenqvist, E. Johansson, Modeling to Understand Plant Protein Structure-Function Relationships—Implications for Seed Storage Proteins, Molecules 25 (2020) 873. https://doi.org/10.3390/molecules25040873.

[241] M. Becidan, Experimental Studies on Municipal Solid Waste and Biomass Pyrolysis, Norwegian University of Science and Technology, 2007.

[242] N. Chen, Q. Wang, M.X. Wang, N. yang Li, A. V. Briones, L. Cassani, M.A. Prieto, M.B. Carandang, C. Liu, C.M. Gu, J.Y. Sun, Characterization of the physicochemical,

thermal and rheological properties of cashew kernel starch, Food Chem X 15 (2022). https://doi.org/10.1016/j.fochx.2022.100432.

[243] R. Rico, M. Bulló, J. Salas-Salvadó, Nutritional composition of raw fresh cashew (*Anacardium occidentale* L.) kernels from different origin, Food Sci Nutr 4 (2016) 329–338. https://doi.org/10.1002/fsn3.294.

[244] F. Canon, Effect of the Structure of Tannins on Their Binding Site on a Human Salivary Proline-Rich Protein, Encyclopedia of Food Chemistry (2019) 510–514. https://doi.org/10.1016/B978-0-08-100596-5.21495-9.

[245] W. Ge, Y. Xu, M. Niu, C. Jia, S. Zhao, The differentiation between condensed and hydrolyzable tannins with different molecular weights in affecting the rheological property of wheat flour-based dough, J Cereal Sci 111 (2023) 103666. https://doi.org/10.1016/j.jcs.2023.103666.

[246] M.A. Bharudin, S. Zakaria, C.H. Chia, Condensed tannins from acacia mangium bark: Characterization by spot tests and FTIR, in: AIP Conf Proc, 2013: pp. 153–157. https://doi.org/10.1063/1.4858646.

[247] M. Chen, J. Luo, R. Shi, J. Zhang, Q. Gao, J. Li, Improved adhesion performance of soy protein-based adhesives with a larch tannin-based resin, Polymers (Basel) 9 (2017) 408. https://doi.org/10.3390/polym9090408.

[248] J. Lisperguer, Y. Saravia, E. Vergara, Structure and thermal behavior of tannin from Acacia dealbata bark and their reactivity toward formaldehyde, J. Chil. Chem. Soc 61 (2016) 3188–3190. https://doi.org/10.4067/S0717-97072016000400007.

[249] F.H.A. Rodrigues, F.C.F. França, J.R.R. Souza, N.M.P.S. Ricardo, J.P.A. Feitosa, Comparison between physico-chemical properties of the technical cashew nut shell liquid (CNSL) and those natural extracted from solvent and pressing, Polimeros 21 (2011) 156–160. https://doi.org/10.1590/S0104-14282011005000028.

[250] S. Shukla, N. Yadav, B. Lochab, Cardanol-Based Benzoxazines and Their Applications, in: Advanced and Emerging Polybenzoxazine Science and Technology, Elsevier, 2017: pp. 451–472. https://doi.org/10.1016/B978-0-12-804170-3.00024-X.

[251] C. Sahin, L. Magomedova, T.A.M. Ferreira, J. Liu, J. Tiefenbach, P.S. Alves, F.J.G. Queiroz, A.S. de Oliveira, M. Bhattacharyya, J. Grouleff, P.C.N. Nogueira, E.R. Silveira,

D.C. Moreira, J.R.S. de A. Leite, G.D. Brand, D. Uehling, G. Poda, H. Krause, C.L. Cummins, L.A.S. Romeiro, Phenolic Lipids Derived from Cashew Nut Shell Liquid to Treat Metabolic Diseases, J Med Chem 65 (2022) 1961–1978. https://doi.org/10.1021/acs.jmedchem.1c01542.

[252] H. Zhao, J.J. Shanahan, S. Samson, Z. Li, G. Ma, N. Prine, L. Galuska, Y. Wang, W. Xia, W. You, X. Gu, Manipulating Conjugated Polymer Backbone Dynamics through Controlled Thermal Cleavage of Alkyl Side Chains, Macromol Rapid Commun 43 (2022). https://doi.org/10.1002/marc.202200533.

[253] Y.N. Chun, H.G. Song, Microwave-induced cracking and reforming of benzene on activated carbon, Chemical Engineering and Processing - Process Intensification 135 (2019) 148–155. https://doi.org/10.1016/J.CEP.2018.11.021.

[254] V. Huchon, E. Martin, F. Pinta, J.M. Commandré, L. Van de steene, Conversion in a char bed reactor of tars and syngas from a wood gasifier, Energy 288 (2024) 129738. https://doi.org/10.1016/J.ENERGY.2023.129738.

[255] A.S. Fedotov, V.I. Uvarov, M.V. Tsodikov, S. Paul, P. Simon, M. Marinova, F. Dumeignil, Production of styrene by dehydrogenation of ethylbenzene on a [Re, W]/γ-Al2O3 (K, Ce)/α-Al2O3 porous ceramic catalytic converter, Chemical Engineering and Processing - Process Intensification 160 (2021) 108265. https://doi.org/10.1016/j.cep.2020.108265.

[256] C. Font Palma, Modelling of tar formation and evolution for biomass gasification: A review, Appl Energy 111 (2013) 129–141. https://doi.org/10.1016/j.apenergy.2013.04.082.

[257] G.P. Assima, A. Paquet, J.-M. Lavoie, Utilization of MSW-Derived Char for Catalytic Reforming of Tars and Light Hydrocarbons in the Primary Syngas Produced During Wood Chips and MSW-RDF Air Gasification, Waste Biomass Valorization 10 (2019) 1203–1222. https://doi.org/10.1007/s12649-017-0138-0.

[258] Q. Wang, H. Song, S. Pan, N. Dong, X. Wang, S. Sun, Initial pyrolysis mechanism and product formation of cellulose: An Experimental and Density functional theory(DFT) study, Sci Rep 10 (2020) 3626. https://doi.org/10.1038/s41598-020-60095-2.

[259] M. Di Gioacchino, F. Bruni, S. Imberti, M.A. Ricci, Hydration of Carboxyl Groups: A Route toward Molecular Recognition?, J Phys Chem B 124 (2020) 4358–4364. https://doi.org/10.1021/acs.jpcb.0c03609.

[260] W. Arayedh, Craquage catalytique du toluène sur un lit de biochars issus de la biomasse, Université de Technologie de Compiègne, 2023.

[261] Q. Yu, C. Brage, G. Chen, K. Sjöström, Temperature impact on the formation of tar from biomass pyrolysis in a free-fall reactor, J Anal Appl Pyrolysis 40–41 (1997) 481–489. https://doi.org/10.1016/S0165-2370(97)00017-X.

Appendices

Appendices

A3.1 Production of cashew nut shells char

In order to study the catalytic cracking of CNS pyrolysis gas, cashew nut shells char was required to study their potential as catalyst. A pilot scale carbonization furnace was used for the production of cashew nut shells char in order to produce large quantity of char. The different parts of the carbonization furnace were detailed, following by the experimental procedure employed to produce the char.

A3.1.1 Description of carbonization furnace

The reactor (Figure A3.1) includes a refractory stainless-steel tube (1) standing at 937 mm with an internal diameter of 264 mm. Within this tube, a set of 10 removable refractory stainless-steel trays (2) measuring 670 mm in height and 252 mm in internal diameter houses the load. Sealing is achieved through a graphite seal.

The entire system is heated by a tubular resistance furnace (3) (ROK 300/1200/11-3Z) from Ceradel Industries, with a height of 1200 mm and an internal diameter of 280 mm, with a maximum power of 20 kW for reaching temperatures up to 1100 °C. This furnace is equipped with three independent heating zones of 400 mm each, ensuring uniform heating of the reactor's wall.

In order to work in an inert environment, the reactor receives nitrogen from below through a 6 m long, 6 mm internal diameter coil (4). This coil, heated in the lower part of the oven, connects to the center of the bottom of the reactor, facilitating the diffusion of the preheated carrier gas under the bed through a nozzle. Nitrogen flow is controlled by a Brooks 5850S mass flow meter, with a maximum flow rate of 30 Nl/min. The use of nitrogen as a carrier gas enhances temperature uniformity within the reactor and aids in the removal of volatile materials towards the post-combustion chamber.

To cool the reactor, forced convection of air occurs between the reactor and the heating elements. Additionally, a flow of cold nitrogen is injected through a bypass system in the serpentine.

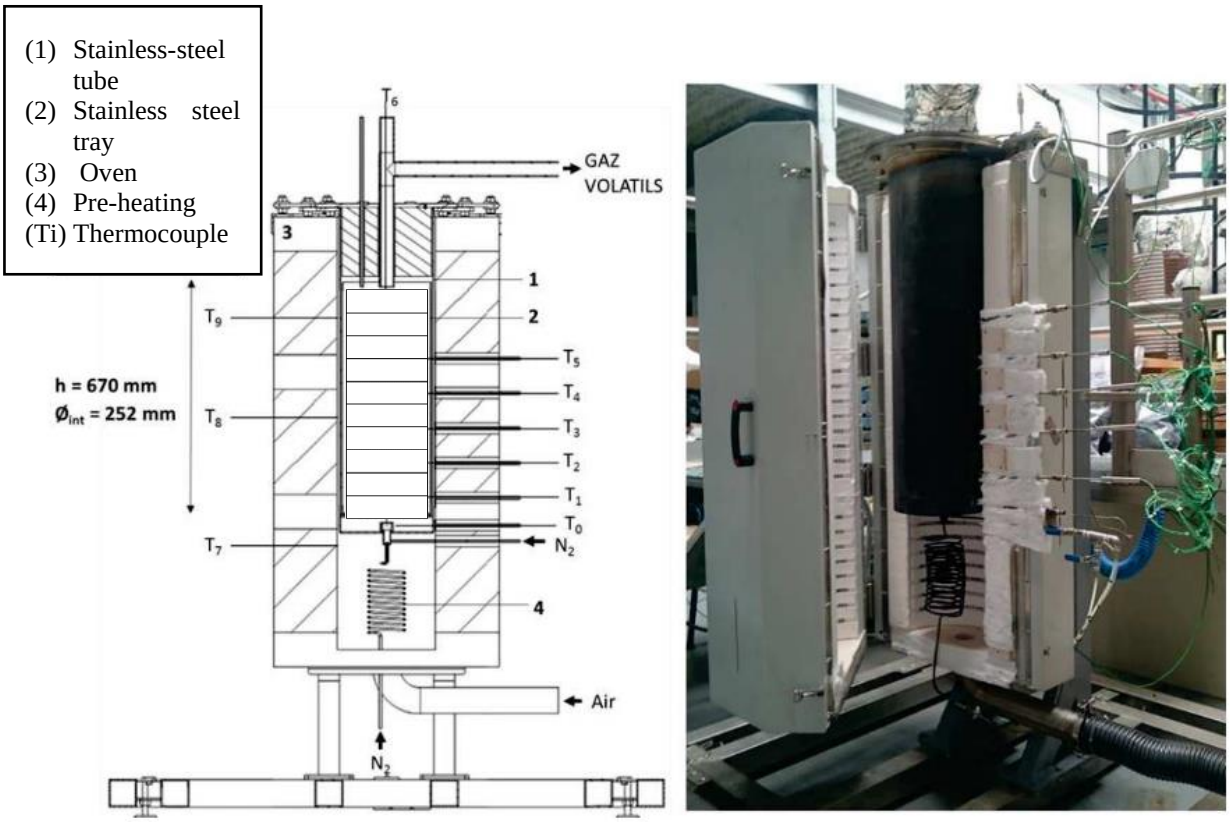

Figure A3.1: Carbonization furnace

A3.1.2 Experimental procedure to produce cashew nut shells char

The temperature rise was carried out under inert nitrogen with a flow rate of 2 Nl/min, as well as cooling with a flow rate of 2 Nl/min. The heating rate was set at 10 °C/min. The final temperature was chosen equal to the maximum temperature planned for the tests of cracking at 910°C to limit residual volatile materials. Dwell time was set for 1 h. The char obtained was then crushed (knife crusher with a 10mm grid) then sieved in the desired particle size cut-off of 1-4 mm.

A3.2 Tars analyzed by GC-MS

Table A3.2.1 Primary tars analyzed by GC-MS

Chemical groups	Chemical compounds
Alcohols	Methanol, Ethylene glycol
Aldehydes	Formaldehyde / Acetaldehyde / Glycol aldehyde
	2-Propanone,1-hydroxy-/2-cyclopenten-1-one
	2-cyclopenten-1-one-3-methyl / 2-Butanone,1-hydroxy-
	3-methyl-1,2-cyclopentanedione / 1-acetyloxy-2-propanone
	Cyclopentanone
Acids	Formic Acid / Acetic Acid / Furans
	Furfural / 2-furanmethanol / Benzofuran
	2-furancarboxaldehyde,5-methyl / 2,5-dimethylfuran
	5-hydroxymethylfurfural / 2(5H)-Furanone
Sugars	Levoglucosan / LAC / DGP
Guaiacols	Phenol-2-methoxy / Phenol-2-methoxy-4-methyl
	2,6-dimethoxyphenol / Phenol-4-ethyl-2-methoxy
	Eugenol / Isoeugenol
	2-methoxy-4-vinylphenol / 2-isopropoxyphenol
	Vanillin / Apocynin
	Guaiacylacetone / Syringaldehyde / Acetosyringone

Table A3.2.2 Secondary tars analyzed by GC-MS

Chemical groups	Chemical compounds
Phenols	Phenol
	Phenol-2-methyl / Phenol-3-methyl+Phenol-4-methyl
	3,4-dimethylphenol / 2,4-dimethylphenol
	1-naphthalenol / 2-naphthalenol
	Hydroquinone / Catechol
Terpenes	1-R-a-pinene

A3.2.3 Tertiary tars analyzed by GC-MS

Chemical groups	Chemical compounds
Anisoles	1,2,3-trimethoxy-5-methylbenzene
	1,2,4-trimethoxybenzene
	3,5-dimethoxy-acetophenone
Nitrogen aromatics	Pyridine / Pyridine-2-methyl
	Quinoline / Isoquinoline
Monocyclic aromatics	Benzene / Toluene / Ethylbenzene
	(m+p)-xylene / o-xylene
	Styrene / Phenylethyne
Alkylated polycyclic aromatics	Naphthalene-1-methyl / Naphthalene-2-methyl
	2-methylindene

PAH : 2 rings	Naphthalene / Biphenyl Indene / Fluorene
PAH : 3 rings	Acenaphthylene / Acenaphthene Phenanthrene / Anthracene Fluoranthene
PAH : 4 rings	Pyrene Benzo(a)anthracene / Chrysene Benzo(b)fluoranthene / Benzo(k)fluranthene
PAH : 5 rings	Benzo(a)pyrene Dibenzo(ah)anthracene Indeno(123cd) pyrene
PAH : 6 rings	Benzo(ghi)pérylène

A6.1 Preparation of char and operating conditions

In this section, the char preparation procedure is first explained. It includes the operating condition for the production of char, followed by a selection procedure of the granulometry of char employed.

The second section consists of the proximate and ultimate analysis of the char. This allows us to predict the behavior of the char during the catalytic cracking experiments.

The third section includes calculations for the porosity of the char bed as well as the residence time of the experiments.

Preparation of char

The char used to form the particle bed in the cracking reactor was produced in the CIRAD carbonization furnace described in Chapter 3 (Annex). It was produced at an average pyrolysis temperature of 910°C for a residence time of approximately one hour. The cashew nut shells char was then ground using a mill with a sieve of 4mm. After that, the milled cashew nut shells char was sieved at different granulometries (1.0-4.0 mm). The objective of separating the milled char was to:

- on the one hand to remove the finest particles and thus limit pressure losses to across the char bed,

- on the other hand in order to have a sufficiently low particle size, allowing good filling the cracking reactor and avoiding creating preferential passages for the gas.

The char yield obtained through sieving is presented in Table A6.1.

Table A6.1: Char yields obtained during char preparation (wt%)

Granulometry	Yield
2.5-4.0 mm	26%
1.6-2.5 mm	43%
1.0-1.6 mm	31%

Most of the char produced had a granulometry between 1.6-2.5 mm. The char with this range of granulometry fills the tube better than the one between 2.5-4.0 mm. For the catalytic cracking experiments, the cashew nut shells char of 1.6-2.5 mm was employed.

Proximate and ultimate analysis of char

The proximate and ultimate analysis of the char selected (1.6-2.5mm) was carried out. It includes humidity content, ash content, volatile matter content and elemental analysis of the char (Table A6.2).

Table A6.2: Characteristics of char used pour cracking of pyrolysis gas

	Parameters	
Proximate (dry basis, db)		
	Humidity (%)	2.78
	Ash (% db)	8.83
	Volatile matter (% db)	6.82
	Fixed carbon (% db)*	84.35
*Calculated by difference : Fixed carbon(%) =100%-Humidity(%)-Ash(%)-Volatile matter(%)		
Ultimate (dry ash free basis, daf)		
	H (% daf)	0.70
	C (% daf)	86.02
	N (% daf)	1.15
	O (% daf) **	12.13
**Calculated by difference : O%=100%-H%-C%-N%		

The CNS char produced has lower humidity than CNS, due to the heat treatment undergone during pyrolysis. The fixed carbon of CNS char is very high, accounting up to 99.23%. In terms of elemental composition, CNS char has a higher carbon, hydrogen and nitrogen content. Even with a higher temperature (910°C), the carbon content is lower than the one of wood chips produced at 670°C [106].

Calculation of porosity and residence time

The apparent density of the char bed can be calculated by Ergun method [31] .

For this, the pressure loss in the bed is measured by sweeping the coal bed with a variable flow rate of nitrogen at different superficial speeds U (corresponding to the nitrogen flow on the section of the reactor).

The porosity of the particles is then obtained according to Eq A6.1:

$$\frac{\Delta P}{L} = 150\frac{(1-\varepsilon)^2}{\varepsilon^3}\frac{\mu U}{d_p^2} + 1.75\frac{(1-\varepsilon)}{\varepsilon^3}\frac{\rho U^2}{d_p} \qquad \textit{Equation A6.1}$$

In our study, the flow regime being laminar, the 2nd term from Eq. A6.1 can be neglected and a linear relationship is obtained between the linear pressure drop and the surface speed U. The porosity and therefore the apparent density can thus be determined (Figure A6.1).

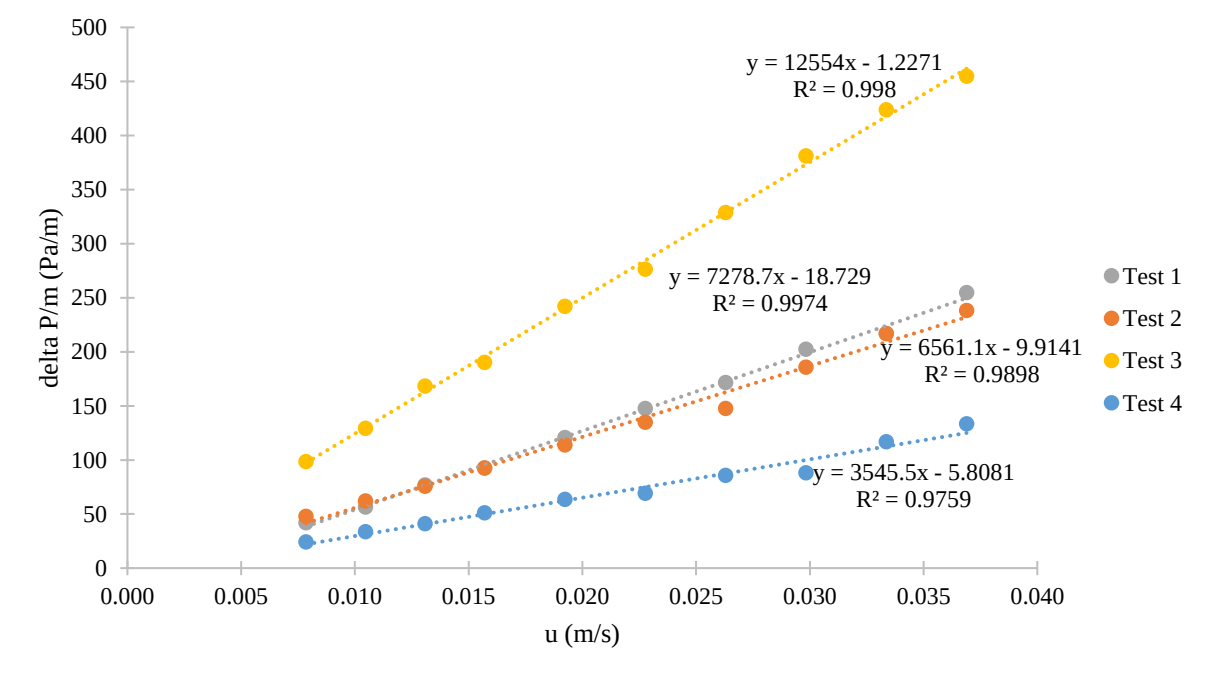

Figure A6.1: Linear pressure drop (Pa/m) vs. surface speed U

By this method, a porosity of 0.34709 +/- 0.06 was measured and therefore a char density of 612.18 kg/m3.The average density of the char bed is 399.7 mg/m3.

When the cracking reactor was heated, the char bed was swept by a flow of nitrogen in order to to keep it inert. Despite being produced at 910°C with a long residence time, the char bed produced a small amount of CO_2. During the experiments at 600°C, this degassing represented up to 700 mg of CO_2. We therefore waited until the microGC no longer detected gas other than N_2 before starting the experiment.

We used a 26 mm i.d. cracking reactor fitted with a sintered plate at a height located 5 cm below the end of the isothermal zone.

For the calculation of the gas residence time, we assumed that the volume and porosity of the gas bed char do not evolve in our operating conditions during an experiment. Residence time gases in the isothermal zone then depends on the initial porosity of the char bed.

The porosity of the bed, ε, was estimated as follows (Equation A6.2):

$$\varepsilon = 1 - \frac{\rho_{lit}}{\rho_{char}} \qquad \textit{Equation A6.2}$$

We can thus calculate the residence time of the gases τ_{hetero} according to Equation A6.3:

$$\tau_{hetero} = \tau_{homo}\varepsilon \qquad \textit{Equation A6.3}$$

Where

τ_{hetero} is the residence time of the gases in the presence of alumine or char in the reactor

τ_{homo} is the residence time of the gases in homogeneous cracking (empty reactor).

The details of the operating condition are summarized in the table below (Table A6.3).

Table A6.3: Operating conditions of thermal cracking and catalytic cracking experiments

	Thermal cracking		**Catalytic cracking**	
	Alumina bed	Tube	Char bed	Tube
Tpyro (°C)	400			
Tcraq (°C)	600			
d_tube (m)	0.026			
Qpyro (mL /min)	500			
Qcraq (mL/min)	500		212	
Flow rate STP (ml/min)	3198		2277	
Real flow rate (m3/s)	5.3E-05		3.8E-05	
Gas velocity (m/s)	1.5E-01	1.0E-01	2.0E-01	7.1E-02
Bed height/ Tube* (m)	0.03	0.22	0.1	0.22
Porosity	0.6922	1	0.35	1
Residence time (s)	0.21	2.19	0.49	2.10
Total residence time (s)	2.4		2.6	

List of figures and tables

List of figures

Figure 1.1: Biomass valorization pathways [33] 38

Figure 1.2: Simplified overall diagram of reactions involved in a gasification process (adapted from S. Salvador) 40

Figure 1.3: Structure of a lignocellulosic biomass [41] 42

Figure 1.4: Hemicelluloses monosaccharides [44] 43

Figure 1.5: Structure of the glucose polymer that forms cellulose [47] 43

Figure 1.6: Lignins structure [49] 44

Figure 1.7: Structure of p-coumaryl alcohol, coniferyl alcohol and synapyl alcohol main structural monomers of lignins [50] 44

Figure 1.8: Proximate and ultimate analysis and different analysis basis [65] 47

Figure 1.9: Photo and pictogram of cashew fruit with apple and nut [78,79] 49

Figure 1.10: Potential applications of CNSL in different fields [76] 51

Figure 2.1: Pyrolysis and the conversion of pyrolysis gas 58

Figure 2.2: Decomposition products of hemicelluloses at different temperatures [129] 60

Figure 2.3: dTG curve of a beech sample and dTG modelling of isolated macromolecules [131] 60

Figure 2.4: Reference species for biomass characterization [143] 60

Figure 2.5 : Composition of typical lignin samples and reference species.[143] 60

Figure 2.6: Reference species and several biomass samples in the H/C vs O/C van Krevelen diagram. [143] 60

Figure 2.7: Multistep kinetic mechanism of cellulose and hemicelluloses pyrolysis. [143] 60

Figure 2.8: Multistep kinetic mechanism of pyrolysis of the three reference lignins.[143] 60

Figure 2.9: Multiple kinetic scheme of biomass pyrolysis [143] 60

Figure 2.10: Structure of main constituents of CNSL 63

Figure 2.11: Soxhlet extraction 65

Figure 2.12: HPLC chromatogram of CNSL [175] 72

Figure 2.13: TG and dTG curves of CNS during pyrolysis [9] 75

Figure 2.14: Plots of deconvoluted DTG curves (solid lines), using Asym2Sig function, against the experimental DTG curves (open circles) of raw cashew nut shells (P-EX: pseudo extractives, P-HC: pseudo hemicelluloses, P-CL: pseudo cellulose, P-LG1:pseudo primary lignins and P-LG2: pseudo secondary lignins) [16] 77

Figure 2.15: Product distribution from CNS pyrolysis from the study of Abrego et al. [14] .. 81

Figure 2.16: Product distribution from de-oiled CNS (left) and CNS pyrolysis (right) [15] ... 81

Figure 2.17: TG and dTG curve of CNSL [12] 86

Figure 2.18: TG and dTG curve of hydrogenated cardanol (Cardanol 15:0) at 10°C/min under air atmosphere [212] 87

Figure 2.19: Step growth polymerization (thermal oligomerization) of cardanol [217] 88

Figure 2.20: TG curves of cardanol monomers and polycardanols (under N_2 and air atmosphere) 20°C/min [218] 89

Figure 2.21: Dealkylation of cardanol and cardol 90

Figure 2.22: Variation of boiling (red) and melting point (blue) of alkanes with different chain lengths [228] 91

Figure 3.1: Cashew nut shells 98

Figure 3.2: Quartering method of biomass [236] 98

Figure 3.3: Soxhlet extraction 100

Figure 3.4: High-Performance Liquid Chromatography coupled with UV 102

Figure 3.5: Thermogravimetric analyzer 104

Figure 3.6: Pyrolysis and tar conversion reactor (PyTar) 106

Figure 3.7: Fixed bed reactor system connected to condensation system and microGC 108

Figure 4.1: Successive triple solvent extraction process 123

Figure 4.2: Calibration curve of anacardic acids 15:0, 15:1, 15:2, et 15:3. 124

Figure 4.3: HPLC chromatogram of the mixture of 12 ACC isomers 125

Figure 4.4: Chromatogram (left) and spectra (right) of anacardic acid isomers (Anacardic acid 15:3, 15:2, 15:1 and 15:0) 127

Figure 4.5: Chromatograms and spectra of cardanol 15:3 and cardol 15:3 127

Figure 4.6: HPLC chromatogram of acetone extractives (1: Cardol 15:3, 2: Cardol 15:2, 3: Anacardic acid 15:3, 4: Cardol 15:1, 5: Cardanol 15:3, 6:Anacardic acid 15:2, 7: Cardanol 15:2, 8: Cardol 15:0, 9: Anacardic acid 15:1, 10: Cardanol 15:1, 11: Anacardic acid 15:0) 129

Figure 4.7: HPLC chromatogram of hexane extractives (1: Anacardic acid 15:3, 2: Cardanol 15:3, 3:Anacardic acid 15:2, 4: Cardol 15:0, 5: Anacardic acid 15:1, 6: Cardanol 15:1, 7: Anacardic acid 15:0) 129

Figure 4.8: Ferric chloride test 132

Figure 4.9: Composition of cashew nut shells (dry basis) 133

Figure 5.1: dTG curves of CNS (10 mg), ACC-free CNS (5.8 mg) and ACC (4.2 mg), 10°C/min 138

Figure 5.2: Decarboxylation reaction of anacardic acid [250] 139

Figure 5.3: dTG curves of CNS and of sum of ACC-free CNS and ACC (10 °C/min)..... 140

Figure 5.4: dTG curves of CNS with different sample masses 2.5, 5 and 10 mg (1 °C/min) 141

Figure 5.5: TG and dTG curves of ACC (160 mg and 1°C/min) 143

Figure 5.6: Composition of ACC residual products in the crucible (g/g ACC) 145

Figure 5.7: Temperature phases selected for ACC conversion analysis 146

Figure 5.8: Composition of ACC residual products in the crucible during first phase (g/g ACC) 147

Figure 5.9: Experimental and theoretical value of mass balance of decarboxylation of anacardic acids (g/g of ACC) 148

Figure 5.10: Composition of ACC residual products in the crucible during second phase (g/g ACC) 150

Figure 5.11: Composition of ACC residual products in the crucible during third phase (g/g ACC) 151

Figure 5.12: Composition of ACC residual products in the crucible during fourth phase (g/g ACC) 152

Figure 5.13: dTG curves of ACC at different sample mass (5, 10, 20, 40, 80 and 160 mg) at 1°C/min (dimensionless mass) 154

Figure 5.14: Mass of anacardic acids (a), cardanols (b) and cardols (c) isomers during pyrolysis at different temperatures (25, 150, 190, 250, 300 and 350°C) (g/g ACC) 157

Figure 5.15: Evolution of permanent gas flow rate (blue) of CNS pyrolysis (400°C, 25°C/min) and of pyrolysis temperature (orange) with time 159

Figure 5.16: Yield of main products of pyrolysis of CNS, ACC-free CNS, ACC, and wood chips at 400 °C (dry and ash-free basis) (%), and composition of condensates (pie charts). 160

Figure 5.17: Mass of quantified tars by chemical families formed during pyrolysis at 400°C (mg/g sample)..... 166

Figure 5.18: Pyrolysis gas composition of CNS and ACC (400, 450 and 500°C)..... 170

Figure 5.19: Permanent gas flow rate (blue) and pyrolysis temperature (black) of ACC pyrolysis at 500°C..... 171

Figure 5.20: ACC-derived char produced by pyrolysis at 500°C 172

Figure 5.21: Distribution of the products of CNS pyrolysis at 400 °C (dry ash free basis)... 173

Figure 5.22 : ACC degradation mechanisms and products during CNS pyrolysis, initial products (black), decarboxylation products (red), polymerization products (blue), thermal degradation and devolatilization products (green),evaporation products (orange)..... 174

Figure 6.1: Temperature profiles of cracking zone 178

Figure 6.2: Cracking zone 179

Figure 6.3: Conversion rate of organic condensates via thermal cracking (800°C) of CNS, ACC, ACC-free CNS and wood chips pyrolysis gas in %..... 181

Figure 6.4: Distribution of condensates (water-free), permanent gas, and water before and after cracking at 800°C (CNS, ACC, ACC-free CNS and wood chips) in % of pyrolysis gas mass 182

Figure 6.5: Variation of individual permanent gas (CNS, ACC, ACC-free CNS and wood chips experiments, 800°C) in mg/g pyrolysis gas 183

Figure 6.6: Variation of main tertiary tars in the condensates (CNS, ACC, ACC-free CNS and wood chips experiments, 800°C) in mg/g pyrolysis gas 185

Figure 6.7: Conversion rate of organic condensates via thermal cracking (800°C) of CNS pyrolysis gas at 3 different temperatures (600,800 and 900°C) in % 187

Figure 6.8: Distribution of condensates (water-free), permanent gas, and water before and after cracking for 3 temperatures (600, 800 and 900°C) in % of pyrolysis gas mass 188

Figure 6.9: Variation of individual permanent gas (600,800 and 900°C) in mg/g pyrolysis gas 189

Figure 6.10: Tars distribution (by group) of thermal cracking of CNS pyrolysis gas (600,800, and 900°C) in mg/g of pyrolysis gas 190

Figure 6.11: Variation of main tertiary tars in the condensates of CNS cracked gas for 3 temperatures (600,800 and 900°C) in mg/g of pyrolysis gas 191

..... 192

Figure 6.12: Distribution of pyrolysis gas (400°C) (a) and cracked gas of CNS (b) and ACC (c) (thermal and catalytic cracking at 600°C) in % of pyrolysis gas mass 192

Figure 6.13: Variation of permanent gas in the CNS and ACC cracked gas (thermal and catalytic cracking) at 600°C in mg/g of pyrolysis gas 193

Figure A3.1: Carbonization furnace 234

Figure A6.1: Linear pressure drop (Pa/m) vs. surface speed U 239

List of tables

Table 1.1: Major components of biomass adapted from Pham (wt% on dry basis) [30] 46

Table 1.2: Proximate and ultimate analysis of biomass. Volatile Matter, Ash, Fixed Carbon, C, H, O, N, S in wt%, High Heating Value in MJ/kg.Fig 48

Table 2.1: Operating conditions of HPLC of CNSL by different studies 67

Table 2.2: Soxhlet extraction yield of CNSL in the CNS (wt%) 68

Table 2.3: Extraction yield of CNSL using other methods than Soxhlet extraction (wt%) 69

Table 2.4: Cashew nut shells composition by different authors 70

Table 2.5: Proximate and ultimate analysis of cashew nut shells (adapted from Melzer et al. [10]). Volatile Matter, Ash, Fixed Carbon, C, H, N, O and S in wt%, High Heating Value in MJ/kg. 71

Table 2.6: HPLC chromatogram of CNSL [174,175] 72

Table 2.7: Proximate and ultimate analysis of CNSL 73

Table 2.8: Physicochemical properties of cashew nut shell liquid (CNSL) 74

Table 2.9: Algebraic expressions of the most frequent reaction models used to describe the kinetics of solid-state reactions [16] 79

Table 2.10: Permanent gas composition of CNS, CNSL and de-oiled CNS pyrolysis (wt%) . 82

Table 2.11: Tar distribution in CNS and CNSL pyrolysis condensates at 500°C (mg/g biomass) [6,10] 83

Table 4.1 : Proximate and ultimate analysis of cashew nut shells 118

Table 4.2: Hemicelluloses, cellulose and lignins content of cashew nut shells (%db) 119

Table 4.3 Extractives yield with single solvent extraction (wt%) 120

Table 4.4: Influence of cashew nut shells granulometry on extractives yield (%) 121

Table 4.5: Influence of extraction duration on extractives yield (%) 122

Table 4.6: Retention times of all ACC isomers (min) 125

Table 4.7: Distribution of ACC constituents in acetone extractives (wt%) 130

Table 4.8 : Proximate and ultimate analysis of acetone extractives 131

Table 5.1 ACC-free CNS and ACC components and their degradation temperatures 139

Table 5.2: ACC degradation mechanisms and their degradation products 153

Table 5.3: Areas of ACC degradation peaks (%) 155

Table 5.4: Distribution of permanent gases (mg/g CNS) in the pyrolysis gas (CNS, ACC-free CNS, ACC and wood chips) at 400 °C. 162

Table 5.5: Distribution of anacardic acids, cardanols and cardols (ACC) in the CNS and ACC pyrolysis condensates (mg/g CNS) at 400 °C. 163

Table 5.6: Anacardic acids in CNS ($n_{AA\ before\ pyrolysis}$) and Cardanols produced during pyrolysis ($n_{CDN\ produced\ during\ pyrolysis}$) at 400°C (mmol/g). 164

Table 5.7 : Major chemical compounds in ACC pyrolysis condensates characterized by GC-MS 168

Table 6.1: Quantified tars in the condensates before and after cracking of pyrolysis gas (CNS and wood chips) (mg/g pyrolysis gas) 184

Table A6.1: Char yields obtained during char preparation (wt%) 237

Table A6.2: Characteristics of char used pour cracking of pyrolysis gas 238

Table A6.3: Operating conditions of thermal cracking and catalytic cracking experiments . 240